Signal Processing for Robust Speech Recognition Motivated by Auditory Processing

Chanwoo Kim

CMU-LTI-10-017

Language Technologies Institute
School of Computer Science
Carnegie Mellon University
5000 Forbes Ave., Pittsburgh, PA 15213
www.lti.cs.cmu.edu

Thesis Committee:

Richard M. Stern, Chair
Alex Rudnicky
Bhiksha Raj
Hynek Hermansky, Johns Hopkins University

Submitted in partial fulfillment of the requirements
for the degree of Doctor of Philosophy
In Language and Information Technologies

SIGNAL PROCESSING FOR ROBUST SPEECH RECOGNITION

MOTIVATED BY AUDITORY PROCESSING

CHANWOO KIM

December 2010

This work was sponsored by the National Science Foundation Grants IIS-10916918 and IIS-0420866, by Samsung Electronics, by the Charles Stark Draper Laboratory URAD Program, and by the DARPA GALE project.

ABSTRACT

Although automatic speech recognition systems have dramatically improved in recent decades, speech recognition accuracy still significantly degrades in noisy environments. While many algorithms have been developed to deal with this problem, they tend to be more effective in stationary noise such as white or pink noise than in the presence of more realistic degradations such as background music, background speech, and reverberation. At the same time, it is widely observed that the human auditory system retains relatively good performance in the same environments. The goal of this thesis is to use mathematical representations that are motivated by human auditory processing to improve the accuracy of automatic speech recognition systems.

In our work we focus on five aspects of auditory processing. We first note that nonlinearities in the representation, and especially the nonlinear threshold effect, appear to play an important role in speech recognition. The second aspect of our work is a reconsideration of the impact of time-frequency resolution based on the observations that the best estimates of attributes of noise are obtained using relatively long observation windows, and that frequency smoothing provide significant improvements to robust recognition. Third, we note that humans are largely insensitive to the slowly-varying changes in the signal components that are most likely to arise from noise components of the input. We also consider the effects of temporal masking and the precedence effect for the processing of speech in reverberant environments and in the presence of a single interfering speaker. Finally, we exploit the excellent performance provided by the human binaural system in providing spatial analysis of incoming signals to develop signal separation systems using two microphones.

Throughout this work we propose a number of signal processing algorithms that are motivated by these observations and can be realized in a computationally efficient fashion using real-time online processing. We demonstrate that these approaches are effective in improving speech recognition accuracy in the presence of various types of noisy and reverberant environments.

CONTENTS

LIST OF FIGURES

1. INTRODUCTION

In recent decades, speech recognition systems have significantly improved. Nevertheless, obtaining good performance in noisy environments still remains a very challenging task. The problem is that recognition accuracy degrades significantly if training conditions are not matched to the corresponding test conditions. These environmental differences might be due to speaker differences, channel distortion, reverberation, additive noise, or other causes.

Many algorithms have been proposed over the past several decades to address this problem. The simplest form of environmental normalization is *cepstral mean normalization* (CMN) [5, 6], which forces the mean of each element of the cepstral feature vector to be zero for all utterances. CMN is known to be able to remove stationary linear filtering, if the impulse response of the filter is short compared to the duration of the analysis frame, and it also can be helpful additive noise as well. *Mean-variance normalization* (MVN) [6] [7] can be considered to be an extension of CMN. In MVN, both the means and the variances of each element of the feature vectors are normalized to zero and one, respectively, for all utterances. In the more general case of *histogram normalization* it is assumed that the cumulative distribution function (CDF) of all features are the same. Recently, it was found that performing histogram normalization on delta cepstra as well as original cepstral coefficients can provide further improvements to performance [8].

A second class of approaches is based on the estimation of the noise components for different clusters and the subsequent use of this information to estimate the original clean spectrum. *Codeword-dependent cepstral normalization* (CDCN) [9] and *vector Taylor series* (VTS) [10] are examples of this approach. These algorithms may be considered to be generalizations of *spectral subtraction* [11], which subtracts the noise spectrum in the spectral domain.

Even though a number of algorithms have shown improvements for stationary noise

(*e.g.*[12, 13]), improvement in non-stationary noise remains a difficult issue (*e.g.* [14]). In these environments, approaches based on human auditory processing (*e.g.*[15]) and missing-feature-based approaches (*e.g.*[16]) are promising. In [15], we observed that improved speech recognition accuracy can be obtained by using a more faithful model of human auditory processing at the level of the auditory nerve.

A third approach is signal separation based on analysis of differences in arrival time (*e.g.* [17, 18, 19]). It is well documented that the human binaural system is remarkable in its ability to separate speech arriving from different angles relative to the ears (*e.g.* [19]). Many models have been developed that describe various binaural phenomena (*e.g.* [20, 21]), typically based on interaural time difference (ITD), interaural phase difference (IPD), interaural intensity difference (IID), or changes of interaural correlation. The *zero crossing amplitude estimation* (ZCAE) algorithm was recently introduced by Park [18], which is similar in some respects to work by Srinivasan *et al.* [17]. These algorithms (and similar ones by other researchers) typically analyze incoming speech in bandpass channels and attempt to identify the subset of time-frequency components for which the ITD is close to the nominal ITD of the desired sound source (which is presumed to be known *a priori*). The signal to be recognized is reconstructed from only the subset of "good" time-frequency components. This selection of "good" components is frequently treated in the computational auditory scene analysis (CASA) literature as a multiplication of all components by a binary mask that is nonzero for only the desired signal components.

The goal of this thesis is to develop robust speech recognition algorithms that are motivated by the human auditory system at the level of peripheral processing and simple binaural analysis. These include time and frequency resolution analysis, auditory nonlinearity, power normalization, and source separation using two microphones.

In time-frequency resolution analysis, we will discuss the duration of the optimal window length for noise compensation. We will also discuss the potential benefits that can be obtained by appropriate frequency weighting (which is sometimes referred to as channel weighting). We will propose an efficient way of normalizing noise components based on these observations.

Next, we will focus on the role that auditory nonlinearity plays in robust speech recognition. While the relationship between the intensity of a sound and its perceived loudness is well known, there have not been many attempts to analyze the effects of rate-level nonlinear-

ity. In this thesis, we discuss several different nonlinearities derived from the rate-intensity relation observed in physiological measurements of the human auditory nerve. We will show that a power function nonlinearity is more robust than the logarithmic nonlinearity that is currently being used in the standard baseline speech features, *mel-frequency cepstral coefficients* (MFCC) [22].

Another important theme of our work is the use of power normalization that is based on the observation that noise power changes less rapidly than speech power. As a convenient measure, we propose the use of the arithmetic mean-to-geometric mean ratio (the AM-to-GM ratio). If a signal is highly non-stationary like speech, then the AM-to-GM ratio will have larger values. However, if the signal changes more smoothly, this ratio will decrease. We develop two algorithms that are based on the estimation of the ideal AM-to-GM ratio from a training database of clean speech: *power-function-based power equalization* (PPE) and *power bias subtraction* (PBS).

This thesis is organized as follows: Chapter 2 provides a brief review of background theories and several related algorithms. We will briefly discuss the key concepts and effectiveness of each idea and algorithm. In Chapter 3, we will discuss time and frequency resolution and its effect on speech recognition. We will see that the window length and frequency weighting have significant impact on speech recognition accuracy. Chapter 4 deals with auditory nonlinearity and how it affects the robustness of speech recognition systems. Auditory nonlinearity is the intrinsic relation between the intensity of the sound and representation in auditory processing, and it plays an important role in speech recognition. In Chapter 8, we introduce a new feature extraction algorithm called *power-normalized cepstral coefficients* (PNCC). PNCC processing can be considered to be an application of some of principles of time-frequency analysis as discussed in Chapter 3, the auditory nonlinearity discussed in Chapter 4, and the power bias subtraction that is discussed in Chapter 6. In Chapter 9, we discuss how to enhance speech recognition accuracy through the us of two microphones. This discussion will focus on a new algorithm called *phase-difference channel weighting* (PDCW). Finally, in Chapter 10 we describe results that are obtained when we combine spatial and temporal masking. We summarize our findings in Chapter 11.

2. REVIEW OF SELECTED PREVIOUS WORK

As had been noted in the Introduction, there has been a great deal of work in robust speech recognition over the decades. In this chapter, we will review the results of a small sample of the previous research in this area that is particularly relevant to this thesis thesis.

2.1 Frequency scales

Frequency scales describe how the physical frequency of an incoming signal is related to the representation of that frequency by the human auditory system. In general, the peripheral auditory system can be modeled as a bank of bandpass filters, of approximately constant bandwidth at low frequencies and of a bandwidth that increases in rough proportion to frequency at higher frequencies. Because different psychoacoustical techniques provide somewhat different estimates of the bandwidth of the auditory filters, several different frequency scales have been developed to fit the psychophysical data. Some of the widely used frequency scales include the MEL scale [23], the BARK scale [24], and the ERB (Equivalent rectangular bandwidth) scale [4]. The popular Mel Frequency Cepstral Coefficients (MFCCs) incorporate the MEL scale, which is represented by the following equation:

$$Mel(f) = 2595 \log(1 + f/700) \tag{2.1}$$

The MEL scale that was proposed by Stevens *et al.* [23] describes how a listener judges the distance between pitches. The reference point is obtained by defining a 1000 Hz tone 40 dB above the listener's threshold to be 1000 mels.

Another frequency scale, called the Bark scale, was proposed by Zwicker [24]:

$$Bark(f) = 13 \arctan(0.00076f) + 3.5 \arctan\left(\frac{f}{7500}\right)^2 \tag{2.2}$$

In the Perceptual Linear Prediction (PLP) feature extraction approach [25], the Bark-

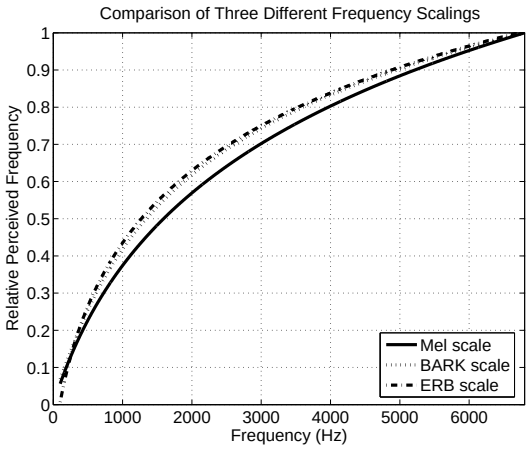

Fig. 2.1: Comparison of the MEL, Bark, and ERB frequency scales.

Frequency relation is based on a similar transformation given by Schroeder:

$$\Omega(f) = 6 \ln \left(\frac{f}{600} + \left(\frac{f}{600} \right)^{0.5} \right) \tag{2.3}$$

More recently, Moore and Glasberg [4] proposed the ERB (Equivalent Rectangular Bandwidth) scale modifying Zwicker's loudness model. The ERB scale is a measure that gives an approximation to the bandwidth of filters in human hearing using rectangular bandpass filters; several different approximations of the ERB scale exist. The following is one of such approximations relating the ERB and the frequency f:

$$ERB(f) = 11.17 \log \left(1 + \frac{46.065 f}{f + 14678.49} \right) \tag{2.4}$$

Fig. 2.1 compares the three different frequency scales in the range between 100 Hz and 8000 Hz. It can be seen that they describe very similar relationships between frequency and its representation by the auditory system.

2.2 Temporal integration times

It is well known that there is a trade-off between time-resolution and frequency resolution that depends on the window length (*e.g.* [26]). Longer windows provide better frequency resolution, but worse time resolution. Usually in speech processing it is assumed that a

signal is quasi-stationary within an analysis window, so typical window durations for speech recognition are on the order of 20 to 30 ms [27].

2.3 Auditory nonlinearity

Auditory nonlinearity is related to how humans process intensity and perceive loudness. The most direct characterization of the auditory nonlinearity is through the use of physiological measurements of the the average firing rates of fibers of the auditory nerve, measured as a function of the intensity of a pure-tone input signal at a specified frequency. As shown in Fig. 2.2, this relationship is characterized by an auditory threshold and a saturation point. The curves in Fig. 2.2 are obtained using the auditory model developed by Heinz *et al.* [1].

Another way of representing auditory nonlinearity is based on psychophysics. One of the well-known psychophysical rules is Steven's power law [28], which relates intensity and perceived loudness in a hearing experiment by fitting data from multiple observers in a subjective magnitude estimation experiment using a power function:

$$L = (I/I_0)^3 \tag{2.5}$$

This rule has been used in Perceptual Linear Prediction (PLP) [25].

Another common relationship used to relate intensity to loudness in hearing is the logarithmic curve, which was originally proposed by Fechner to relate the intensity-discrimination results of Weber to a psychophysical transfer function. MFCC features, for example, use a logarithmic function to relate input intensity to putative loudness, and the definition of sound pressure level (SPL) is also based on the logarithmic transformation:

$$L_p = 20 \log_{10} \left(\frac{p_{rms}}{p_{ref}} \right) \tag{2.6}$$

The commonly-used value for the reference pressure p_{ref} is 20μPa, which was once considered to be the threshold of human hearing, when the definition was first established.

In Fig. 2.3, we compare these nonlinearities. In addition to the nonlinearities mentioned in this Sec., we included another power-law nonlinearity which is an approximation to the physiological model of Heinz *et al.* between 0 and 50 dB SPL in the Minimum Mean Square Error (MMSE) sense. In this approximation, the estimated power coefficient is around 1/10.

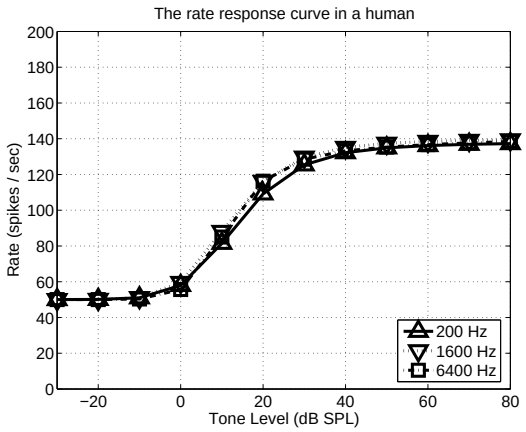

Fig. 2.2: The rate-intensity function of the human auditory system as predicted by the model of Heinz et al. *[1] for the auditory-nerve response to sound.*

In Fig. 2.3(a), we compare these curves as a function of sound pressure directly as measured in Pa. In this figure, with the exception of the cube power root, all three curves are very similar. Nevertheless, if we plot the curves using the logarithmic scale (dB SPL) to represent sound pressure level, we can observe a significant difference between the power-law nonlinearity and the logarithmic nonlinearity in the region below the auditory threshold. As will be discussed in Chap. 4, this difference plays an important role for robust speech recognition.

2.4 Feature Extraction Systems

The most widely used forms of feature extraction are Mel Frequency Cepstral Coefficient (MFCC) and Perceptual Linear Prediction (PLP) [25]. These feature extraction systems are based on the theories briefly reviewed in Secs. 2.1 to 2.3. Fig. 2.8 contains block diagrams of MFCC and PLP, which we briefly review and discuss in this section.

MFCC processing begins with pre-emphasis, typically using a first-order high-pass filter. Short-time Fourier Transform (STFT) analysis is performed using a hamming window, and triangular frequency integration is performed for spectral analysis. The logarithmic nonlinearity stage follows, and the final features are obtained through the us of a Discrete Cosine

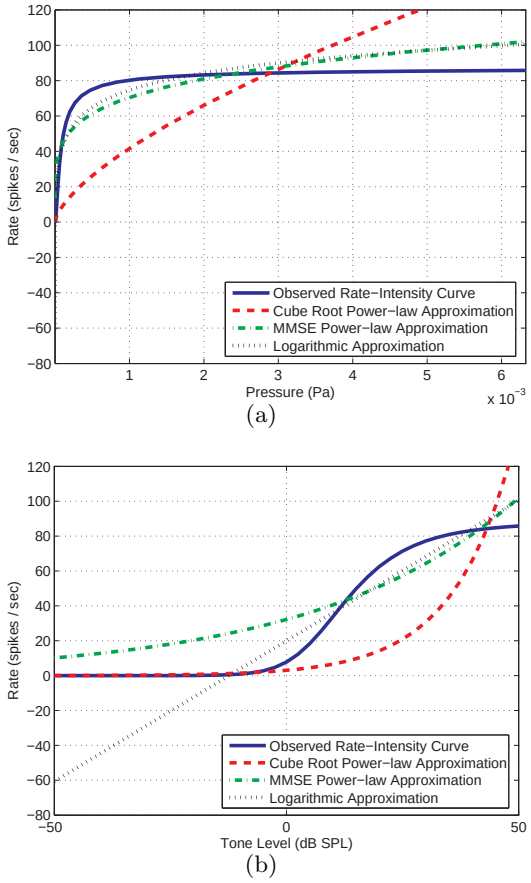

Fig. 2.3: Comparison of the cube-root power law nonlinearity, the MMSE power-law nonlinearity, and logarithmic nonlinearity. Plots are shown using two different intensity scales: pressure expressed directly in Pa (upper panel) and pressure after the log transformation in dB SPL (lower panel).

Transform (DCT).

PLP processing, which is similar to MFCC processing in some ways, begins with STFT analysis followed by critical-band integration using trapezoidal frequency-weighting functions. In contrast to MFCC, pre-emphasis is performed based on an equal-loudness curve after frequency integration. The nonlinearity in PLP is based on the power-law nonlinearity proposed by Stevens [25]. After this stage, Inverse Fast Fourier Transform (IFFT) and Linear Prediction (LP) analysis are performed in sequence. Cepstral recursion is also usually performed to obtain the final features from the LP coefficients [29].

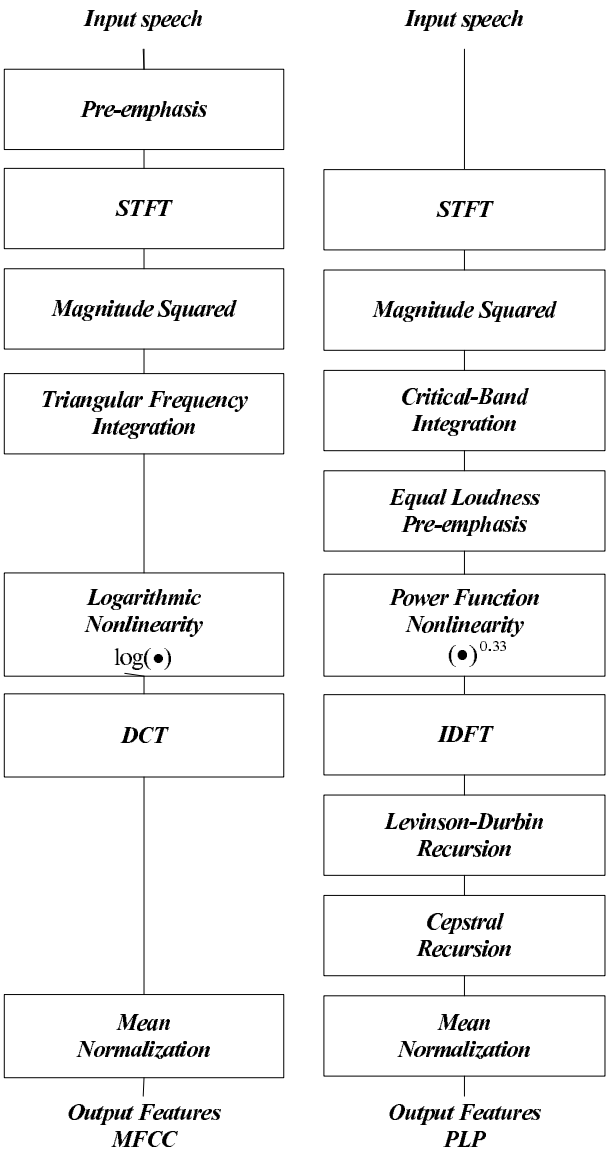

Fig. 2.4: Block diagrams of MFCC and PLP processing.

Fig. 2.5 compares the speech recognition accuracy obtained under various types of noisy conditions. We used subsets of 1600 utterances for training and 600 utterances for testing from the DARPA Resource Management 1 Corpus (RM1). In other experiments, which are shown in Fig. 2.6, we used the DARPA Wall Street Journal WSJ0-si84 training set and WSJ0 5k test set. For training the acoustical models we used `SphinxTrain 1.0` and for decoding, we used `Sphinx 3.8`.

For MFCC processing, we used `sphinxe_fe` included in `sphinxbase 0.4.1`. For PLP processing, we used both `HTK 3.4` and the MATLAB package provided by Dan Ellis and colleagues at Columbia University [30]. Both of the PLP packages show similar performance, except for the for reverberation and interfering speaker environments, where the version of PLP included in HTK provided better performance.

In all these experiments, we used 12^{th}-order feature vectors including the zeroth coefficient, along with the corresponding delta and delta-delta cepstra. As shown in these figures, MFCC and PLP show provide speech recognition accuracy. Nevertheless, in our experiments we found that RASTA processing is not as helpful as conventional Cepstral Mean Normalization (CMN).

2.5 Noise Power Subtraction Algorithms

In this section we discuss conventional ways of accomplishing noise power compensation, focussing on the original spectral subtraction technique of Boll [11] and Hirsch [31]. The biggest difference between the Boll's and Hirsch's approaches is how to estimate noise level. In the Boll's approach, *voice activity detector* (VAD) runs first, and noise level is estiamted from the non-speech segment. In Hirsch's approach, the noise level is conditionally updated by comparing the current power level and the estimated noise level.

2.5.1 Boll's approach

Boll proposed the first noise subtraction technique, of which dozens if not hundreds of variants have been proposed since Boll's original algorithm. The first step in Boll's historic approach is the use of a Voice Activity Detector (VAD) which determines whether or not the current frame contains speech, and an estimate of the noise spectrum is obtained by averaging power spectra from frames in which speech is absent. Frames in which speech is present are modified by subtracting the noise in the following fashion:

$$|\tilde{X}[m,l]| = \max(|X(m,l)| - N(m,l), \delta|X(m,l)|) \tag{2.7}$$

where $N(m,l)$ is the noise spectrum, $X(m,l)$ is the corrupt speech spectrum, and δ is a small constant to prevent the subtracted spectrum from having a negative spectrum value. The

indices m and l denote the frame number and channel number, respectively.

2.5.2 Hirsch's approach

Hirsch [31] proposed a noise-compensation method that was similar to that of Boll, but with the fixed estimate of the power spectrum of the noise replaced by a running average estimate using a simple difference equation:

$$|N(m,l)| = \lambda|N(m-1,l)| + (1-\lambda)|X(m,l)| \quad \text{if} |X(m,l)| < \beta|N(m,l)| \tag{2.8}$$

where m is the frame index and l is the frequency index. We note that the above equation is realizes in effect a first-order IIR lowpass filter. If the magnitude spectrum is larger than $\beta N(m,l)$, the estimate noise spectrum is not updated. Hirsch suggested using a value between 1.5 and 2.5 for β.

2.6 Algorithms Motivated by Modulation Frequency

It has long been believed that modulation frequency plays an important role in human listening. For example, it has been observed that the human auditory system is most sensitive to modulation frequencies that are less than 20 Hz (*e.g.* [32] [33] [34]). On the other hand, very slowly-changing components (*e.g.* less than 5 Hz) are usually related to noisy sources (*e.g.* [35] [36] [37]). In some studies (*e.g* [2]) it has been argued that speaker-specific information dominates for frequencies below $10Hz$, while speaker-independent information dominates higher frequencies. Based on these observations, many researchers have tried to utilize modulation-frequency information to enhance speech recognition accuracy in noisy environments. Typical approaches use high-pass or band-pass filtering in either the spectral, log-spectral, or cepstral domains.

In [2], Hirsch *et al.* investigated the effects of high-pass filtering the spectral envelopes of each subband after the initial bandpass filtering that is commonly used in signal processing based on auditory processing. Unlike the RASTA processing proposed by Hermansky in [3], Hirsch *et al.* conducted the high-pass filtering in the power domain (rather than in the log power domain). They compared FIR filtering with IIR filtering, and concluded that the latter approach is more effective. Their final system used the following first-order IIR filter:

$$H(z) = \frac{1 - z^{-1}}{1 - 0.7z^{-1}} \tag{2.9}$$

where λ is a coefficient that adjusts the cut-off frequency. This is a simple high-pass filter with a cut-off frequency at around 4.5 Hz.

It has been observed that online implementation of Log Spectral Mean Subtraction (LSMS) is largely similar to RASTA processing. Mathematically, the online mean log-spectral subtraction is equivalent to online CMN:

$$\mu_L(m, l) = \lambda \mu_Y(m - 1, l) + (1 - \lambda) Y(m, l) \tag{2.10}$$

where

$$Y(m, l) = P(m, l) - \mu_P(m, l) \tag{2.11}$$

This is also a high-pass filter like Hirsch's approach, but the major difference is that Hirsch conducted the high-pass filtering in the power domain, while in the LSMS, subtraction is done after applying the log-nonlinearity. Theoretically speaking, filtering in the power domain should be helpful in compensating for additive noise, while filtering in the log-spectral domain should be better for ameliorating the effects of linear filtering including reverberation [6].

RASTA processing in [3] is similar to online cepstral mean subtraction and online LSMS. While online cepstral mean subtraction is basically first-order high-pass filtering, RASTA processing is actually bandpass processing motivated by the modulation-frequency concept. This processing was based on the observation that the human auditory system is most sensitive to modulation frequencies between 5 and 20 Hz (*e.g.* [33] [34]). Hence, signal components outside this modulation frequency range are not likely to originate from speech. In RASTA processing, Hermansky proposed the following fourth-order bandpass filtering:

$$H(z) = 0.1z^4 \frac{2 + z^{-1} - z^{-3} - 2z^{-4}}{1 - 0.98z^{-1}} \tag{2.12}$$

As in the case of online CMN, RASTA processing is performed after the nonlinearity is applied.

Hermansky [3] showed that band-pass filtering approach results in better performance than high-pass filtering. In the original RASTA processing in Eq. (2.12), the pole location

was at $z = 0.98$; later, Hermansky suggested that $z = 0.94$ seems to be optimal [3]. Nevertheless, in some articles (*e.g.* [6]), it has been reported that online CMN (which is a form of high-pass filtering) provides slightly better speech recognition accuracy than RASTA processing (which is a form of band-pass filtering). As mentioned above, if we perform filtering after applying the log-nonlinearity, then it would be more helpful for reverberation, but it might not be very helpful for additive noise.

Hermansky and Morgan also proposed a variation of RASTA, called J-RASTA (or Lin-Log RASTA) that uses the following function:

$$y = \log(1 + Jx) \tag{2.13}$$

This model has characteristics of both the linear model and the logarithmic nonlinearity and in principle compensates for additive noise at low SNRs and for linear filtering at higher SNRs.

2.7 Normalization Algorithms

In this section, we discuss some algorithms that are designed for enhancing robustness against noise by matching the statistical characteristics of the training and testing environments. Many of these algorithms operate in the feature domain including Cepstral Mean Normalization (CMN), Mean Variance Normalization (MVN), Code-Dependent Cepstral Normalization (CDCN), and Histogram Normalization (HN). The original form of VTS (Vector Taylor Series) works in the log-spectral domain.

2.7.1 CMN, MVN, HN, and DCN

The simplest way of performing normalization is using CMN or MVN. Histogram normalization (HN) is a generalization of these approaches. CMN is the most basic form of noise compensation schemes, and it can remove the effects of linear filtering if the impulse response of the filter is shorter then the window length [38]. By assuming that the mean of each element of the feature vector from all utterances is the same, CMN is also helpful for additive

noise as well. CMN can be expressed mathematically as follows:

$$\tilde{c}_i[j] = c_i[j] - \mu_{c_i}, \quad 0 \leq i \leq I-1,\ 0 \leq j \leq J-1 \tag{2.14}$$

where μ_{c_i} is the mean of the i^{th} element of the cepstral vector. In the above equation, $c_i[j]$ and $\tilde{c}_i[j]$ represent the original and normalized cepstral coefficients for the i^{th} element of the vector at the j^{th} frame index. I denotes the dimensionality of the feature vector and J denotes the number of frames in the utterance.

MVN is a natural extension of CMN and is defined by the following equation:

$$\tilde{c}_i[j] = \frac{c_i[j] - \mu_{c_i}}{\sigma_{c_i}}, \quad 0 \leq i \leq I-1,\ 0 \leq j \leq J-1 \tag{2.15}$$

where μ_{c_i} and σ_{c_i} are the mean and standard deviation of the i-th element of the cepstral vector.

As mentioned in Sec. 2.6, CMN can be implemented as an online algorithm (*e.g.* [7] [39] [40]) where the mean of the cepstral vector is updated recursively.

$$\mu_{c_i}[j] = \lambda \mu_{c_i}[j-1] + (1-\lambda) c_i[j], \quad 0 \leq i \leq I-1,\ 0 \leq j \leq J-1 \tag{2.16}$$

This online mean is subtracted from the current cepstral vector.

As in RASTA and online log-spectral mean subtraction, the initialization of the mean value is very important in online CMN. Otherwise, the performance would be significantly degraded (*e.g.* [6] [7]). It has been shown that using values obtained from the previous utterances is a good means of initialization. Another method is to run a VAD to detect the first non-speech-to-speech transition (*e.g.* [7]). If the center of the initialization window coincides with the first non-speech-to-speech transition, then good performance is preserved, but this method requires a small amount of processing delay.

In HN, it is assumed that the Cumulative Distribution Function (CDF) for an element of a feature is the same for all utterances.

$$\tilde{c}_i[j] = F^{-1}_{c_i^{tr}}\left(F_{c_i^{te}}(c_i[j])\right) \tag{2.17}$$

In the above equation, $F_{c_i^{te}}$ denotes the CDF of the current test utterance and $F^{-1}_{c_i^{tr}}$ denotes the inverse CDF from the entire training corpus. Using (2.17) we can make the distribution

of the element of the test utterance the same as that of the entire training corpus. We can also perform HN in a slightly different way by assuming that every element of the feature follows a Gaussian distribution with zero mean and unit variance. In this case, $F_{c_i^{tr}}^{-1}$ is just the inverse CDF of the Gaussian distribution with zero mean and unity variance. If we use this approach, then the training database also needs to be normalized.

Recently, Obuchi [8] showed that if we do apply histogram normalization on the delta cepstrum as well as on the original cepstrum, recognition accuracy is better than with the original HN. This approach is called DCN (delta cepstrum normalization).

Fig. 2.9 shows speech recognition accuracy obtained using the RM1 database. First, we observe that CMN provides significant benefit for noise robustness. MVN performs somewhat better than CMN. Although HN is a very simple algorithm, it shows significant improvements for the white noise and street noise environments. DCN provides the largest threshold shift among all these algorithms. Fig. 2.10 shows the the results of similar experiments conducted on the WSJ0 5k test set, using WSJ0-si84 dataset for training.

Although these approaches show improvements in noisy environments, they are also very sensitive to the length of silence that precedes the speech, as shown in Fig. 2.11. This is because in these approaches it is assumedd that all distributions are the same and if we prepend or append silences this assumption no longer remains valid. As a consequence, DCN provides better accuracy than Vector Taylor Series (VTS) in the RM white noise and street noise environments, but the former is doing worse than the latter in the WSJ0 5k experiment, which include more silences. Experimental results obtained using VTS will be described in more detail in the next section.

2.7.2 CDCN and VTS

More advanced algorithms including CDCN (Code-Dependent Cepstral Normalization) and VTS (Vector Taylor Series) attempt to simultaneously compensate for the effects of additive noise and linear filtering. In this section we briefly review a selection of these techniques.

In CDCN and VTS the underlying assumption is that speech is corrupted by unknown additive noise and linear filtering by an unknown channel [41]. This assumption can be

represented by the following equation:

$$\begin{aligned} P_z(e^{jw_k}) &= P_x(e^{jw_k})|H(e^{jw_k})|^2 + P_n(e^{jw_k}) \\ &= P_x(e^{jw_k})|H(e^{jw_k})|^2 \left(1 + \frac{P_n(e^{jw_k})}{P_x(e^{jw_k})|H(e^{jw_k})|^2}\right) \end{aligned} \tag{2.18}$$

Noise compensation can be performed either in the log spectral domain [10] or in the cepstral domain [9]. In this subsection we describe compensation in the log spectral domain. Let x, n, q, and z denote the logarithms of the powewr spectral densities $P_x(e^{jw_k})$, $P_n(e^{jw_k})$, $|H(e^{jw_k})|^2$, and $P_z(e^{jw_k})$, respectively. For simplicity, we will remove the frequency index w_k in the following discussions. Then (2.18) can be expressed in the following form:

$$z = x + q + \log(1 + e^{n-x-q}) \tag{2.19}$$

This equation can be rewritten in the form of

$$z = x + q + r(x, n, q) = x + f(x, n, q) \tag{2.20}$$

where $f(x, n, q)$ is called the "environment function" [41].

Thus, our objective is inverting the effect of the environment function $f(x, n, q)$. This inversion consists of two independent problems. The first problem is estimating the parameters needed for the environment function. The second problem is finding the Minimum Mean Square Error (MMSE) estimate of x given z in (2.20).

In the CDCN approach, it is assumed that x is represented by the following Gaussian mixture and n and q are unknown constants:

$$f(x) = \sum_{k=0}^{M-1} c_k N(\mu_{x,k}, \Sigma_{x,k}) \tag{2.21}$$

The vectors $\hat{n}$ and $\hat{q}$ are obtained by maximizing the following likelihood:

$$(\hat{n}, \hat{q}) = arg \max_{n,q} p(z|q, n) \tag{2.22}$$

The maximization of the above equation is performed using the Expectation Maximization (EM) algorithm. After obtaining $\hat{n}$ and $\hat{q}$, $\hat{x}$ is obtained in the Minimum Mean Square Error (MMSE) sense. In CDCN it is assumed that n and q are constants for that utterance, so CDCN cannot efficiently handle non-stationary noise [42].

In the VTS approach, it is assumed that the probability density function (PDF) of the log spectral density of clean utterance is represented by a GMM (Gaussian Mixture Model) and that noise is represented by a single Gaussian component.

$$f(x) = \sum_{k=0}^{M-1} c_k N(\mu_{x,k}, \Sigma_{x,k}) \tag{2.23}$$

$$f(n) = N(\mu_n, |\Sigma_n) \tag{2.24}$$

The VTS approach attempts to reverse the effect of the environment function in Eq. (2.20). Because this function is nonlinear, it is not easy to find an environmental function which maximizes the likelihood. This problem is made more tractable by using the first-order Taylor series approximation. From (2.20), we consider the following first-order Taylor series expansion of the environment function $f(x, n, q)$:

$$\begin{aligned} \mu_z &= E\left[x + f(n_0, x_0, q_0)\right] + E\left[\frac{\delta}{\delta x} f(x_0, n_0, q_0)(x - x_0))\right] \\ &\quad E\left[\frac{\delta}{\delta n} f(x_0, n_0, q_0)(n - n_0))\right] + E\left[\frac{\delta}{\delta q} f(x_0, n_0, q_0)(q - q_0))\right] \end{aligned} \tag{2.25}$$

The resulting distribution z is also Gaussian if x is Gaussian.

In a similar fashion, we also obtain the covariance matrix:

$$\begin{aligned} \Sigma_z &= \left(I + \frac{d}{dx} f(n_0, x_0, q_0)\right)^T \Sigma_x \left(I + \frac{d}{dx} f(n_0, x_0, q_0)\right) \\ &\quad \left(\frac{d}{dx} f(n_0, x_0, q_0)\right)^T \Sigma_n \left(\frac{d}{dx} f(n_0, x_0, q_0)\right) \end{aligned} \tag{2.26}$$

Using the above approximations for the means and covariances of the Gaussian components, q, μ_n, and hence μ_z and Σ_z are obtained using the EM method to maximize the likelihood.

Finally, feature compensation is conducted in the MMSE sense as shown below.

$$\hat{x}_{MMSE} = E[X|z] \tag{2.27}$$

$$= \int x p(x|z) dx \tag{2.28}$$

[COMMENTS/DISCUSSION OF FIGS. 2.11 AND 2.12 SEEMS TO BE MISSING]

2.8 ZCAE and related algorithms

It has been long observed that human beings are remarkable in their ability to separate sound sources. Many research results (*e.g.* [43, 44, 45]) have supported the contention that binaural interaction plays an important role in sound source separation. For low frequencies, the use of interaural time delay (ITD) is primarily used for sound source separation; for high frequencies, interaural intensity difference (IID) plays an important role. This is because for high frequencies, spatial aliasing occurs, which prevents the effective use of ITD information, although ITDs of the low-frequency *envelopes* of high-frequency signals may be used in localization.

In ITD-based sound source separation approaches (*e.g.* [46] [18]), we frequently use a smaller distance between two microphones than the actual distance between two ears to avoid spatial aliasing problems.

The conventional way of calculating the ITD (and the way the human binaural system is believed to calculate ITDs) by computing the cross-correlation of the signals to the two microphones after they are passed through the bank of bandpass filters that is used to model the frequency selectivity of the peripheral auditory system. In more recent work [18], it has been shown that a zero-crossing approach is more effective than the cross-correlation approach for accurately estimating the ITD, and resulting in better speech recognition accuracy, at least in the absence of reverberation. This approach is called Zero Crossing Amplitude Estimation (ZCAE).

However, one critical problem of ZCAE is that the zero crossing point is heavily affected by in-phase noise and reverberation. Thus, as shown in [19] and [46], the ZCAE method does not produce successful results in environments that include reverberation and/or omni-directional noise.

2.9 Discussion

While it is generally agreed that a window length between 20 ms and 30 ms is appropriate for speech analysis, as mentioned in Section 2.2, there is no guarantee that this window length will remain optimal for the estimation of or the compensation for additive-noise components.

Since the noise characteristics are usually stationary compared to speech, it is expected that longer windows might be more helpful for noise compensation purposes. In this thesis we will consider what would be the optimal window length for noise compensation purposes. We note that even though longer duration windows may be used for noise compensation, we still need short duration windows for the actual speech recognition. We will discuss methods for accomplishing this in Chapter 3 of this thesis.

In Section 2.3, we discussed several different rate-level nonlinearities based on different data. Up until now, there has not been much discussion or analysis of the type of nonlinearity that is best for feature extraction. For a nonlinearity to be appropriate, it should satisfy some of the following characteristics:

- It should be robust with respect to the presence of additive noise and reverberation.
- It should discriminate each phone reasonably well.
- The nonlinearity should be independent of the absolute input sound pressure level, or at worst, a simple normalization should be able to remove the effect of the input sound pressure level.

Based on the above criteria, we will discuss in Chapter 4 of this thesis the nature of appropriate nonlinearities to be used for feature extraction.

We discussed conventional spectral subtraction techniques in Section 2.5. The problem with conventional spectral subtraction is that the structure is complicated and the performance depends on the accuracy of the VAD. Instead of using this conventional approach, since speech power changes faster than noise power, we can use the rate of power change as a measure for power normalization.

Although algorithms like VTS are very successful for stationary noise, they have some intrinsic problems. First, VTS is computationally costly, since it is based on a large number of mixture components and an iterative EM algorithm, which is used for maximizing the likelihood. Second, this model assumes that the noise component is modeled by a single Gaussian component in the log spectral domain. This assumption is reasonable in many cases, but it is not always true. A more serious problem is that the noise component is assumed to be stationary, which is not quite true for non-stationary noise, like music noise.

Finally, since VTS requires maximizing the likelihood using the values in the current test set, it is not straightforward to implement this algorithm for real-time applications.

In the work described in later chapters of this thesis, we will develop an algorithm that is motivated by auditory observations, that imposes a smaller computational burden, and that can be implemented as an online algorithm that operates in sub-real time with only a very small delay. Instead of trying to estimate the environment function and maximizing the likelihood, which is very computationally costly, we will simply use the rate of power change or power distribution of the test utterance.

While the ZCAE algorithm described in Section 2.8 shows remarkable performance, it does not provide much benefit in reverberant environments [19][46]. Another problem is that this algorithm requires large computation[46], since it needs bandpass filtering. for these reasons we consider various two-microphone approaches that provide greater robustness with respect to reverberation in Chapters 9 and 10 of this thesis. We summarize our major conclusions and provide suggestions for future work in Chapter 11.

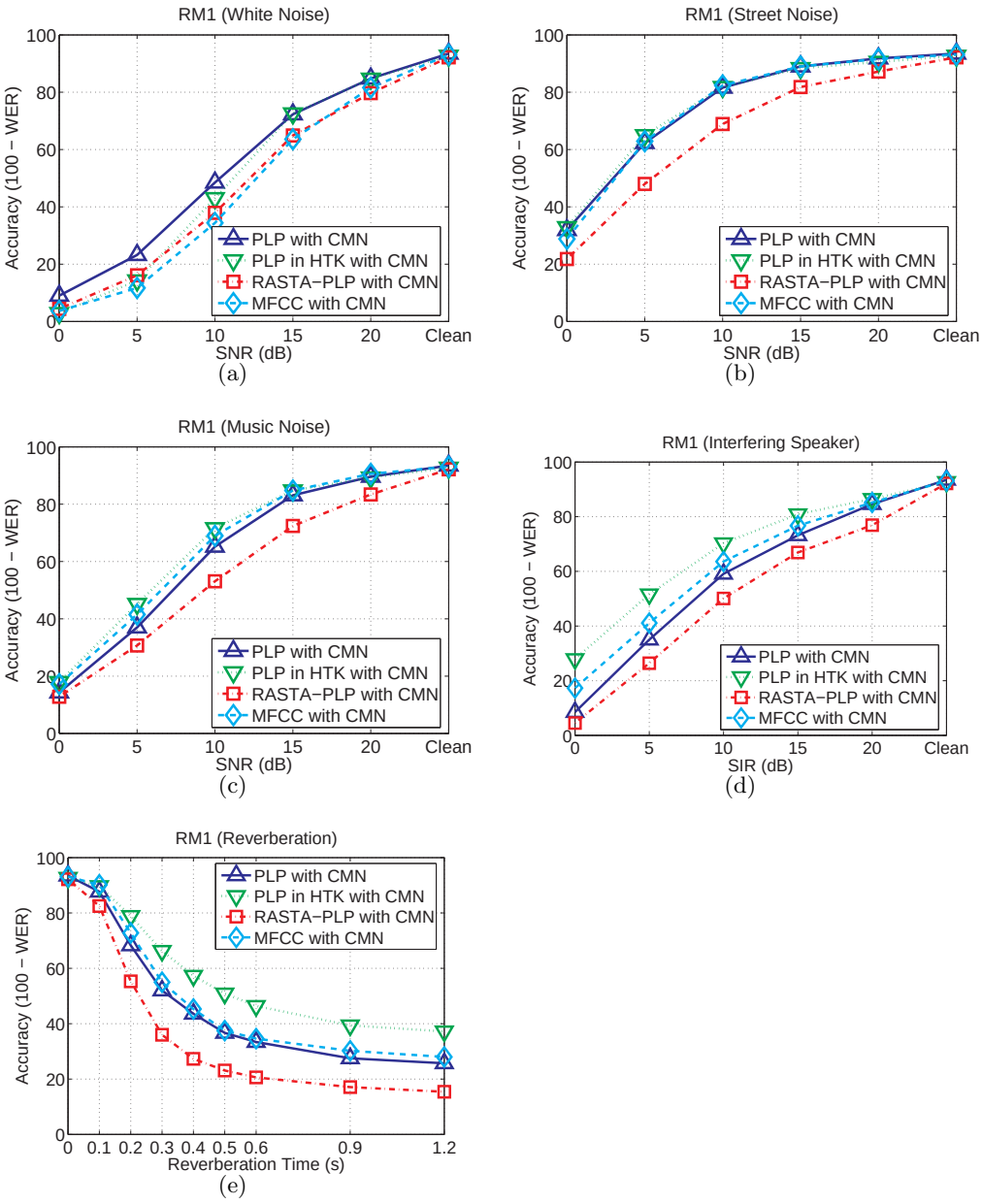

Fig. 2.5: Comparison of MFCC and PLP processing in different environments using the RM1 test set: (a) additive white gaussian noise, (b) street noise, (c) background music, (c) interfering speaker, and (d) reverberation.

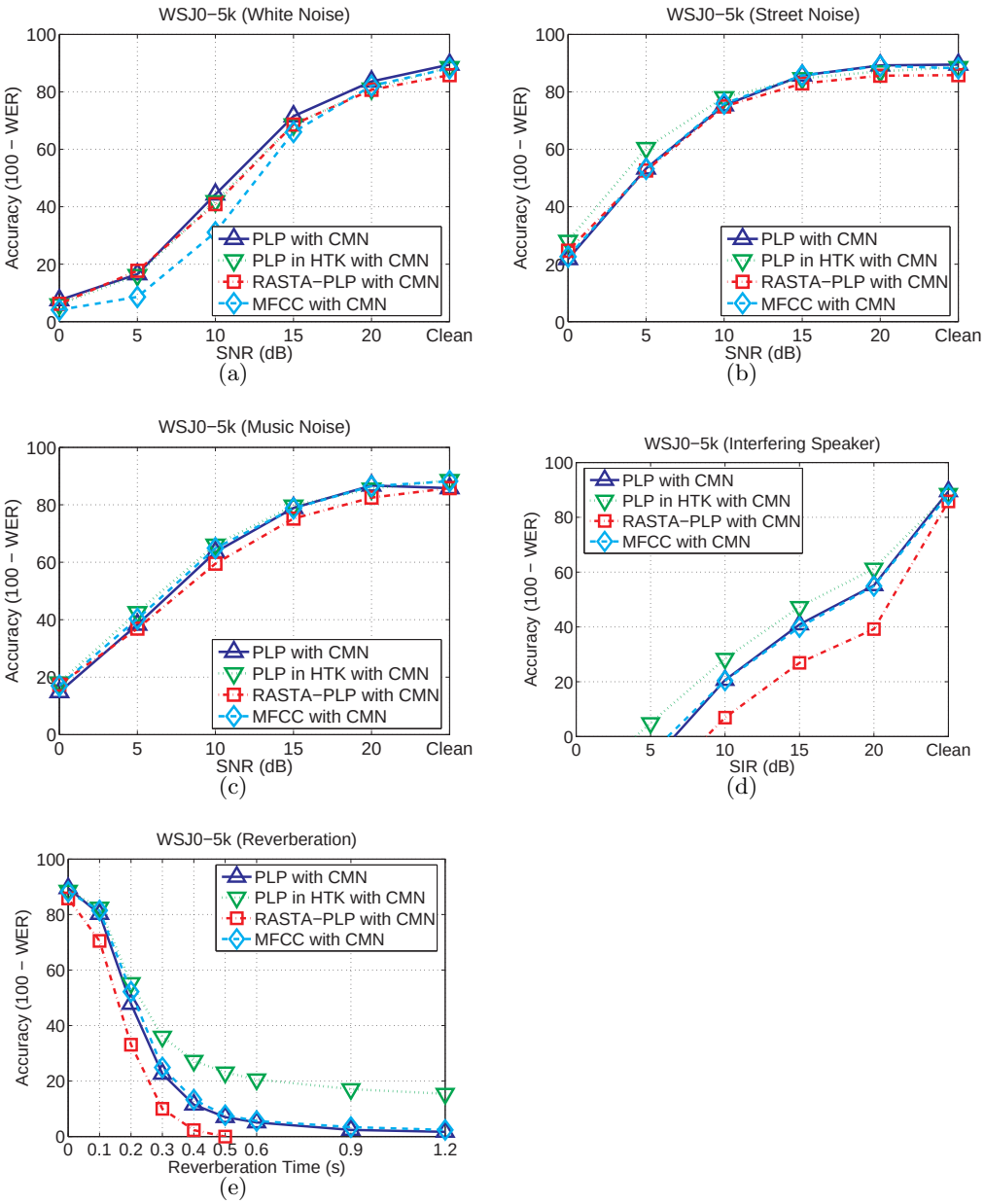

Fig. 2.6: Comparison of MFCC and PLP in different environments using the WSJ0 5k test set: (a) additive white gaussian noise, (b) street noise, (c) background music, (c) interfering speaker, and (d) reverberation.

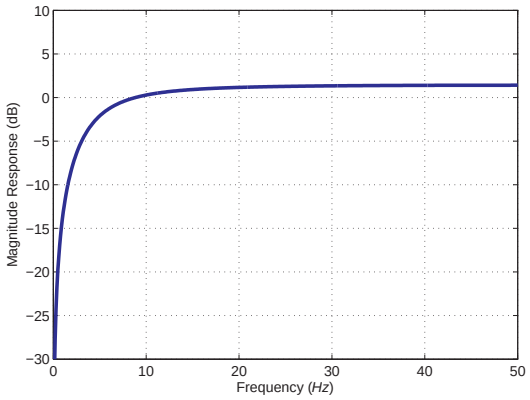

Fig. 2.7: The frequency response of the high-pass filter proposed by Hirsch et al. *[2]*

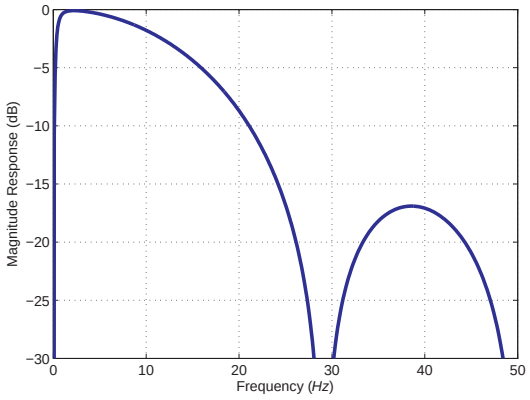

Fig. 2.8: The frequency response of the band-pass filter proposed by Hermansky et al. [3].

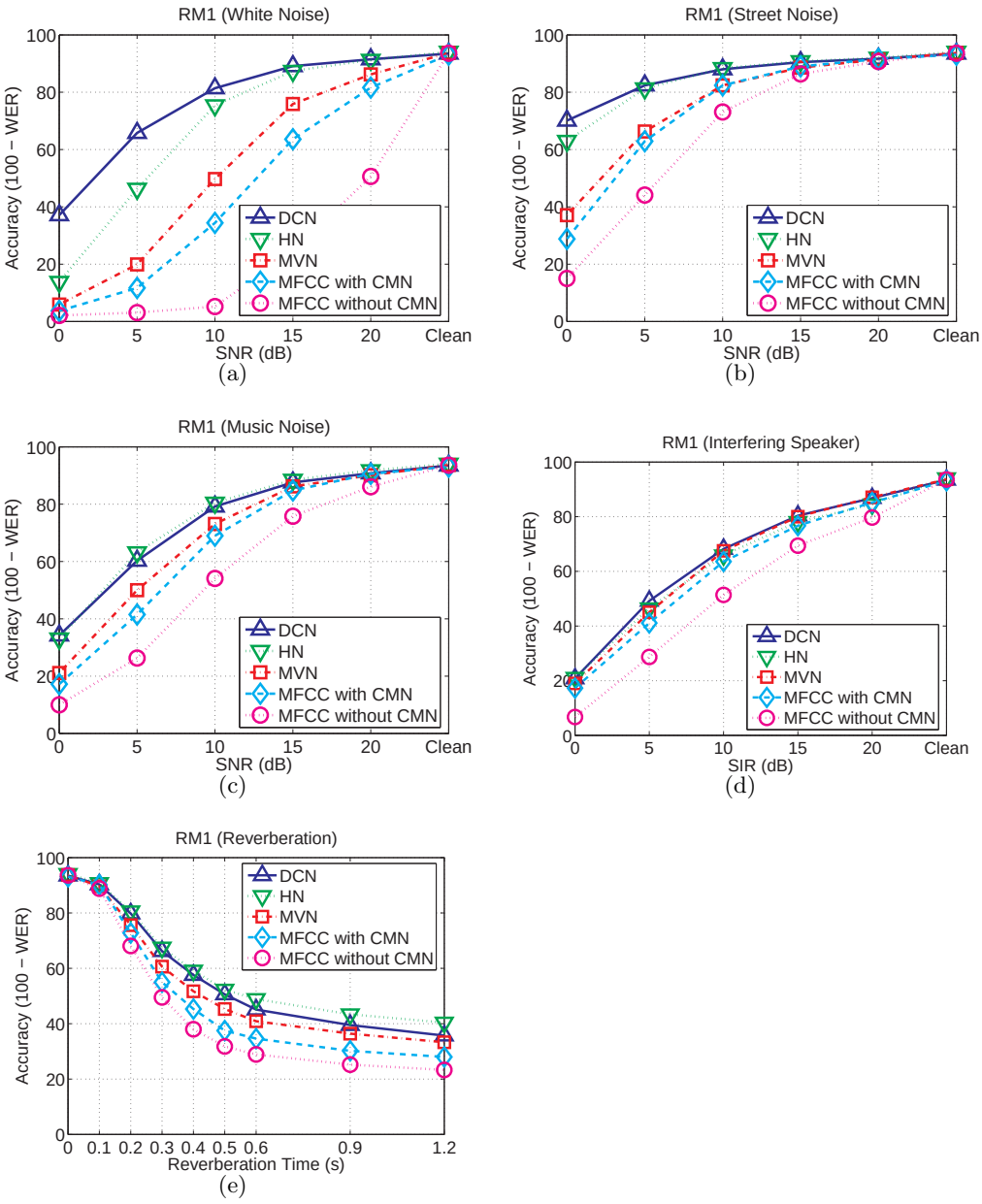

Fig. 2.9: Comparison of different normalization approaches in different environments on the RM1 test set: (a) additive white gaussian noise, (b) street noise, (c) background music, (c) interfering speaker, and (d) reverberation.

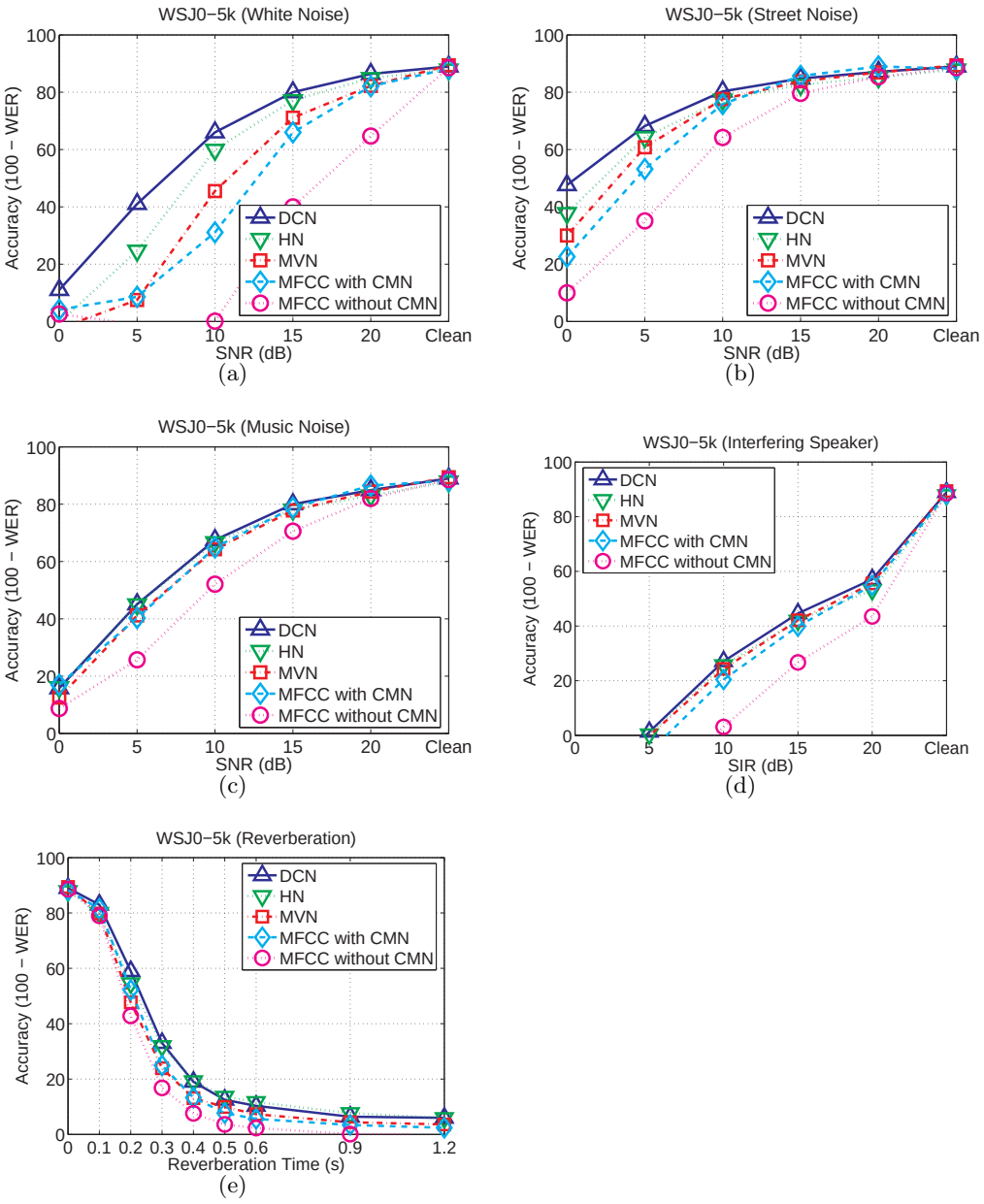

Fig. 2.10: Comparison of different normalization approaches in different environments on the WSJ0 5k test set: (a) additive white gaussian noise, (b) street noise, (c) background music, (c) interfering speaker, and (d) reverberation.

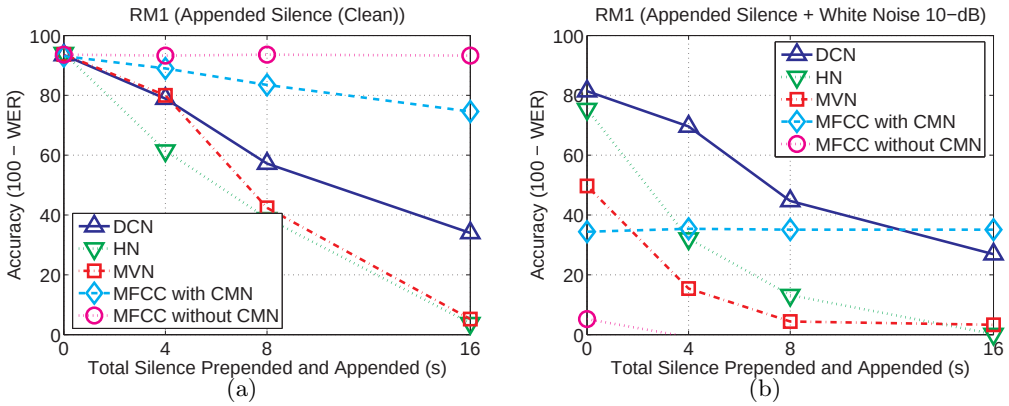

Fig. 2.11: Recognition accuracy as a function of appended and prepended silence without (left panel) and with (right panel) white Gaussian noise added at an SNR of 10 dB.

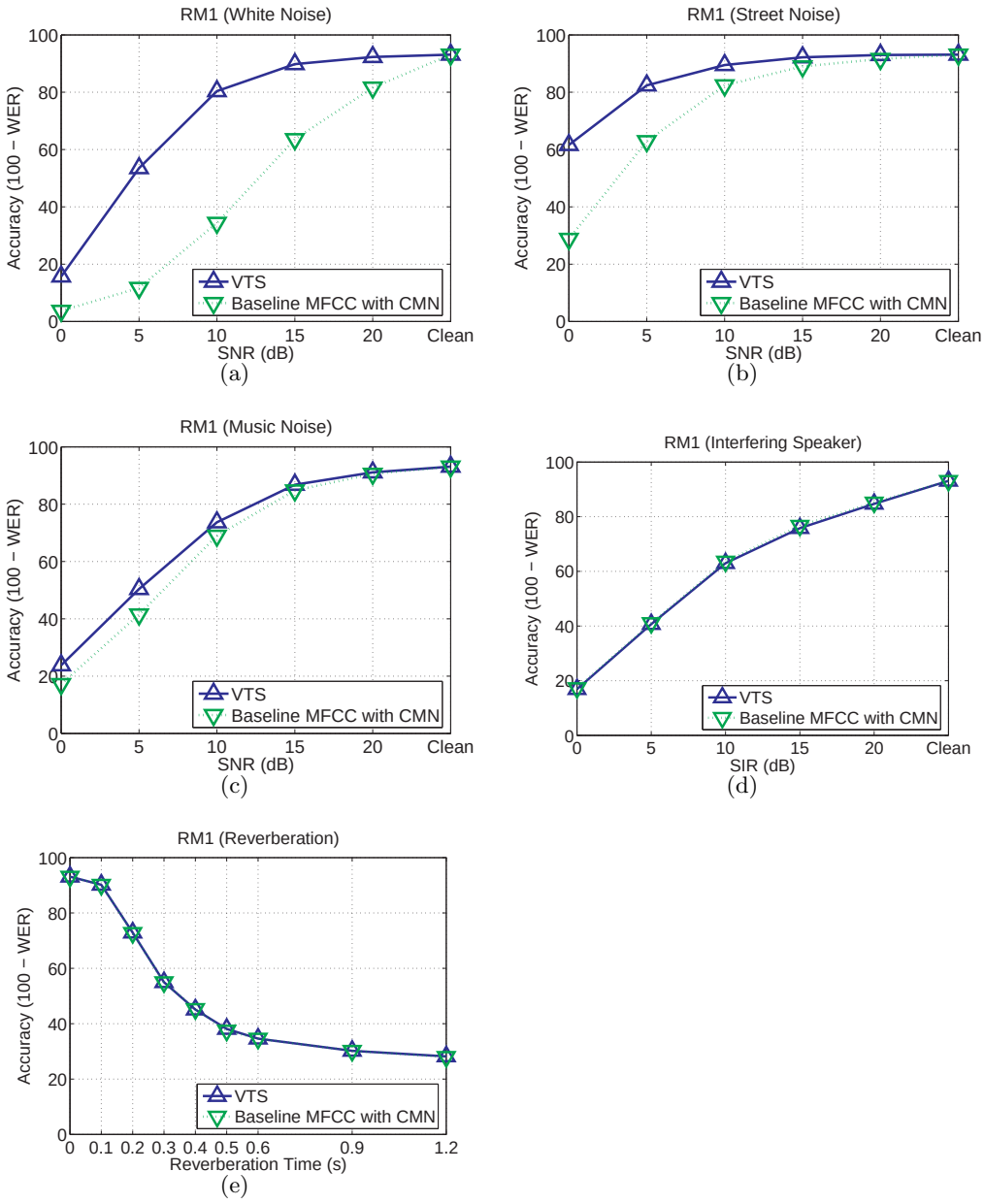

Fig. 2.12: Comparison of different normalization approaches in different environments using the RM1 test set: (a) additive white gaussian noise, (b) street noise, (c) background music, (c) interfering speaker, and (d) reverberation.

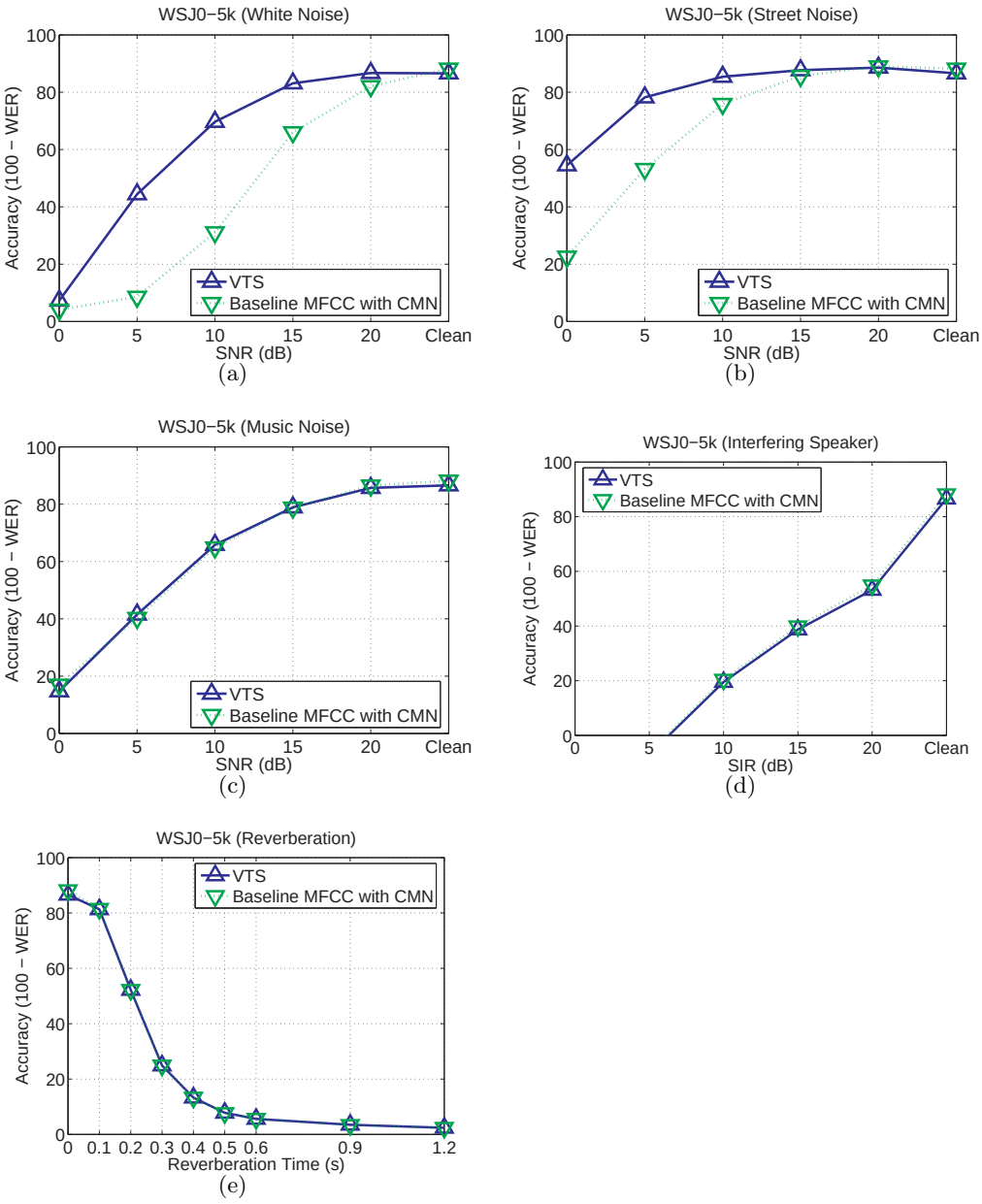

Fig. 2.13: Comparison of different normalization approaches in different environments using the WSJ0 test set: (a) additive white gaussian noise, (b) street noise, (c) background music, (c) interfering speaker , and (d) reverberation.

3. TIME AND FREQUENCY RESOLUTION

It is widely known that there is a trade-off between time resolution and frequency resolution when we select an appropriate window length for frequency-domain analysis (*e.g.* [27]). If we want to obtain better frequency-domain resolution, a longer window is more appropriate since the Fourier transform of a longer window is closer to a delta function in the frequency domain. However, a longer window is worse in terms of time resolution, and this is especially true for highly non-stationary signals like speech. In speech analysis, we want the signal within a single window to be stationary. As a compromise between these tradeoffs, a window length between 20 ms and 30 ms has been widely used in speech processing (*e.g.* [27]).

Although a window of 20-30 ms is suitable for analyzing speech signals, if the statistical characteristics of a certain signal do not change very quickly a longer window will be better. If we use a longer window, we can analyze the noise spectrum in a better way. Also from large sample theory, if we use more data in estimating statistics, then the variance of the estimate will be reduced. Since noise power changes more slowly than speech signal power, longer windows are expected to be better for estimating the noise power or noise characteristics. Nevertheless, even if we use longer windows for noise compensation or normalization, we still need to use short windows for feature extraction. In this section, we discuss two general approaches to accomplish this goal, the Medium-duration-window Analysis and Synthesis (MAS) method, and the Medium-duration-window Running Average (MRA) method.

We know from large sample theory that statistical parameter estimation provides estimates with smaller variance as the amount of available data increases. While we previously addressed this concept in terms of the duration of the analysis window used for speech processing, we now consider integration along the frequency axis as well. In the analysis-and-synthesis approach, we perform frequency analysis by directly estimating parameters for each discrete-time frequency index. Nevertheless, we observe that the channel-weighting

approach provides better performance, as will be described and discussed below in more detail. We believe that this occurs for the same reason that we observed better performance with the medium-duration window. If we make use of information from adjacent frequency channels, we can estimate noise components more reliably by averaging over frequency.

We consider several different weighting schemes such as triangular response weighting or gammatone response weighting for frequency integration (or weighting), and we compare the impact of window shape on recognition accuracy.

3.1 Time-frequency resolution trade-offs in short-time Fourier analysis

Before discussing the medium-duration-window processing for robust speech recognition, we will review the time-frequency resolution trade-off in short-time Fourier analysis. This trade-off has been known for a long time and has been extensively discussed in many articles (*e.g.* [27]).

Suppose that we obtain a short-time signal $v[n]$ by multiplying the originial signal $x[n]$ by a finite-duration window $w[n]$. In the time domain, this windowing procedure is represented by the equation:

$$v[n] = x[n]w[n] \tag{3.1}$$

In the frequency domain, it is represented by the relation:

$$V(e^{j\omega}) = \frac{1}{2\pi} X(e^{j\omega}) * W(e^{j\omega}) \tag{3.2}$$

where the asterisk in this case represents circular convolution along the frequency axis over an interval of 2π. Ideally, we want $V(e^{j\omega})$ to approach $X(e^{j\omega})$ as closely as possible. To achieve this goal, $W(e^{j\omega})$ needs to be close to the delta function in the frequency domain [26]. In the time domain, this corresponds to a constant value of $w[n] = 1$ with infinite duration. As the length of the window increases, the magnitude spectrum becomes closer and closer to the delta function. Hence, a longer window results in better frequency resolution.

Unfortunately, speech is a highly non-stationary signal, and in spectral analysis, we want to assume that the short-time signal $v[n]$ is stationary. If we increase the window length to obtain better frequency resolution, then the statistical characteristics of $v[n]$ would be

more and more time-varying, which means that we would fail to capture those time changes faithfully. Thus, to obtain better time resolution, we need to use a shorter window.

The above discussion is the well-known time-frequency resolution trade-offs. Due to this trade-offs, in speech processing, we usually use a window length between 20 ms and 30 ms.

3.2 Time Resolution for Robust Speech Recognition

In this section, we discuss two different ways of using the medium-duration window for noise compensation: the Medium-duration-window Analysis and Synthesis (MAS) method, and the Medium-duration-window Running Average (MRA) method. These methods enable us to use short windows for speech analysis while noise compensation is performed using a longer window. Fig. 3.2.1 summarizes the MAS and MRA methods in block diagram form. The main objective of these approaches is the same, but they differ in how to obtain this objective. In the case of the MRA approach, frequency analysis is performed using short windows, but parameters are smoothed over time using a running average. Since frequency analysis is conducted using short windows, the features can be obtained directly without re-synthesizing the speech. In the case of the MAS approach, frequency analysis is performed using a medium-duration window, and the waveform is re-synthesized after normalization. Using the re-synthesized speech, we can apply feature extraction algorithms using short windows. While the idea of using a longer window is actually very simple and obvious in conventional normalization algorithms, this idea has not been extensively used previously and the theoretical analysis has not been thoroughly performed.

3.2.1 Medium-duration running average (MRA) method

A block diagram for the medium-duration running average (MRA) method is shown in Fig. 3.4(f). In the MRA method, we segment the input speech by applying a short hamming window with a length between 20 ms and 30 ms, which is the length conventionally used in speech analysis. Let us consider a certain type of variable for each time-frequency bin and represent it by $P[m, l]$, where m is the frame index, and l is the channel index. Then, the medium-duration variable $Q[m, l]$ is defined by the following equation:

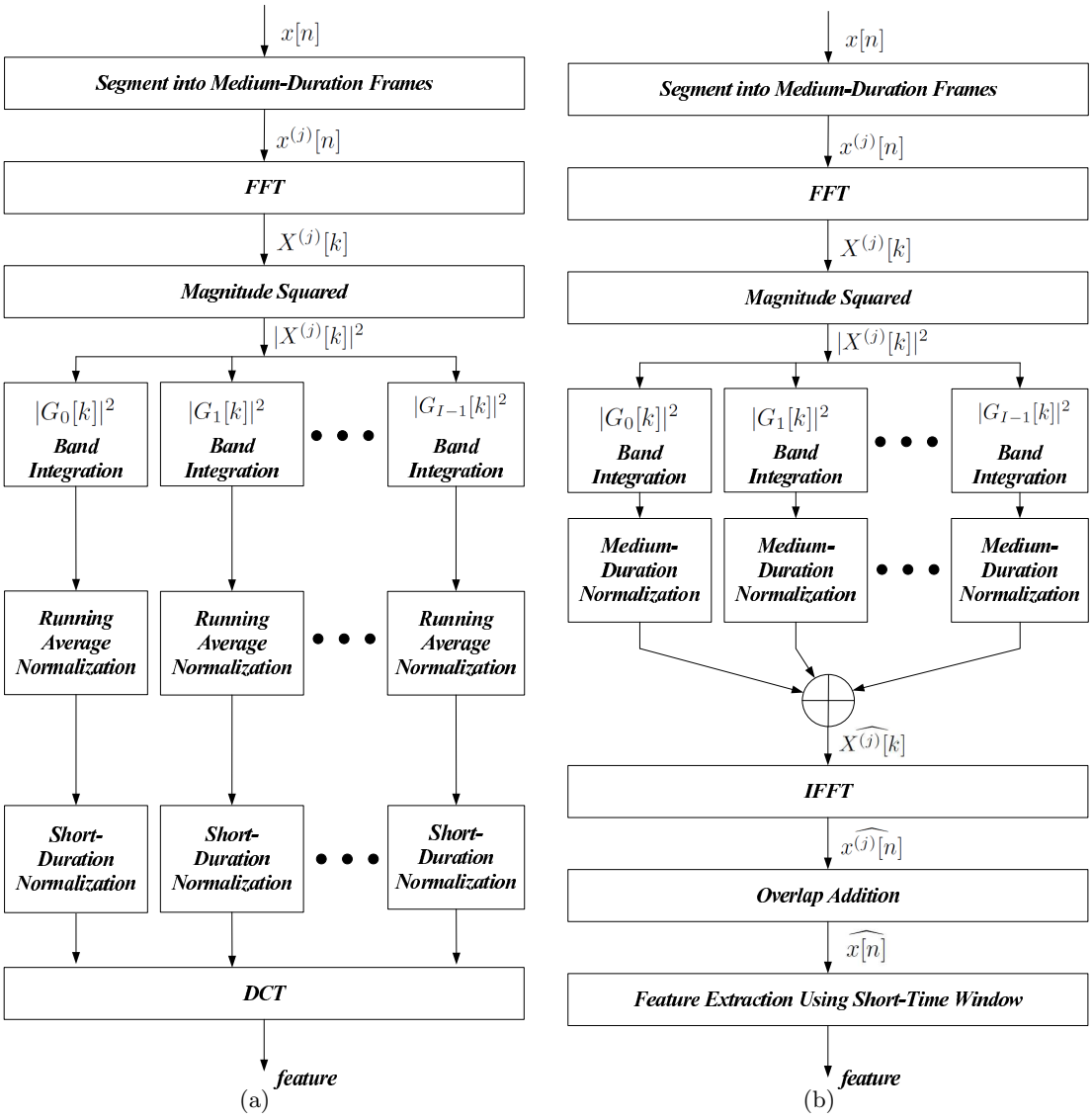

Fig. 3.1: (a) Bock diagram of the Medium-duration-window Running Average (MRA) Method. (b) Block diagram of the Medium-duration-window Analysis Synthesis (MAS) Method.

$$Q[m,l] = \frac{1}{2M+1} \sum_{m'=m-M}^{m+M} P[m',l] \quad \text{Averaging stage} \tag{3.3}$$

Averaging power across adjacent frames can be represented as a filtering operation with

the following transfer function:

$$H(z) = \sum_{n=-M}^{M} z^{-n} \tag{3.4}$$

This operation can be considered to be a low-pass filtering with the system's frequency response given by:

$$H(e^{j\omega}) = \frac{\sin\left(\left(\frac{2M+1}{2}\right)\omega\right)}{\sin\left(\frac{\omega}{2}\right)}, \tag{3.5}$$

and these responses for different M values are shown in 3.2. However we observe that if we directly perform low-pass filtering, then it has the effect of making the spectrogram quite blurred, so in many cases, it induces the negative effects as shown in Fig. 3.3.

Thus, instead of performing normalization using the original power $P[m, l]$, we perform normalization on $Q[m, l]$ as defined in Eq. (8.3). However, instead of using the normalized medium-duration power $\tilde{Q}[m, l]$ directly to obtain the features, the weighting coefficient is multiplied by $P[m, l]$ to obtain the normalized power $\tilde{P}[m, l]$. This procedure is represented in the following equation:

$$\tilde{P}[m, l] = \frac{\tilde{Q}[m, l]}{Q[m, l]} P[m, l] \tag{3.6}$$

An example of MRA is the Power Normalized Cepstral Coefficient (PNCC) algorithm, which is explained in Subsection 8. In the case of PBS, when we used a 25.6-ms window length with a 10-ms frame period, $M = 2 \sim 3$ showed the best speech recognition accuracy in noisy environments. So, this approximately corresponds to a window length of $75.6 \sim 85.6$ ms.

3.2.2 Medium duration window analysis and re-synthesis approach

As noted above, the other approach using a longer window for normalization is the MAS method. This method is described in block diagram form in Fig. 3.4(e). In this method, we directly apply a longer window to the speech signal to obtain a spectrum. From this spectrum, we perform normalization. Since we need to use features obtained from short windows, we cannot directly use the normalized spectrum from a longer window. Thus, a

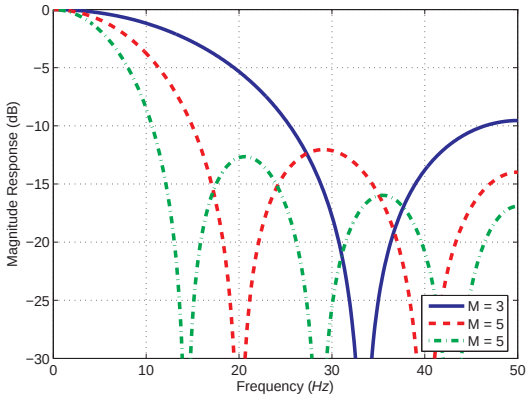

Fig. 3.2: Frequency response as a function of the medium-duration parameter M.

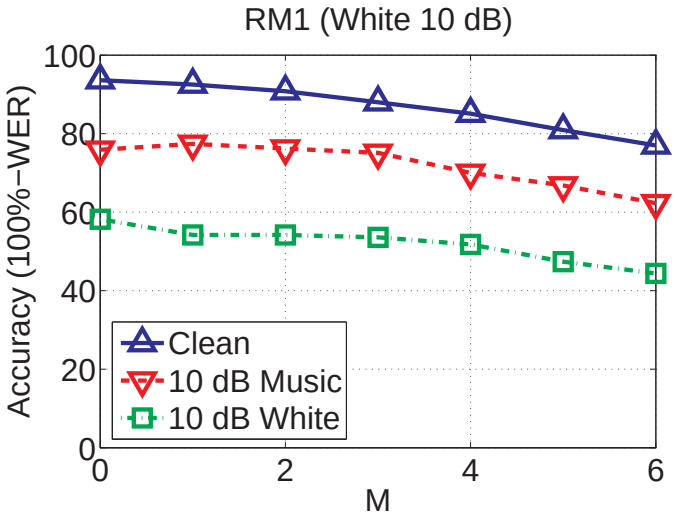

Fig. 3.3: Speech recognition accuracy as a function of the medium-duration parameter M.

spectrum from a longer window needs to be re-synthesized using IFFTs and the overlap-add (OLA) method. This approach is an integral part of the Power-function-based Power Distribution Normalization (PPDN) algorithm, which is explained in Sec. 6, as well as the Phase Difference Channel Weighting (PDCW) algorithm, which is explained in Chapter 9. Even though PPDN and PDCW are unrelated algorithms, the optimal window length for noisy environments is around $75ms \sim 100ms$ in both algorithms.

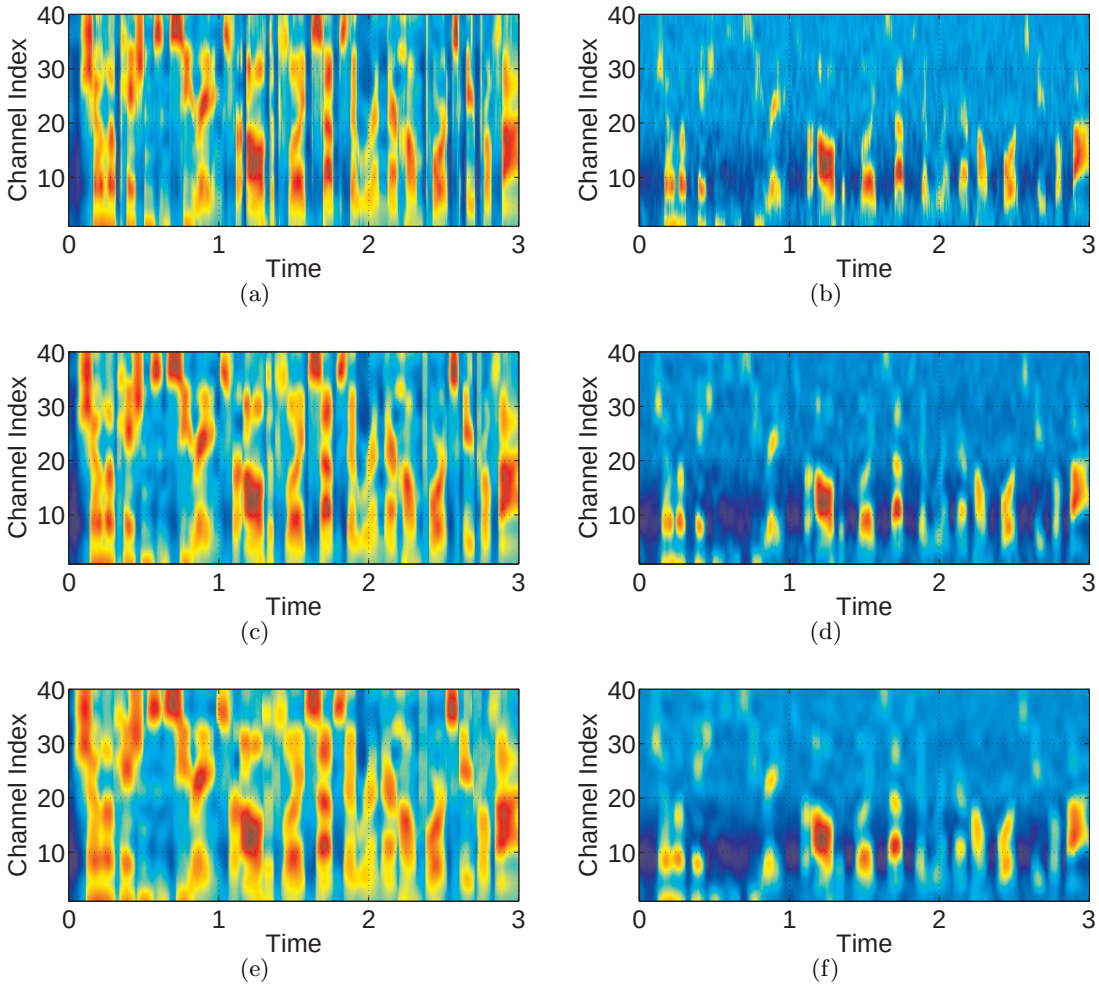

Fig. 3.4: (a) Spectrograms of clean speech with $M = 0$, (b) with $M = 2$, and (c) with $M = 4$. (d) Spectrograms of speech corrupted by additive white noise at an SNR of 5 dB with $M = 0$, (e) with $M = 2$, and (f) with $M = 4$.

3.3 Channel Weighting

3.3.1 Channel Weighting after Binary Masking

In many cases there are high correlations among adjacent frequencies, so performing channel weighting is helpful in obtaining more reliable information about noise and for smoothing purposes. This is especially true for environmental compensation algorithms in which a binary mask is used to select a subset of time-frequency channels that are considered to

contain a valid representation of the speech signal. If we make a binary decision about whether or not a particular time-frequency bin is corrupted by the effects of environmental degradation, there are likely to be some errors in the mask values as a consequence of the limitations of binary decision making. The use of a weighted average across adjacent frequencies enables the system to make better decisions, which is expected to lead to better system performance.

Suppose that $\xi[m,l]$ is a component of a binary mask for the l^{th} frequency index in the m^{th} frame.

$$w[m,l] = \frac{\sum_{k=0}^{\frac{N-1}{2}} \xi[m,k]\,|X[m,k]H_l[k]|}{\sum_{k=0}^{\frac{N-1}{2}} |X[m,l]H_l[l]|} \tag{3.7}$$

where $X[m,l]$ is the spectral component of the signal for this time-frequency bin and $H_i[l]$ is the frequency response of the i^{th} channel. Usually, the number of channels is much less than the FFT size. After obtaining the channel weighting coefficient $w[m,l]$ using (9.11), we obtain the smoothed weighting coefficient $\mu_g[m,l]$ using the following equation:

$$\mu_g[m,l] = \frac{\sum_{i=0}^{I-1} w[m,l]\,|H_i[l]|}{\sum_{l=0}^{I-1} |H_i[l]|} \tag{3.8}$$

Finally, the reconstructed spectrum is given by:

$$\tilde{X}[m,l] = \max\left(\mu_g(m,l), \eta\right)\, X[m,l] \tag{3.9}$$

where again η is a small constant used as a floor.

Using $\tilde{X}[m,l]$, we can re-synthesize speech using the IFFT and OLA algorithms. This approach has been used in Phase Difference Channel Weighting (PDCW), and experimental results using PDCW may be found in Chapter 8 of this thesis.

3.3.2 Averaging continuous weighting factors across channels

In the previous section we discussed channel weighting for systems that use binary masks. The same general approach can also be applied to systems that use continuous weighting functions as well.

Suppose that we have the values for a noise-corrupted power coefficient $P[m,l]$ and the corresponding enhanced power $\tilde{P}[m,l]$ for a particular time-frequency bin where as before m represents the frame index and l represents the channel index.

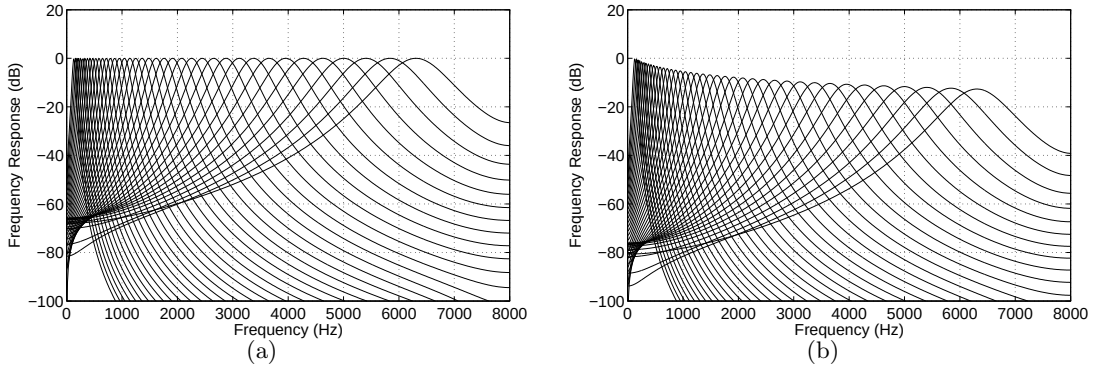

Fig. 3.5: (a) Gammatone Filterbank Frequency Response and (b) Normalized Gammatone Filterbank Frequency Response

Instead of directly using $\tilde{P}[m,l]$ as the enhanced power, the weighting factor averaging scheme works as follows:

$$\hat{P}[m,l] = \left(1/(l_2 - l_1 + 1) \sum_{l'=l_1}^{l_2} \frac{\tilde{P}[m,l']}{P[m,l]} \right) P[m,l] \tag{3.10}$$

where $l_2 = \min(l+N, N_{ch}-1)$ and $l_1 = \max(l-N, 0)$. In the equation above, averaging is performed using a rectangular window across frequency. Substitution of the rectangular window by a Hamming or Bartlett windows did not appear to affect recognition error very much in pilot

This approach has been used in Power Normalized Cesptral Coefficient (PNCC) and Small Power Boosting (SPB), with experimental results to be found in Chapters 5 and 6.

3.3.3 Comparison between the triangular and the gammatone filter bank

In the previous subsection, we discussed obtaining performance improvement by using the channel-weighting scheme. Usually, in conventional speech feature extraction such as MFCC or PLP, frequency-domain integration has been already employed in the form of triangular or trapezoidal frequency response integration. In this section, we compare the triangular frequency integration and the gammatone frequency integration in terms of speech recognition accuracy. The gammatone frequency response is shown in Fig 3.5. This figure was obtained using Slaney's auditory toolbox [47]. Figure 3.6 shows speech recognition accuracies obtained

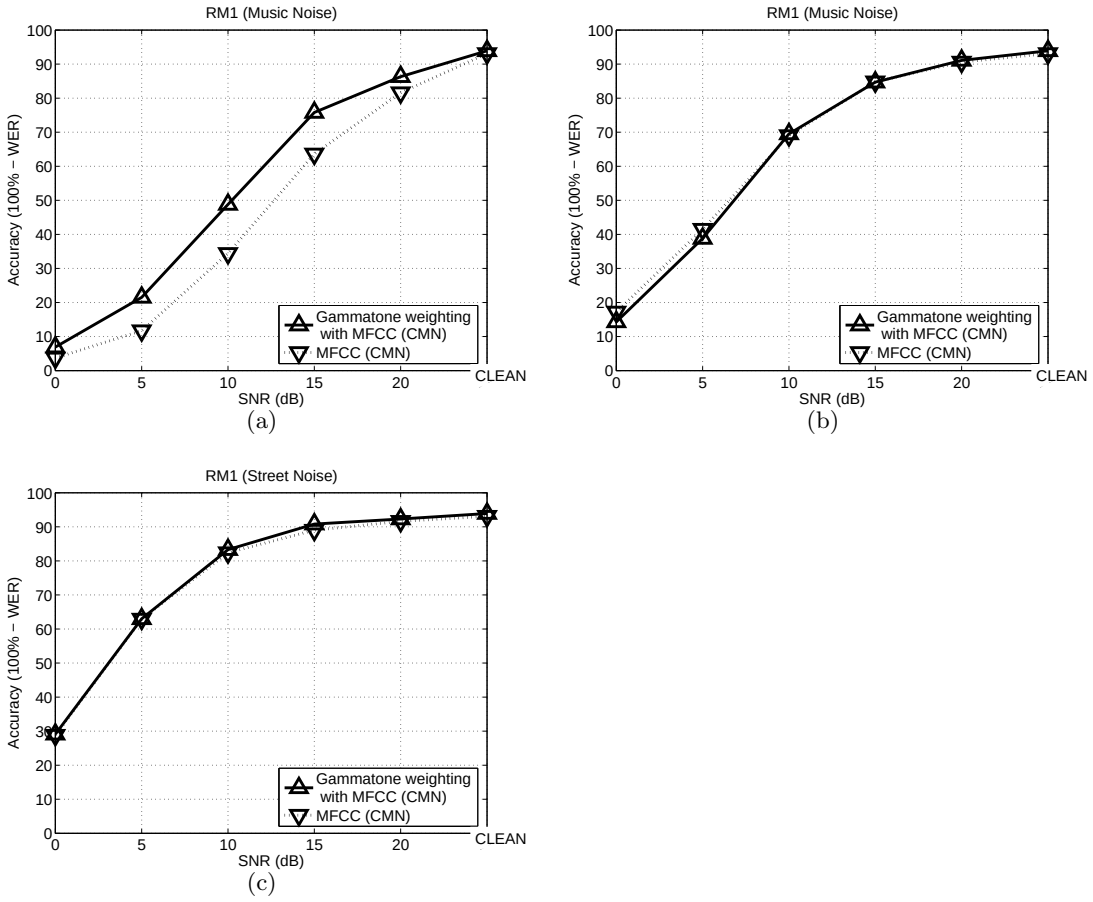

Fig. 3.6: Speech recognition accuracies when the gammatone and mel filter banks are employed under different noisy conditions: (a) white noise, (b) musical noise, and (c) street noise.

using the gammatone and mel filter bank weightings are employed. As shown in this figure, the difference in WER is somewhat small. In much of the work that is performed in this thesis we will use gammatone weighting, because it is more faithful to the actual human auditory response, even though the impact of the shapes of the filters in the filterbank on the final results may be less than that of other model components.

4. AUDITORY NONLINEARITY

4.1 Introduction

In this chapter, we discuss auditory nonlinearities and their role in robust speech recognition. The relation between sound pressure level and human perception has been studied for some time (*e.g.* [48] [49]). Auditory nonlinearities have been an important part of many speech feature extraction systems. Inarguably, the most widely used features extraction procedures presently used in speech recognition and speaker identification are MFCC (Mel Frequency Cepstral Coefficients) and PLP (Perceptual Linear Prediction coefficients). The MFCC procedure uses a logarithmic nonlinearity motivated in part by the work of Fechner while PLP includes a power-law nonlinearity that is motivated by Steven's power law of hearing [28]. In this chapter we will discuss the role of nonlinearity in feature extraction in terms of phone discrimination ability, noise robustness, and speech recognition accuracy in different noisy environments.

4.2 Physiological auditory nonlinearity

The putative nonlinear relationship between signal intensity and perceived loudness has been investigated by many researchers. Due to the difficulty of conducting physiological experiments on actual human nervous systems, researchers perform experiments on animals like cats which have similar auditory systems [50], with results extrapolated to reflect presumed human values *e.g.* [1]. Fig. 4.1 illustrates the results of simulations of the relation between the average rate of response and the input SPL (Sound Pressure Level) for a pure sinusoidal signal using the auditory model proposed by Heinz *et al.* [1]. In Fig. 4.1(a) and Fig. 4.1(b), we can observe the rate-intensity relation at different frequencies obtained from the cat's nerve model and from a modification that is believed to describe the human auditory

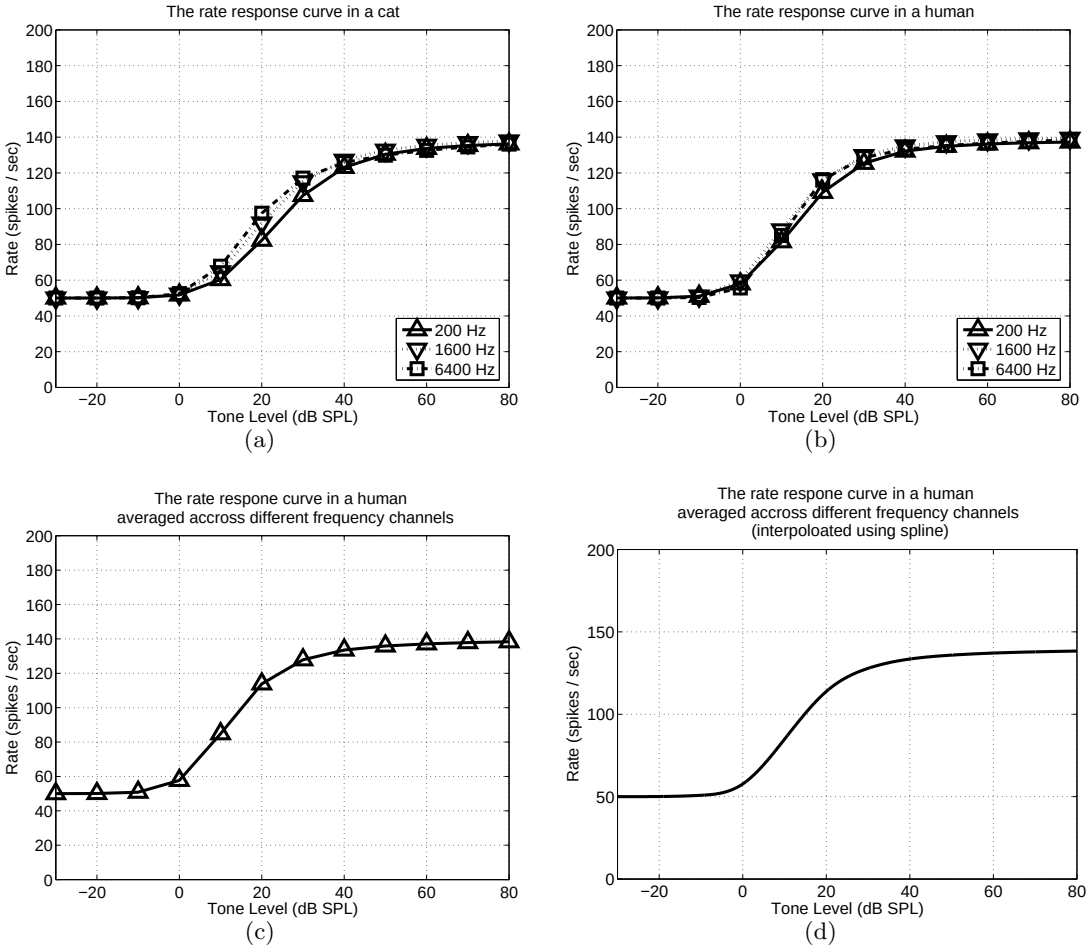

Fig. 4.1: Simulated relations between signal intensity and response rate for fibers of the auditory nerve using the model developed by Heinz *et al.* [1] to describe the auditory-nerve response of cats. (a) response as a function of frequency, (b) response with parameters adjusted to describe putative human response, (c) average of the curves in (b) across different frequency channels, and (d) is the smoothed version of the curves of (c) using spline interpolation.

physiology. In this figure, especially in the case of the putative human neural response, this intensity-relation does not change significantly with respect to the frequency of the pure tone. Fig. 4.1(c) illustrates the model human rate-level response averaged across frequency, which is smoothed in Fig. 4.1(d) using spline interpolation. In the discussion that follows we will use the curve of Fig. 4.1(c) for speech recognition experiments. As can be seen in

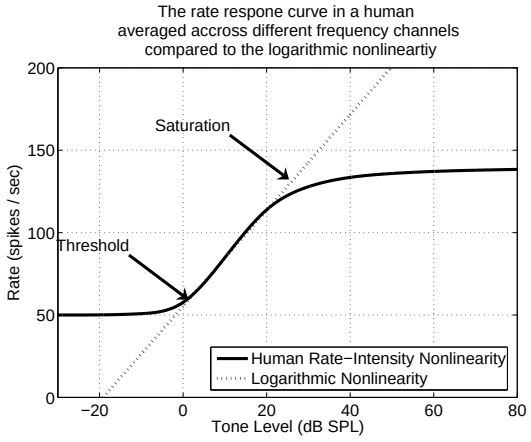

Fig. 4.2: The comparison between the intensity and rate response in the human auditory model [1] and the logarithmic curve used in MFCC. A linear transformation is applied to fit the logarithmic curve to the rate-intensity curve.

Fig. 4.1(c) and Fig. 4.2, this curve can be divided into three distinct regions. If the input sound pressure level (SPL) is less than 0 dB, the rate is almost a constant referred to as the *spontaneous rate*. In the region between 0 and 20 dB, the rate increases linearly with respect to the input SPL. If the input SPL of the pure tone is more than 30 dB, then the rate curve is largely constant. The distance between the threshold and the saturation points is around 25 dB SPL. As will be discussed later, this relative range in dB of this linear region causes problems in applying the original human rate-intensity curve to speech recognition systems.

The MFCC procedure uses a logarithmic nonlinearity in each channel, which is given by the following equation

$$g(m,l) = \log_{10}\left(p(m,l)\right) \tag{4.1}$$

where $p(m,l)$ is the power for l^{th} channel at time m and $g(m,l)$ is the corresponding output of the nonlinearity. Defining $\eta(m,l)$ as

$$\eta(m,l) = 20\log_{10}\left(\frac{p(m,l)}{p_{ref}}\right) \tag{4.2}$$

Thus, if we represent $g(m,l)$ in terms of $\eta(m,l)$, it appears as:

$$g(m,l) = \log_{10}(p_{ref}) + \frac{\eta(m,l)}{20} \tag{4.3}$$

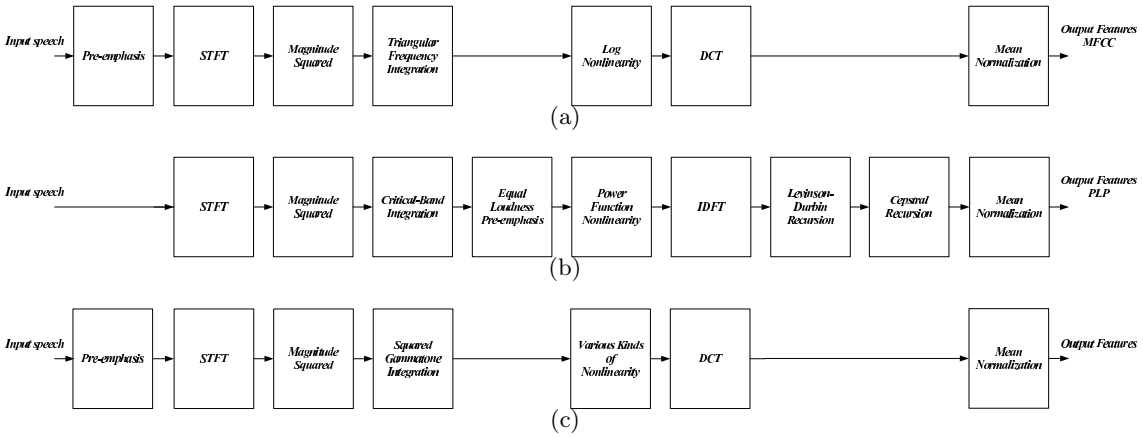

Fig. 4.3: Block diagram of three feature extraction systems: (a) MFCC, (b) PLP, and (c) a general nonlinearity system.

From the above equation, we can see that the relation is just basically a linear function. In speech recognition, the coefficients of this linear equation are not important as long as we consistently use the same coefficient for all of the training and test utterances. If we match this linear function to the linear region of Fig. 4.1(d), then we obtain Fig. 4.2. As is obvious from this figure, the biggest difference between logarithmic nonlinearity and the human auditory nonlinearity is that human auditory nonlinearity has threshold and saturation points. Because the logarithmic nonlinearity used in MFCC features does not exhibit threshold behavior, for speech segments of low power the output of the logarithmic nonlinearity will produce large output changes even if the changes in input are small. This characteristic, which can degrade speech recognition accuracy, becomes very obvious as the input approaches zero. If the power in a certain time-frequency bin is small, then even a very small additive noise, will produce a very different output because of the nonlinearity. Hence, we argue that the threshold point has a very important role for robust speech recognition.

In the following discussion, we will discuss the role of the threshold and the saturation points in actual speech recognition. Although the importance of auditory nonlinearity has been confirmed in several studies (*e.g.* [15]), there has been relatively little analysis of the effects of peripheral nonlinearities.

4.3 Speech recognition using different nonlinearities

In the following discussion, to test the effectiveness of different nonlinearities, we will use the feature extraction system shown in Fig 4.3(c) using different nonlinearities. As a comparison, we will also provide MFCC and PLP speech recognition results, which are shown in Fig. 4.8, respectively. Throughout this chapter, we will provide speech recognition results while changing the nonlinearity in 4.3(c). We will use the traditional triangular frequency-domain integration using MFCC processing, while for PLP processing we will make use of the critical band integration used by Hermansky [51]. For the system in Fig 4.3(c), we use gammatone frequency integration. In all of the following experiments, we used 40 channels. For the MFCC processing in Fig. 4.3(a) and the general feature extraction system in Fig. 4.3(c), a pre-emphasis filter of the form $H(z) = 1 - 0.97z^{-1}$ is applied first. The STFT analysis is performed using Hamming windows of duration 25.6 ms, with 10 ms between frames for a sampling frequency of 16 kHz. Both the MFCC and PLP procedures include intrinsic nonlinearities: PLP passes the amplitude-normalized short-time power of critical-band filters through a cube-root nonlinearity to approximate the power law of hearing [51, 52]. In contrast, the MFCC procedure passes its filter outputs through a logarithmic function.

4.4 Recognition results using the hypothesized human auditory nonlinearity

Using the structure shown in Fig. 4.3(c) and the nonlinearity shown in Fig. 4.2, we conducted speech recognition experiments using the CMU `Sphinx 3.8` system with `Sphinxbase 0.4.1` and `SphinxTrain 1.0` used to train the acoustic models. For comparison purposes, we also obtained MFCC and PLP features using `sphinx_fe` and `HTK 3.4`, respectively. All experiments were conducted under the same conditions, and delta and delta-delta components were appended to the original features. For training and testing, we used subsets of 1600 utterances and 600 utterances, respectively, from the DARPA Resource Management (RM1) database. To evaluate the robustness of the feature extraction approaches, we digitally added three different types of noise: white noise, street noise, and background music. The background music was obtained from a musical segment of the DARPA Hub 4 Broadcast News database, while the street noise was recorded on a busy street. For reverberation

simulation, we used he Room Impulse Response (RIR) software [53]. We assumed a room of dimensions $5 \times 4 \times 3$ m with a distance of 2 m between the microphone and the speaker.

Since the rate-intensity curve is highly nonlinear, it is expected that the recognition accuracy that is obtained will be dependent on the speech power level. We conducted experiments at several different input intensity levels to measure this effect. In Fig. 4.4, β dB represents the intensity at which the average SPL falls slightly below the middle point of the linear region of the rate-intensity curve. As can be seen in Fig. 4.4(a), for speech in the presence of white noise, increasing the input intensity causes the recognition accuracy to degrade, which is due to the fact that the benefit provided by limiting the response in the threshold region affects a smaller percentage of the incoming speech frames. For street noise, the performance improvement is small, and for music and reverberation, increasing the intensity reduces the accuracy compared to the baseline condition.

Up until now, we discussed the characteristics of the human rate-intensity curve and compared it with the log nonlinearity curve used in the MFCC. We observe both the advantages and disadvantages of the human rate-intensity curve. The biggest advantage of the human rate-intensity curve compared to the log nonlinearity is that it uses the threshold point, which provides a significant improvement in noise robustness in speech recognition experiments. However, one clear disadvantage is that speech recognition performance depends on the input sound pressure level. Thus, the optimal input sound pressure level needs to be obtained empirically, and if we use a different input sound pressure level for training and testing, recognition will degrade because of the environmental mismatch.

4.5 Shifted Log Function and the Power Function

In the previous section, we saw that the human auditory rate-intensity curve is more robust against stationary additive noise. However, we also observed that performance depends heavily on the input speech intensity, which is not desirable, and the input intensity must be obtained empirically. Additionally, if there are mismatches between the input sound pressure level between the training and testing utterances, performance will degrade significantly. Another problem is that even though the feature extraction system with this human rate-intensity curve shows improvement for stationary noisy environments, the performance is

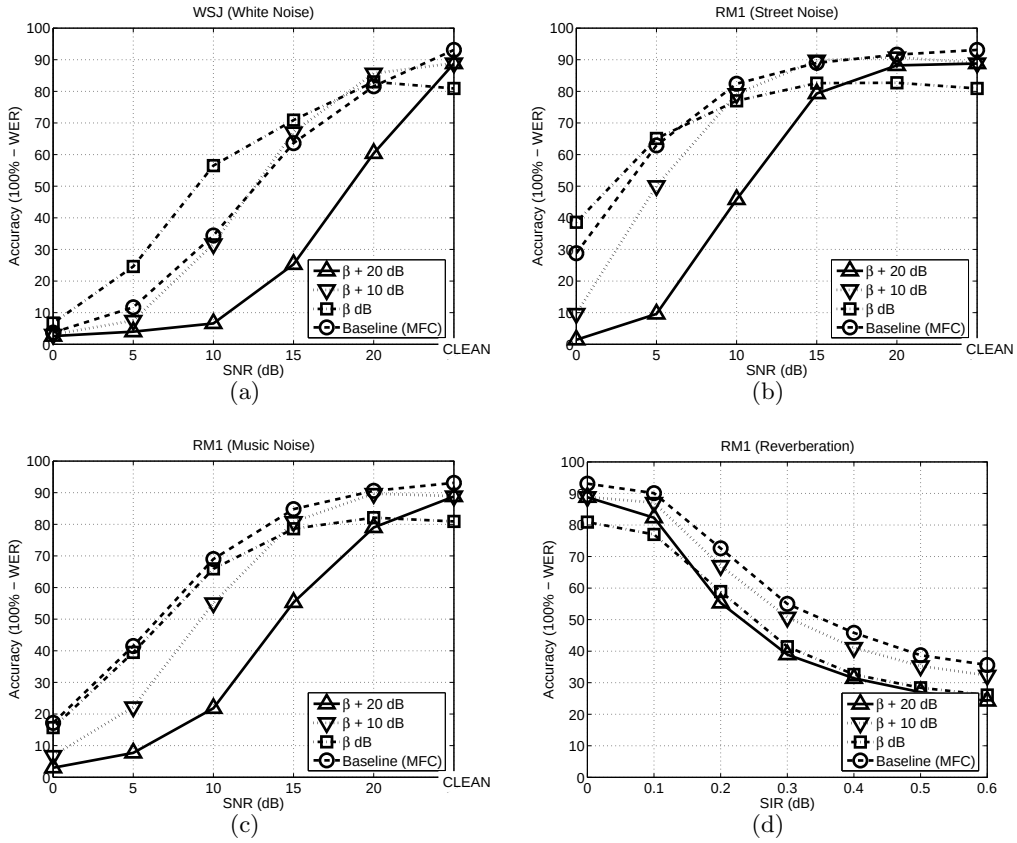

Fig. 4.4: Speech recognition accuracy obtained in different environments using the human auditory rate-intensity nonlinearity: (a) additive white gaussian noise, (b) street noise, (c) background music, and (d) reverberation.

worse than baseline when the SNR is high. For highly non-stationary noise like music, the human rate-intensity curve does not provide an improvement.

In the previous section, we argued that the thresholding the log function provides benefits in recognition accuracy. A natural question that arises is how performance will look if we ignore the saturation portion and use only the threshold portion of the human auditory rate-intensity curve. This nonlinearity can be modeled by the following shifted-log function as shown in Fig. 4.5:

$$g(m,l) \quad = \quad log_{10}(p(m,l) + \alpha P_{max}) \tag{4.4}$$

where P_{max} is defined to be the 95-th percentile of all $p(m,l)$. The value of the threshold

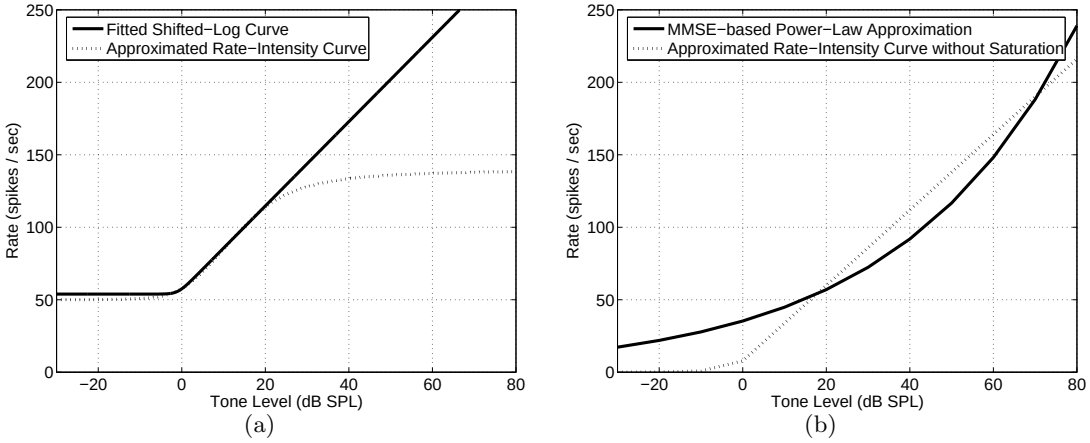

Fig. 4.5: (a) Extended rate-intensity curve based on the shifted log function. (b) Power function approximation to the extended rate-intensity curve in (a).

point depends on the choice of the parameter α.

The solid curve in Fig. 4.5(a) is basically an extended version of the linear portion of the rate-intensity curve. The dotted curve in Fig. 4.5(b) is virtually identical to the solid curve in Fig. 4.5(a), but translated downward so that for small intensities the output is zero (rather than the physiologically-appropriate spontaneous rate of 50 spikes/s). The solid power function in that panel is the MMSE-based best-fit power function to the piecewise-linear dotted curve. The reason for choosing the power-law nonlinearity instead of the dotted curve in Fig. 4.5(b) is that the dynamic behavior of the output does not depend critically on the input amplitude. For greater input intensities, this solid curve is a linear approximation to the dynamic behavior of the rate-intensity curve between 0 and 20 dB. Hence, this solid curve exhibits threshold behavior but no saturation. We prefer to model the higher intensities with a curve that continues to increase linearly to avoid spectral distortion caused by the saturation seen in the dotted curve in the right panel of Fig. 4.5. This nonlinearity, which is what is used in the PNCC feature extraction procedure to be described in Chapter 4 of this thesis, is described by the equation

$$y = x^{a_0} \tag{4.5}$$

with the best-fit value of the exponent observed to be between 1/10 and 1/15. We note that this exponent differs somewhat from the power-law exponent of 0.33 used for PLP fea-

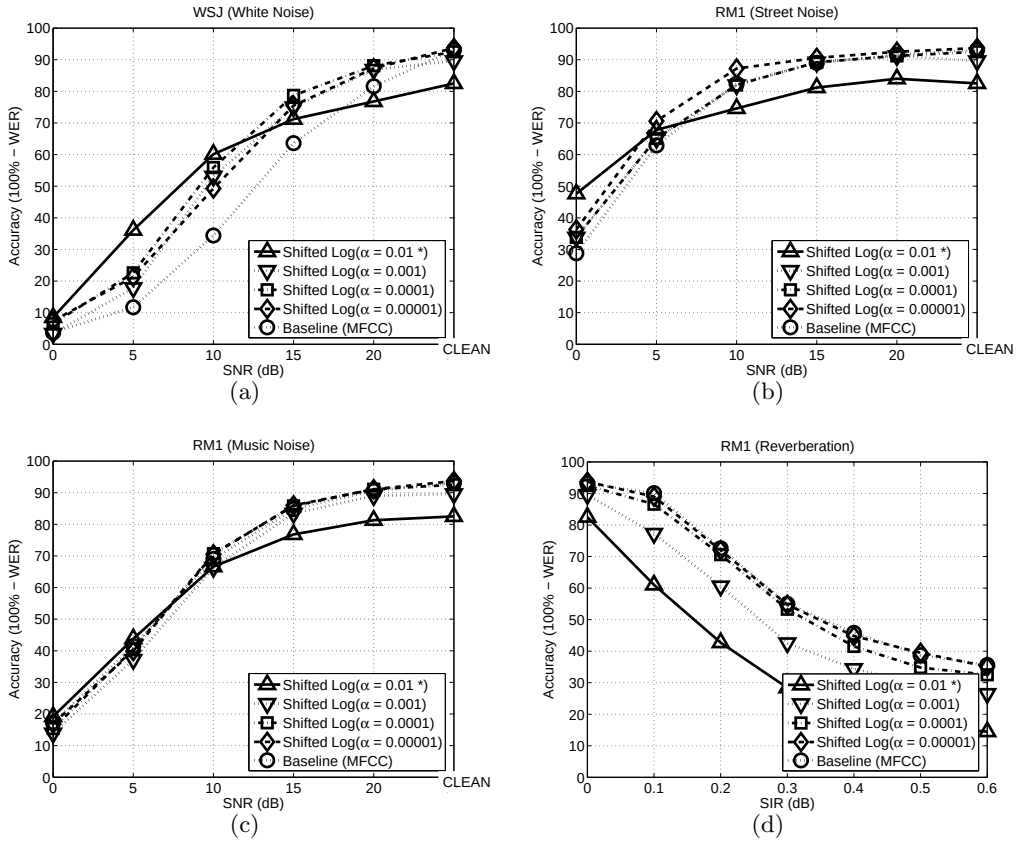

Fig. 4.6: Speech recognition accuracy obtained in different environments using the shifted-log nonlinearity: (a) additive white gaussian noise, (b) street noise, (c) background music, and (d) reverberation.

tures, which was based on Steven's power law of hearing [52] derived from psychoacoustical experiments. While our power-function nonlinearity may appear to be only a crude approximation of the physiological rate-intensity function, we will show that it provides a substantial improvement in recognition accuracy compared to the traditional log nonlinearity used in MFCC processing.

4.6 Comparison of Speech Recognition Results using Several Different Nonlinearities

In this section, we compare the recognition accuracy obtained using the various different nonlinearities that were described in the previous sections. These nonlinearities include the

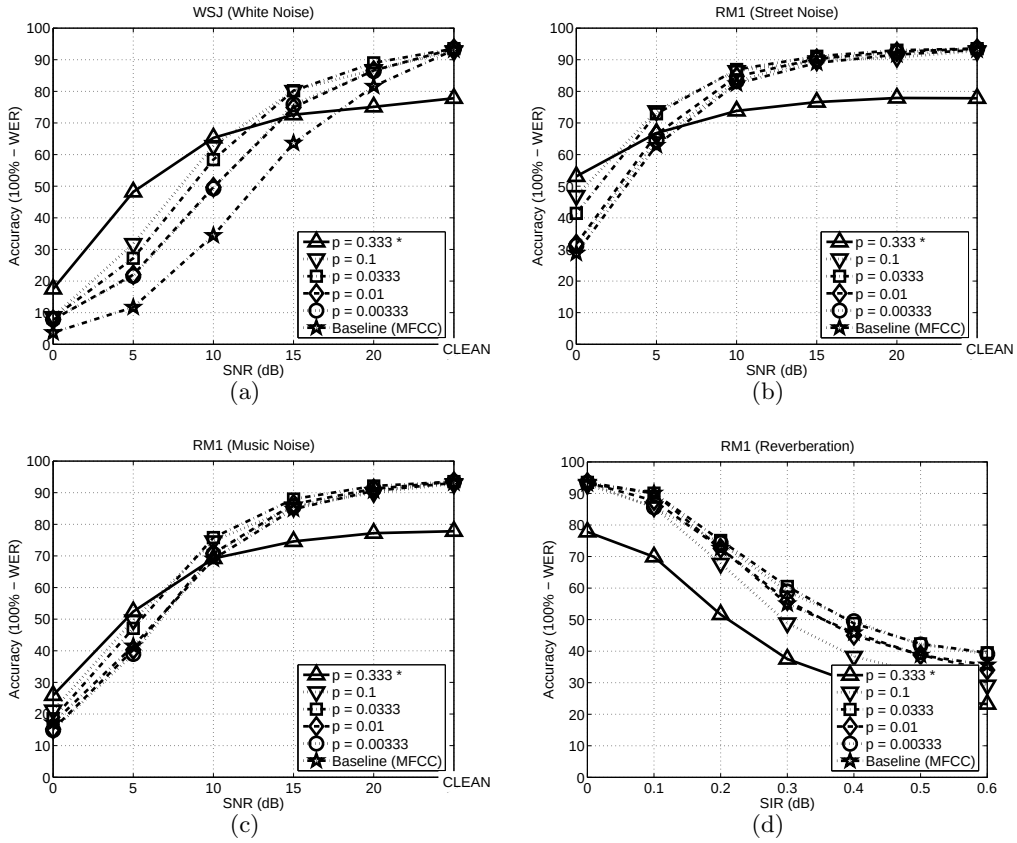

Fig. 4.7: Comparison of speech recognition accuracy obtained in different environments using the power function nonlinearity: (a) additive white gaussian noise, (b) street noise, (c) background music, and (d) reverberation.

human rate-intensity curve, the shifted-log curve, and the power function approximation to the shifted-log curve. As discussed earlier, the human rate-intensity curve depends on the sound pressure level of the utterance. On the other hand, the shifted-log and power-function nonlinearities depend on their intrinsic parameters. In comparing the performance of these algorithms we selected parameter values which provided reasonably good recognition accuracy from the previous data shown in Figs. 4.4, 4.6, and 4.7.

The results of these comparisons are summarized in Fig. 4.8. For white noise there are not substantial differences in performance in terms of the threshold shift (of the S-shaped curve that describes performance as a function of SNR), and a shift of around 5 dB is observed. Since the threshold point is the common characteristic of all three nonlinearities, we can

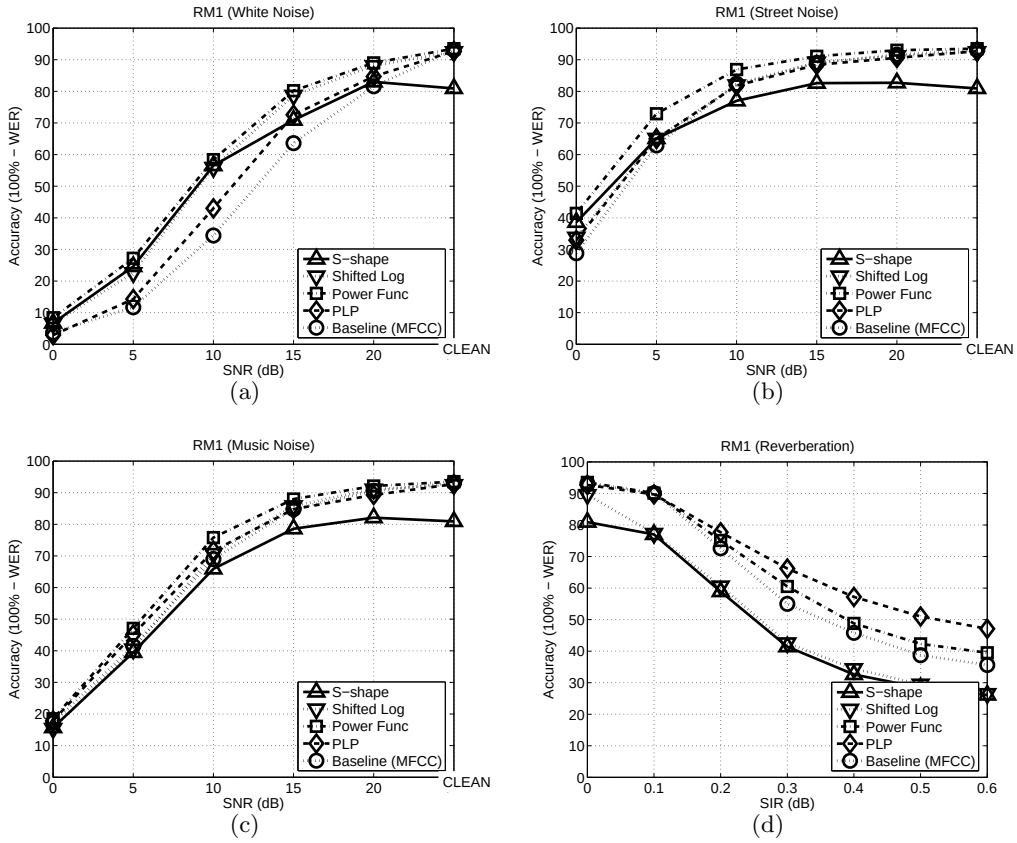

Fig. 4.8: Comparison of different nonlinearities (human rate-intensity curve, under different environments: (a) additive white gaussian noise, (b) street noise, (c) background music, (d) Reverberation

infer that the threshold point plays an important role for additive noise. Nevertheless, when the SNR is relatively high the human auditory rate-intensity nonlinearity falls behind other nonlinearities that do not include saturation, so it appears that that the saturation is actually harming performance. This tendency of losing performance for high SNR is observed in the various types of noise shown in Fig 4.8. For street noise and music noise, the threshold shift is significantly reduced compared to white noise. The power-function-based nonlinearity still shows some improvements compared to the baseline. In this figure, we can also note that even though PLP also uses the power function, it is not doing as well as the power function based feature extraction system described in this chapter. However, for reveberation, PLP shows better performance, as shown in Fig. 4.8(d).

4.7 Summary

In this Chapter, we compared different nonlinearities and compared speech recognition accuracies. We observe that the logarithmic nonlinearity is very vulnerable to additive noise, since it ignores the auditory threshold which is an important characteristic in the human rate-intensity relation. In a series of speech recognition experiments, we showed that human rate-intensity curve shows better robustness in the additive noise environments than MFCC. However, there are two problems with this "S-shape" rate-intensity nonlinearity of the human auditory system, which is characterized by the threshold and saturation points. The first problem is that since the curve is highly nonlinear, if the input is scaled (different SPL), then the output spectrum is also very different. This phenomena causes problems in speech recognition. The second problem is, the saturation point does not give us any evident benefits in speech recognition results. We compared "shifted-log" and "S-shape" nonlinearities, and observed that both of them show similar robustness against additive noise, but the "shifted-log" approach usually performs slightly better than "S-shape" curve for high SNR regions. From the above discussion, we conclude that a good nolinearity for speech recognition systems need to have the following characteristics. First, it needs to have the auditory threshold characteristic. It should not be affected by scaling effects, or at least, the effect of scaling needs to be easily reversible. Based on these discussion and experimental results, we conclude that a power function is a good choice for modelling the auditory nonlinearity. We further discuss auditory nonlinearity in Chapter 5 and Chapter 8.

5. THE SMALL-POWER BOOSTING ALGORITHM

5.1 Introduction

Recent studies show that for non-stationary disturbances such as background music or background speech, algorithms based on missing features (*e.g.* [16, 54]) or auditory processing are more promising than simple baseline approaches such as the CDCN algorithm or the use of PLP coefficients (*e.g* [9, 15, 55, 56, 25]). Still, the improvement in non-stationary noise remains less than the improvement that is observed in stationary noise. In previous work [55] and in the previous section, we also observed that the "threshold point" of the auditory nonlinearity plays an important role in improving performance in additive noise. Let us imagine a specific time-frequency bin with small power. Even if a relatively small distortion is applied to this time-frequency bin, due to the nature of compressive nonlinearity the distortion can become quite large.

In this chapter we explain the structure of the small-power boosting (SPB) algorithm, which reduces the variability introduced by the nonlinearity by applying a floor to the possible value that each time-frequency bin may take on. There are two different implementations of the SPB algorithm. In the first approach, we apply small-power boosting to each time-frequency bin in the spectral domain, and then resynthesize speech (SPB-R). The resynthesized speech is fed to the feature extraction system. This approach is conceptually straightforward but less computationally efficient (because of the number of FFTs and IFFTs that must be performed). In the second approach, we use SPB to obtain feature values directly (SPB-D). This approach does not require IFFT operations and the system is consequently more compact. As we will discuss below, effective implementation of SPB-D requires smoothing in the spectral domain.

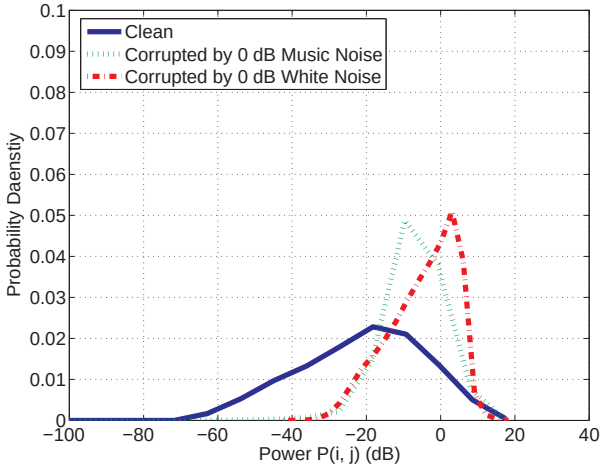

(a) Probability Density Functions (PDFs) obtained with the conventional log nonlinearity.

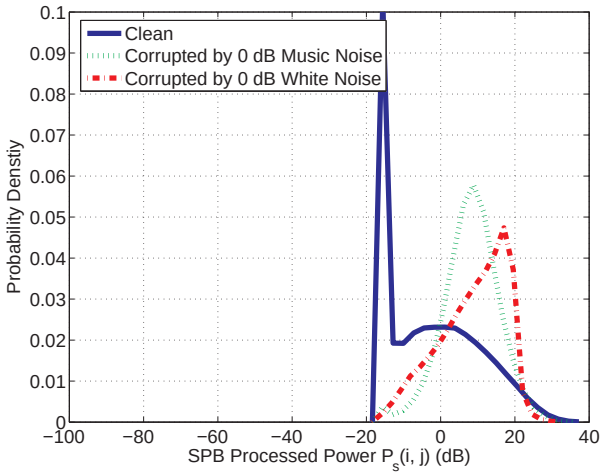

(b) Probability Density Functions (PDFs) obtained using the SPB algorithm with the power boosting coefficient in Eq. (5.2) set equal to 0.02.

Fig. 5.1: Comparison of the Probability Density Functions (PDFs) obtained in three different environments : clean, 0-dB additive background music, and 0-dB additive white noise.

5.2 The principle of small-power boosting

Before presenting the structure of the SPB algorithm, we first review how we obtain spectral power in our system, which is similar to the system in [46]. Pre-emphasis in the form of $H(z) = 1 - 0.97z^{-1}$ is applied to an incoming speech signal sampled at 16 kHz. A short-

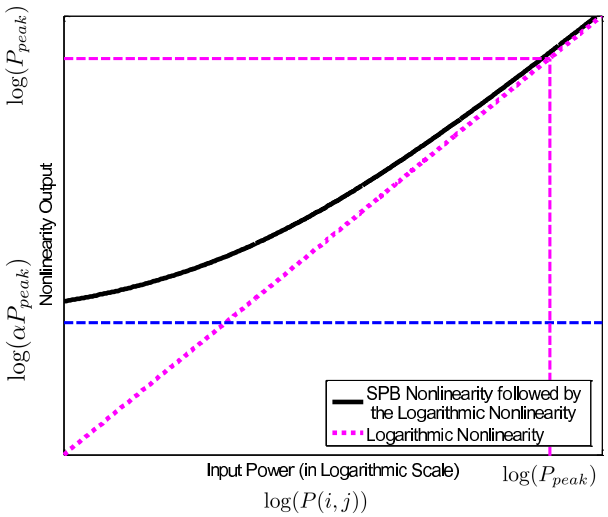

Fig. 5.2: The total nonlinearity consists of small-power boosting and the subsequent logarithmic nonlinearity in the SPB algorithm

time Fourier transform (STFT) is calculated using Hamming windows of a duration of 25.6 ms. Spectral power is obtained by integrating the magnitudes of the STFT coefficients over a series of weighting functions [57]. This procedure is represented by the following equation:

$$P(i,j) = \sum_{k=0}^{N-1} |X(e^{j\omega_k}; j) H_i(e^{j\omega_k})|^2 \tag{5.1}$$

In the above equation i and j represent the channel and frame indices respectively, N is the FFT size, and $H_i(e^{jw_k})$ is the frequency response of the i-th Gammatone channel. $X(e^{j\omega_k}; j)$ is the STFT for the j-th frame. w_k is defined by $\omega_k = \frac{2\pi k}{N}, \quad 0 \leq k \leq N-1$.

In Fig. 5.1(a), we observe the distributions of $\log(P(i,j))$ for clean speech, speech in 0-dB music, and speech in 0-dB white noise. We used a subset of 50 utterances to obtain these distributions from the training portion of the DARPA Resource Management 1 (RM1) database. In plotting the distributions, we scaled each waveform to set the 95^{th} percentile of $P(i,j)$ to be 0 dB. We note in Fig. 5.1(a) that higher values of $P(i,j)$ are (unsurprisingly) less affected by the additive noise, but the values that are small in power are severely distorted by additive noise. While the conventional approach to this problem is spectral subtraction (*e.g.* [11]), this goal can also be achieved by intentionally boosting power for all utterances, thereby rendering the small-power regions less affected by the additive noise. We implement

the SPB algorithm with the following nonlinearity:

$$P_s(i,j) = \sqrt{P(i,j)^2 + (\alpha P_{peak})^2} \tag{5.2}$$

where P_{peak} is defined to be the 95^{th} percentile in the distribution of $P(i,j)$. We refer to the parameter α as the "small-power boosting coefficient" or "SPB coefficient". In our algorithm, further explained in Secs. 5.3 and 5.3, after obtaining $P_s(i,j)$, either resynthesis or smoothing is performed, followed by the logarithmic nonlinearity. Thus, if we plot the entire nonlinearity defined by Eq. (5.2) and the subsequent logarithmic nonlinearity, then the total nonlinearity is represented by Fig. 5.2. Suppose that the power of clean speech at a specific time-frequency bin $P(i,j)$ is corrupted by additive noise ν. The log spectral distortion is represented by the following equation:

$$\begin{aligned} d(i,j) &= \log(P(i,j)+\nu) - \log(P(i,j)) \\ &= \log\left(1 + \frac{1}{\eta(i,j)}\right) \end{aligned} \tag{5.3}$$

where $\eta(i,j)$ is the Signal-to-Noise Ratio (SNR) for this time-frequency bin defined by:

$$\eta(i,j) = \frac{P(i,j)}{\nu} \tag{5.4}$$

Applying the nonlinearity of Eq. (5.2) and the logarithmic nonlinearity, the remaining distortion is represented by:

$$\begin{aligned} d_s(i,j) &= \log(P_s(i,j)+\nu) - \log(P_s(i,j)) \\ &= \log\left(1 + \frac{1}{\sqrt{\eta(i,j)^2 + \left(\frac{\alpha P_{peak}}{\nu}\right)^2}}\right) \end{aligned} \tag{5.5}$$

The largest difference between $d(i,j)$ and $d_s(i,j)$ occurs when $\eta(i,j)$ is relatively small. For time-frequency regions with small power $\eta(i,j)$ will become relatively large, even if ν is not large, and in Eq. (5.3), the distortion will diverge to infinity as $\eta(i,j)$ approaches zero. In contrast, in Eq. (5.5), even if $\eta(i,j)$ approaches zero, the distortion converges to $\log\left(1 + \frac{\nu}{\alpha P}\right)$.

Consider now the power distribution for SPB-processed time-frequency segments. Figure 5.1(b) compares the distributions for the same conditions as Fig. 5.1(a). It is clear that the distortion is greatly reduced.

While it has been noted in the previous chapter and in [55] that nonlinearities motivated by human auditory processing such as the "S"-shaped nonlinearity and the power-law nonlinearity curves also reduce variability due to low signal power, these approaches are less effective than the SPB approach described in this chapter. The key difference is that in other approaches the nonlinearity is directly applied for each time-frequency bin. As will be discussed in Sec. 5.4, directly applying the non-linearity results in reduced variance for regions of small power, thus reducing the ability to discriminate small differences in power and finally, to differentiate speech sounds. We explain this issue in detail in Section 5.4 and propose an alternate approach.

5.3 Small-power boosting with re-synthesized speech (SPB-R)

In this section, we discuss the SPB-R system, which resynthesizes speech as an intermediate stage in feature extraction. The block diagram for this approach is shown in Fig. 5.3. The blocks leading up to Overlap-Addition (OLA) are for small-power boosting and resynthesizing speech, which is finally fed to conventional feature extraction. The only difference between the conventional MFCC features and our features is the use of the gammatone-shaped frequency integration with the equivalent rectangular bandwidth (ERB) scale [4] instead of the triangular integration using the MEL scale [23]. The advantages of gammatone integration are described in [55], where gammatone-based integration was found to be more helpful in additive noise environments. In our system we use an ERB scale with 40 channels spaced between 130 Hz and 6800 Hz, as discussed in Sec. 2.1. From Eq. (5.2), the weighting coefficient $w(i,j)$ for each time-frequency bin is given by:

$$w(i,j) = \frac{P_s(i,j)}{P(i,j)} = \sqrt{1 + \left(\frac{\alpha P_{peak}}{P(i,j)}\right)^2} \tag{5.6}$$

Using $w(i,j)$, we apply the spectral reshaping expressed in [46]:

$$\mu_g(k,j) = \frac{\sum_{i=0}^{I-1} w(i,j) \left|H_i\left(e^{j\omega_k}\right)\right|}{\sum_{i=0}^{I-1} \left|H_i\left(e^{j\omega_k}\right)\right|} \tag{5.7}$$

where I is the total number of channels, and k is the discrete frequency index. The reconstructed spectrum is obtained from the original spectrum $X\left(e^{j\omega_k}; j\right)$ by using $\mu_g(k,j)$ in Eq.

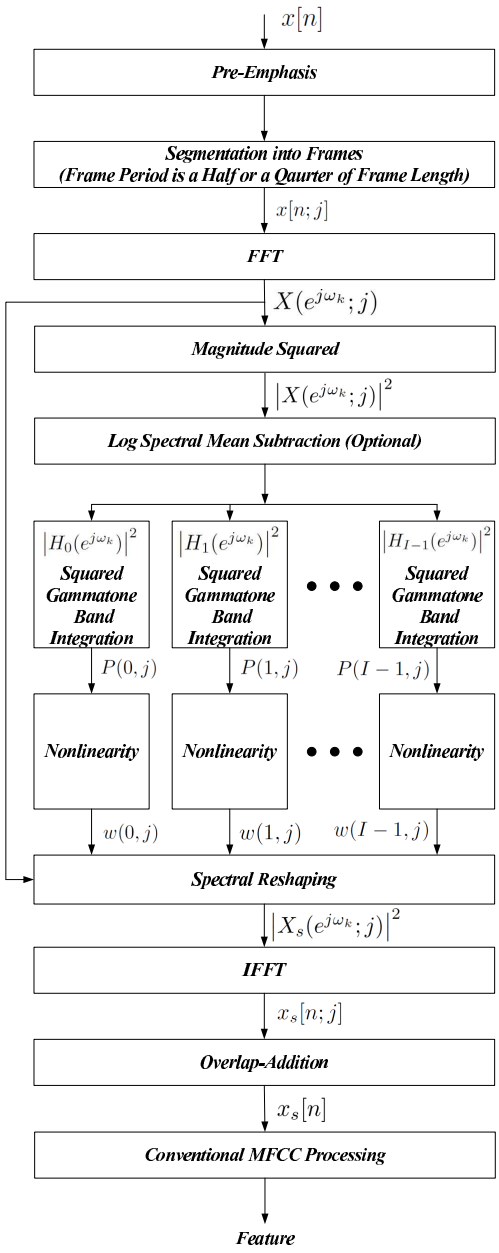

Fig. 5.3: Small-power boosting algorithm which resynthesizes speech (SPB-R). Conventional MFCC processing is followed after resynthesizing the speech.

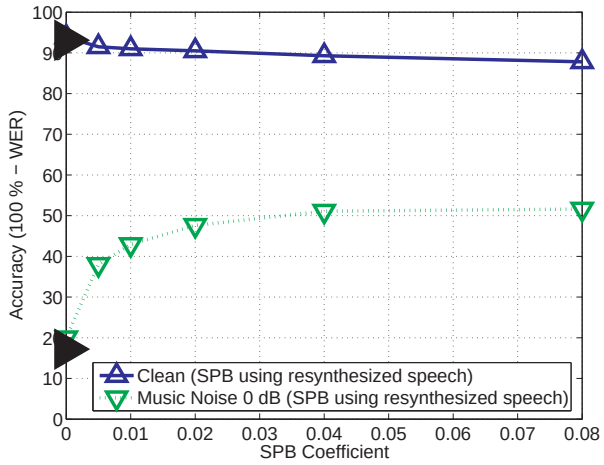

Fig. 5.4: Word error rates obtained using the SPB-R algorithm as a function of the value of the SPB coefficient. The filled triangles along the vertical axis represent baseline MFCC performance for clean speech (upper triangle) and for speech in additive background music noise at 0 dB SNR (lower triangle).

(9.13) as follows:

$$X_s\left(e^{j\omega_k};j\right) = \mu_g(k,j)X\left(e^{j\omega_k};j\right) \tag{5.8}$$

Speech is resynthesized using $X_s\left(e^{j\omega_k};j\right)$ by performing an IFFT and using OLA with hamming windows of 25 ms duration and 6.25 ms between adjacent frames, which satisfy the OLA constraint for undistorted reconstruction. Fig. 5.4 plots the WER against the SPB coefficient α. The experimental configuration is as described in Sec. 5.6. As can be seen, increasing the boosting coefficient results in much better performance for highly non-stationary noise even at 0 dB SNR; while losing some performance when training and testing using clean speech. Based on this trade-off between clean and noisy performance, we typically select a value for the SPB coefficient α in the range of $0.01 - 0.02$.

5.4 Small-power boosting with direct feature generation (SPB-D)

In the previous section we discussed the SPB-R system which resynthesizes speech as an intermediate step. Because resynthesizing the speech is quite computationally costly, we

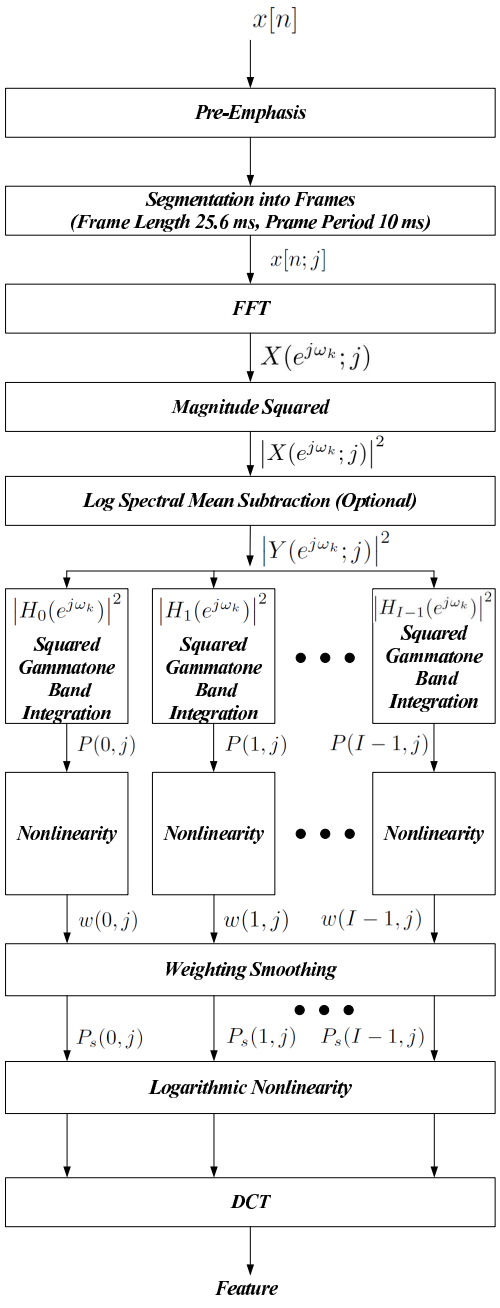

Fig. 5.5: Small-power boosting algorithm with direct feature generation (SPB-D).

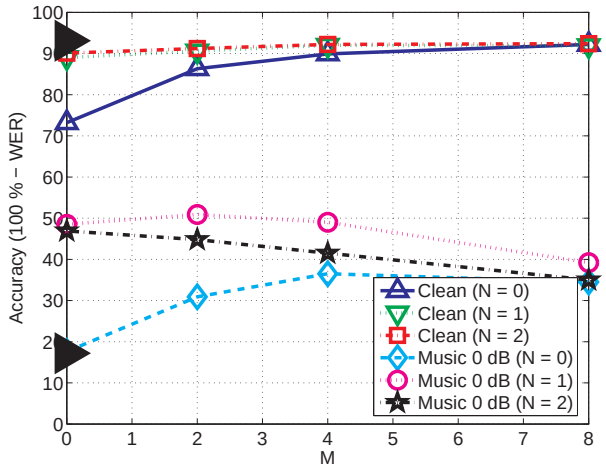

Fig. 5.6: The effects of smoothing of the weights on recognition accuracy using the SPB-D algorithm for clean speech and for speech corrupted by additive background music at 0 dB. The filled triangles along the vertical axis represent baseline MFCC performance for clean speech (upper triangle) and speech in additive background music at an SNR of 0 dB (lower triangle). The SPB coefficient α was 0.02.

discuss an alternate approach in this section that generates SPB-processed features without the resynthesis step.The most obvious approach towards this end would be simply to apply the Discrete Cosine Transform (DCT) to the SPB-processed power $P_s(i, j)$ terms in Eq. (5.2). Since this direct approach is basically a feature extraction system itself, it will of course require that the values of the window length and frame period used for segmentation into frames for SPB processing be the same as are used in conventional feature extraction. Hence we use a window length of 25.6 ms with 10 ms between successive frames. We refer to this direct system as small-power boosting with direct feature generation (SPB-D), and it is described in block diagram form in Fig. 5.5.

Figure 5.6 describes the dependence of recognition accuracy on the values of the system parameters N and M that specify the degree of temporal and spectral smoothing, respectively, as discussed in Chap. 3. Comparing the WER corresponding to $M = 0$ and $N = 0$ in Fig. 5.6 to the performance of SPB-R in Fig. 5.4, it is easily seen that SPB-D in its original form described above performs far worse than the SPB-R algorithm. These differences in

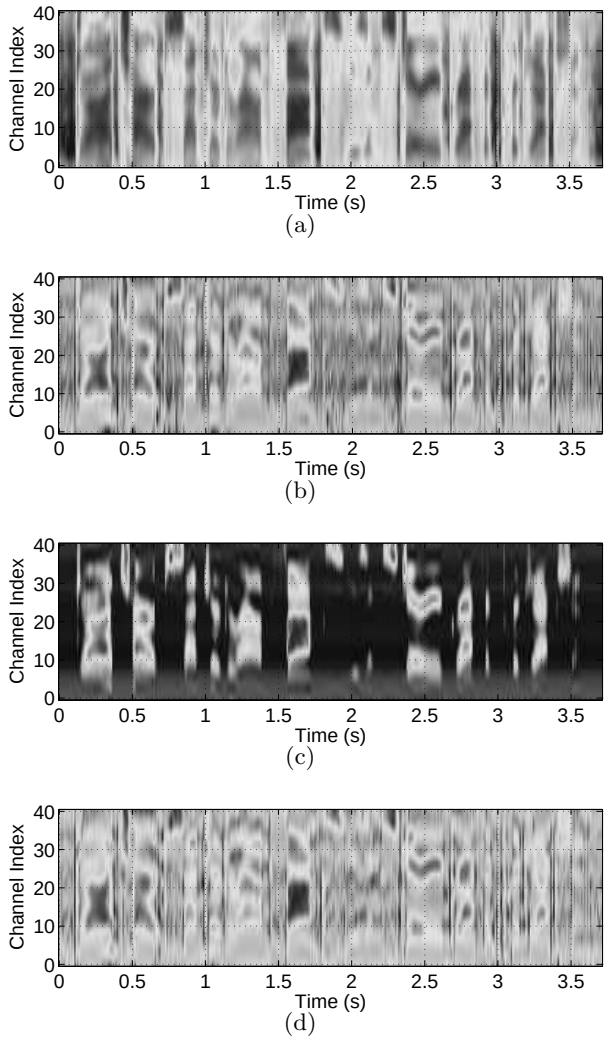

Fig. 5.7: Spectrograms obtained from a clean speech utterance using different types of processing: (a) conventional MFCC processing, (b) SPB-R processing, (c) SPB-D processing without any weight smoothing, and (d) SPB-D processing with weight smoothing using $M = 4, N = 1$ *in Eq.* (5.9)*. A value of* 0.02 *was used for the SPB coefficient* α*.*

performance are reflected in the corresponding spectrograms, as can be seen by comparing Fig. 5.7(c) to the SPB-R-derived spectrogram in Fig. 5.7(b)). In Fig. 5.7(c), the variance in time-frequency regions of small power is very small [concentrated at αP_{peak} in Fig. 5.2 and Eq. (5.2)], thus losing the power to discriminate sounds which have small power. Small variance is harmful in this context because the PDFs developed during the training process are modeled by Gaussians with very narrow peaks. As a consequence, small perturbations

in the feature values from their means lead to large changes in log-likelihood scores. Hence variances that are too small in magnitude should be avoided.

We also note that there exist large overlaps in the shape of gammatone-like frequency responses, as well as an overlap between successive frames. Thus, the gain in one time-frequency bin is correlated with that in an adjacent time-frequency bin. In the SPB-R approach, similar smoothing was achieved implicitly by the spectral reshaping from Eq. (9.13) and Eq. (5.8), and in the OLA process. With the SPB-D approach the spectral values must be smoothed explicitly.

Smoothing of the weights can be done horizontally (along the time axis) as well as vertically (along the frequency axis). The smoothed weights are obtained by:

$$\tilde{w}(i,j) = \exp\left(\frac{\sum_{j'=j-N}^{j+N}\sum_{i'=i-M}^{i+M}\log\left(w(i',j')\right)}{(2N+1)(2M+1)}\right) \tag{5.9}$$

where M and N respectively indicate smoothing along the time and frequency axes. The averaging in Eq. (5.9) is performed in the logarithmic domain (equivalent to geometric averaging) since the dynamic range of $w(i,j)$ is very large. (If we had performed a normal arithmetic averaging instead of geometric averaging in Eq. (5.9), the resulting averages would be dominated inappropriately by the values of $w(i,j)$ of greatest magnitude.)

Results of speech recognition experiments using different values of N and M are reported in Fig. 5.6. The experimental configuration is the same as was used for the data shown in Fig. 5.4. We note that the smoothing operation is quite helpful, and that with suitable smoothing the SBP-D algorithm works as well as the SPB-R. In our subsequent experiments, we used values of $N = 1$ and $M = 4$ in the SPB-D algorithm with 40 gammatone channels. The corresponding spectrogram obtained with this smoothing is shown in Fig. 5.7(d), which is similar to that obtained using SPB-R in Fig. 5.7(b).

5.5 Log spectral mean subtraction

In this section, we discuss log spectral mean subtraction (LSMS) and its potential use as an optional pre-processing step in the SPB approach. We compare the performance of LSMS computed for each frequency index with that of LSMS computed for each gammatone channel. LSMS is a standard technique which has been commonly applied for robustness to

environmental mismatch, and this technique is mathematically equivalent to the well known cepstral mean normalization (CMN) procedure. Log spectral mean subtraction is commonly performed for $\log\left(P(i,j)\right)$ for each channel i as shown below.

$$\tilde{P}(i,j) = \frac{P(i,j)}{\exp(\frac{1}{2L+1}\sum_{j'=j-L}^{j+L}\log\left(P(i,j')\right))} \tag{5.10}$$

Hence, this normalization is performed between the squared gammatone integration in each band and the nonlinearity. It is also reasonable to apply LSMS for $X(e^{j\omega_k};j)$ for each frequency index k before performing the gammatone frequency integration. This can be expressed as:

$$\tilde{X}(e^{j\omega_k;j}) = \frac{\left|X(e^{j\omega_k;j})\right|}{\exp(\frac{1}{2L+1}\sum_{j'=j-L}^{j+L}\log\left(|X(e^{j\omega_k;j'})|\right))} \tag{5.11}$$

Fig. 5.8 depicts the results of speech recognition experiments using the two different approaches to LSMS (without including SPB). In that figure, the moving average window length indicates the length corresponding to $2L+1$ in Eq. (5.10) and Eq. (5.11). We note that the approach in Eq. (5.10) provides slightly better performance for white noise, but that the performance difference diminishes as the window length increases. However, the LSMS based on Eq. (5.11) shows consistently better performance in the presence of background music, which is consistent across all window lengths. This may be explained due to the rich discrete harmonic components in music, which makes frequency-index-based LSMS more effective. In the next section we examine the performance obtained when LSMS as described by Eq. (5.11) is used in combination with SPB.

5.6 Experimental results

In this section we present experimental results using the SPB-R algorithm described in Sec. 5.3 and the SPB-D algorithm described in Sec. 5.4. We also examine the performance of SPB is combination with LSMS as described in Sec. 5.5. We conducted speech recognition experiments using the CMU `Sphinx 3.8` system with `Sphinxbase 0.4.1`. For training the acoustic model, we used `SphinxTrain 1.0`. For the baseline MFCC feature, we used `sphinx_fe` included in `Sphinxbase 0.4.1`. All experiments in this and previous sections were conducted under identical conditions, with delta and delta-delta components appended

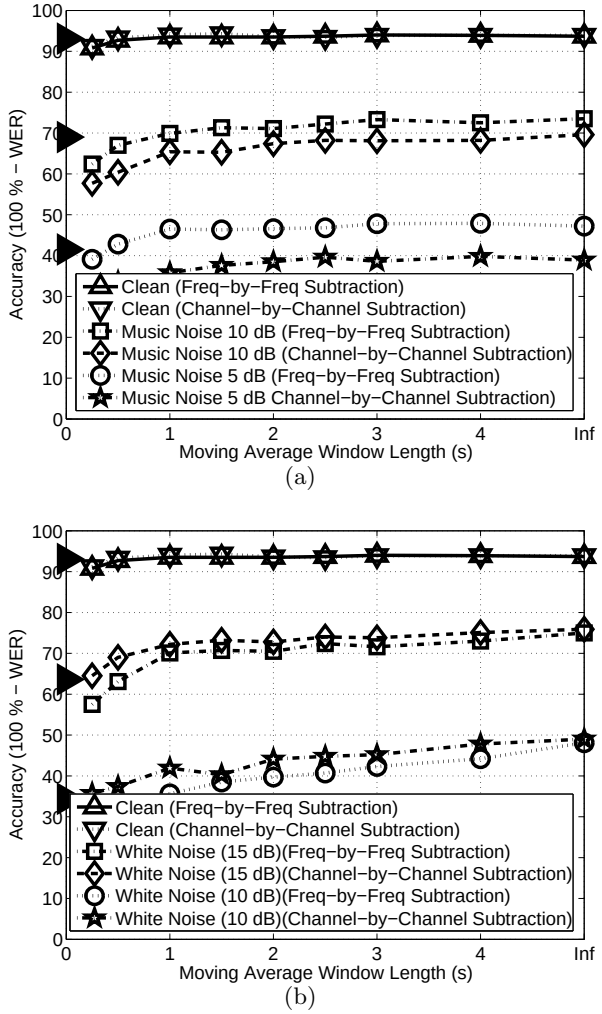

Fig. 5.8: The impact of Log Spectral Subtraction on recognition accuracy as a function of the length of the moving window for (a) background music and (b) white noise. The filled triangles along the vertical axis represent baseline MFCC performance.

to the original features. For training and testing we used subsets of 1600 utterances and 600 utterances respectively from the DARPA Resource Management (RM1) database. To evaluate the robustness of the feature extraction approaches we digitally added white Gaussian noise and background music noise. The background music was obtained from musical segments of the DARPA HUB 4 database.

In Fig. 5.9, SPB-D is the basic SPB system described in Sec. 5.4. While we noted in a previous paper [46] that gammatone frequency integration provides better performance than

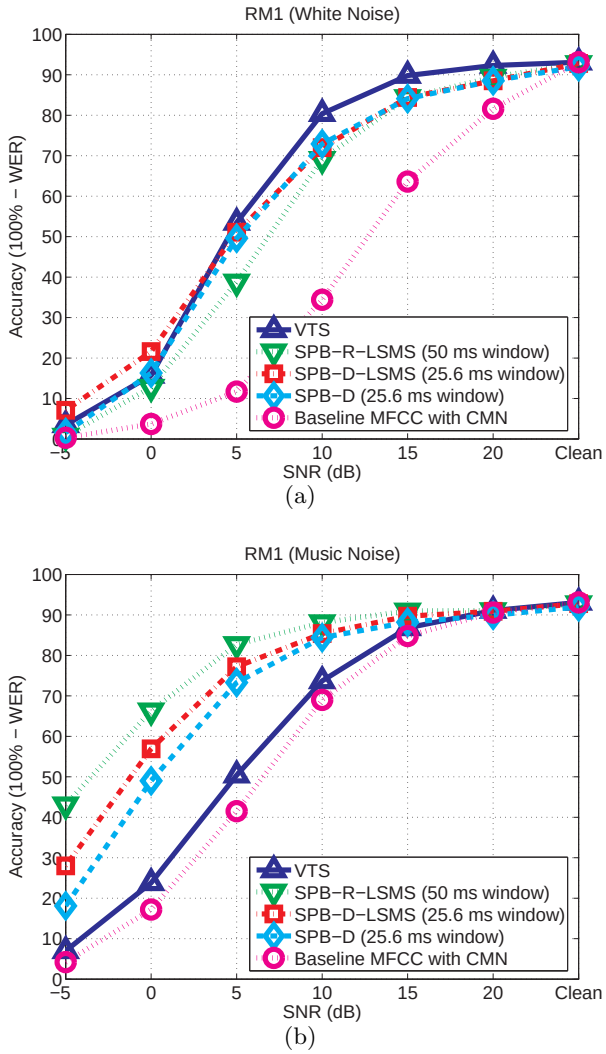

Fig. 5.9: Comparison of recognition accuracy between VTS, SPB-CW and MFCC processing: (a) additive white noise, (b) background music.

conventional triangular frequency integration, the effect is minor in these results. Thus, the performance boost of SPB-D over the baseline MFCC is largely due to the SPB nonlinearity in Eq. (5.2) and subsequent smoothing across time and frequency. SPB-D-LSMS refers to the combination of the SPB-D and LSMS techniques. For both the SPB-D and SPB-D-LSMS systems we used a window length of 25.6 ms with $10ms$ between adjacent frames. Even though not explicitly plotted in this figure, SPB-R shows nearly the same performance as SPB-D as mentioned in Sec. 5.4 and shown in Fig. 5.4.

We prefer to characterize the improvement in recognition accuracy by the amount of

lateral threshold shift provided by the processing. For white noise, SPB-D and SPB-D-LSMS provides an improvement of about 7 dB to 8 dB compared to MFCC, as shown in Fig. 5.9. SPB-R-LSMS results in slightly smaller threshold shift. For comparison, we also conduct experiments using the Vector Taylor Series (VTS) algorithm [10], as shown in Fig. 5.9. For white noise, the performance of SPB family is slightly worse than that obtained using VTS.

Compensation for the effects of music noise, on the other hand, is considered to be much more difficult (*e.g.* [42]). The SPB family of algorithms provides a very impressive improvement in performance with background music. An implementation of SPB-R-LSMS with window durations of 50 ms provides the greatest threshold shift (amounting to about 10 dB), and SPB-D provides a threshold shift of around 7 dB. VTS provides a performance improvement of about 1 dB for the same data.

5.7 Conclusions

In this chapter we presented the robust speech recognition algorithm called Small-Power Boosting (SPB), which is very helpful for difficult noise environments such as music noise. The SPB algorithm works by intentionally boosting the representation of time-frequency segments that are observed to have small power. We also noted that we should not boost power in each time-frequency bin independently as adjacent time-frequency bins are highly correlated. This correlation is achieved implicitly in SPB-R and by applying smoothing of the weights in SPB-D over both time and frequency. We also observed that direct application of the nonlinearity results in excessively small variance for time-frequency regions of small power, which is harmful for robustness and speech sound discrimination. Finally, we also note that for music noise the application of LSMS on a frequency-by-frequency basis is more effective than the channel-by-channel implementation of the algorithm.

6. ENVIRONMENTAL COMPENSATION USING POWER DISTRIBUTION NORMALIZATION

Even though many speech recognition systems have provided satisfactory results in clean environments, one of the biggest problems in the field of speech recognition is that recognition accuracy degrades significantly if the test environment is different from the training environment. These environmental differences might be due to additive noise, channel distortion, acoustical differences between different speakers, etc. Many algorithms have been developed to enhance the environmental robustness of speech recognition systems (*e.g.*[58, 59, 10, 15, 16, 54, 41, 13, 12]). Cepstral mean normalization (CMN) [5] and mean-variance Normalization (MVN) (*e.g.*[58]) are the simplest kinds of these techniques [6]. In these approaches, it is assumed that the mean or the mean and variance of the cepstral vectors should be the same for all utterances. These approaches are especially useful if the noise is stationary and its effect can be approximated by a linear function in the cepstral domain. Histogram Equalization (HEQ) (*e.g.* [59]) is a more powerful approach that assumes that the cepstral vectors of all the utterances have the same probability density function. Histogram normalization can be applied either in the waveform domain (*e.g.* [60]), the spectral domain (*e.g.* [61]), or the cepstral domain (*e.g.*[62]). Recently it has been observed that applying histogram normalization to delta cepstral vectors as well as the original cepstral vectors can also be helpful for robust speech recognition [59].

Even though many of these simple normalization algorithms have been applied successfully in the feature (or cepstral) domain rather than in the time or spectral domains, normalization in the power or spectral domain has some advantages. First, temporal or spectral normalization can be easily used as a pre-processing stage for many kinds of feature extraction systems and can be used in combination with other normalization schemes. In addition, these approaches can be also used as part of a speech enhancement scheme. In the present

study, we perform normalization in the spectral domain, resynthesizing the signal using the inverse Fast Fourier Transform (IFFT) and combined with the overlap-add method (OLA).

One characteristic of speech signals is that their power level changes very rapidly while the background noise power usually changes more slowly. In the case of stationary noise such as white or pink noise, the variation of power approaches zero if the length of the analysis window becomes sufficiently large, so the power distribution is centered at a specific level. Even in the case of non-stationary noise like music noise, the noise power does not change as fast as the speech power. Because of this, the distribution of the power can be effectively used to determine the extent to which the current frame is affected by noise, and this information can be used for equalization. One effective way of doing this is measuring the ratio of arithmetic mean to geometric mean (*e.g.* [55]). This statistic is useful because if power values do not change much, the arithmetic and geometric mean will have similar values, but if there is a great deal of variation in power the arithmetic mean will be much larger than the geometric mean. This ratio is directly related to the shaping parameter of the gamma distribution, and it also has been used to estimate the signal-to-noise ratio (SNR) [63].

In this paper we introduce a new normalization algorithm based on the distribution of spectral power. We observe that the the ratio of the arithmetic mean to geometric mean of power in a particular frequency band (which we subsequently refer to as the *AM–GM ratio* in that band) depends on the amount of noise in the environment [55]. By using values of the AM–GM ratio obtained from a database of clean speech, a nonlinear transformation (specifically a power function) can be exploited to transform the output powers so that the AM–GM ratio in each frequency band of the input matches the corresponding ratio observed in the clean speech used for training the normalization system. In this fashion speech can re-synthesized resulting in greatly improved sound quality as well as better recognition results for noisy environments. In many applications such as voice communication or real-time speech recognition, we want the normalization to work in online pipelined fashion, processing speech in real time. In this paper we also introduce a method to find appropriate power coefficients in real time.

As we have observed in previous work [55, 46], even though windows of duration between 20 and 30 ms are optimal for speech analysis and feature extraction, longer-duration windows

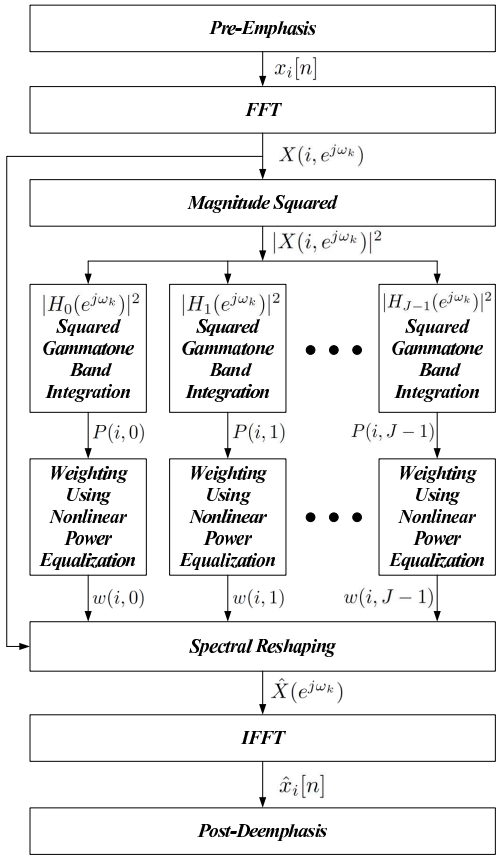

Fig. 6.1: The block diagram of the power-function-based power distribution normalization system.

between 50 ms and 100 ms tend to be better for noise compensation. We also explore the effect of window length in power-distribution normalization and find the same tendency is be observed for this algorithm as well.

The rest of the paper is organized as follows: Sec. 6.1 describes our power-function-based power distribution normalization algorithm at a general level. We describe the online implementation of the normalization algorithm in Sec. 6.2. Experimental results are discussed in Sec.6.3 and we summarize our work in Sec. 6.4.

6.1 Power function based power distribution normalization algorithm

6.1.1 Structure of the system

Figure 6.1 shows the structure of our power-distribution normalization algorithm. The input speech signal is pre-emphasized and then multiplied by a medium duration (75-ms) Hamming window. This signal is represented by $x_m[n]$ in Fig. 6.1 where m denotes the frame index. We use a 75-ms window length and 10 ms between frames. The reason for using the longer window will be discussed later. After windowing, the FFT is computed and integrated over frequency using gammatone weighting functions to obtain the power $P[m,l]$ in the m^{th} frame and l^{th} frequency band as shown below:

$$P[m,l] = \sum_{k=0}^{\frac{K}{2}-1} |X([m,e^{j\omega_k})H_l(e^{j\omega_k})|^2 \tag{6.1}$$

where k is a dummy variable representing the discrete frequency index, and K is the DFT size. The discrete frequency ω_k is defined by $\omega_k = \frac{2\pi k}{K}$. Since we are using a 75-ms window, for 16-kHz audio samples N is 2048. $H_l(e^{j\omega_k})$ is the frequency response of the gammatone filter bank for the l^{th} channel evaluated at frequency index k with center frequencies distributed according to the Equivalent Rectangular Bandwidth (ERB) scale [4]. $X[m,e^{j\omega_k})$ is the short-time spectrum of the speech signal for this m^{th} frame. L in Fig. 6.1 denotes the total number of gammatone channels, and we are using $L = 40$ for obtaining the spectral power.

The frequency response of the gammatone filterbank that we used is shown in Fig. 9.6. In each channel the area under the squared transfer function is normalized to unity to satisfy the equation as we did in [64]:

$$\int_0^{8000} |H_l(f)|^2 df = 1 \tag{6.2}$$

where $H_l(f)$ is the frequency response of the l^{th} gammatone channel. To reduce the amount of computation, we modified the gammatone filter responses slightly by setting $H_l(f)$ equal to zero for all values of f for which the unmodified $H_l(f)$ would be less than 0.5 percent (corresponding to -46 dB) of its maximum value. Note that we are using exactly the same gammatone weigthing as in [64].

After power equalization, which will be explained in the following subsections, we perform spectral reshaping and compute the IFFT using OLA to obtain enhanced speech.

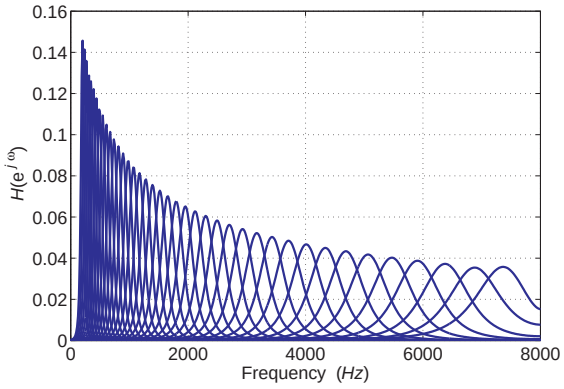

Fig. 6.2: The frequency response of a gammatone filterbank with each area of the squared frequency response normalized to be unity. Characteristic frequencies are uniformly spaced between 200 and 8000 Hz according to the Equivalent Rectangular Bandwidth (ERB) scale [4].

6.1.2 Normalization based on the AM–GM ratio

In this subsection, we examine how the frequency-dependent AM–GM ratio behaves. As described previously, the AM–GM ratio of of $P[m,l]$ for each channel is given by the following equation:

$$g[l] = \frac{\frac{1}{N_f}\sum_{m=0}^{N_f-1} P[m,l]}{\left(\prod_{m=0}^{N_f-1} P[m,l]\right)^{\frac{1}{N_f}}} \tag{6.3}$$

where N_f represents the total number of frames. Since addition is easier to handle than multiplication and exponentiation to $1/N_f$, we will use the logarithm of the above ratio in the following discussion.

$$G[l] = \log\left(\frac{1}{N_f}\sum_{m=0}^{N_f-1} P[m,l]\right) - \frac{1}{N_f}\sum_{m=0}^{N_f-1}\log P[m,l] \tag{6.4}$$

Figure 6.3 illustrates $G[l]$ for clean and noisy speech corrupted by 10-dB additive white noise. To obtain statistics in Fig. 6.3, we used randomly selected 100 utterances from the WSJ SI-84 training set. We calculated the AM–GM ratios from the speech segment of these 100 utterances using a Voice Activity Detector (VAD).

It can be seen that as noise is added the values of $G[l]$ significantly decreases. We define the function $G_{cl}[l]$ to be the value of $G[l]$ obtained from the speech segment of clean

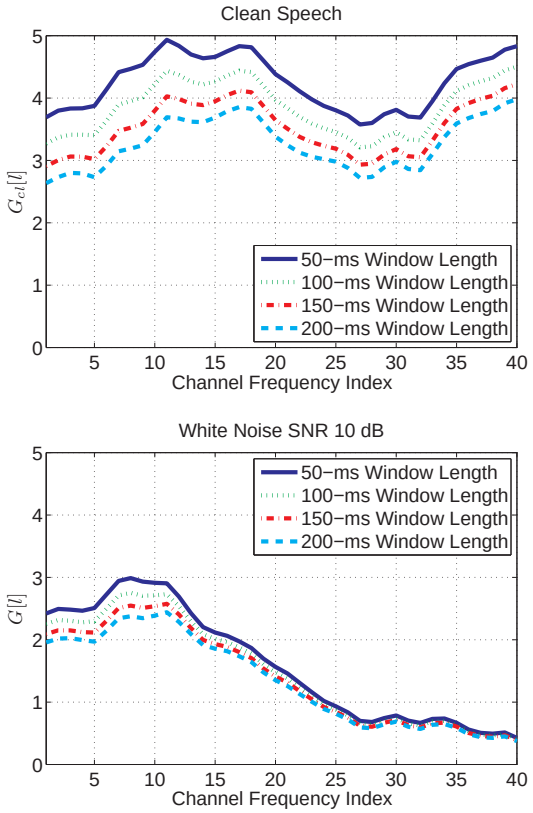

Fig. 6.3: The logarithm of the AM–GM ratio of spectral power of clean speech (upper panel) and of speech corrupted by 10-dB white noise (lower panel).

utterances. In our implementation, we used $G_{cl}[l]$ values obtained from the above-mentioned 100 utterances, which is shown in Fig. 6.3. We now proceed to normalize differences in $G[l]$ using a power function.

$$Q[m,l] = k_l P[m,l]^{a_l} \tag{6.5}$$

In the above equation, $P[m,l]$ is the medium-duration power of the noise-corrupted speech, and $Q[m,l]$ is the normalized medium-duration power. We want the AM–GM ratio representing normalized spectral power to be equal to the corresponding ratio at each frequency of the clean database. The power function is used because it is simple and the exponent can be easily estimated. We proceed to estimate k_l and a_l using this criterion.

Substituting $Q[m,l]$ into (6.4) and canceling out k_l, the ratio $\tilde{G}_{cl}[l|a_l)$ from this trans-

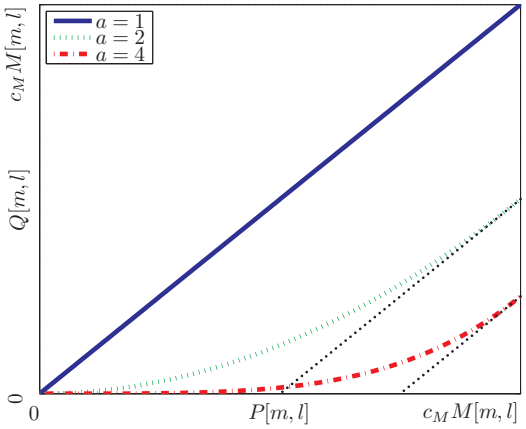

Fig. 6.4: The assumption about the relationship between $S[m,l]$ and $P[m,l]$. Note that the slope of the curve relating $P[m,l]$ to $Q[m,l]$ is unity when $P[m,l] = c_M M[m,l]$

formed variable $Q[m,l]$ can be represented by the following equation:

$$\tilde{G}_{cl}[l|a_l) = \log\left(\frac{1}{M}\sum_{m=0}^{M-1} P[m,l]^{a_l}\right) - \frac{1}{M}\sum_{m=0}^{M-1}\log P[m,l]^{a_l} \tag{6.6}$$

For a specific channel l, we see that a_l is the only unknown variable in $\tilde{G}_{cl}(j|a_l)$. From the following equation:

$$\tilde{G}_{cl}[l|a_l) = G_{cl}[l] \tag{6.7}$$

we can obtain a value for a_l using the Newton-Raphson method.

The parameter k_l in Eq. (6.5) is obtained by assuming that the derivative of $Q[m,l]$ with respect to $P[m,l]$ is the unity at $max_i P[m,l]$ for this channel l, we set up the following constraint:

$$\left.\frac{dQ[m,l]}{dP[m,l]}\right|_{max_m P[m,l]} = 1 \tag{6.8}$$

The above constraint is illustrated in Fig 6.4. The meaning of the above equation is that the slope of the nonlinearity is unity for the largest power of the l^{th} channel. This constraint

might look arbitrary, but it makes sense for additive noise case, since the following equation will hold:

$$P[m,l] = S[m,l] + N[m,l] \tag{6.9}$$

where $S[m,l]$ is the true clean speech power, and $N[m,l]$ is the noise power. By differentiating the above equation with respect to $P[m,l]$ we obtain:

$$\frac{dS[m,l]}{dP[m,l]} = 1 - \frac{dN[m,l]}{dP[m,l]} \tag{6.10}$$

At the peak value of $P[m,l]$, the variation of $N[m,l]$ will be much smaller for a given variation of $P[m,l]$, which means that the variation of $P[m,l]$ around its largest value would be mainly due to variations of the speech power rather than the noise power. In other words, the second term on the right hand side of Eq. (6.10) would be very small, yielding Eq.(6.8). By substituting (6.8) into (6.5), we obtain a value for k_l:

$$k_l = \frac{1}{a_l} \max_m P[m,l]^{1-a_l} \tag{6.11}$$

Using the above equation with (6.5), we obtain normalized power $Q[m,l]$, which is given by:

$$Q[m,l] = \frac{1}{a_l} \max_m P[m,l]^{1-a_l} P[m,l]^{a_l} \tag{6.12}$$

We apply a suitable flooring to $Q[m,l]$. This procedure is explained in Sec. 6.2.3. For each time-frequency bin, the weight $w[m,l]$ is given by the following equation.

$$w[m,l] \quad = \quad \frac{R[m,l]}{P[m,l]} \tag{6.13}$$

where $R[m,l]$ is the floored power obtained from $Q[m,l]$. After obtaining the weight $w[m,l]$ for each gammatone channel, we reshape the original spectrum $X[m,e^{j\omega_k})$ using the following equation for the m^{th} frame:

$$Y[m,e^{j\omega_k}) = \frac{\sum_{l=0}^{L-1} \sqrt{w[m,l]}|H_l(e^{j\omega_k})|}{\sum_{l=0}^{L-1} |H_l(e^{j\omega_k})|} X[m,e^{j\omega_k}) \tag{6.14}$$

The above approach is similar to what we used in [46, 65]. In Fig. 6.1, the above procedure is represented by the "spectral reshaping" block. As mentioned before, $H_l(e^{j\omega_k})$ is the spectrum of the l^{th} channel of the gammatone filter bank, and L is the total number of channels.

$\hat{X}[m, e^{j\omega_k})$ is the resultant enhanced spectrum. After doing this, we compute the IFFT of $\hat{X}[m, e^{j\omega_k})$ to retrieve the time-domain signal and perform de-emphasis to compensate for the effect of the previous pre-emphasis. The speech waveform is resynthesized using OLA.

6.1.3 Medium-duration windowing

Even though short-time windows of 20 to 30 ms duration are best for feature extraction for speech signals, in many applications we observe that longer windows are better for normalization purposes (*e.g.* [55] [46] [35] [66]). The reason for this is that noise power changes more slowly than the rapidly-varying speech signal. Hence, while good performance is obtained using short-duration windows for ASR, longer-duration windows are better for parameter estimation for noise compensation. Figure describes recognition accuracy as a function of window length. As can be seen in the figure a window of length between 75 ms and 100 ms provides the best parameter estimation for noise compensation and normalization. We will refer to a window of approximately this duration as a "medium-time window" as in [64].

6.2 Online implementation

In many applications the development of a real-time "online" algorithm for speech recognition and speech enhancement is desired. In this case we cannot use (6.6) for obtaining the coefficient a_l, since this equation requires the knowledge about the entire speech signal. In this section we discuss how an online algorithm of the power equalization algorithm can be implemented.

6.2.1 Power coefficient estimation

In this section, we discuss how to obtain a power coefficient a_l for each channel l, which satisfies (6.7) using an "online" algorithm. We define two terms $S_1[m, l|a_l)$ and $S_2[m, l|a_l)$ with a forgetting factor λ of 0.995 as follows.

$$S_1[m, l|a_l) = \lambda S_1[m, l-1) + (1-\lambda) Q_l[m]^{a_l} \tag{6.15}$$

$$S_2[m, l|a_l) = \lambda S_2[m, l-1) + (1-\lambda) \ln Q_l[m]^{a_l} \tag{6.16}$$

$$a_l = 1, 2, ..., 10$$

In our online algorithm, we calculate $S_1[m,l|a_l)$ and $S_2[m,l|a_l)$ for integer values of a_l in $1 \leq a_l \leq 10$ for each frame. From (6.6), we can define the online version of $G[l]$ using $S_1[m,l]$ and $S_2[m,l]$.

$$\begin{aligned} \tilde{G}_{cl}[m,l|a_l) &= \log(S_1[m,l|a_l)) - S_2[m,l|a_l) \\ & a_l = 1,2,..10 \end{aligned} \tag{6.17}$$

Now, $\hat{a}[m,l]$ is defined as the solution to the equation:

$$\tilde{G}_{cl}[m,l|\hat{a}[m,l]) = G_{cl}[m] \tag{6.18}$$

Note that the solution would depend on time, so the estimated power coefficient $\hat{a}[m,l]$ is now a function of both the frame index and the channel. Since we are updating $G_{cl}[m,l|a_l)$ for each frame using integer values of a_l in $1 \leq a_l \leq 10$, we use linear interpolation of $\tilde{G}_{cl}[m,l|a_l)$ in (6.17) with respect to a_l to obtain the solution to (6.18).

6.2.2 Online peak estimation using asymmetric filtering

For estimating k_l using (6.11), we need to obtain the peak power. Because speech power exhibits a very large dynamic range we use the following compressive nonlinearity before obtaining the on-line peak power:

$$T[m,l] = P[m,l]^{a_0} \tag{6.19}$$

where $a_0 = \frac{1}{15}$. This power function nonlinearity was proposed and evaluated in our previous research (*e.g.* [35, 67]). In our experiments, we observe that if $T[m,l]$ is applied to the asymmetric filtering which is explained below, the performance is usually slightly better than directly applying $P[m,l]$ to the same filtering.

To obtain the peak value using an online algorithm, we use asymmetric filtering, which is defined by the following equation [64]:

$$U[m,l] = \begin{cases} \lambda_a U[m-1,l] + (1-\lambda_a)T[m,l], \\ \qquad \text{if } T[m,l] \geq U[m-1,l] \\ \lambda_b U[m-1,l] + (1-\lambda_b)T[m,l], \\ \qquad \text{if } T[m,l] < U[m-1,l] \end{cases} \tag{6.20}$$

where m is the frame index, l is the channel index as before, $T[m,l]$ is the input to the filter, and $U[m,l]$ is the output of the filter. As shown in (8.4), the asymmetric filter resembles a first-order IIR filter, but the filter coefficients are different depending on whether the current input $T[m,l]$ is equal to or larger than the previous filter $U[m-1,l]$. More specifically, if $1 > \lambda_a > \lambda_b > 0$, then as shown in Fig. 6.5, the nonlinear filter function as a conventional *upper envelope detector*. In contrast, if $1 > \lambda_b > \lambda_a > 0$, the filter output $U[m,l]$ tends to follow the *lower envelope* of $T[m,l]$. As in [64], we will use the following notation

$$U[m,l] = \mathcal{AF}_{\lambda_a,\lambda_b}[T[m,l]] \tag{6.21}$$

to represent the nonlinear filter described by (8.4). In the examples in Fig. 6.5, $T_{up}[m,l] = \mathcal{AF}_{0.995,0.5}[T[m,l]]$ and $T_{low}[m,l] = \mathcal{AF}_{0.5,0.995}[T[m,l]]$. From $T_{up}[m,l]$, the moving peak value $V[m,l]$ is obtained using the following equation:

$$V[m,l] = T_{up}[m,l]^{\frac{1}{a_0}} \tag{6.22}$$

where $a_0 = \frac{1}{15}$ as in (6.19). Thus, Eq. (6.22) decompresses the effect of the compressive nonlinearity in Eq. (6.19).

For the actual peak level, we use the following value:

$$V_o[m,l] = c_0 V[m,l] \tag{6.23}$$

where we use c_0 of 1.5. We use this multiplicative factor, since the power $T[m,l]$ can be larger than $T_{up}[m,l]$ for some peaks.

One problem with the above procedure is the initialization of the asymmetric filter in (8.4). Usually, the first frames (when $m = 0$) belong to non-speech segments, so the peak values in this part are likely to be be much smaller than those of the speech segments. We observe that this characteristic has a negative effect on performance. In our implementation, we resolve this issue by using the average values of $T_{up}[m,l]$ for each channel l from the speech segments of 100 utterances selected from WSJ0 SI-84, which was also used for obtaining AM–GM ratio in Sec. 6.1.2. Let us denote these average values for each channel by $\mu_T[l]$. The initial value $T_{up}[0,l]$ is obtained by the following equation:

$$T_{up}[0,l] = (\mu_T[l]^{\frac{1}{a_0}} + P[0,l])^{a_0} \tag{6.24}$$

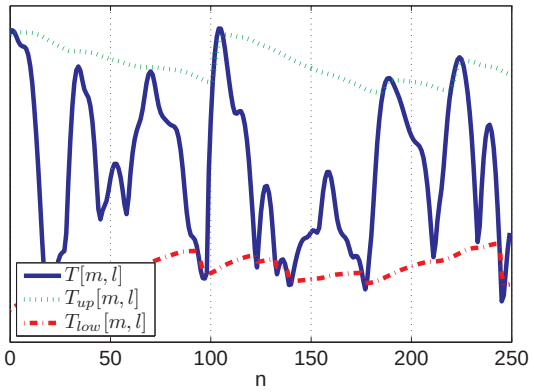

Fig. 6.5: The relationship between $T[m,l]$, the upper envelope$T_{up}[m,l] = \mathcal{AF}_{0.995,0.5}[T[m,l]]$, and the lower envelope $T_{low}[m,l] = \mathcal{AF}_{0.5,0.995}[T[m,l]]$. In this example, the channel index l is 10.

In the above equation, power to $\frac{1}{a_0}$ is applied $\mu_T[l]$, since we need to add power in the non-compressed domain. After addition, we apply a compressive nonlinearity (power to a_0) once again as shown in (6.24).

6.2.3 Power flooring and resynthesis

In our previous research it has been frequently observed that appropriate power flooring is valuable in obtaining noise robustness (*e.g.* [64, 65, 35]), and we make use of this approach in the present work.

We apply power flooring using the following equation:

$$R[m,l] = \max\left\{Q[m,l], \delta V[m,l]\right\} \tag{6.25}$$

where we use a δ is a flooring coefficient and $V[m,l]$ is the online peak power defined in (6.22). For the flooring coefficient δ, we observed that $\delta = 1e-4$ is appropriate.

Using $w[m,l] = \frac{R[m,l]}{P[m,l]}$ in (6.14), we can normalize the spectrum and resynthesize speech using IFFT and OLA. In our implementation, no look-ahead buffer is used in processing the remaining speech.

Figure 6.7 depicts spectrograms of the original speech corrupted by various types of additive noise, and corresponding spectrograms of processed speech using the online PPDN

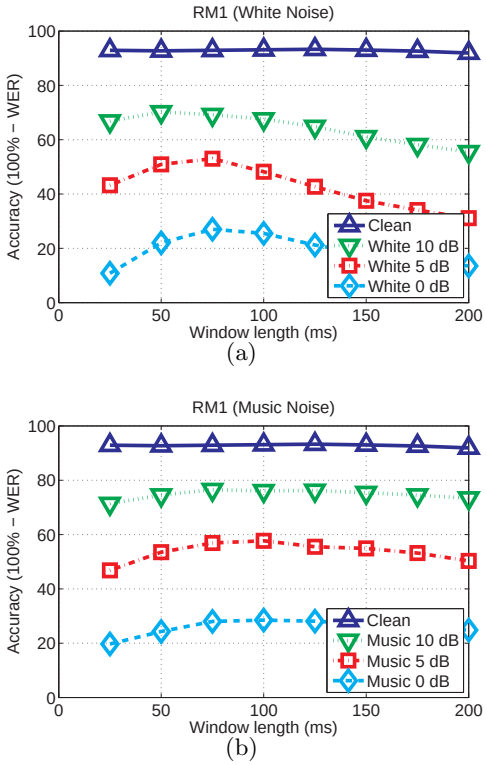

Fig. 6.6: Speech recognition accuracy as a function of window length for noise compensation corrupted by white noise and background music.

explained in this section. As seen in 6.7(b), for additive Gaussian white noise, improvement is observable even at 0-dB SNR. For the 10-dB music and 5-dB street noise samples, which are more realistic, as shown in 6.7(d) and 6.7(f), we can clearly observe that processing provides improvement. In the next section, we present speech recognition results using the online PPDN algorithm.

6.3 Simulation results using the online power equalization algorithm

In this section we describe experimental results obtained on the DARPA Resource Management (RM) database using the online processing as described in Section 6.2. We first observe that the online PPDN algorithm improves the subjective quality of speech, as can be assessed by the reader by comparing processed and unprocessed speech in the demo package at `http://www.cs.cmu.edu/~robust/archive/algorithms/IEEETran_PPDN`

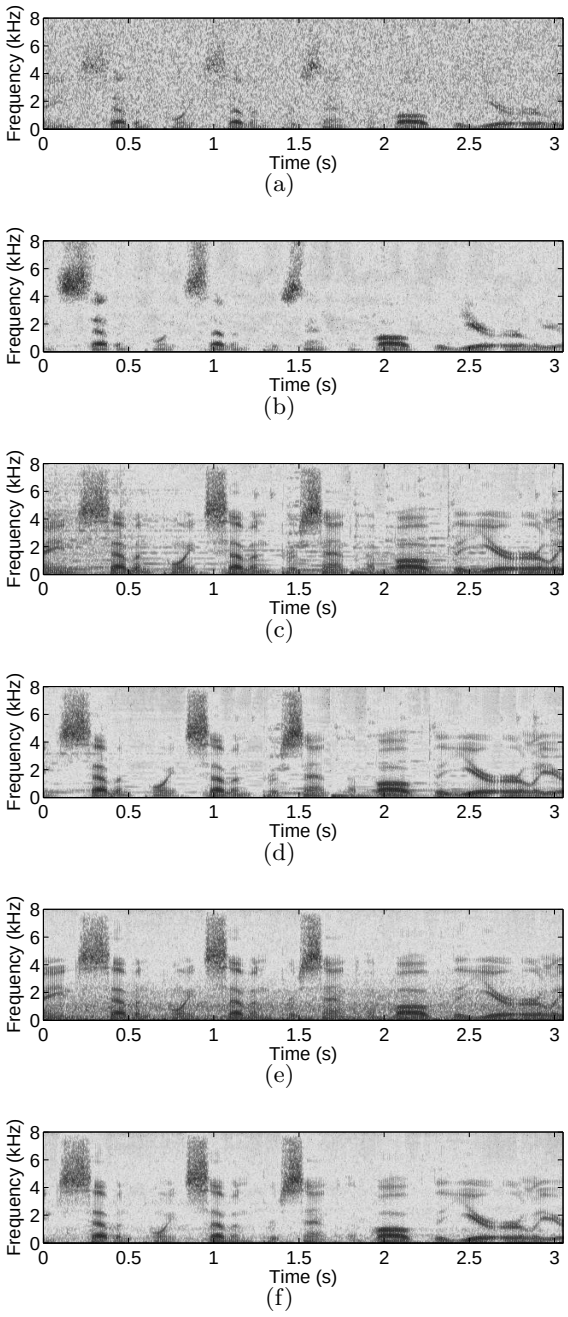

Fig. 6.7: Sample spectrograms illustrating the effects of online PPDN processing. (a) original speech corrupted by 0-dB additive white noise, (b) processed speech corrupted by 0-dB additive white noise (c) original speech corrupted by 10-dB additive background music (d) processed speech corrupted by 10-dB additive background (e) original speech corrupted by 5-dB street noise (f) processed speech corrupted by 5-dB street noise

For quantitative evaluation of PPDN we used 1,600 utterances from the DARPA Resource Management (RM) database for training and 600 utterances for testing. We used `SphinxTrain 1.0` for training the acoustic models, and `Sphinx 3.8` for decoding. For feature extraction we used `sphinx_fe` which is included in `sphinxbase 0.4.1`. In Fig. 6.8(a), we used test utterances corrupted by additive white Gaussian noise, and in Fig. 6.8(b), noise recorded on a busy street was added to the test set. In Fig. 6.8(c) we used test utterances corrupted by musical segments of the DARPA Hub 4 Broadcast News database.

We prefer to characterize the improvement in recognition accuracy as the amount by which curves depicting WER as a function of SNR shift laterally when processing is applied. We refer to this statistic as the "threshold shift". As shown in these figures, PPDN provided 10-dB threshold shifts for white noise, 6.5-dB threshold shifts for street noise and 3.5-dB shifts for background music. Note that obtaining improvements for background music is not easy.

For comparison, we also obtained similar results using the state-of-the-art noise compensation algorithm Vector Taylor series (VTS) [10]. For PPDN, further application of Mean Variance Normalization (MVN) provided slightly better recognition accuracy than the application of CMN. Nevertheless, for VTS, we could not observe any improvement in performance by applying MVN in addition, so we compared the MVN version of PPDN and the CMN version of VTS. For white noise, the PPDN algorithm outperforms VTS if the SNR is equal to or less than 5 dB, and the threshold shift is also larger. If the SNR is greater than or equal to 10 dB, VTS provides doing somewhat better recognition accuracy. In street noise, PPDN and VTS exhibited similar performance. For background music, which is considered to be more difficult, the PPDN algorithm produced threshold shifts of approximately 3.5 dB, along with better accuracy than VTS for all SNRs.

6.4 Conclusions

We describe a new power equalization algorithm, PPDN, that is based on applying a power function that normalizes the ratio of the arithmetic mean to the geometric mean of power in each frequency band. PPDN is simple and easier to implement than many other normalization algorithms. PPDN is quite effective in combatting the effects of additive noise and

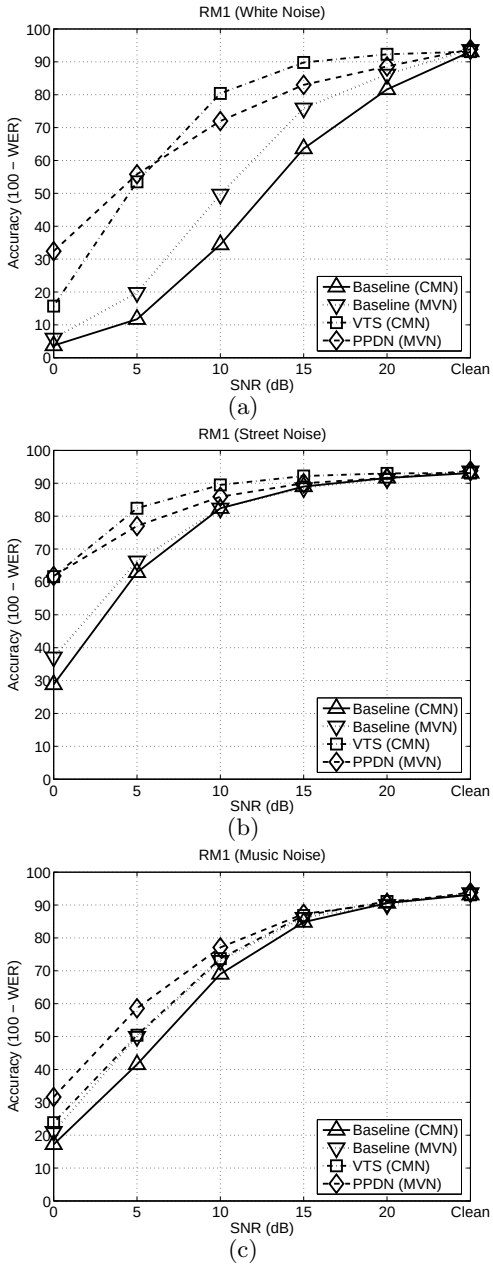

Fig. 6.8: Comparison of recognition accuracy for the DARPA RM database corrupted by (a) white noise, (b) street noise, and (c) music noise.

it provides comparable or somewhat better recognition accuracy than the VTS algorithm. Since PPDN resynthesizes the speech waveform, it can also be used for speech enhancement or as a pre-processing stage in conjunction with other algorithms that work in the cepstral domain. PPDN can also be implemented as an online algorithm without any look-ahead

buffer. This characteristic makes the algorithm potentially useful for applications such as real-time speech recognition or real-time speech enhancement. We also noted above that windows used to extract parametric information for noise compensation should be roughly three times the duration of those that are used for feature extraction. We used a window length of 100 ms for our normalization procedures.

6.5 Open Source Software

We provide the software used to implement PPDN in open source form at `http://www.cs.cmu.edu/~robust/archive/IEEETran_PPDN`. [68]. The code in this directory was used for obtaining the results described in this chapter.

7. ONSET ENHANCEMENT

In this chapter we introduce an onset enhancement algorithm which is referred to as Suppression of Slowly-varying components and the Falling edge (SSF) of the power envelope. It has long been believed that modulation frequency plays an important role in human hearing. For example, it is observed that the human auditory system is more sensitive to modulation frequencies less than 20 Hz (*e.g.* [33] [34]). On the other hand, very slowly changing components (*e.g.* less than 5 Hz) are usually related to noisy sources (*e.g.*[35] [36] [37]). Based on these observations, researchers have tried to utilize modulation frequency information to enhance the speech recognition performance in noisy environments. Typical approaches use highpass or bandpass filtering in either the spectral, log-spectral, or cepstral domains (*e.g.* [32]). In [2], Hirsch *et al.* investigated the effects of highpass filtering of spectral envelopes of each frequency subband. Hirsch conducted highpass filtering in the log spectral domain, using the transfer function:

$$H(z) = \frac{1 - z^{-1}}{1 - 0.7z^{-1}} \tag{7.1}$$

This first-order IIR filter can be implemented by subtracting an exponentially weighted moving average from the current log spectral value. For robust speech recognition the other common difficulty is reverberation. Many hearing scientists believe that human speech perception in reverberation is enabled by the "precedence effect", which refers to the emphasis that appears to be given to the first-arriving wave-front of a complex signal in sound localization and possibly speech perception (*e.g.* [69]). To detect the first wave-front, we can either measure the envelope of the signal or energy in the frame (*e.g.* [70] [71]).

In this chapter we introduce an approach that we refer to as SSF processing, which represents Suppression of Slowly-varying components and the Falling edge of the power envelope. This processing mimics aspects of both the precedence effect and modulation spectrum analysis. SSF processing operates on frequency weighted power coefficients as they

evolve over time, as described below. The DC-bias term is first removed in each frequency band by subtracting an exponentially-weighted moving average. When the instantaneous power in a given frequency channel is smaller than this average, the power is suppressed, either by scaling by a small constant or by replacement by the scaled moving average. The first approach results in better sound quality for non-reverberated speech, but the latter results in better speech recognition accuracy in reverberant environments. SSF processing is normally applied to both training and testing data in speech recognition applications.

In speech signal analysis, we normally use a short-duration window with duration between 20 and 30 ms. With the SSF algorithm, we observe that windows longer than this length are more appropriate for estimating or compensating for noise components, which is consistent with our observations in previous work (*e.g.* [55][46][35]). Nevertheless, even if we use a longer-duration window for noise estimation, we must use a short-duration window for speech feature extraction. After performing frequency-domain processing we use an IFFT and the overlap-add method (OLA) to re-synthesize speech, as in [36]. Feature extraction and subsequent speech recognition can be performed on the re-synthesized speech. We refer to this general approach as the medium-duration analysis and synthesis approach (MAS).

7.1 Structure of the SSF algorithm

Figure 7.1 shows the structure of the SSF algorithm. The input speech signal is pre-emphasized and then multiplied by a medium-duration Hamming window as in [36]. This signal is represented by $x_m[n]$ in Fig. 7.1 where m denotes the frame index. We use a 50-ms window and 10 ms between frames. After windowing, the FFT is computed and integrated over frequency using gammatone weighting functions to obtain the power $P[m,l]$ in the m^{th} frame and l^{th} frequency band as shown below:

$$P[m,l] = \sum_{k=0}^{N-1} |X[m,e^{j\omega_k})H_l(e^{j\omega_k})|^2, \quad 0 \le l \le L-1 \tag{7.2}$$

where k is a dummy variable representing the discrete frequency index, and N is the FFT size. The discrete frequency is $\omega_k = 2\pi k/N$. Since we are using a 50-ms window, for 16-kHz audio samples N is 1024. $H_l(e^{j\omega_k})$ is the spectrum of the gammatone filter bank for the l^{th} channel evaluated at frequency index k, and $X[m,e^{j\omega_k})$ is the short-time spectrum of the

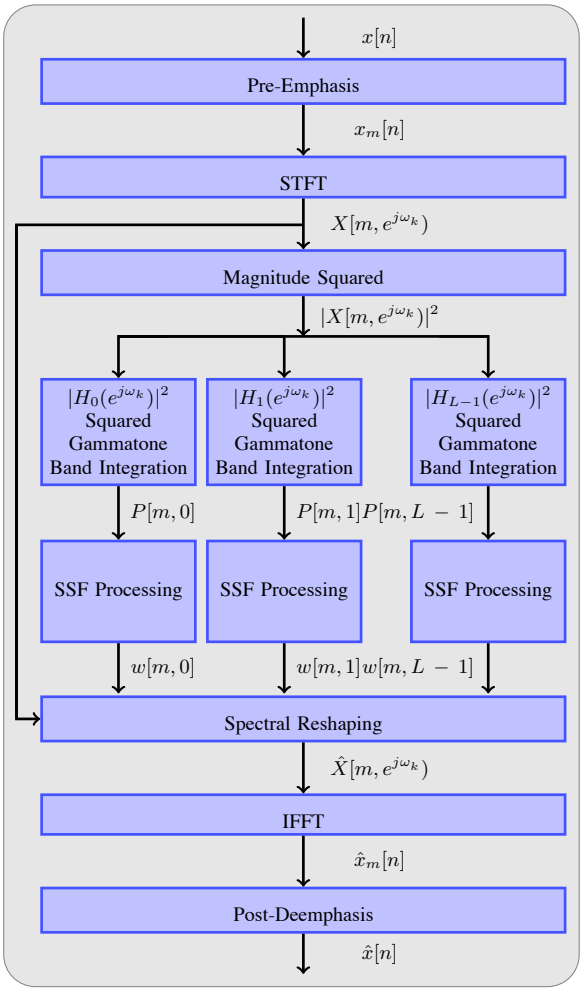

Fig. 7.1: The block diagram of the SSF processing system

speech signal for the m^{th} frame, where $L = 40$ is the total number of gammatone channels. After the SSF processing described below, we perform spectral reshaping and compute the IFFT using OLA to obtain enhanced speech.

7.2 SSF Type-I and SSF Type-II Processing

In SSF processing, we first obtain the lowpassed power $M[m, l]$ from each channel:

$$M[m, l] = \lambda M[m - 1, l] + (1 - \lambda)P[m, l] \tag{7.3}$$

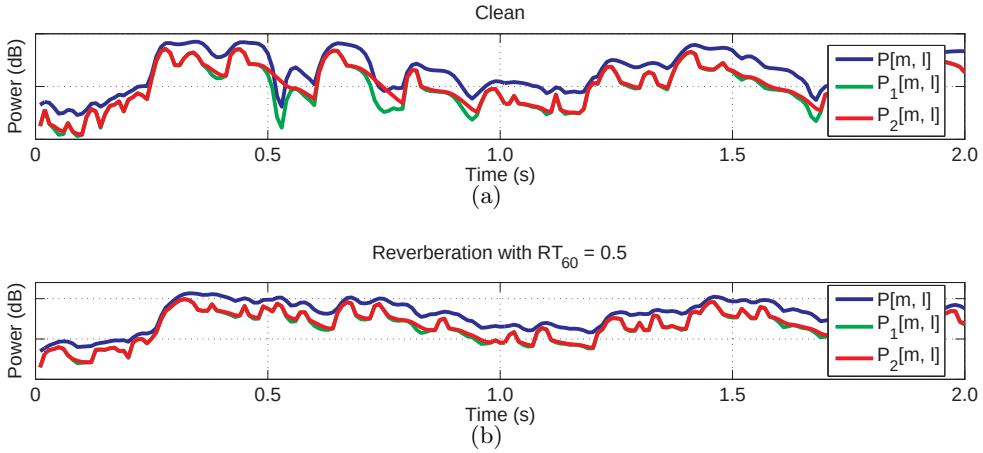

Fig. 7.2: Power contour $P[m,l]$, $P_1[m,l]$ (processed by SSF Type-I processing), and $P_2[m,l]$ (processed by SSF Type-II processing) for the 10^{th} channel in a clean environment (a) and in a reverberant environment (b).

where λ is a forgetting factor that is adjusted for the bandwidth of the lowpass filter. The processed power is obtained by the following equation:

$$P_1[m,l] = \max\left(P[m,l] - M[m,l], c_0 P[m,l]\right) \tag{7.4}$$

where c_0 is a small fixed coefficient to prevent $P[m,l]$ from becoming negative. In our experiments we find that $c_0 = 0.01$ is appropriate for suppression purposes. As is obvious from Eq. (7.4), $P_1[m,l]$ is intrinsically a highpass filter signal, since the lowpassed power $M[m,l]$ is subtracted from the original signal power $P[m,l]$. From Eq. (7.4), we observe that if the power $P[m,l]$ is larger than $M[m,l] + c_0 P_1[m,l]$ then, $P_1[m,l]$ is the highpass filter output. However, if $P[m,l]$ is smaller than the latter, the power is suppressed. These operations have the effect of suppressing the falling edge of the power contour. We call processing using Eq. (7.4) SSF Type-I.

A similar approach uses the following equation instead of Eq. (7.4):

$$P_2[m,l] = \max\left(P[m,l] - M[m,l], c_0 M[m,l]\right) \tag{7.5}$$

We call this processing SSF Type-II.

The only difference between Eq. (7.4) and Eq. (7.5) is one term, but as shown in Fig 7.3 and 7.4, this term has a major impact on recognition accuracy in reverberant environments. We also note that using SSF Type-I processing, if $0.2 \leq \lambda \leq 0.4$, substantial improvements

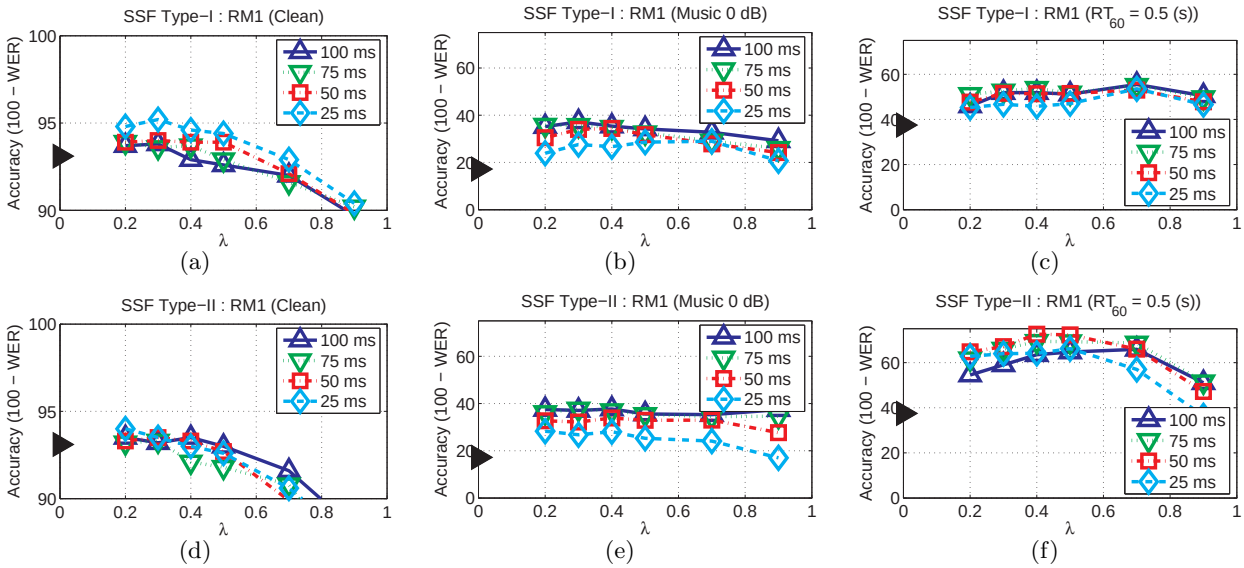

Fig. 7.3: The dependence of speech recognition accuracy on the forgetting factor λ and the window length. In (a), (b), and (c), we used Eq. (7.4) for normalization. In (d), (e), and (f), we used Eq. (7.5) for normalization. The filled triangles along the vertical axis represent the baseline MFCC performance in the same environment.

are observed for clean speech compared to baseline processing. In the power contour of Fig. 7.2, we observe that if we use SSF Type-II, the falling edge is smoothed (since $M[m,l]$ is basically a lowpass signal), which significantly reduces spectral distortion between clean and reverberant environments.

Fig. 7.3 shows the dependence of performance dependence on the forgetting factor λ and the window length. For additive noise, a window length of 75 or 100 ms provided the best performance. On the other hand, a value of 50 ms provided the best performance for reverberation. For these reasons we use $\lambda = 0.4$ and a window length of 50 ms.

7.3 Spectral reshaping

After obtaining the processed power $\tilde{P}[m,l]$ (which is either $P_1[m,l]$ in Eq. (7.4) or $P_2[m,l]$ Eq. (7.5)), we obtain a processed spectrum $\tilde{X}[m,e^{j\omega_k}]$. To achieve this goal, we use a similar spectral reshaping approach as in [36] and [46]. Assuming that the phases of the original and the processed spectra are identical, we modify only the magnitude spectrum.

First, for each time-frequency bin, we obtain the weighting coefficient $w[m,l]$ as a ratio of the processed power $\tilde{P}[m,l]$ to $P[m,l]$.

$$w[m,l] = \frac{\tilde{P}[m,l]}{P[m,l]}, \qquad 0 \le l \le L-1 \tag{7.6}$$

Each of these channels is associated with H_l, the frequency response of one of a set of gammatone filters with center frequencies distributed according to the Equivalent Rectangular Bandwidth (ERB) scale [4]. The final spectral weighting $\mu[m,k]$ is obtained using the above weight $w[m,l]$

$$\begin{aligned} \mu[m,k] &= \frac{\sum_{l=0}^{L-1} w[m,l] \left| H_l\left(e^{j\omega_k}\right)\right|}{\sum_{l=0}^{L-1} \left|H_l\left(e^{j\omega_k}\right)\right|}, \\ & \qquad 0 \le k \le N/2-1, 0 \le l \le L-1 \end{aligned} \tag{7.7}$$

After obtaining $\mu[m,k]$ for the lower half of the frequencies ($0 \le k \le N/2$), we can obtain the upper half by applying Hermitian symmetry:

$$\mu[m,k] = \mu[m,N-k], \qquad N/2 \le k \le N-1 \tag{7.8}$$

Using $\mu[m,k]$, the reconstructed spectrum is obtained by:

$$\tilde{X}[m,e^{j\omega_k}) = \mu[m,k]X[m,e^{j\omega_k}), \;\; 0 \le k \le N-1 \tag{7.9}$$

The enhanced speech $\hat{x}[n]$ is re-synthesized using the IFFT and the overlap-add method as in previous chapters.

7.4 Experimental results

In this section we describe experimental results obtained on the DARPA Resource Management (RM) database using the SSF algorithm. For quantitative evaluation of SSF we used 1,600 utterances from the DARPA Resource Management (RM) database for training and 600 utterances for testing. We used `SphinxTrain 1.0` for training the acoustic models, and `Sphinx 3.8` for decoding. For feature extraction we used `sphinx_fe` which is included in `sphinxbase 0.4.1`. Even though SSF was developed for reverberant environments, we also conducted experiments in additive noise as well. In Fig. 7.4(a), we used test utterances corrupted by additive white Gaussian noise, and in Fig. 7.4(b), we used test utterances corrupted by musical segments of the DARPA Hub 4 Broadcast News database.

As in previous chapters we characterize improvement as the amount by which curves depicting WER as a function of SNR shift laterally when processing is applied. We refer to this statistic as the "threshold shift". As shown in these figures, SSF provides 8-dB threshold shifts for white noise and 3.5-dB shifts for background music. As in the case of the algorithms previously considered, obtaining large improvements in the presence of background music is usually quite difficult. For comparison, we also obtained similar results using vector Taylor series (VTS) [10]. We also conducted experiments using an open source RASTA-PLP implementation [30]. For white noise, VTS and SSF provide almost the same recognition accuracy, but for background music, SSF provides significantly better performance. In additive noise, both SSF Type-I and SSF Type-II provide almost the same accuracy. For clean utterances, SSF Type-I performs slightly better than SSF Type-II.

To simulate the effects of room reverberation, we used the software package Room Impulse Response (RIR) [53]. We assumed a room of dimensions of $5 \times 4 \times 3$ m , a distance between the microphone and the speaker of 2 m, with the microphones located at the center of the room. In reverberant environments, as shown in Fig. 7.4(c), SSF Type-II shows the best performance by a very large margin. SSF Type-I shows the next performance, but the performance difference between SSF Type-I and SSF-Type-II is large. On the contrary, VTS does not provide any performance improvement, and PLP-RASTA provides worse performance than MFCC.

7.5 Conclusions

In this chapter we present a new algorithm that is especially robust with respect to reverberation. Motivated by modulation frequency considerations and the precedence effect, we apply first-order high-pass filtering to power coefficients. The falling edges of power contours are suppressed in two different ways. We observe that using the lowpassed signal for the falling edge is especially helpful for reducing spectral distortion for reverberant environments. Experimental results show that this approach is more effective than previous algorithms in reverberant environments.

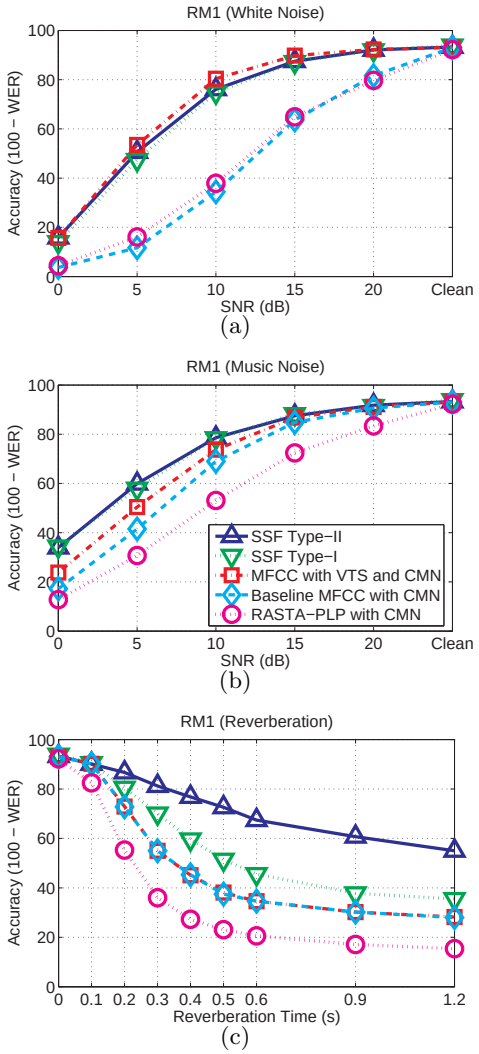

Fig. 7.4: Comparison of speech recognition accuracy using the two types of SSF, VTS, and baseline MFCC and PLP processing for (a) white noise, (b) musical noise, and (c) reverberant environments.

7.6 Open source MATLAB code

MATLAB code for the SSF algorithm may be found at [URL here] . This code was used to obtain the results in Section 7.4.

8. POWER NORMALIZED CEPSTRAL COEFFICIENT

In this chapter, we discuss our new feature PNCC processing. PNCC incorporates concepts we discussed in Chap. 3, 4, and 7.

8.1 Introduction

In recent decades following the introduction of hidden Markov models (*e.g.* [72]) and statistical language models (*e.g.*[73]), the performance of speech recognition systems in benign acoustical environments has dramatically improved. Nevertheless, most speech recognition systems remain sensitive to the nature of the acoustical environments within which they are deployed, and their performance deteriorates sharply in the presence of sources of degradation such as additive noise, linear channel distortion, and reverberation.

One of the most challenging contemporary problems is that recognition accuracy degrades significantly if the test environment is different from the training environment and/or if the acoustical environment includes disturbances such as additive noise, channel distortion, speaker differences, reverberation, and so on. Over the years dozens if not hundreds of algorithms have been introduced to address this problem. Many of these conventional noise compensation algorithms have provided substantial improvement in accuracy for recognizing speech in the presence of quasi-stationary noise (*e.g.* [9, 10, 7, 41, 12, 74]). Unfortunately these same algorithms frequently do not provide significant improvements in more difficult environments with transitory disturbances such as a single interfering speaker or background music (*e.g.* [42]).

Virtually all of the current systems developed for automatic speech recognition, speaker identification, and related tasks are based on variants of one of two types of features: *mel frequency cepstral coefficients* (MFCC) [22] or *perceptual linear prediction* (PLP) coefficients [25]. In this chapter we describe the development of a third type of feature set for speech

recognition which we refer to as *power-normalized cepstral coefficients* (PNCC). As we will show, PNCC features provide superior recognition accuracy over a broad range of conditions of noise and reverberation using features that are computable in real time using "online" algorithms, and with a computational complexity that is comparable to that of traditional MFCC and PLP features.

In the subsequent subsections of this Introduction we discuss the broader motivations and overall structure of PNCC processing. We specify the key elements of the processing in some detail in Sec. 8.2. In Sec. 8.3 we compare the recognition accuracy provided by PNCC processing under a variety of conditions with that of other processing schemes, and we consider the impact of various components of PNCC on these results. We compare the computational complexity of the MFCC, PLP, and PNCC feature extraction algorithms in Sec. 8.6 and we summarize our results in the final section.

8.1.1 Broader motivation for the PNCC algorithm

The development of PNCC feature extraction was motivated by a desire to obtain a set of practical features for speech recognition that are more robust with respect to acoustical variability in their native form, without loss of performance when the speech signal is undistorted, and with a degree of computational complexity that is comparable to that of MFCC and PLP coefficients. While many of the attributes of PNCC processing have been strongly influenced by consideration of various attributes of human auditory processing, we have favored approaches that provide pragmatic gains in robustness at small computational cost over approaches that are more faithful to auditory physiology in developing the specific processing that is performed.

Some of the innovations of the PNCC processing that we consider to be the most important include:

- The replacement of the log nonlinearity in MFCC processing by a power-law nonlinearity that is carefully chosen to approximate the nonlinear relation between signal intensity and auditory-nerve firing rate. We believe that this nonlinearity provides superior robustness by suppressing small signals and their variability, as discussed in Sec. 8.2.7.

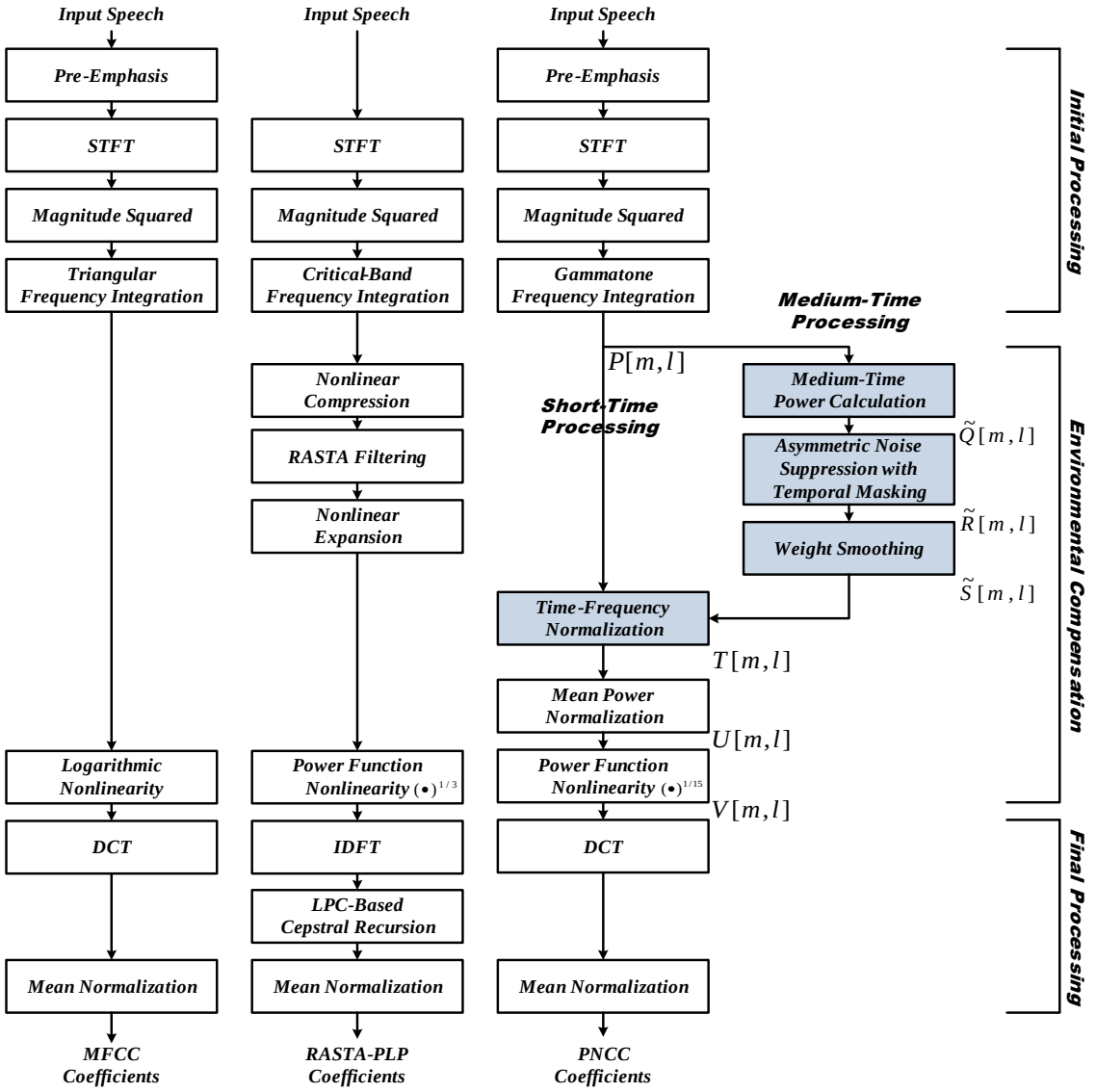

Fig. 8.1: Comparison of the structure of the MFCC, PLP, and PNCC feature extraction algorithms. The modules of PNCC that function on the basis of "medium-time" analysis (with a temporal window of 65.6 ms) are plotted in the rightmost column. If the shaded blocks of PNCC are omitted, the remaining processing is referred to as *simple power-normalized cepstral coefficients (SPNCC)*.

- The use of "medium-time" processing with a duration of 50-120 ms to analyze the parameters characterizing environmental degradation, in combination with the tradi-

tional short-time Fourier analysis with frames of 20-30 ms used in conventional speech recognition systems. We believe that this approach enables us to estimate environmental degradation more accurately while maintaining the ability to respond to rapidly-changing speech signals, as discussed in Sec. 8.2.2.

- The use of a form of "asymmetric nonlinear filtering" to estimate the level of the acoustical background noise for each time frame and frequency bin. We believe that this approach enables us to remove slowly-varying components easily without needing to deal with many of the artifacts associated with over-correction in techniques such as spectral subtraction [11], as discussed in Sec. 8.2.3. As shown in Sec. 8.3.3, this approach is more effective than RASTA processing [3].

- The development of computationally-efficient realizations of the algorithms above that support "online" real-time processing.

8.1.2 Structure of the PNCC algorithm

Figure 8.1 compares the structure of conventional MFCC processing [22], PLP processing [25, 3], and the new PNCC approach which we introduce in this chapter. As was noted above, the major innovations of PNCC processing include the redesigned nonlinear rate-intensity, along with the series of processing elements to suppress the effects of background acoustical activity based on medium-time analysis.

As can be seen from Fig. 8.1, the initial processing stages of PNCC processing are quite similar to the corresponding stages of MFCC and PLP analysis, except that the frequency analysis is performed using gammatone filters [57]. This is followed by the series of nonlinear time-varying operations that are performed using the longer-duration temporal analysis that accomplish noise subtraction as well as a degree of robustness with respect to reverberation. The final stages of processing are also similar to MFCC and PLP processing, with the exception of the carefully-chosen power-law nonlinearity with exponent 1/15, which will be discussed in Sec. 8.2.7 below.

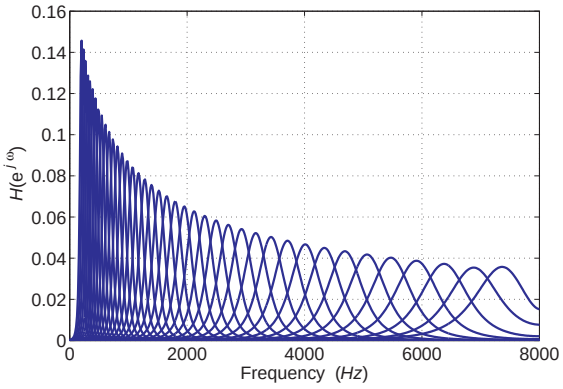

Fig. 8.2: The frequency response of a gammatone filterbank with each area of the squared frequency response normalized to be unity. Characteristic frequencies are uniformly spaced between 200 and 8000 Hz according to the Equivalent Rectangular Bandwidth (ERB) scale [4].

8.2 Components of PNCC processing

In this section we describe and discuss the major components of PNCC processing in greater detail. While the detailed description below assumes a sampling rate of 16 kHz, the PNCC features are easily modified to accommodate other sampling frequencies.

8.2.1 Initial processing

As in the case of MFCC, a pre-emphasis filter of the form $H(z) = 1 - 0.97z^{-1}$ is applied. A short-time Fourier transform (STFT) is performed using Hamming windows of duration 25.6 ms, with 10 ms between frames, using a DFT size of 1024. Spectral power in 40 analysis bands is obtained by weighting the magnitude-squared STFT outputs for positive frequencies by the frequency response associated with a 40-channel gammatone-shaped filter bank [57] whose center frequencies are linearly spaced in Equivalent Rectangular Bandwidth (ERB) [4] between 200 Hz and 8000 Hz, using the implementation of gammatone filters in Slaney's Auditory Toolbox [47]. In previous work [55] we observed that the use of gammatone frequency weighting provides slightly better ASR accuracy in white noise, but the differences compared to the traditional triangular weights in MFCC processing are small. The frequency response of the gammatone filterbank is shown in Fig. 9.6. In each channel the area under

the squared transfer function is normalized to unity to satisfy the equation:

$$\int_0^{8000} |H_l(f)|^2 df = 1 \tag{8.1}$$

where $H_l(f)$ is the frequency response of the l^{th} gammatone channel. To reduce the amount of computation, we modified the gammatone filter responses slightly by setting $H_l(f)$ equal to zero for all values of f for which the unmodified $H_l(f)$ would be less than 0.5 percent (corresponding to -46 dB) of its maximum value.

We obtain the short-time spectral power $P[m, l]$ using the squared gammatone summation as below:

$$P[m, l] = \sum_{k=0}^{(K/2)-1} |X[m, e^{j\omega_k}) H_l(e^{j\omega_k})|^2 \tag{8.2}$$

where K is the DFT size, m and l represent the frame and channel indices, respectively, and $\omega_k = 2\pi k/F_s$, with F_s representing the sampling frequency. $X[m, e^{j\omega_k})$ is the short-time spectrum of the m^{th} frame of the signal.

8.2.2 Temporal integration for environmental analysis

Most speech recognition and speech coding systems use analysis frames of duration between 20 ms and 30 ms. Nevertheless, it is frequently observed that longer analysis windows provide better performance for noise modeling and/or environmental normalization (*e.g.* [35, 36]), because the power associated with most background noise conditions changes more slowly than the instantaneous power associated with speech.

In PNCC processing we estimate a quantity we refer to as "medium-time power" $\tilde{Q}[m, l]$ by computing the running average of $P[m, l]$, the power observed in a single analysis frame, according to the equation:

$$\tilde{Q}[m, l] = \frac{1}{2M+1} \sum_{m'=m-M}^{m+M} P[m', l] \tag{8.3}$$

where m represents the frame index and l is the channel index. We will apply the tilde symbol to all power estimates that are performed using medium-time analysis.

We observed experimentally that the choice of the temporal integration factor M has a substantial impact on performance in white noise (and presumably other types of broadband

background noise). This factor has less impact on the accuracy that is observed in more dynamic interference or reverberation, although the longer temporal analysis window does provide some benefit in these environments as well [75]. We chose the value of $M = 2$ (corresponding to five consecutive windows with a total net duration of 65.6 ms) on the basis of these observations.

Since $\tilde{Q}[m,l]$ is the moving average of $P[m,l]$, $\tilde{Q}[m,l]$ is a low-pass function of m. If $M = 2$, the upper frequency is approximately 15 Hz. Nevertheless, if we were to use features based on $\tilde{Q}[m,l]$ directly for speech recognition, recognition accuracy would be degraded because onsets and offsets of the frequency components would become blurred. Hence in PNCC, we use $\tilde{Q}[m,l]$ only for noise estimation and compensation, which are used to modify the information based on the short-time power estimates $P[m,l]$. We also apply smoothing over the various frequency channels, which will discussed in Sec. 8.2.5 below.

8.2.3 Asymmetric noise suppression

In this section, we discuss a new approach to noise compensation which we refer to as *asymmetric noise suppression* (ANS). This procedure is motivated by the observation mentioned above that the speech power in each channel usually changes more rapidly than the background noise power in the same channel. Alternately we might say that speech usually has a higher-frequency modulation spectrum than noise. Motivated by this observation, many algorithms have been developed using either high-pass filtering or band-pass filtering in the modulation spectrum domain (*e.g.* [3, 32]). The simplest way to accomplish this objective is to perform high-pass filtering in each channel (*e.g.* [31, 66]) which has the effect of removing slowly-varying components.

One significant problem with the application of conventional linear high-pass filtering in the power domain is that the filter output can become negative. Negative values for the power coefficients are problematic in the formal mathematical sense (in that power itself is positive). They also cause problems in the application of the compressive nonlinearity and in speech resynthesis unless a suitable floor value is applied to the power coefficients (*e.g.* [66]). Rather than filtering in the power domain, we could perform filtering after applying the logarithmic nonlinearity, as is done with conventional cepstral mean normalization in MFCC

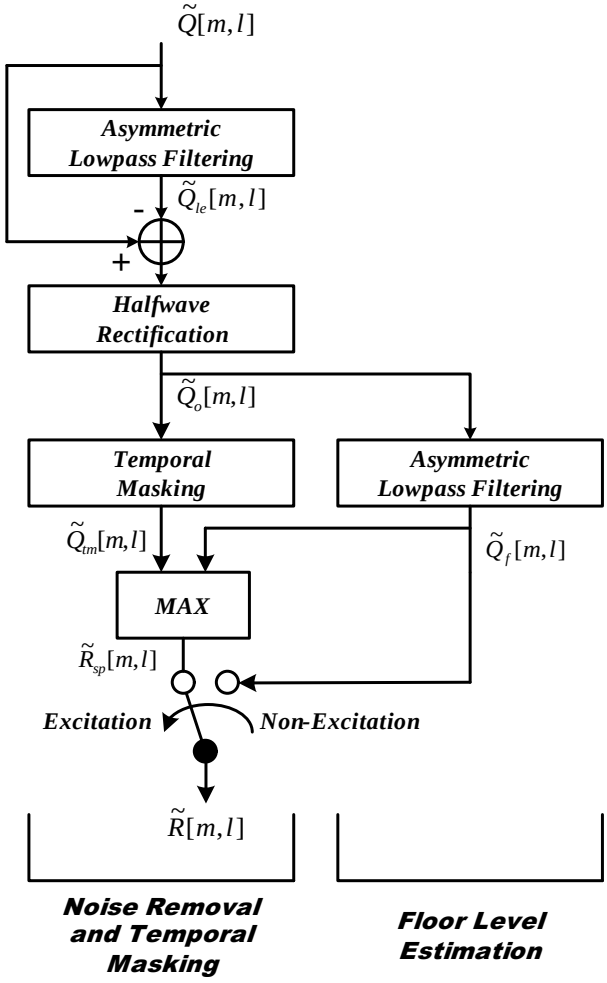

Fig. 8.3: Functional block diagram of the modules for asymmetric noise suppression (ANS) and temporal masking in PNCC processing. All processing is performed on a channel-by-channel basis. $\tilde{Q}[m,l]$ is the medium-time-averaged input power as defined by Eq.(8.3), $\tilde{R}[m,l]$ is the speech output of the ANS module, , and $\tilde{S}[m,l]$ is the output after temporal masking (which is applied only to the speech frames). The block labelled Temporal Masking is depicted in detail in Fig. 8.7

processing. Nevertheless, as will be seen in Sec. 8.3, this approach is not very helpful for environments with additive noise. Spectral subtraction is another way to reduce the effects of noise, whose power changes slowly (*e.g.* [11]). In spectral subtraction techniques, the noise level is typically estimated from the power of non-speech segments (*e.g.* [11]) or through

the use of a continuous-update approach (*e.g.* [31]). In the approach that we introduce, we obtain a running estimate of the time-varying noise floor using an asymmetric nonlinear filter, and subtract that from the instantaneous power.

Figure 8.3 is a block diagram of the complete asymmetric nonlinear suppression processing with temporal masking. Let us begin by describing the general characteristics of the asymmetric nonlinear filter that is the first stage of processing. This filter is represented by the following equation for arbitrary input and output $\tilde{Q}_{in}[m,l]$ and $\tilde{Q}_{out}[m,l]$, respectively:

$$\tilde{Q}_{out}[m,l] = \begin{cases} \lambda_a \tilde{Q}_{out}[m-1,l] + (1-\lambda_a)\tilde{Q}_{in}[m,l], \\ \qquad \text{if } \tilde{Q}_{in}[m,l] \geq \tilde{Q}_{out}[m-1,l] \\ \lambda_b \tilde{Q}_{out}[m-1,l] + (1-\lambda_b)\tilde{Q}_{in}[m,l], \\ \qquad \text{if } \tilde{Q}_{in}[m,l] < \tilde{Q}_{out}[m-1,l] \end{cases} \tag{8.4}$$

where m is the frame index and l is the channel index, and λ_a and λ_b are constants between zero and one.

If $\lambda_a = \lambda_b$ it is easy to verify that Eq. 8.4 reduces to a conventional IIR filter that is lowpass in nature because of the positive values of the λ parameters, as shown in Fig. 8.4(a). In contrast, If $1 > \lambda_b > \lambda_a > 0$, the nonlinear filter functions as a conventional "upper" envelope detector, as illustrated in Fig. 8.4(b). Finally, and most usefully our purposes, if $1 > \lambda_a > \lambda_b > 0$, the filter output $\tilde{Q}_{out}$ tends to follow the *lower envelope* of $\tilde{Q}_{in}[m,l]$, as seen in Fig. 8.4(c). In our processing, we will use this slowly-varying lower envelope in Fig. 8.4(c) to serve as a model for the estimated medium-time noise level, and the activity above this envelope is assumed to represent speech activity. Hence, subtracting this low-level envelope from the original input $\tilde{Q}_{in}[m,l]$ will remove a slowly varying non-speech component.

We will use the notation

$$\tilde{Q}_{out}[m,l] = \mathcal{AF}_{\lambda_a,\lambda_b}[\tilde{Q}_{in}[m,l]] \tag{8.5}$$

to represent the nonlinear filter described by Eq. (8.4). We note that that this filter operates only on the frame indices m for each channel index l.

Keeping the characteristics of the asymmetric filter described above in mind, we may now consider the structure shown in Fig. 8.3. In the first stage, the lower envelope $\tilde{Q}_{le}[m,l]$, which represents the average noise power, is obtained by ANS processing according to the

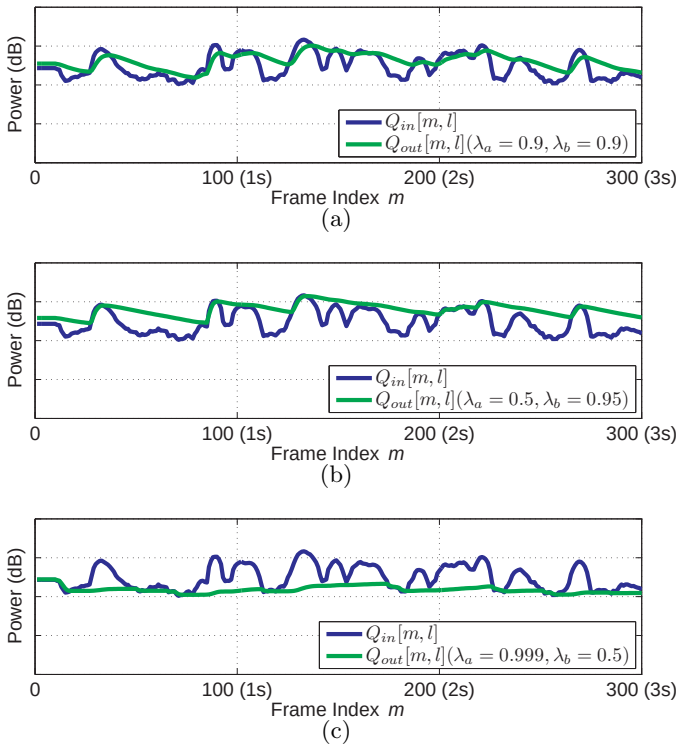

Fig. 8.4: Sample inputs (solid curves) and outputs (dashed curves) of the asymmetric nonlinear filter defined by Eq. (8.4) for conditions when (a) $\lambda_a = \lambda_b$ (b) $\lambda_a < \lambda_b$, and (c) $\lambda_a > \lambda_b$. In this example, the channel index l is 8.

equation

$$\tilde{Q}_{le}[m,l] = \mathcal{AF}_{0.999,0.5}[\tilde{Q}[m,l]] \tag{8.6}$$

as depicted in Fig. 8.4(c). $\tilde{Q}_{le}[m,l]$ is subtracted from the input $\tilde{Q}[m,l]$, effectively highpass filtering the input, and that signal is passed through an ideal half-wave linear rectifier to produce the rectified output $\tilde{Q}_0[m,l]$. The impact of the specific values of the forgetting factors λ_a and λ_b on speech recognition accuracy is discussed below.

The remaining elements of ANS processing in the right-hand side of Fig. 8.3 (other than the temporal masking block) are included to cope with problems that develop when the rectifier output $\tilde{Q}_0[m,l]$ remains zero for an interval, or when the local variance of $\tilde{Q}_0[m,l]$ becomes excessively small. Our approach to this problem is motivated by our previous work [35] in which it was noted that applying a well-motivated flooring level to power is very

important for noise robustness. In PNCC processing we apply the asymmetric nonlinear filter for a second time to obtain the lower envelope of the rectifier output $\tilde{Q}_f[m,l]$, and we use this envelope to establish this floor level. This envelope $\tilde{Q}_f[m,l]$ is obtained using asymmetric filtering as before:

$$\tilde{Q}_f[m,l] = \mathcal{AF}_{0.999,0.5}[\tilde{Q}_0[m,l]] \tag{8.7}$$

As shown in Fig. 8.3, we use the lower envelope of the rectified signal $\tilde{Q}_f[m,l]$ as a floor level for the ANS processing output $\tilde{R}[m,l]$ after temporal masking:

$$\tilde{R}_{sp}[m,l] = \max\left(\tilde{Q}_{tm}[m,l], \tilde{Q}_f[m,l]\right) \tag{8.8}$$

where $\tilde{Q}_{tm}[m,l]$ is the temporal masking output depicted in Fig. 8.3. Temporal masking for speech segments is discussed in Sec. 8.2.4.

We have found that applying lowpass filtering to the non-excitation segments improves recognition accuracy in noise by a small amount, and for that reason we use the lower envelope of the rectified signal $\tilde{R}_{le}[m,l]$ directly for these non-excitation segments. This operation, which is effectively a further lowpass filtering, is not performed for the speech segments because blurring the power coefficients for speech degrades recognition accuracy.

Excitation/non-excitation decisions for this purpose are obtained for each value of m and l in a very simple fashion:

$$\text{“excitation segment” if} \quad \tilde{Q}[m,l] \geq c\tilde{Q}_{le}[m,l] \tag{8.9a}$$

$$\text{“non-excitation segment” if} \quad \tilde{Q}[m,l] < c\tilde{Q}_{le}[m,l] \tag{8.9b}$$

where $\tilde{Q}_{le}[m,l]$ is the lower envelope of $\tilde{Q}[m,l]$ as described above, and in and c is a fixed constant. In other words, a particular value of $\tilde{Q}[m,l]$ is not considered to be a sufficiently-large excitation if it is less than a fixed multiple of its own lower envelope.

We observed experimentally that while a broad range of values of λ_b between 0.25 and 0.75 appear to provide reasonable recognition accuracy, the choice of $\lambda_a = 0.9$ appears to be best under some circumstances as shown in Fig. 8.5. The parameter values used for the current standard implementation are $\lambda_a = 0.999$ and $\lambda_b = 0.5$, which were chosen in part to maximize the recognition accuracy in clean speech as well as performance in noise. We

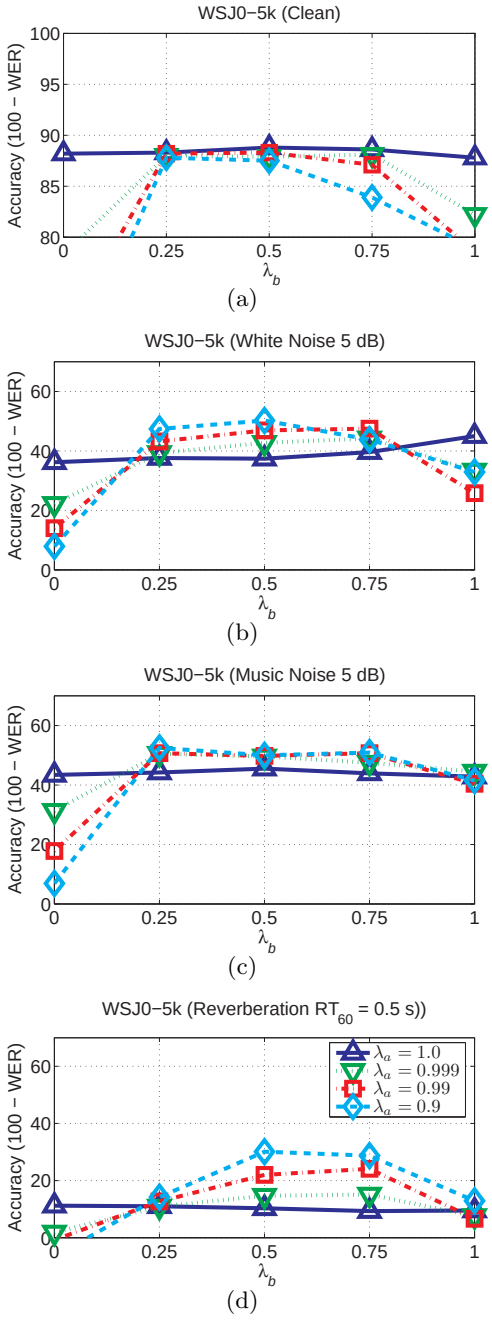

Fig. 8.5: The corresponding dependence of speech recognition accuracy on the forgetting factors λ_a and λ_b. The filled triangle on the y-axis represents the baseline MFF result for the same test set: (a) Clean, (b) 5-dB Gaussian white noise, (c) 5-dB musical noise, and (d) reverberation with $RT_{60} = 0.5$

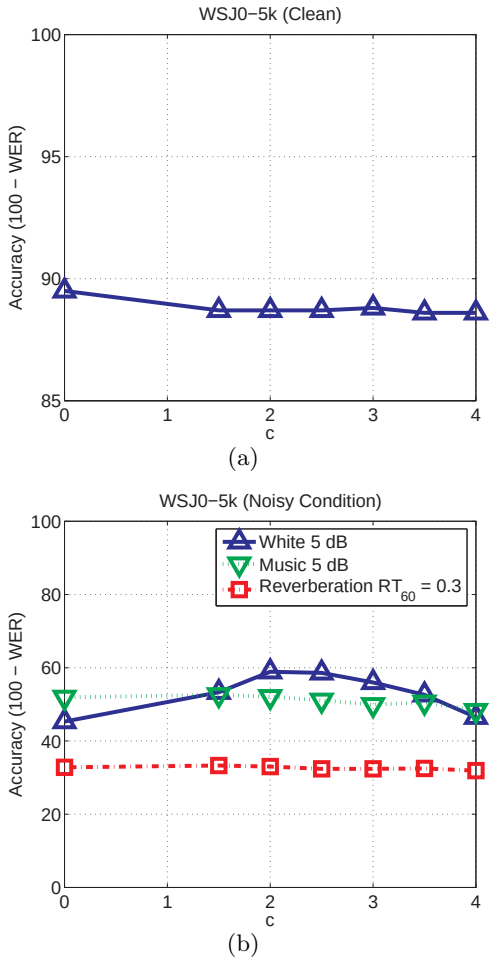

Fig. 8.6: The dependence of speech recognition accuracy on the speech/non-speech decision coefficient c in (8.9) : (a) clean and (b) noisy environment

also observed (in experiments in which the temporal masking described below was bypassed) that the threshold-parameter value $c = 2$ provides the best performance for white noise (and presumably other types of broadband noise) as shown in Fig. 8.6. The value of c has little impact on performance in background music and in the presence of reverberation.

8.2.4 Temporal masking

Many authors have noted that the human auditory system appears to focus more on the onset of an incoming power envelope rather than the falling edge of that same power envelope (*e.g.* [76, 77]). This observation has led to several onset enhancement algorithms (*e.g.* [70, 66, 78]).

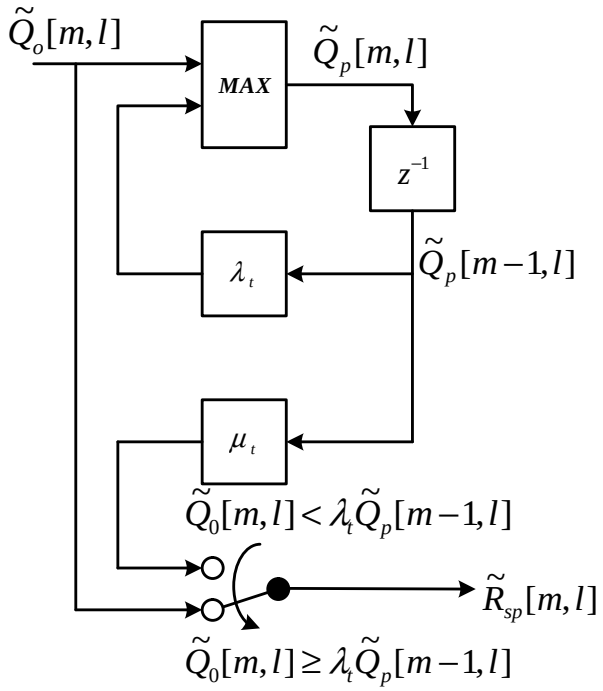

Fig. 8.7: Block diagram of the components that accomplish temporal masking in Fig. 8.3

In this section we describe a simple way to incorporate this effect in PNCC processing, by obtaining a moving peak for each frequency channel l and suppressing the instantaneous power if it falls below this envelope.

The processing invoked for temporal masking is depicted in block diagram form in Fig. 8.7. We first obtain the on-line peak power $Q_p[m,l]$ for each channel using the following equation:

$$\tilde{Q}_p[m,l] = \max\left(\lambda_t \tilde{Q}_p[m-1,l], \tilde{Q}_0[m,l]\right) \tag{8.10}$$

where λ_t is the forgetting factor for obtaining the on-line peak. As before, m is the frame index and l is the channel index. Temporal masking for speech segments is accomplished using the following equation:

$$\tilde{R}_{sp}[m,l] = \begin{cases} \tilde{Q}_0[m,l], & \tilde{Q}_0[m,l] \geq \lambda_t \tilde{Q}_p[m-1,l] \\ \mu_t \tilde{Q}_p[m-1,l], & \tilde{Q}_0[m,l] < \lambda_t \tilde{Q}_p[m-1,l] \end{cases} \tag{8.11}$$

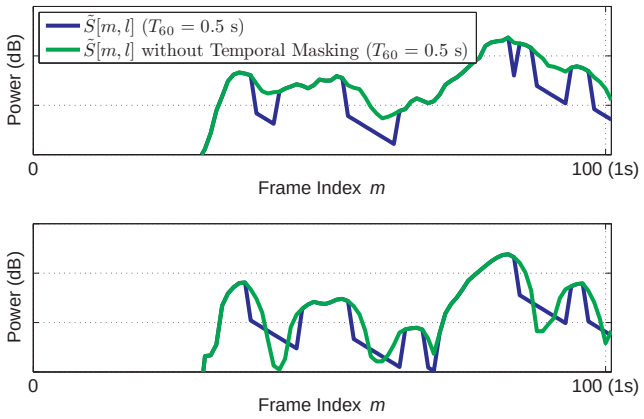

Fig. 8.8: Demonstration of the effect of temporal masking in the ANS module for speech in simulated reverberation with $T_{60} = 0.5$ s (upper panel) and clean speech (lower panel). In this example, the channel index l is 18.

Fig. 8.9 shows how recognition accuracy depends on the forgetting factor λ_t and the suppression factor μ_t. Experimental configuration is described in Subsection 8.3.1. In obtaining speech recognition results in this figure, we used the entire PNCC structure shown in Fig. 8.1 and changed only the forgetting factor λ_t and the suppression factor μ_t.

In clean environment, as shown in Fig. 8.9(a), if the forgetting factor is equal to or less than 0.85 and if $\mu_t \leq 0.2$, then performance remains almost constant. However, if λ_t is larger than 0.85, then performance degrades. Similar tendency is also observed in additive noise such as white and music noise as shown in Fig. 8.9(b) and in Fig. 8.9(c). For reverberation, as shown in Fig. 8.9(d), we observe that by applying the temporal masking scheme, we observe substantial benefit. As will be shown in Subsection 8.3.2, this temporal masking scheme also shows a remarkable improvement in a very difficult environment like a single-channel interfering speaker case.

Figure 8.8 illustrates the effect of this temporal masking. In general, with temporal masking the response of the system is inhibited for portions of the input signal $\tilde{R}[m,l]$ other than rising "attack transients". The difference between the signals with and without masking is especially pronounced in reverberant environments, for which the temporal processing module is especially helpful.

The final output of the asymmetric noise suppression and temporal masking modules is

$\tilde{R}[m.l] = \tilde{R}_{sp}[m,l]$ for the excitation segments and $\tilde{R}[m,l] = \tilde{Q}_f[m,l]$ for the non-excitation segments.

8.2.5 Spectral weight smoothing

In our previous research on speech enhancement and noise compensation techniques (*e.g.*, [55, 35, 36, 46, 37]) it has been frequently observed that smoothing the response across channels is helpful. This is true especially in processing schemes such as PNCC where there are nonlinearities and/or thresholds that vary in their effect from channel to channel, as well as processing schemes that are based on inclusion of responses only from a subset of time frames and frequency channels (*e.g.* [46]) or systems that rely on missing-feature approaches (*e.g.* [16]).

From the discussion above, we can represent the combined effects of asymmetric noise suppression and temporal masking for a specific time frame and frequency bin as the transfer function $\tilde{R}[m,l]/\tilde{Q}[m,l]$. Smoothing the transfer function across frequency is accomplished by computing the running average over the channel index l of the ratio $\tilde{R}[m,l]/\tilde{Q}[m,l]$. Hence, the frequency averaged weighting function $\tilde{T}[m,l]$ (which had previously been subjected to temporal averaging) is given by:

$$\tilde{S}[m,l] \;=\; \left(\frac{1}{l_2 - l_1 + 1} \sum_{l'=l_1}^{l_2} \frac{\tilde{R}[m,l']}{\tilde{Q}[m,l']} \right) \tag{8.12}$$

where $l_2 = \min(l+N, L)$ and $l_1 = \max(l-N, 1)$, and L is the total number of channels.

The time-averaged frequency-averaged transfer function $\tilde{T}[m,l]$ is used to modulate the original short-time power $P[m,l]$:

$$T[m,l] = P[m,l]\tilde{U}[m,l] \tag{8.13}$$

In the present implementation of PNCC, we use a value of $N = 4$, and a total number of $L = 40$ gammatone channels, again based on empirical optimization from the results of pilot studies [75]. We note that if we were to use a different number of channels L, the optimal value of N would be also different.

8.2.6 Mean power normalization

In conventional MFCC processing, multiplication of the input signal by a constant scale factor produces only an additive shift of the C_0 coefficient because a logarithmic nonlinearity is included in the processing, and this shift is easily removed by cepstral mean normalization. In PNCC processing, however, the replacement of the log nonlinearity by a power-law nonlinearity as discussed below, causes the response of the processing to be affected by changes in absolute power, even though we have observed that this effect is usually small. In order to further minimize the potential impact of amplitude scaling in PNCC we invoke a stage of mean power normalization.

While the easiest way to normalize power would be to divide the instantaneous power by the average power over the utterance, this is not feasible for real-time online processing because of the "look ahead" that would be required. For this reason, we normalize input power in the present online implementation of PNCC by dividing the incoming power by a running average of the overall power. The mean power estimate $\mu[m]$ is computed from the simple difference equation:

$$\mu[m] = \lambda_\mu \mu[m-1] + \frac{(1-\lambda_\mu)}{L} \sum_{l=0}^{L-1} T[m,l] \tag{8.14}$$

where m and l are the frame and channel indices, as before, and L represents the number of frequency channels. We use a value of 0.999 for the forgetting factor λ_μ.

The normalized power is obtained directly from the running power estimate $\mu[m]$:

$$U[m,l] = k\frac{T[m,l]}{\mu[m]} \tag{8.15}$$

where the value of the constant k is arbitrary. In pilot experiments we found that the speech recognition accuracy obtained using the online power normalization described above is comparable to the accuracy that would be obtained by normalizing according to a power estimate that is computed over the entire estimate in offline fashion.

8.2.7 Rate-level nonlinearity

Several studies in our group (*e.g.* [55, 37]) have confirmed the critical importance of the nonlinear function that describes the relationship between incoming signal amplitude in a

given frequency channel and the corresponding response of the processing model. This "rate-level nonlinearity" is explicitly or implicitly a crucial part of every conceptual or physiological model of auditory processing (*e.g.* [79, 80, 50]). In this section we summarize our approach to the development of the rate-level nonlinearity used in PNCC processing.

It is well known that the nonlinear curve relating sound pressure level in decibels to the auditory-nerve firing rate is compressive (*e.g* [1] [81]). It has also been observed that the average auditory-nerve firing rate exhibits an overshoot at the onset of an input signal. As an example, we compare in Fig. 8.11 the average onset firing rate versus the sustained rate as predicted by the model of Heinz *et al.* [1]. The curves in this figure were obtained by averaging the rate-intensity values obtained from sinusoidal tone bursts over seven frequencies, 100, 200, 400, 800, 1600, 3200, and 6400 Hz. For the onset-rate results we partitioned the response into bins of length of 2.5 ms, and searched for the bin with maximum rate during the initial 10 ms of the tone burst. To measure the sustained rate, we averaged the response rate between 50 and 100 ms after the onset of the signals. The curves were generated under the assumption that the spontaneous rate is 50 spikes/second. We observe in Fig. 8.11 that the sustained firing rate (broken curve) is S-shaped with a threshold around 0 dB SPL and a saturating segment that begins at around 30 dB SPL. The onset rate (solid curve), on the other hand, increases continuously without apparent saturation over the conversational hearing range of 0 to 80 dB SPL. We choose to model the onset rate-intensity curve for PNCC processing because of the important role that it appears to play in auditory perception.

Figure 8.13 compares the onset rate-intensity curve depicted in Fig. 8.11 with various analytical functions that approximate this function. The curves are plotted as a function of dB SPL in the lower panel of the figure and as a function of absolute pressure in Pascals in the upper panel, and the putative spontaneous firing rate of 50 spikes per second is subtracted from the curves in both cases.

The most widely used current feature extraction algorithms are Mel Frequency Cepstral Coefficients (MFCC) and Perceptual Linear Prediction (PLP) coefficients. Both the MFCC and PLP procedures include an intrinsic nonlinearity, which is logarithmic in the case of MFCC and a cube-root power function in the case of PLP analysis. We plot these curves relating the power of the input pressure p to the response s in Fig. 8.13 using values of the arbitrary scaling parameters that are chosen to provide the best fit to the curve of the Heinz

et al. model, resulting in the following equations:

$$s_{cube} = 4294.1p^{2/3} \tag{8.16}$$

$$s_{log} = 120.2\log(p) + 1319.3 \tag{8.17}$$

We note that the exponent of the power function is doubled because we are plotting power rather than pressure. Even though scaling and shifting by fixed constants in Eqs. (8.16) and (8.17) do not have any significance in speech recognition systems, we included them in the above equation to fit these curves to the rate-intensity curve in Fig. 8.13(a). The constants in Eqs. (8.16) and (8.17) are obtained using an MMSE criterion for the sound pressure range between 0 dB (20μPa) and 80 dB (0.2 Pa) from the linear rate-intensity curve in the upper panel of Fig. 8.11.

As shown in Fig. 8.12, the power function coefficient obtained from the MMSE power-fit gives us performance benefit compared to conventional logarithmic processing. If we use a bigger coefficient such as 1/5, it gives us better performance for white noise, but it loses performance in other environments as well as in clean environment. From this figure, we observe that larger values of the pressure exponent such as 1/5 provide better performance in white noise, but they degrade the recognition accuracy that is obtained for clean speech . We consider the value 1/15 for the pressure exponent to represent a pragmatic compromise that provides reasonable accuracy in white noise without sacrificing recognition accuracy for clean speech, producing the power-law nonlinearity

$$V[m,l] = U[m,l]^{1/15} \tag{8.18}$$

where again $U[m,l]$ and $V[m,l]$ have the dimensions of power. This curve is closely approximated by the equation

$$s_{power} = 1389.6p^{0.1264} \tag{8.19}$$

which is also plotted in Fig. 8.13. The exponent of 0.1264 happens to be the best fit to the Heinz *et al.* data as depicted in the upper panel of Fig. 8.11. As before, this estimate was developed in the MMSE sense over the sound pressure range between 0 dB (20μPa) and 80 dB (0.2 Pa).

The power low function was chosen for PNCC processing for several reasons. First, it is a relationship that is not affected in form by multiplying the input by a constant. Second, it has the attractive property that its asymptotic response at very low intensities is zero rather than negative infinity, which reduces variance in the response to low-level inputs such as spectral valleys or silence segments. Finally, the power law has been demonstrated to provide a good approximation to the "psychophysical transfer functions" that are observed in experiments relating the physical intensity of sensation to the perceived intensity using direct magnitude-estimation procedures (*e.g.* [52]).

Figure 8.14 is a final comparison of the effects of the asymmetric noise suppression, temporal masking, channel weighting, and power-law nonlinearity modules discussed in Secs. 8.2.3 through 8.2.7. The curves in both panels compare the response of the system in the channel with center frequency 490 Hz to clean speech and speech in the presence of street noise at an SNR of 5 dB. The curves in the upper panel were obtained using conventional MFCC processing, including the logarithmic nonlinearity and without ANS processing or temporal masking. The curves in the lower panel were obtained using PNCC processing, which includes the power-law transformation described in this section, as well as ANS processing and temporal masking. We note that the difference between the two curves representing clean and noisy speech is much greater with MFCC processing (upper panel), especially for times during which the signal is at a low level.

8.3 Experimental results

In this section we present experimental results that are intended to demonstrate the superiority of PNCC processing over competing approaches in a wide variety of acoustical environments. We begin in Sec. 8.3.1 with a review of the experimental procedures that were used. We provide some general results for PNCC processing, we assess the contributions of its various components in PNCC in Sec. 8.3.2, and we compare PNCC to a small number of other approaches in Sec. 8.3.3.

It should be noted that in general we selected an algorithm configuration and associated parameter values that provide very good performance over a wide variety of conditions using a single set of parameters and settings, without sacrificing word error rate in clean conditions

relative to MFCC processing. In previous work we had described slightly different feature extraction algorithms that provide even better performance for speech recognition in the presence of reverberation [35] and in background music [66], but these approaches do not perform as well as MFCC processing in clean speech. We used five standard testing environments in our work: (1) digitally-added white noise, (2) digitally-added noise that had been recorded live on urban streets, (3) digitally-added single-speaker interference, (4) digitally-added background music, and (5) passage of the signal through simulated reverberation. The street noise was recorded by us on streets with steady but moderate traffic. The masking signal used for single-speaker-interference experiments consisted of other utterances drawn from the TIMIT database, and background music was selected from music segments from the original DARPA Hub 4 Broadcast News database. The reverberation simulations were accomplished using the *Room Impulse Response* open source software package [53] based on the image method [82]. The room size used was $3 \times 4 \times 5$ meters, the microphone is in the center of the room, the spacing between the target speaker and the microphone was assumed to be 1.5 meters, and reverberation time was manipulated by changing the assumed absorption coefficients in the room appropriately.

8.3.1 Experimental Configuration

The PNCC feature described in this chapter was evaluated by comparing the recognition accuracy obtained with PNCC introduced in this chapter to that obtained using MFCC and RASTA-PLP processing. We used the version of conventional MFCC processing implemented as part of `sphinx_fe` in `sphinxbase 0.4.1` both from the CMU Sphinx open source codebase [83]. We used the PLP-RASTA implementation that is available at [30]. In all cases decoding was performed using the publicly-available CMU Sphinx 3.8 system [83] using training from `SphinxTrain 1.0`. We also compared PNCC with the *vector Taylor series* (VTS) noise compensation algorithm [10] and the *ETSI advanced front end* (AFE) which has several noise suppression algorithms included [74]. In the case of the ETSI AFE, we excluded the log energy element because this resulted in better results in our experiments. A bigram language model was used in all experiments. In all experiments, we used feature vectors of length of 39 including delta and delta-delta features. For experiments using the DARPA

Resource Management (RM1) database we used subsets of 1600 utterances of clean speech for training and 600 utterances of clean or degraded speech for testing. For experiments based on the DARPA Wall Street Journal (WSJ) 5000-word database we trained the system using the WSJ0 SI-84 training set and tested it on the WSJ0 5K test set.

We typically plot word recognition accuracy, which is 100 percent minus the word error rate (WER), using the standard definition for WER of the number of insertions, deletions, and substitutions divided by the number of words spoken.

8.3.2 General performance of PNCC in noise and reverberation

In this section we describe the recognition accuracy obtained using PNCC processing in the presence of various types of degradation of the incoming speech signals. Figures 8.15 and 8.16 describe the recognition accuracy obtained with PNCC processing in the presence of white noise, street noise, background music, and speech from a single interfering speaker as a function of SNR, as well as in the simulated reverberant environment as a function of reverberation time. These results are plotted for the DARPA RM database in Fig. 8.15 and for the DARPA WSJ database in Fig. 8.16. For the experiments conducted in noise we prefer to characterize the improvement in recognition accuracy by the amount of lateral shift of the curves provided by the processing, which corresponds to an increase of the effective SNR. For white noise using the RM task, PNCC provides an improvement of about 12 dB to 13 dB compared to MFCC processing, as shown in Fig. 8.15. In the presence of street noise, background music, and interfering speech, PNCC provides improvements of approximately 8 dB, 3.5 dB, and 3.5 dB, respectively. We also note that PNCC processing provides considerable improvement in reverberation, especially for longer reverberation times. PNCC processing exhibits similar performance trends for speech from the DARPA WSJ0 database in similar environments, as seen in Fig. 8.16, although the magnitude of the improvement is diminished somewhat, which is commonly observed as we move to larger databases.

The curves in Figs. 8.15 and 8.16 are also organized in a way that highlights the various contributions of the major components. It can be seen from the curves that a substantial improvement can be obtained by simply replacing the logarithmic nonlinearity of MFCC

processing by the power-law rate-intensity function described in Sec. 8.2.7. The addition of the ANS processing provides a substantial further improvement for recognition accuracy in noise. Although it is not explicitly shown in Figs. 8.15 and 8.16, the temporal masking is particularly helpful in improving accuracy for reverberated speech and for speech in the presence of interfering speech.

8.3.3 Comparison with other algorithms

Figures 8.17 and 8.18 provide comparisons of PNCC processing to the baseline MFCC processing with cepstral mean normalization, MFCC processing combined with the vector Taylor series (VTS) algorithm for noise robustness [10], as well as RASTA-PLP feature extraction [3]. The experimental conditions used were the same as those used to produce Figs. 8.15 and 8.16.

We note in Figs. 8.17 and 8.18 that PNCC provides substantially better recognition accuracy than both MFCC and RASTA-PLP processing for all conditions examined. It also provides recognition accuracy that is better than the combination of MFCC with VTS, and at a substantially lower computational cost than the computation that is incurred in implementing VTS. We also note that the VTS algorithm provides little or no improvement over the baseline MFCC performance in difficult environments like background music noise, single-channel interfering speaker or reverberation.

The ETSI AFE [74] generally provides slightly better recognition accuracy than VTS in noisy environments, but accuracy that does not approach that obtained with PNCC processing. Both the ETSI AFE and VTS do not improve recognition accuracy in reverberant environments compared to MFCC features, while PNCC shows measuremable improvements in reverberation and a closely related algorithm [66] provides even greater recognition accuracy in reverberation (at the expense of somewhat worse performance in clean speech).

8.4 Experimental results under multi-style training condition

In the above sections, we presented speech recognition results using clean training set. These days, in many large-scale speech recognition systems, we use multi-style noisy training set. So, we also evaluated the performance of PNCC for multi-style training set. In Fig. 8.19,

we used a training set corrupted by street noise at 5 different SNR levels (0, 5, 10, 15, 20) and clean. Each utterance in the training set was randomly corrupted to one of these 6 different SNR levels. As shown in Fig. 8.19, PNCC shows improvements in all kinds of cases. Especially, we observe that for interfering speaker noise, MFCC using noisy training set is doing even worse than MFCC using the clean training set. Another interesting observation is that for the clean test set, PNCC shows significantly better performance than MFCC. The reason is now clean test set is unmatched condition since we used noisy training set, and PNCC does better than MFCC for unmatched conditions.

Experiments in Fig. 8.20 are similar to the experiments in Fig. 8.19. But we used 4 different types of noise (white, street, music, and interfering speaker noise) at 5 different SNR levels (0, 5, 10, 15, 20 dB). So, in total, the utterances in the clean training set was randomly selected to one of these 21 possible cases and was corrupted. In this experiment, as shown in Fig. 8.20, PNCC is still doing better than MFCC even though the difference is reduced compared to the clean training set.

Experiments in Fig. 8.21 is similar to experiments in Fig. 8.19, but we used WSJ0-si84 for acoustic model training and WSJ0-5k for decoding. Experiments in Fig.8.22 is the same as experiments in Fig. 8.20, but we used WSJ0-si84 for acoustic model training and WSJ0-5k for decoding.

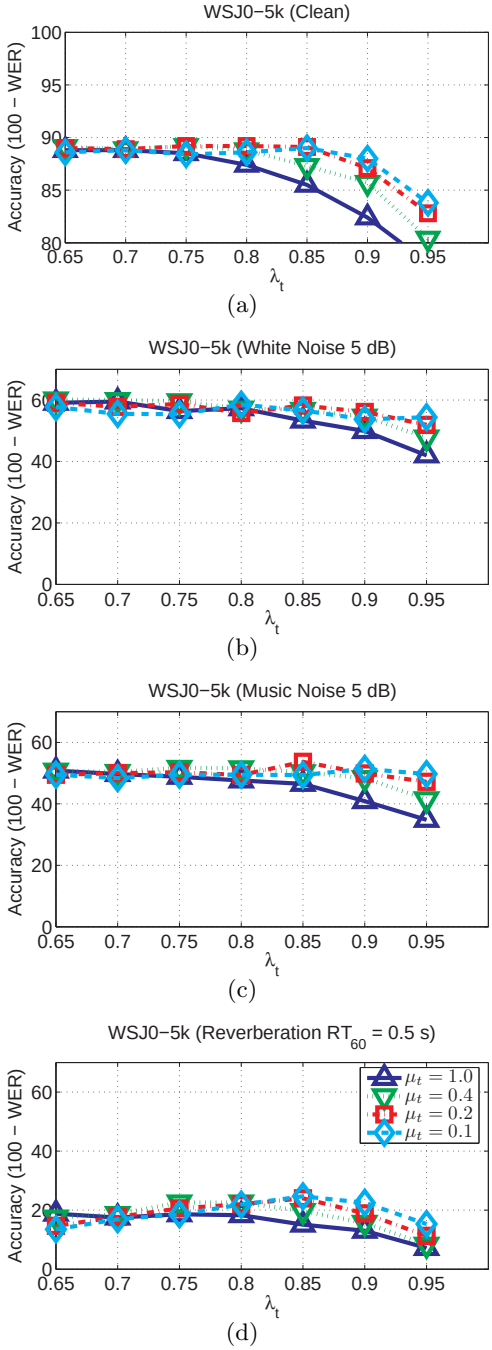

Fig. 8.9: The dependence of speech recognition accuracy on the forgetting factor λ_t and the suppression factor μ_t , which are used for temporal masking block. The filled triangle on the y-axis represents the baseline MFCC result for the same test set: (a) Clean, (b) 5-dB Gaussian white noise, (c) 5-dB musical noise, and (d) reverberation with $RT_{60} = 0.5$

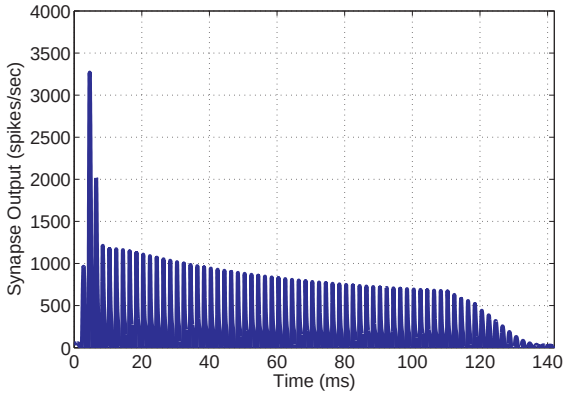

Fig. 8.10: Synapse output for a pure tone input with a carrier frequency of 500 Hz at 60 dB SPL. This synapse output is obtained using the auditory model by Heinz et al. [1].

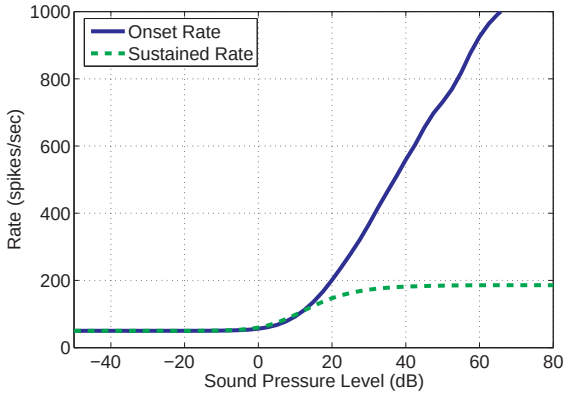

Fig. 8.11: Comparison of the onset rate (solid curve) and sustained rate (dashed curve) obtained using the model proposed by Heinz *et al.* [1]. The curves were obtained by averaging responses over seven frequencies. See text for details.

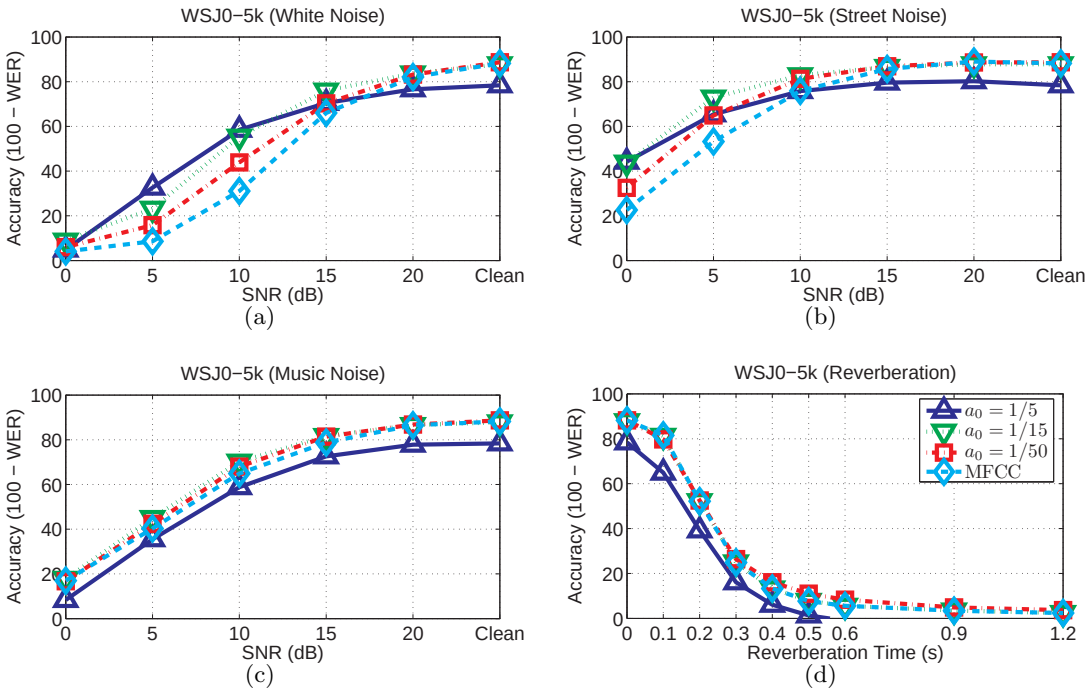

Fig. 8.12: Dependence on speech recognition accuracy on power coefficient in different environments: (a) additive white gaussian noise, (b) street noise, (c) background music, and (d) reverberant environment.

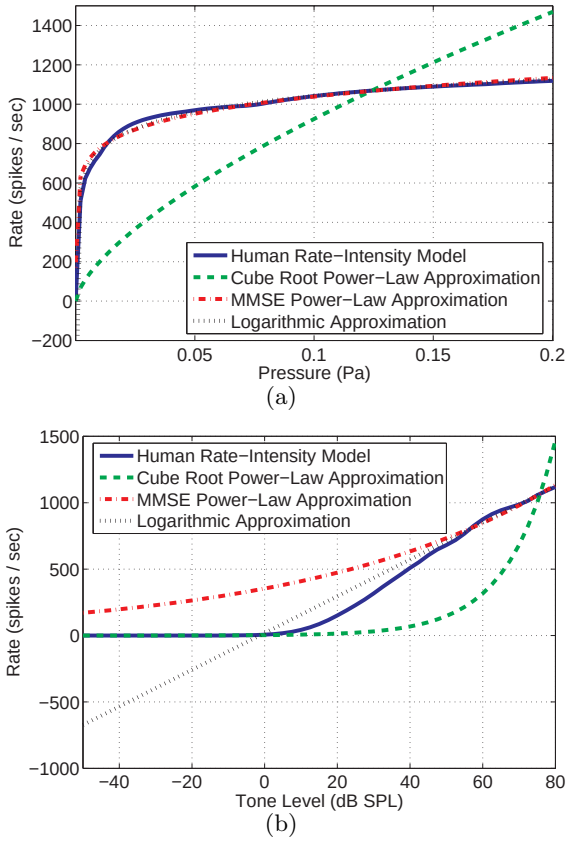

Fig. 8.13: Comparison between a human rate-intensity relation using the auditory model developed by Heinz *et al.* [1], a cube root power-law approximation, an MMSE power-law approximation, and a logarithmic function approximation. Upper panel: Comparison using the pressure (Pa) as the x-axis. Lower panel: Comparison using the sound pressure level (SPL) in dB as the x-axis.

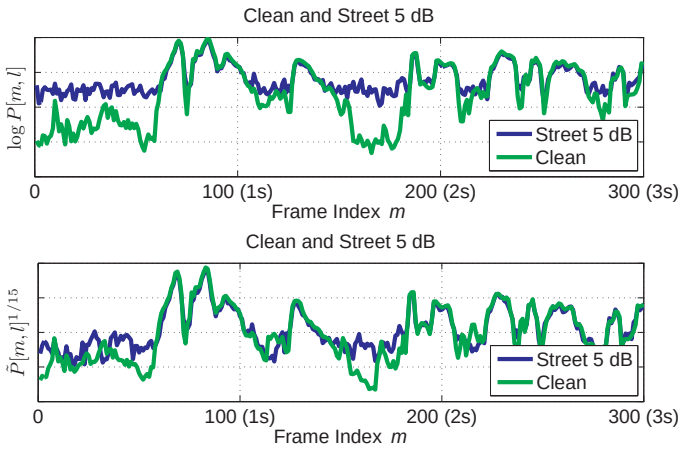

Fig. 8.14: The effects of the asymmetric noise suppression, temporal masking, and the rate-level nonlinearity used in PNCC processing. Shown are the outputs of these stages of processing for clean speech and for speech corrupted by street noise at an SNR of 5 dB when the logarithmic nonlinearity is used without ANS processing or temporal masking (upper panel), and when the power-law nonlinearity is used with ANS processing and temporal masking (lower panel). In this example, the channel index l is 8.

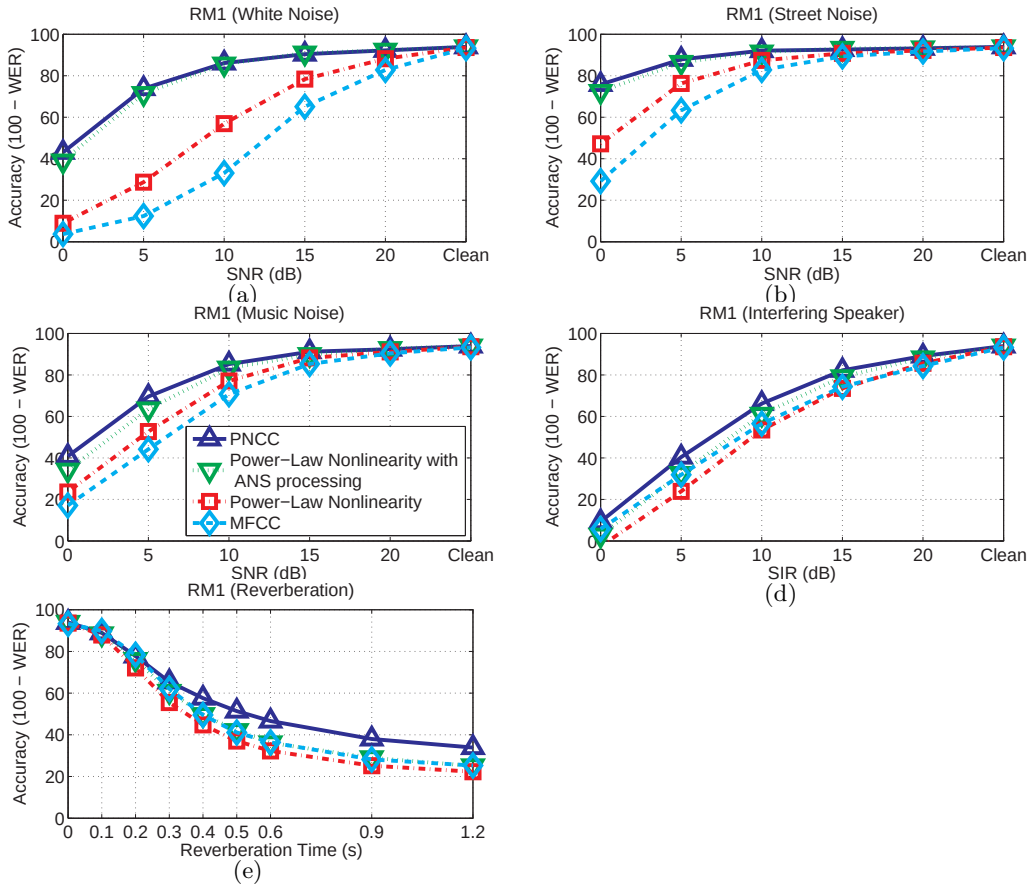

Fig. 8.15: Recognition accuracy obtained using PNCC processing in various types of additive noise and reverberation. Curves are plotted separately to indicate the contributions of the power-law nonlinearity, asymmetric noise suppression, and temporal masking. Results are described for the DARPA RM1 database in the presence of (a) white noise, (b) street noise, (c) background music, (d) interfering speech, and (e) artificial reverberation.

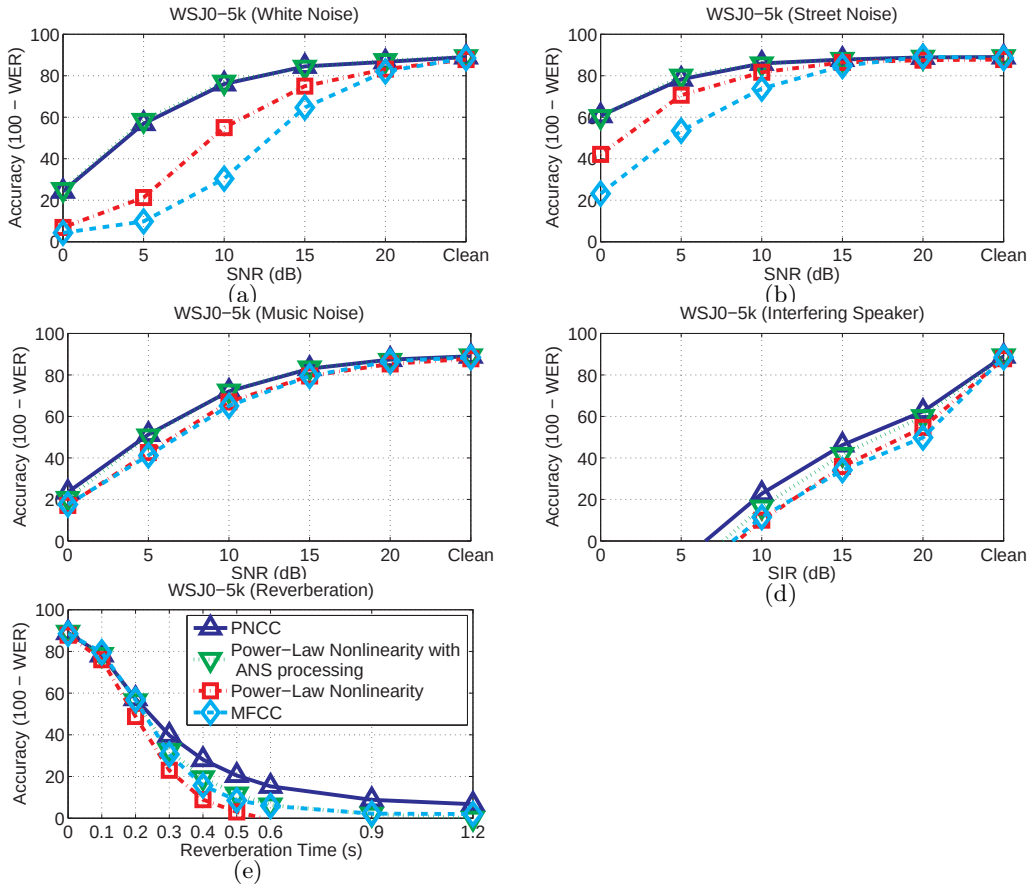

Fig. 8.16: Recognition accuracy obtained using PNCC processing in various types of additive noise and reverberation. Curves are plotted separately to indicate the contributions of the power-law nonlinearity, asymmetric noise suppression, and temporal masking. Results are described for the DARPA WSJ0 database in the presence of (a) white noise, (b) street noise, (c) background music, (d) interfering speech, and (e) artificial reverberation.

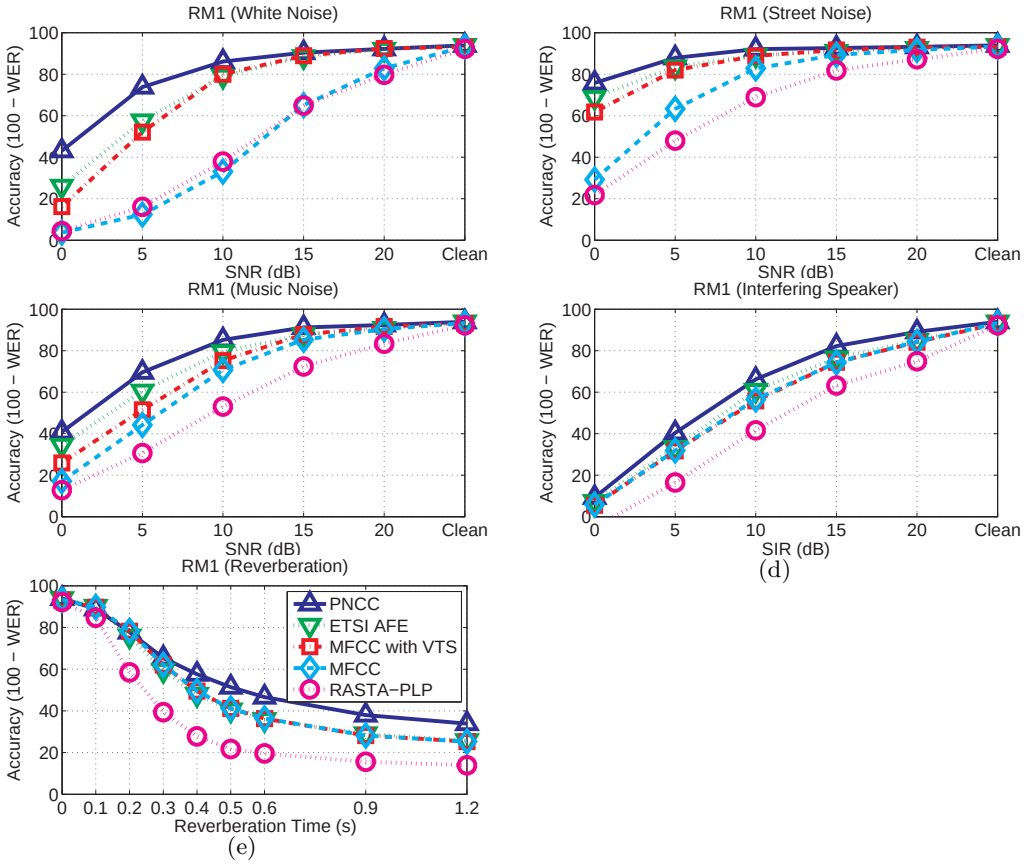

Fig. 8.17: Comparison of recognition accuracy for PNCC with processing using MFCC features, the ETSI AFE, MFCC with VTS, and RASTA-PLP features using the DARPA RM1 corpus. Environmental conditions are (a) white noise, (b) street noise, (c) background music, (d) interfering speech, and (e) reverberation.

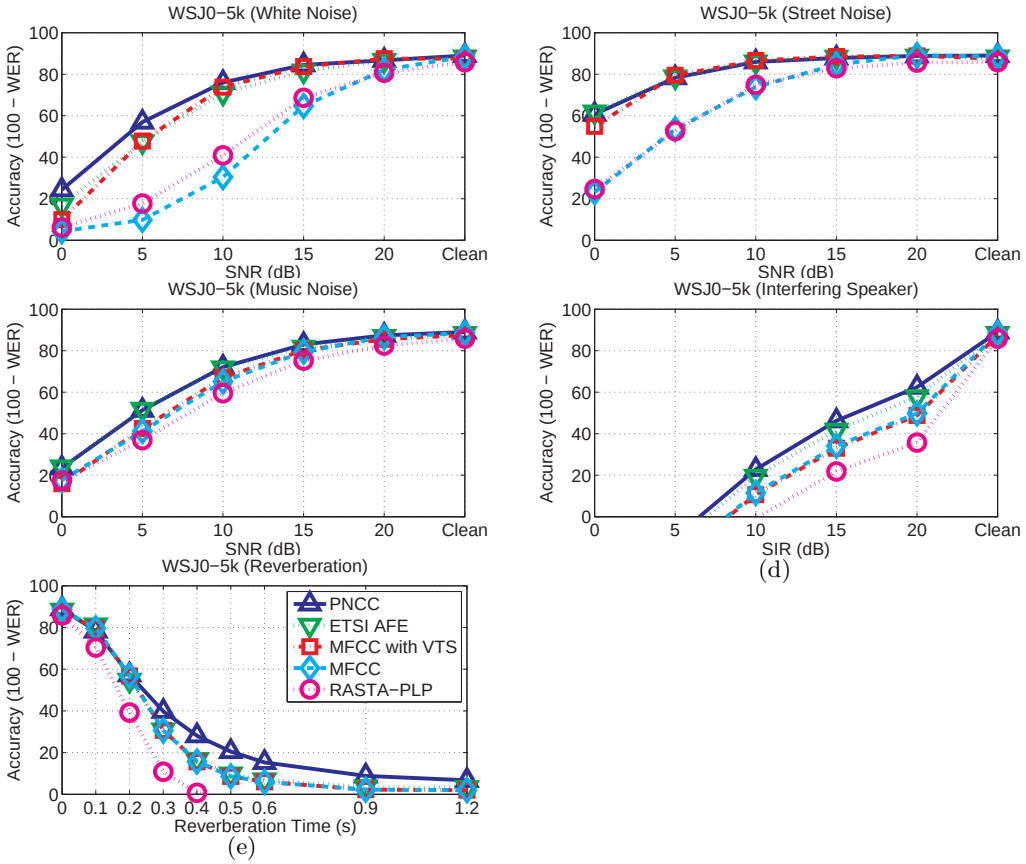

Fig. 8.18: Comparison of recognition accuracy for PNCC with processing using MFCC features, ETSI AFE, MFCC with VTS, and RASTA-PLP features using the DARPA RM1 corpus. Environmental conditions are (a) white noise, (b) street noise, (c) background music, (d) interfering speech, and (e) reverberation.

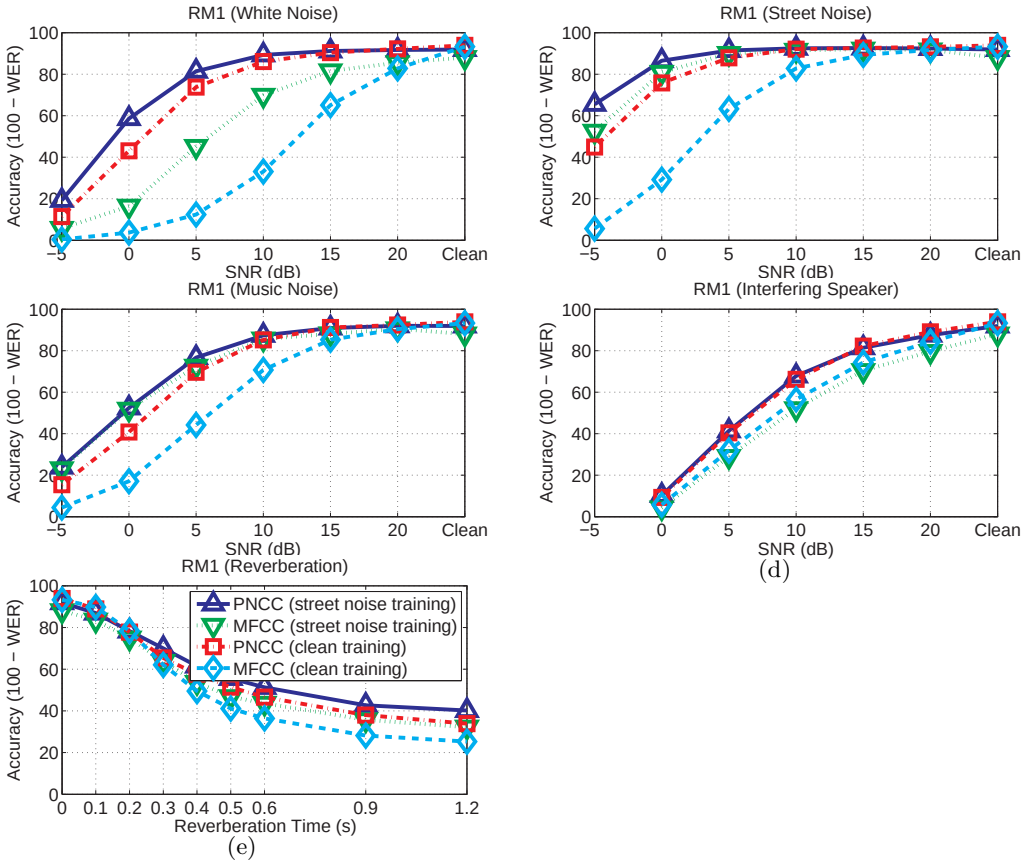

Fig. 8.19: Comparison of recognition accuracy for PNCC with processing using MFCC features using the DARPA RM1 corpus. Training database was corrupted by street noise at 5 different levels plus clean. Environmental conditions are (a) white noise, (b) street noise, (c) background music, (d) interfering speech, and (e) reverberation.

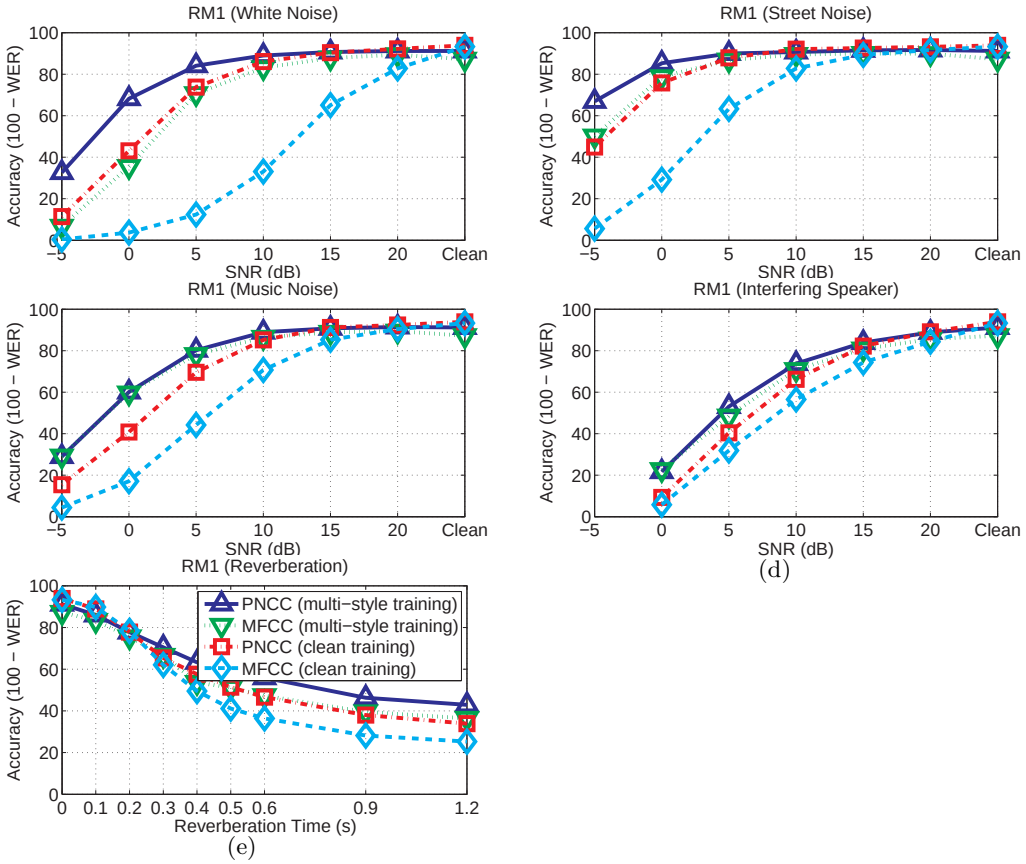

Fig. 8.20: Comparison of recognition accuracy for PNCC with processing using MFCC features using the DARPA RM-1 corpus. Training database was corrupted by street noise at 5 different levels plus clean. Environmental conditions are (a) white noise, (b) street noise, (c) background music, (d) interfering speech, and (e) reverberation.

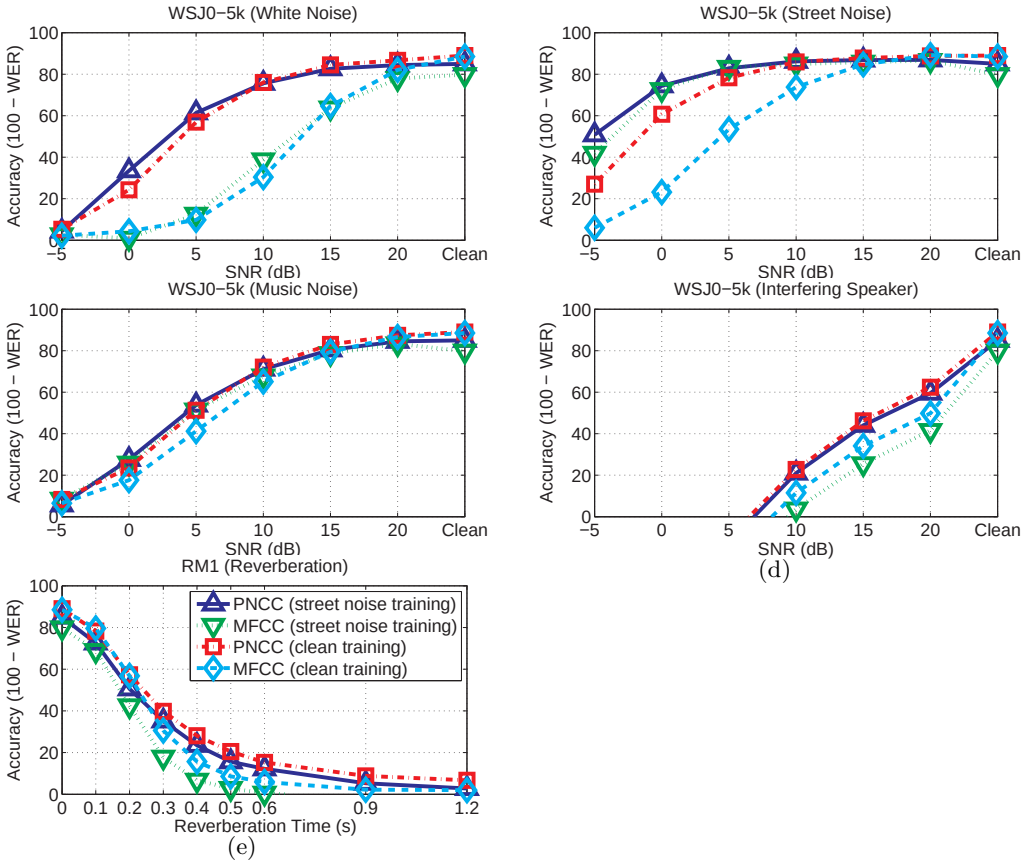

Fig. 8.21: Comparison of recognition accuracy for PNCC with processing using MFCC features using the WSJ0 5k corpus. Training database was corrupted by street noise at 5 different levels plus clean. Environmental conditions are (a) white noise, (b) street noise, (c) background music, (d) interfering speech, and (e) reverberation.

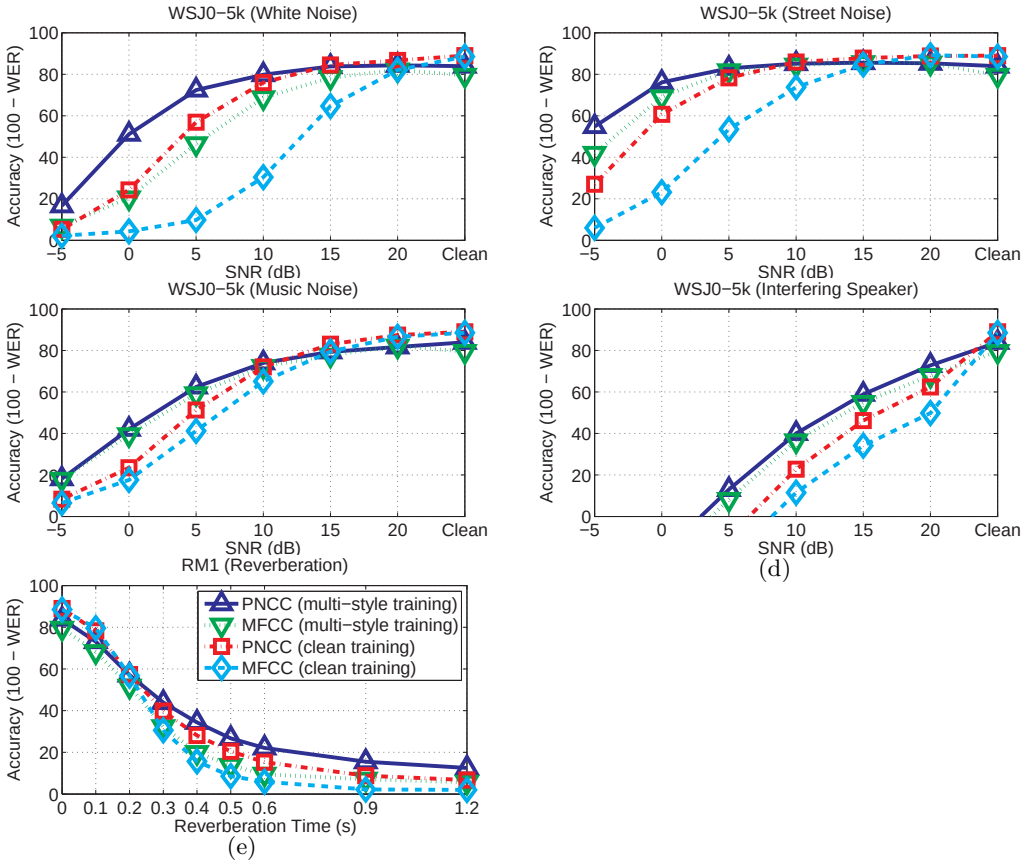

Fig. 8.22: Comparison of recognition accuracy for PNCC with processing using MFCC features using the WSJ0 5k corpus. Training database was corrupted by street noise at 5 different levels plus clean. Environmental conditions are (a) white noise, (b) street noise, (c) background music, (d) interfering speech, and (e) reverberation.

8.5 Experimental results using MLLR

Maximum likelihood linear regression (MLLR) has become very popular in speech recognition. It has been observed that MLLR is a very powerful technique, in many cases, robustness algorithm does not show substantial improvement compared to MFCC if MLLR is incorporated. To evaluate the performance of PNCC in combination of MLLR, we conducted speech recognition experiments using four different types of MLLR configuration.

8.5.1 Clean training and multi-style MLLR adaptation set

Figure 8.23 shows speech recognition accuracies, when we used the clean training set, and MLLR was performed on the noisy test set "speaker-by-speaker" basis. We used RM1 for acoustic model training and decoding. We used 600 utterances for test and 600 utterances for MLLR model adaptation (development set). In the test set, there are 40 different speakers, and we adapted HMM model "speaker-by-speaker" basis using this adaptation set. As in the previous section, for the MLLR adaptation set, multi-style noise was intentionally added to the adaptation set. We used 4 different types of noise, white, street, music, and interfering speaker noise at 5 different SNR levels (0, 5, 10, 15, 20 dB). Including the clean case, there are 21 possible cases, and for each utterance in the MLLR adaptation set, one of these conditions are randomly selected to make multi-style MLLR adaptation set. In this experiment, MLLR was performed under supervised mode. For each speaker, 15 utterances from the adaptation set (corrupted by multi-style noise) was used for HMM model adaptation under supervised mode (using the correct transcript for the adaptation set), and the adapted model was used for decoding the test set. This process was performed each speaker.

As shown in Fig. 8.23, PNCC shows improvements under all types of noise except reverberation. For the reverberation set, we later observed that if we use PNCC using "off-line" peak normalization, then it still shows some small improvement. For white, street, and interfering speaker noise, MFCC with MLLR processing is even worse than PNCC without MLLR processing. Thus, we can observe that PNCC is still a very useful technique when it is combined with MLLR.

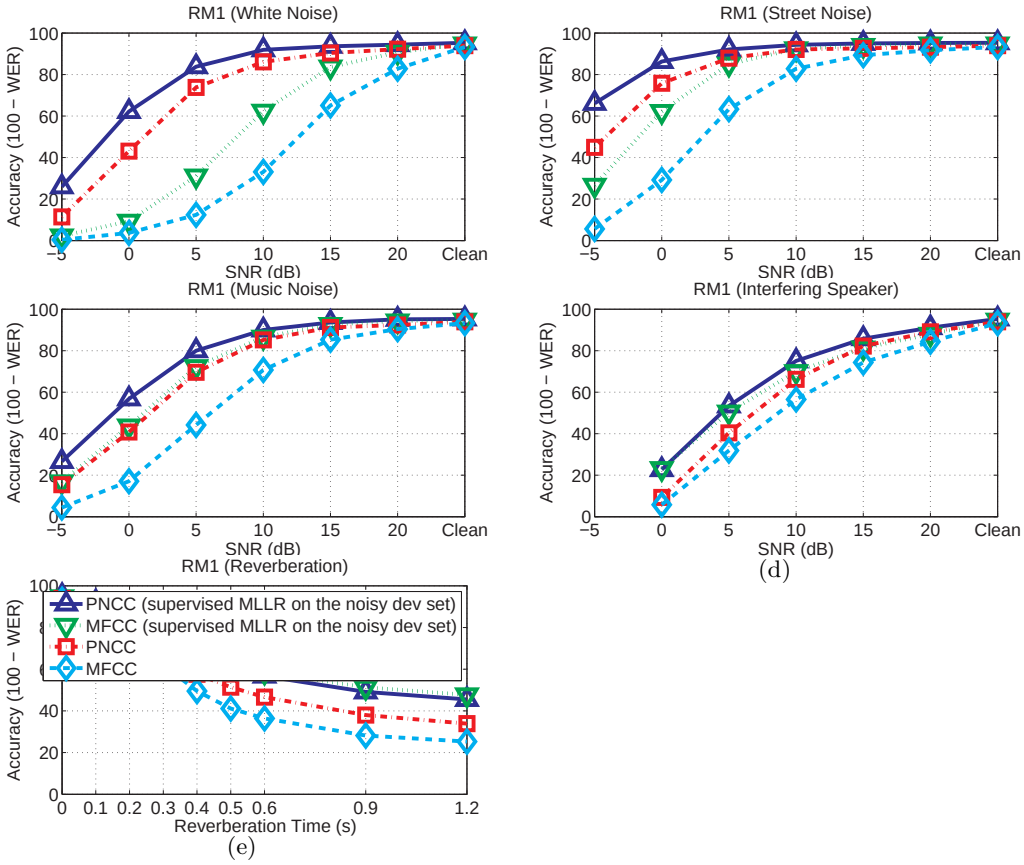

Fig. 8.23: Comparison of recognition accuracy for PNCC with processing using MFCC features using the RM1 corpus. Clean training set was used, and MLLR was directly performed spk-by-spk basis using the multi-style development set. MLLR was performed in the unsupervised mode. Environmental conditions are (a) white noise, (b) street noise, (c) background music, (d) interfering speech, and (e) reverberation.

8.5.2 Multi-style training and multi-style MLLR adaptation set

Experiments in Fig. 8.24 is similar to the experiments in Fig. 8.23. The only difference is that instead of using the clean training set, we used "multi-style" training set in this experiment. As before, we corrupted the training database using white, street, music, and interfering speaker noise at 5 different SNR levels (0, 5, 10, 15, and 20 dB). The MLLR adapation set is exactly the same as Sec. 8.5.1.

Figure 8.24 shows the speech recognition results. As shown in this figure, PNCC shows improvements under all different noise conditions. As in the result in the previous subsection, MFCC with MLLR performs even worse than PNCC without MLLR.

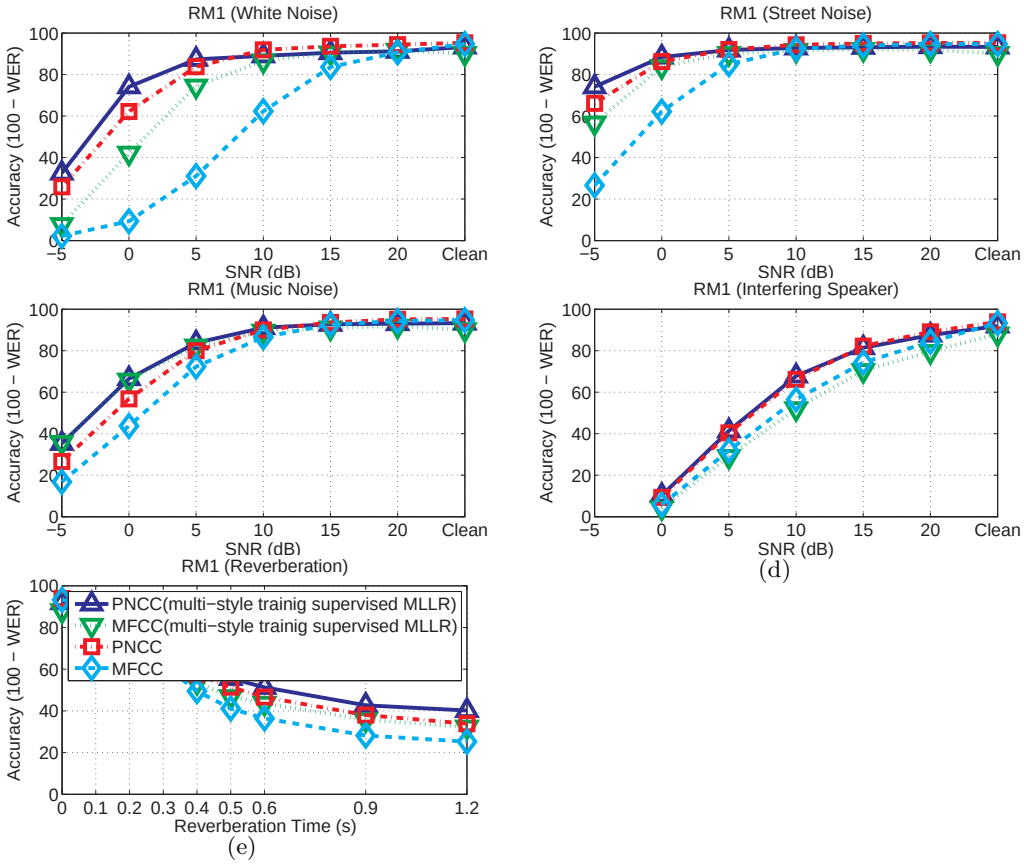

Fig. 8.24: Comparison of recognition accuracy for PNCC with processing using MFCC features using the RM1 corpus. Multi-style training set was used, and MLLR was directly performed spk-by-spk basis using the multi-style development set. MLLR was performed in the unsupervised mode. Environmental conditions are (a) white noise, (b) street noise, (c) background music, (d) interfering speech, and (e) reverberation.

8.5.3 Multi-style training and MLLR under the matched condition

In this experiment, we use the same multi-style training set as Sec. 8.5.2, but MLLR is performed under the matched condition. For example, if the test utterance is corrupted by 5-dB street noise, then the exactly same kind of noise type and level were used for MLLR adaptation. As before, MLLR is performed "speaker-by-speaker" basis. Since MLLR is performed under matched condition, recognition accuracies are very high even under very noisy environment, so unlike previous figures, we used a different y-scale (70 % – 100 %) in Fig. 8.25. As shown in Fig. 8.25, PNCC still shows improvements for all conditions even though the difference between PNCC and MFCC is much reduced. We also note that for clean environment, MFCC performs significantly poorer than PNCC, which is consistently being observed if we use multi-style training set.

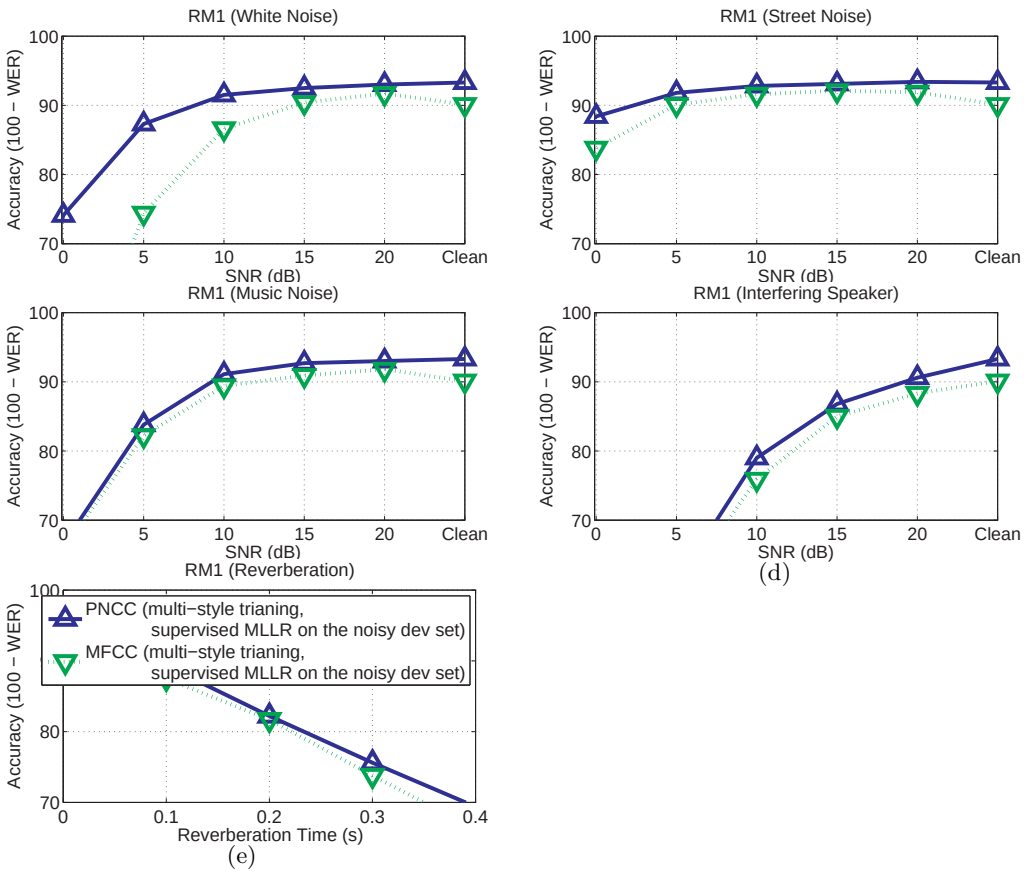

Fig. 8.25: Comparison of recognition accuracy for PNCC with processing using MFCC features using the RM1 corpus. Multi-style training set was used, and MLLR was directly performed spk-by-spk basis under "the matched condition". MLLR was performed in the unsupervised mode. Environmental conditions are (a) white noise, (b) street noise, (c) background music, (d) interfering speech, and (e) reverberation.

8.5.4 *Multi-style training and unsupervised MLLR using the test set itself*

In this experiment, we used "unsupervised MLLR" on the test set itself. Since we use the test utterances themselves as the MLLR adaptation set, we can no longer use the supervised MLLR. Thus, in the first path, the decoder runs and we obtained the hypothesis. Using this hypothesis, we ran MLLR. Like the experiments in Sec. 8.5.3, MLLR is performed under completely matched condition, but the difference is in the previous subsection, we used a separate adaptation set, but in this experiment, we used the test itself as the adaptation set. Experimental results are shown in Fig. 8.26. Again, PNCC shows improvements for all kinds of conditions, even though the difference between MFCC and PNCC is now reduced.

8.6 *Computational Complexity*

Table 8.1 provides estimates of the computational demands MFCC, PLP, and PNCC feature extraction. (The RASTA processing is not included in these tabulations.) As before we use the standard open source Sphinx code in `sphinx_fe` [83] for the implementation of MFCC, and the implementation in [30] for PLP. We assume that the window length is 25.6 ms and that the interval between successive windows is 10 ms. The sampling rate is assumed to be 16 kHz, and we use a 1024-pt FFT for each analysis frame.

It can be seen in Table 8.1 that because all three algorithms use 1024-point FFTs, the greatest difference from algorithm to algorithm in the amount of computation required is associated with the spectral integration component. Specifically, the triangular weighting used in the MFCC calculation encompasses a narrower range of frequencies than the trapezoids used in PLP processing, which is in turn considerably narrower than the gammatone filter shapes, and the amount of computation needed for spectral integration is directly proportional to the effective bandwidth of the channels. For this reason, as mentioned in Sec. 8.2.1, we limited the gammatone filter computation to those frequencies for which the filter transfer function is 0.5 percent or more of the maximum filter gain. In Table 8.1, for all spectral integration types, we considered filter portion whose magnitude is 0.5 or more of the maximum filter gain.

As can be seen in Table 8.1, PLP processing by this tabulation is about 32.9 percent more costly than baseline MFCC processing. PNCC processing is approximately 34.6 percent more

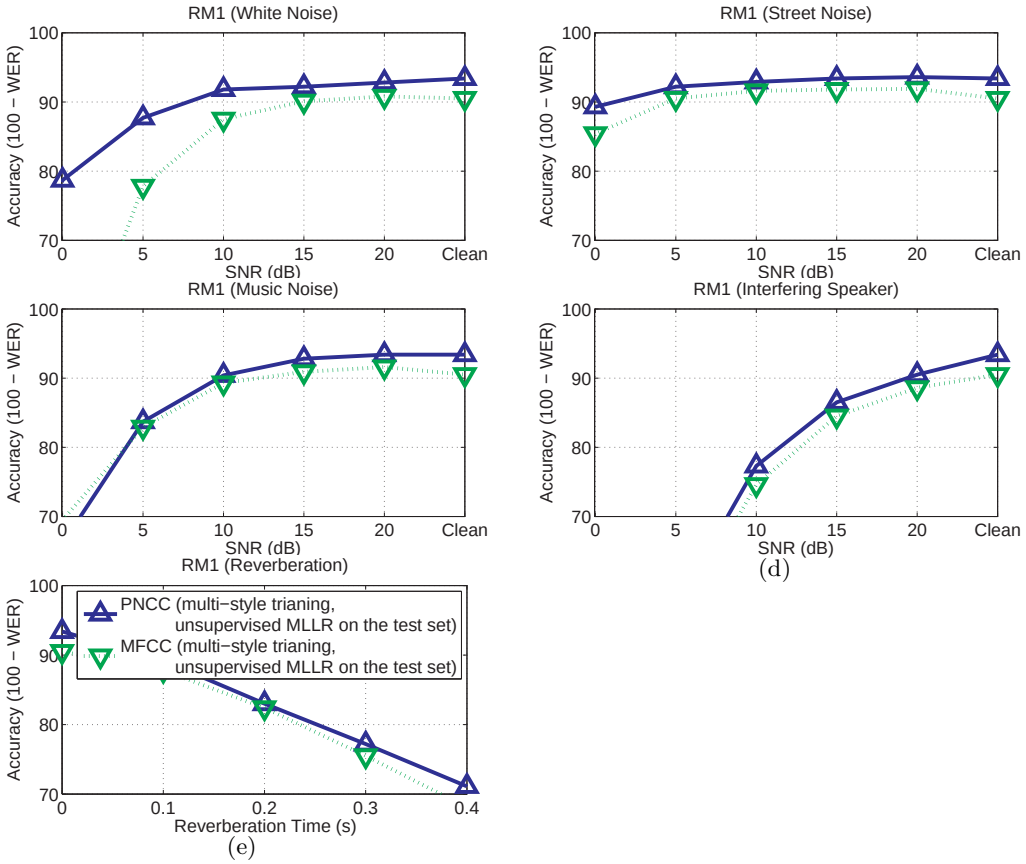

Fig. 8.26: Comparison of recognition accuracy for PNCC with processing using MFCC features using the RM1 corpus. Multi-style training set was used, and MLLR was directly performed on "the test set itself" speaker-by-speaker basis. MLLR was performed in the unsupervised mode. Environmental conditions are (a) white noise, (b) street noise, (c) background music, (d) interfering speech, and (e) reverberation.

costly than MFCC processing and 1.31 percent more costly than PLP processing.

8.7 Summary

In this chapter we introduce power-normalized cepstral coefficients (PNCC), which we characterize as a feature set that provides better recognition accuracy than MFCC and RASTA-PLP processing in the presence of common types of additive noise and reverberation. PNCC processing is motivated by the desire to develop computationally efficient feature extrac-

Tab. 8.1: Number of multiplications and divisions in each frame

Item	**MFCC**	**PLP**	**PNCC**
Pre-emphasis	410		410
Windowing	410	410	410
FFT	10240	10240	10240
Magnitude squared	512	512	512
Medium-time power calculation			40
Spectral integration	958	4955	4984
ANS filtering			200
Equal loudness pre-emphasis		512	
Temporal masking			120
Weight averaging			120
IDFT		504	
LPC and cepstral recursion		156	
DCT	480		480
Sum	13010	17289	17516

tion for automatic speech recognition that is based on a pragmatic abstraction of various attributes of auditory processing including the rate-level nonlinearity, temporal and spectral integration, and temporal masking. The processing also includes a component that imple-

ments suppression of various types of common additive noise. PNCC processing requires only about 33 percent more computation compared to MFCC.

Open Source MATLAB code for PNCC may be found at `http://www.cs.cmu.edu/~robust/archive/algorithms/PNCC_IEEETran`. The code in this directory was used for obtaining the results for this chapter.

9. COMPENSATION WITH 2 MICROPHONES

9.1 Introduction

Speech researchers have proposed many types of algorithms to enhance the noise robustness of speech recognition systems, and many of these algorithms have shown provided improvements in the presence of stationary noise (*e.g.* [12, 13, 9]). Nevertheless, improvement in non-stationary noise remains a difficult issue (*e.g.* [14]). In these environments, auditory processing (*e.g.* [37] [55]) and missing-feature-based approaches (*e.g.* [16]) are promising.

An alternative approach is signal separation based on analysis of differences in arrival time (*e.g.* [17, 18, 19]). It is well documented that the human binaural system has a remarkable ability to separate speech that arrives from different azimuths (*e.g.* [19] [84]). It has been observed that various types of cues are used to segregate the target signal from interfering sources. Motivated by these observations, many models and algorithms have been developed using inter-microphone time differences (ITDs), inter-microphone intensity difference (IIDs), inter-microphone phase differences (IPDs), and other cues (*e.g.* [17, 18, 85, 75]). IPD and ITD have been extensively used in binaural processing because this information can be easily obtained by spectral analysis (*e.g.* [85] [86] [46]). ITD can be estimated using either phase differences (*e.g.* [46]), cross-correlation (*e.g.* [87], [78]), or zero-crossings (*e.g.* [18]).

In many of the algorithms above, either binary or continuous "masks" are developed to indicate which time-frequency bins are dominated by the target source. Studies have shown that continuous-mask techniques provide better performance than the binary masking technique but they usually require that we know the exact location of the noise source (*e.g.* [18]). Binary masking techniques (*e.g.* [55]) might be more realistic for situations when multiple noise sources arise from all directions ("omnidirectional noise") but we still need to know which estimated source arrival anagle should serve as the threshold that determines

whether a particular time-frequency segment should be considered to be part of the desired target speech or part of the unwanted noise source. Typically this is performed by sorting the time-frequency bins according to ITD (either calculated directly or inferred from estimated IPD). In either case, performance depends on how the threshold ITD for selection is selected, and the optimal threshold depends on the configuration of the noise sources including their locations and strength. If the optimal ITD from a particular environment is applied to a somewhat different environment, the system performance will be degraded. In addition, the characteristics of the environment typically vary with time.

The Zero Crossing Amplitude Estimation (ZCAE) algorithm recently introduced by Park [18] is similar in some respects to earlier work by Srinivasan *et al.* [17]. These algorithms (and similar ones by other researchers) typically analyze incoming speech in bandpass channels and attempt to identify the subset of time-frequency components for which the ITD is close to the nominal ITD of the desired sound source (which is presumed to be known *a priori*). The signal to be recognized is reconstructed from only the subset of "good" time-frequency components. This selection of "good" components is frequently treated in the computational auditory scene analysis (CASA) literature as a multiplication of all components by a binary mask that is nonzero for only the desired signal components. Although ZCAE provides impressive performance even at low signal-to-noise ratios (SNRs), it is very computationally intensive, which makes it unsuitable for hand-held devices.

Our own work on signal separation is motivated by human binaural processing. Sound sources are localized and separated by the human binaural system primarily through the use of ITD information at low frequencies and IID information at higher frequencies, with the crossover point between these two mechanisms considered to be based on the physical distance between the two ears and the need to avoid spatial aliasing (which would occur when the ITD between two signals exceeds half a wavelength). In our work we focus on the use of ITD cues and avoid spatial aliasing by placing the two microphones closer together than occurs anatomically. When multiple sound sources are presented, it is generally assumed that humans attend to the desired signal by attending only to information at the ITD corresponding to the desired sound source.

The goals of the present paper are threefold. First, we would like to obtain improvements in word error rate (WER) for speech recognition systems that operate in real world envi-

ronments that include noise (possibly multiple noisy sources) and reverberation. For this purpose, we investigated into the effects of temporal resolution. We also perform channel weighting to enhance speech recognition accuracy in real-world environments. In addition, the performance of sound source separation system ITD heavily depends on the ITD threshold. In this work, we investigate into an efficient way of finding an appropriate ITD threshold blindly. Second, we also would like to develop a computationally efficient algorithm than can run in real time in embedded systems. In the present ZCAE algorithm much of the computation is taken up in the bandpass filtering operations. We found that computational cost could be significantly reduced by estimating the ITD through examination of the phase difference between the two sensors in the frequency domain. We describe in the sections below how the binary mask is obtained using frequency information. We also discuss the duration and shape of the analysis windows, which can contribute to further improvements in WER. Third, and most important, we describe a method by which the threshold ITD that separates time-frequency segments belonging to the target from the masker segments can be obtained automatically and adaptively, without any *a priori* knowledge of the location of the sound sources or the acoustics of the environment.

In many cases, we can assume knowledge of the location of the target source, but we don't have control of the number or locations of the noise sources. When target identification is obtained by a binary masked based on an ITD threshold, the value of that threshold is typically estimated from development test data. As noted above, the optimal ITD threshold itself will depend on the number of noise sources and their locations, both of which may be time-varying. If the azimuth of the noise source is very different from that of the target, a threshold that ITD is relatively far from that of the target may be helpful. On the other hand, if an interfering noise source is very close to the target and we use a similar ITD threshold, the system will also classify many components of the interfering signal as part of the target signal. If there is more than one noise source, or if the noise sources are moving, the problem becomes even more complicated.

In our approach, which is summarized in Fig. 9.2, we construct two complementary masks using a binary threshold. Using these two complementary masks, we obtain two different spectra: one for the target and the other for everything except for the target. From these spectra, we obtain the short-time power for the target and the interference. These power

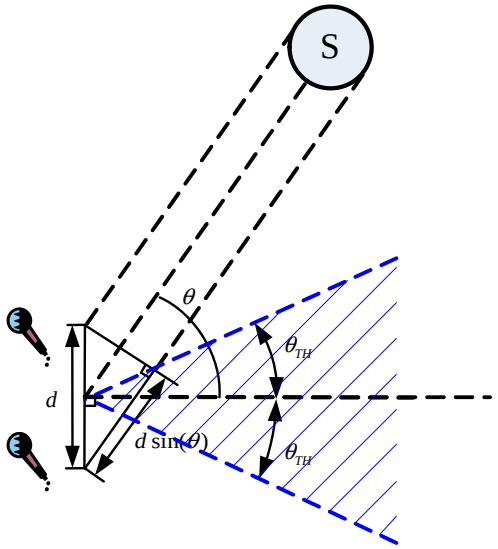

Fig. 9.1: Selection region for the binaural sound source separation system: if the location of a sound source is inside the shaded region, the sound source separation system assumes that it is the target. If the location of a sound source is outside this shaded region, then it is assumed to be arising from a nose source and is suppressed by the sound source separation system.

sequences are passed through a compressive nonlinearity. We compute the cross-correlation coefficient and normalized coefficient for the two resulting power sequences, and we obtain the ITD threshold by minimizing these coefficients.

The rest of the paper is organized as follows: in Sec. 9.2, we explain the entire system structure of the basic PDCW algorithm, including the estimation of the ITD from phase difference information and further improvements in speech recognition accuracy that are obtained through the use of a medium-time window and gammatone channel weighting. In Sec. 9.3 we explain the method by which we obtain the optimal ITD threshold through the construction of the complementary masks for speech and noise. We present experimental results in Section 10.2.

9.2 Structure of the PDCW-AUTO Algorithm

In this section, we explain the structure of our sound source separation system. While the detailed description below assumes a sampling rate of 16 kHz, this algorithm is easily modified to accommodate other sampling frequencies. Our processing approach crudely emulates human binaural processing. Our binaural sound source separation system is referred to as Phase Difference Channel Weighting (PDCW). If the automatic threshold selection algorithm is employed to obtain the target ITD threshold, as described in Sec. 9.3, we refer to the entire system as PDCW-AUTO. The block diagram of the PDCW-AUTO system is shown in Fig. 9.2. If we use a fixed ITD threshold at angle θ_{TH}, which might be empirically chosen, we refer to this system as PDCW-FIXED. We refer the system without the channel weighing to as the Phase Difference (PD) system. As in the case of PDCW, if we use the automatic threshold selection algorithm, this system is referred to as PD-AUTO. If a fixed threshold is used with PD, this algorithm is referred to as PD-FIXED.

The system first performs a short-time Fourier transform (STFT) which decomposes the two input signals in time and in frequency. We use Hamming windows of duration 75 ms with 37.5 ms between frames, and a DFT size of 2048. The reason for choosing this window length will be discussed in Sec. 9.2.3. The ITD is estimated indirectly by comparing the phase information from the two microphones at each frequency. The time-frequency mask identifying the subset of ITDs that are "close" to the ITD of the target speaker is identified using the ITD threshold selection algorithm which is explained in Sec. 9.3. To obtain better speech recognition accuracy in noisy environments, instead of directly applying the binary mask, we apply a gammatone channel weighting approach, Finally, the time domain signal is obtained using the overlap-add method.

9.2.1 Source Separation Using ITDs

In the binaural sound source separation system, we usually assume that we have *a priori* knowledge about the target location. This is a reasonable assumption, because we usually have control over the target. For example, if the target is a user holding a hand-held device equipped with two microphones, the user might be instructed to hold the device at a particular orientation relative to his or her mouth. In this paper, we assume that the target

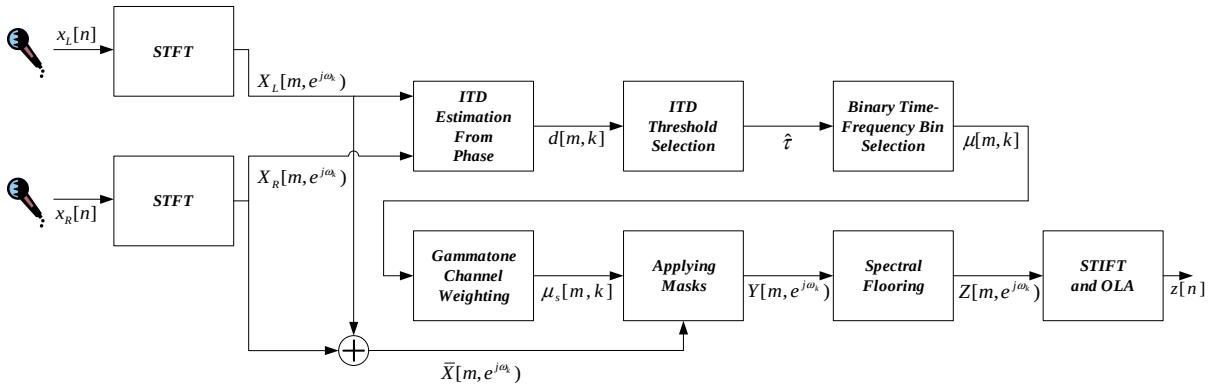

Fig. 9.2: Block diagram of a sound source separation system using the Phase Difference Channel Weighting (PDCW) algorithm and the automatic ITD threshold selection algorithm.

is located along the perpendicular bisector to the line connecting two microphones. Under this assumption, let us consider a selection area as shown in Fig. 9.1, which is defined by an angle θ_{TH}. If the sound source is determined to be inside the shaded region in this figure, then we assume that it is a target. As shown in Fig. 9.1, suppose that there is a sound source S along a line with angle θ. Then we can set up a decision criterion as follows:

$$\begin{cases} \text{Considered to be a target:} & |\theta| < \theta_{TH} \\ \text{Considered to be a noise source:} & |\theta| \geq \theta_{TH} \end{cases} \tag{9.1}$$

In Fig. 9.1, if the sound source is located along the line of angle θ, then using simple geometry, we find that the inter-microphone distance d_i is given by:

$$d_i = d\sin(\theta) \tag{9.2}$$

where d is the distance between two microphones. In the discrete-time domain, the inter-microphone time melay (ITD) (in units of discrete samples) is given by the following equation:

$$\tau = \frac{d\sin(\theta)}{c_0} f_s \tag{9.3}$$

where c_0 is the speed of sound and f_s is the sampling rate. Since d, c_0, and f_s are all fixed constants, θ is the only factor that determines the ITD τ. Hence, the decision criterion in

Eq. (9.1) can be expressed as follows:

$$\begin{cases} \text{considered to be a target:} & |\tau| < \tau_{TH} \\ \text{considered to be a noise source:} & |\tau| \geq \tau_{TH} \end{cases} \tag{9.4}$$

where $\tau_{TH} = \frac{d\sin(\theta_T H)}{c_0} f_s$. Thus, if we obtain a suitable ITD threshold using Eq. (9.4), we can make a binary decision to determine whether the source is in the shaded region in Fig. 9.1. In our sound source separation system the ITD is obtained for each-time frequency bin using phase information according to Eq. (9.4) is made for each-time frequency bin. This procedure will be explained in detail in Sec. 9.2.2.

9.2.2 Obtaining the ITD from phase information

In this subsection we review the procedure for obtaining the ITD from phase information (*e.g.* [46]). Let $x_L[n]$ and $x_R[n]$ be the signals from the left and right microphones, respectively. We assume that we know where the target source is located and, without loss of generality, we assume that it is placed along the perpendicular bisector of the line between two microphones, which means that its ITD is zero.

Suppose that the total number of interfering sources is S. Each source $s, 1 \leq s \leq S$ has an ITD of $tau_s[m,k]$ where m is the frame index and k is the frequency index. Note that both S and $tau_s[m,k]$ are unknown. We assume that $x_0[n]$ represents the target signal and that the notation $x_s[n], 1 \leq s \leq S$, represents signals from each interfering source received from the "left" microphone. In the case of signals from the "right" microphone, the target signal is still $x_0[n]$, but the interfering signals are delayed by $tau_s[m,k]$. Note that for the target signal $x_0[n]$, $d_0[m,k] = 0$ for all m and k by the above assumptions.

To perform spectral analysis, we obtain the following short-time signals by multiplication with a Hamming window $w[n]$:

$$x_L[n;m] = x_L[n - mL_{fp}]w[n] \tag{9.5a}$$

$$x_R[n;m] = x_R[n - mL_{fp}]w[n] \tag{9.5b}$$

$$\text{for } 0 \leq n \leq L_{fl} - 1$$

where m is the frame index, L_{fp} is the number of samples between frames, and L_{fl} is the frame length. The window $w[n]$ is a Hamming window with a length of L_{fl}. We use a 75-ms window length based on previous findings described in [46]. The short-time Fourier transforms of Eq. (9.5) can be represented as

$$X_L[m, e^{j\omega_k}) = \sum_{s=0}^{S} X_s[m, e^{j\omega_k}) \tag{9.6a}$$

$$X_R[m, e^{j\omega_k}) = \sum_{s=0}^{S} e^{-jw_k\tau_s[m,k]} X_s[m, e^{j\omega_k}) \tag{9.6b}$$

where $w_k = 2\pi k/N$ and N is the FFT size. We represent the strongest sound source for a specific time-frequency bin $[m, k]$ as $s^*[m, k]$. This leads to the following approximation:

$$X_L[m, e^{j\omega_k}) \approx X_{s^*[m,k]}[m, e^{-jw_k}) \tag{9.7a}$$

$$X_R[m, e^{j\omega_k}) \approx e^{-jw_k\tau_{s^*[m,k]}[m,k]} \times X_{s^*[m,k]}[m, e^{-jw_k}) \tag{9.7b}$$

Note that $s^*[m, k]$ may be either 0 (the target source) or $1 \le s \le S$ (any of the interfering sources). From Eq. (9.7), The ITD for a particular time-frequency bin $[m, k]$ is given by

$$|\tau_{s^*[m,k]}[m, k]| \approx \frac{1}{|w_k|} \min_r \Big| \angle X_R[m, e^{-jw_k}) - \angle X_L[m, e^{-jw_k}) - 2\pi r \Big| \qquad 0 \le k \le \frac{N}{2} \tag{9.8}$$

Thus, by examining whether the obtained ITD from Eq. (9.8) is within a certain range from the target ITD, we can make a simple binary decision concerning whether the time-frequency bin $[m, k]$ is likely to belong to the target speaker or not.

From here on we will use the notation $\tau[m, k]$ instead of $\tau_{s^*[m,k]}[m, k]$ for simplicity. From Eqs. (9.4) and (9.8), we obtain the mask for the target for τ_{TH} for $0 \le k \le N/2$:

$$\mu[m, k] = \begin{cases} 1, & \text{if } |\tau_{TH}[m, k]| \le \tau_{TH} \\ \delta, & \text{otherwise} \end{cases} \qquad 0 \le k \le \frac{N}{2} \tag{9.9}$$

In other words, we assume that time-frequency bins for which $|\tau(m,k)| < \tau_{TH}$ are presumed to belong to the target speaker, and that time-frequency bins for which$|\tau(m,k)| > \tau_{TH}$ belong to the noise source. We are presently using a value of 0.01 for the floor constant δ.

The mask $\mu[m,k]$ in Eq. (9.9) may be directly applied to $\bar{X}[m,e^{j\omega_k})$, the averaged signal spectrogram from the two microphones:

$$\bar{X}[m,e^{j\omega_k}) \;=\; \frac{1}{2}\left(X_L[m,e^{j\omega_k}) + X_R[m,e^{j\omega_k}\right) \tag{9.10}$$

The mask is applied by multiplying $\bar{X}[m,e^{j\omega_k})$ by the mask value in Eq. (9.9). As mentioned before, if we directly apply $\mu[m,k]$ to the spectrum, this approach is referred to as the Phase Difference (PD) approach. Even though the PD approach is able to separate sound sources, in some cases, the mask in Eq. (9.9) is too noisy to be employed directly. In Sec. 9.2.4 we discuss a channel weighting algorithm in detail that resolves this issue.

9.2.3 Temporal resolution

While the basic procedure described in Sec. 9.2.2 provides signals that are audibly separated, the mask estimates are generally too noisy to provide useful speech recognition accuracy. Figures 9.5(c) and 9.5(d) show the mask and the resynthesized speech that is obtained by directly applying the mask $\mu[m,k]$. As can be seen in these figures, there are a lot of artifacts in the spectrum of resynthesized speech that occur as a consequence of discontinuities in the mask. In this and the following subsection, we discuss the implementation of two methods that smooth the estimates over frequency and time.

In conventional speech coding and speech recognition systems, we generally use a length of approximately 20 to 30 ms for the Hamming window $w[n]$ in order to capture effectively the temporal fluctuations of speech signals. Nevertheless, longer observation durations are usually better for estimating environmental parameters as shown in our previous works (*e.g.* [36, 37, 35, 66, 55]). Using the configuration described in Sec. 10.2, we evaluated the effect of window length on recognition accuracy using the PD-FIXED structure described in Sec. 9.2.2. While we defer a detailed description of our experimental procedures to Sec. 10.2, we describe in Fig. 9.4(b) the results of a series of pilot experiments that describe the dependence of recognition accuracy on window length, obtained using the DARPA RM1 database. These results indicate that best performance is achieved with window length of

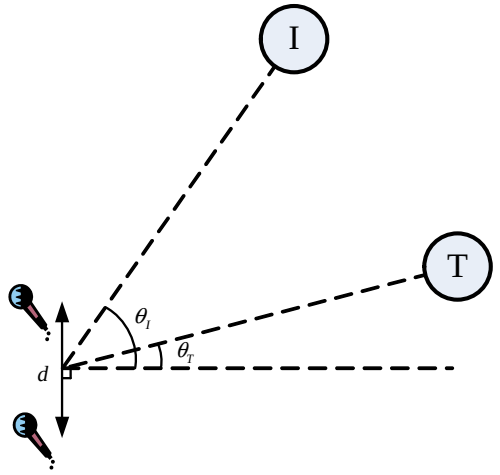

Fig. 9.3: The configuration for a single target (represented by T) and a single interfering source (represented by I).

about 75 ms. In the experiments described below we Hamming windows of duration 75 ms with 37.5 ms between successive frames.

9.2.4 Gammatone channel weighting and mask application

As noted above, the estimates produced by Eq. (9.9) are generally noisy and must be smoothed. To achieve smoothing along frequency, we use a gammatone weighting that functions in a similar fashion to that of the familiar triangular weighting in MFCC feature extraction. Specifically, we obtain the gammatone channel weighting coefficients $w[m, l]$ according to the following equation:

$$w[m,l] = \frac{\sum_{k=0}^{\frac{N}{2}} \mu[m,k] \left| \bar{X}[m; e^{j\omega k}) H_l(e^{j\omega k}) \right|}{\sum_{k=0}^{\frac{N}{2}} \left| \bar{X}[m; e^{j\omega k}) H_l(e^{j\omega k}) \right|} \tag{9.11}$$

where $\mu[m, k]$ is the original binary mask that is obtained using Eq. (9.9). With this weghting we effectively map the ITD for each of the 256 original frequencies to an ITD for what we refer to as one of $L = 40$ channels. Each of these channels is associated with H_i, the frequency response of one of a set of gammatone filters with center frequencies distributed according to the Equivalent Rectangular Bandwidth (ERB) scale [4].

The frequency response of the gammatone filterbank is shown in Fig. 9.6. In each channel

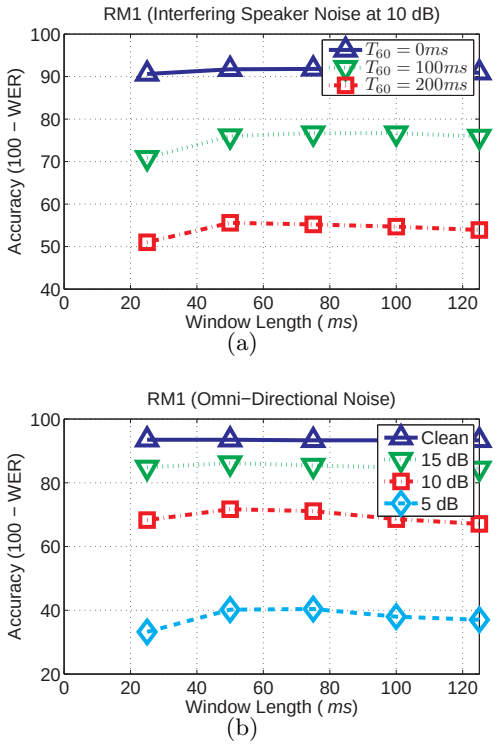

Fig. 9.4: The dependence of word recognition accuracy (100%-WER) on window length under different conditions: (a) interfering source at angle $\theta_I = 45°$. SIR 10 dB. (b) omnidirectional natural noise. In both case PD-FIXED is used with a threshold angle of $\theta_{TH} = 20°$.

the area under the squared transfer function is normalized to unity to satisfy the equation

$$\int_0^{8000} |H_l(f)|^2 df = 1 \tag{9.12}$$

where $H_l(f)$ is the frequency response of the l^{th} gammatone channel. To reduce the amount of computation, we modified the gammatone filter responses slightly by setting $H_l(f)$ equal to zero for all values of f for which the unmodified $H_l(f)$ would be less than 0.5 percent (corresponding to -46 dB) of its maximum value. Note that we are using exactly the same gammatone weigthing as in [64].

The final spectrum weighting is obtained using the gammatone mask μ_s

$$\mu_s[m,k] = \frac{\sum_{l=0}^{L-1} w[m,k] \left| H_l\left(e^{j\omega k}\right)\right|}{\sum_{l=0}^{L-1} \left|H_l\left(e^{j\omega k}\right)\right|} \qquad 0 \le k \le \frac{N}{2} \tag{9.13}$$

Examples of $\mu[m,k]$ in Eq. (9.9) and $\mu_s[m,k]$ in Eq. (9.13) are shown shown for a typical spectrum in Figs. 9.5(c) and 9.5(e), respectively, with an SNR of 0 dB as before. The reconstructed spectrum is given by:

$$\begin{aligned} Y[m,e^{j\omega k}) &= \max\{\mu_s[m,k],\eta\}\,\bar{X}[m,e^{j\omega k}) \\ & \qquad 0 \le k \le \frac{N}{2} \end{aligned} \tag{9.14}$$

where again we use $\eta = 0.01$ as in (9.9), and $\bar{X}[m,e^{j\omega k})$ is the averaged spectrum defined in Eq. (9.10).

In the discussion up to now we have considered spectral components for frequency indicies $0 \le k \le \frac{N}{2}$. For $\frac{N}{2}+1 \le k \le N-1$, we obtain $Y[m,e^{j\omega k})$ using the Hermition symmetry property of Fourier transforms of real time functions:

$$Y[m,e^{j\omega k}) = Y[m,e^{j\omega(N-k)}) \tag{9.15}$$

$$\angle Y[m,e^{j\omega k}) = -\angle Y[m,e^{j\omega(N-k)}) \tag{9.16}$$

9.2.5 Spectral flooring

In our previous work (*e.g.* [37] [35]), it has been frequently observed that an appropriate flooring helps in improving noise robustness. For this reason we also apply a flooring level to the spectrum, that is described by the equation:

$$Y_f = \delta_f \sqrt{\frac{1}{N_f N} \sum_{m=0}^{N_f-1} \sum_{k=0}^{N-1} |Y[m,e^{j\omega k})|^2} \tag{9.17}$$

where δ_f is the flooring coefficient, N_f is the number of frames in the utterance, N is the FFT size, and Y_f is the obtained threshold. We use a value of 0.01 for the flooring coefficient δ_f.

Using the flooring level Y_f, the floored spectrum $Z[m,e^{j\omega k}), 0 \le k \le N$ is obtained as follows:

$$|Z[m,e^{j\omega k})| = \max\{|Y[m,e^{j\omega k})|, Y_f\} \tag{9.18a}$$

$$\angle Z[m,e^{j\omega k}) = \angle Y[m,e^{j\omega k}) \tag{9.18b}$$

The above equations mean that the magnitude spectrum is floored by a minimum value of Y_f while the phase remains unchanged.

Using $Z[m, e^{j\omega k})$, speech is resynthesized using IFFT and OverLap Addition (OLA).

In Sec. 9.3, we discuss how to obtain the optimal threshold without prior knowledge about the noise sources.

9.3 Optimal ITD threshold selection using complementary masks

In the previous section we used a fixed ITD threshold to construct binary masks. Unfortunately, in a real-world environment we typically do not have control over the locations of the noise sources. It is reasonable to assume that the value of the ITD threshold will vary depending on the types and locations of the noise sources. In this section we discuss how to obtain an optimal threshold automatically without prior knowledge about the nature and locations of the noise sources. Before explaining our algorithm in great detail we will discuss the general dependence of speech recognition accuracy on the locations of the target and interfering sources.

9.3.1 Dependence of speech recognition accuracy on the locations of the target and interfering source

To examine the dependence of the optimal threshold on the interfering source location, let us consider the simulation configuration shown in Fig. 9.3. To simplify the discussion, we assume that there is a single single interfering source along the line of angle θ_I. As before, the distance between two microphones is 4 cm. In the first set of experiments we assumed that the target angle θ_T is zero. For the interfering source angle θ_I we used three different values (30°, 45°, and 75°). Signal-to-Interference Ratio (SIR) is assumed to be 0 dB and we assume that the room is anechoic. For speech recognition experiments, we used the configuration explained in Sec. 10.2.

Figure 9.7 describes the dependence of speech recognition accuracy on the threshold angle θ_{TH} and the interfering source angle θ_I. We use the PD-FIXED and PDCW-FIXED processing algorithms in Figs. 9.7(a) and 9.7(b), respectively. When the interfering source angle is θ_I, we obtain best speech recognition accuracy when θ_{TH} is roughly equal to or or slightly larger than $\theta_I/2$. When θ_{TH} is larger than θ_I, the system fails to separate the

sound sources, which is is reflected in very poor speech recognition accuracy. In another set of experiments we used natural omnidirectional stereo noises, but but maintaining the target angle $\theta_T = 0^\circ$ as before. Speech recognition results for this experiment are shown in Fig. 9.7, fixing the SNR at 5 dB and measuring recognition accuracy as a function of threshold angle θ_{TH}. In this experiment the best speech recognition accuracy is obtained at a much smaller value of θ_T. Figure 9.9 describes the dependence of recognition accuracy on SNR when the ITD threshold θ_{TH} is fixed at either 10° or 20°. As can been in the figure, the smaller threshold angle ($\theta_{TH} = 10^\circ$) is more helpful than in the case of single-speaker interference. As before, a greater difference in recognition accuracy provided by the PD-FIXED and PDCW-FIXED algorithms is observed when the smaller threshold angle θ_{TH} is 10° is used.

In the previous discussion we observed that the optimal threshold angle $\hat{\theta}_{TH}$ depends heavily on the noise source location. In a real environment there is one more complication. Up to now we have assumed that the target is placed at $\theta_T = 0^\circ$. Even if we had control over the target location there may still be some errors in estimating or controlling it. For example, even if a user of a hand-held device is instructed to hold the device at a particular angle, there is no way of ensuring that the user could accomplish this task perfectly. To understand the impact of this issue we implemented an additional experiment using the configuration shown in Fig. 9.7, but we changing the target angles to be one of the five values (-20°, -10°, 0°, 10°, and 20°) while holding the interfering angle fixed at $\theta_I = 45^\circ$. Results of this experiment are shown in Fig. 9.10(a). From the figure we observe that if we choose a very small value for θ_{TH}, then the sound source separation system is not very robust with respect to mis-estimation of the target angle.

In this section, we observed that the optimal ITD threshold depends on both the target angle θ_T, the interfering source angle θ_I, and the noise type. If the ITD threshold is inappropriately selected, speech recognition accuracy becomes significantly degraded. From this observation we conclude that we need to develop an automatic threshold selection algorithm which obtains a suitable value for the ITD threshold without prior knowledge about the noise sources, and that at the same time is robust with respect to error in the location of the target angle θ_T.

9.3.2 The optimal ITD threshold algorithm

The algorithm we introduce in this section is based on two complementary binary masks, one that identifies time-frequency components that are believed to belong to the target signal and a second that identifies the components that belong to the interfering signals (*i.e.* everything except the target signal). These masks are used to construct two different spectra corresponding to the power sequences representing the target and the interfering sources. We apply a compressive nonlinearity to these power sequences, and define the threshold to be the separating ITD threshold that minimizes the cross-correlation between these two output sequences (after the nonlinearity).

Computation is performed in discrete fashion, considering a set $\mathcal{T}$ of a finite number of possible ITD threshold candidates. The set $\mathcal{T}$ is defined by the following minimum and maximum values of the ITD threshold.

$$\tau_{min} = \frac{dsin(\theta_{TH,min})}{c} f_s \tag{9.19a}$$

$$\tau_{max} = \frac{dsin(\theta_{TH,max})}{c} f_s \tag{9.19b}$$

where d is the distance between two microphones, c is the speed of sound, and f_s is the sampling rate as in Eq. (9.3). $\theta_{TH,min}$ and $\theta_{TH,max}$ are the minimum and the maximum values of the threshold angle. In the present implementation, we use values of $\theta_{TH,min} = 5^\circ$ and $\theta_{TH,max} = 45^\circ$. We use a set of candidate ITD thresholds $\mathcal{T}$ that consist of the 20 linearly-spaced values of θ_{TH} that lie between $\theta_{TH,min}$ and $\theta_{TH,max}$.

We determine which element of this set is the most appropriate ITD threshold by performing an exhaustive search over the set T. Let us consider one element of this set, τ_0. Using this procedure, we obtain the target spectrum $X_T[m, e^{j\omega_k}|\tau_0), \quad 0 \leq k \leq \frac{N}{2}$ as shown below:

$$X_T[m, e^{j\omega_k}|\tau_0) = \bar{X}[m, e^{j\omega_k})\mu_T[m, e^{j\omega_k}) \tag{9.20}$$

In the above equation we explicitly include τ_0 to show that the masked spectrum depends on the ITD threshold. Using this spectrum $X_T[m, e^{j\omega_k})$, we obtain the target power and the power of the interfering sources. Since everything which is not the target is considered to

be an interfering source, the power associated with the target and interfering sources can be obtained by the following equations:

$$P_T[m|\tau_0) = \sum_{k=0}^{N-1} \left| X_T[m, e^{j\omega_k}) \right|^2 \tag{9.21a}$$

$$P_I[m|\tau_0) = P_{tot}[m] - P_T[m|\tau_0) \tag{9.21b}$$

where $P_{tot}[m]$ is the total power at frame index m, given by:

$$P_{tot}[m] = \sum_{k=0}^{N-1} \left| \bar{X}[m, e^{j\omega_k}) \right|^2. \tag{9.22}$$

A compressive nonlinearity is invoked because the power signals in Eq. (9.21) have a very large dynamic range. A compressive nonlinearity will reduce the dynamic range, and it may be considered to represent a transformation that yields the perceived loudness of the sound. While many nonlinearities have been proposed to characterize the relationship between signal intensity and perceived loudness [88] we chose the following power-law nonlinearity motivated by previous work (*e.g.* [55][35][64]):

$$R_T[m|\tau_0) = P_T[m|\tau_0)^{a_0} \tag{9.23a}$$

$$R_I[m|\tau_0) = P_I[m|\tau_0)^{a_0} \tag{9.23b}$$

where $a_0 = 1/15$ is the power coefficient as in [35, 64].

In general, the optimal ITD threshold is determined by identifying the value of τ_0 that minimizes the cross-correlation between the signals $R_T[m|\tau_0)$ and $R_I[m|\tau_0)$ from Eq. (9.23), but there are several plausible ways of computing this cross-correlation. The first method considered, which was used in an earlier paper [67], is based on the cross-correlation coefficient of the signals in Eq. (9.23):

$$\rho_{T,I}(\tau_0) = \frac{\frac{1}{N}\sum_{m=1}^{M} R_T[m|\tau_0) R_I[m|\tau_0) - \mu_{R_T}\mu_{R_I}}{\sigma_{R_T}\sigma_{R_I}} \tag{9.24}$$

where μ_{R_1} and μ_{R_2}, and σ_{R_T} and σ_{R_I}, are the means and standard deviations of $R_T[m|\tau_0)$ and $R_I[m|\tau_0)$, respectively. (This statistic is also known as the Pearson product-moment correlation or the normalized covariance.)

The optimal ITD threshold τ_0 is selected to minimize the absolute value of the cross-correlation coefficient:

$$\hat{\tau}_1 = \arg\min_{\tau_0} |\rho_{T,I}(\tau_0)| \tag{9.25}$$

We refer to this approach as the "Type-I" statistic, and it has provided good speech recognition accuracy as shown in Fig. 9.11, especially at low SNRs such as 0 or 5 dB. Nevertheless, at moderate SNRs such 10 or 15 dB, the speech recognition accuracies obtained using "Type-I" processing are even worse than those obtained using the PDCW-FIXED algorithm. PDCW-AUTO processing using the Type-I statistic also provides poor recognition accuracy in the presence of omnidirectional natural noise, as shown in Fig. 9.12. We have also found in pilot studies that the cross-correlation-based statistic in Eq. 9.24 is not a helpful measure in situations where there is a single interfering source with power that is comparable to that of the target, or where there are multiple interfering sources.

To address this problem, we consider a second related statistic, the normalized correlation:

$$r_{T,I}(\tau_0) = \frac{\frac{1}{N}\sum_{m=1}^{M} R_T[m|\tau_0)R_I[m|\tau_0)}{\sigma_{R_T}\sigma_{R_I}} \tag{9.26}$$

$$\hat{\tau}_2 = \arg\min_{\tau_0} |r_{T,I}(\tau_0)| \tag{9.27}$$

We refer to implementations of PD-AUTO or PDCW-AUTO using $\hat{\tau}_2$ as "Type-II" systems.

The final ITD threshold $\hat{\tau}_3$ is obtained easily by calculating the minimum of τ_1 and τ_2 as shown below:

$$\hat{\tau}_3 = \min(\hat{\tau}_1, \hat{\tau}_2) \tag{9.28}$$

We refer to implementations of PD-AUTO or PDCW-AUTO using $\hat{\tau}_3$ as "Type-III" systems. As can be seen in Figs. 9.11 and 9.12, systems using the "Type-III" stastistic consistently provide recognition accuracy that is similar to or better than that obtained using either the "Type-I" or "Type-II" approaches. For these reasons we adopt "Type-3" processing as our default approach, and if the threshold type of a PD-AUTO or PD-AUTO system is not mentioned explicitly, the reader should assume that a Type-III threshold statistic is used.

In this section we present experimental results using the PDCW-AUTO algorithm described in this paper. To evaluate the effectiveness of the automatic ITD threshold selection algorithm and the channel weighting, we compare the PDCW-AUTO system to the PDCW-FIXED and PD-AUTO systems. We also compare our approach with an earlier state-of-the-art technique, the ZCAE algorithm described above [18]. The ZCAE algorithm is implemented with binary masking for the present comparisons because the better-performing continuous-masking implementation requires that there should be only one interfering source with a known location, which is an unrealistic requirement in many cases. As we have done previously (*e.g.* [19] [89]), we convert the gammatone filters to a zero-phase form in order to impose identical group delay on each channel. The impulse responses of these filters $h_l(t)$ are obtained by the following equation:

$$h_l(t) = h_{g,l}(t) * h_{g,l}(-t) \tag{9.29}$$

where l is the channel index and $h_{g,l}(t)$ is the original gammatone response. While this approach compensates for the difference in group delay from channel to channel, it also causes the magnitude response to become squared, which results in bandwidth reduction. To compensate for this, we intentionally double the bandwidths of the original gammatone filters at the outset.

In all speech recognition experiments described in this paper we perform feature extraction using the version of MFCC processing implemented in `sphinx_fe` in `sphinxbase 0.4.1`. For acoustic model training, we used `SphinxTrain 1.0`, and decoding was performed suing the `CMU Sphinx 3.8`, all of which are readily available in Open Source form [83]. We used subsets of 1600 utterances and 600 utterances, respectively, from the DARPA Resource Management (RM1) database for training and testing. A bigram language model was used in all experiments. In all experiments, we used feature vectors of length of 39 including delta and delta-delta features. We assumed that the distance between two microphones is 4 cm.

We conducted three different sets of experiments in this section. The first two sets of experiments, described in Secs. 9.4.1 and 9.4.2, involve simulated reverberant environments in which the target speaker is masked by a single interfering speaker (in Sec. 9.4.1) or by three interfering speakers (in Sec. 9.4.2). The reverberation simulations were accomplished

using the *Room Impulse Response* open source software package [53] based on the image method [82]. The third set of experiments, decscribed in Sec. 9.4.3, involve the use of additive omnidirectional noise recorded in several natural environments.

9.4.1 Experimental results using a single interfering speaker

In the experiments in this section we assume a room of dimensions 5 x 4 x 3 m, with microphones that are located at the center of the room, as in Fig. 9.3. Both the target and interfering sources are 1.5 m away from the microphone. For the fixed-ITD threshold systems such as PDCW-FIXED, we used the threshold angle $\theta_{TH} = 20^\circ$ based on the experimental results described in Sec. 9.3.1. We conducted three different kinds of experiments using this scenario.

In the first set of experiments we assume that the target is located along the perpendicular bisector of the line between two microphones, which means $\theta_T = 0^\circ$. We assume that the interfering source is located at $\theta_I = 30^\circ$. We repeated the experiments by changing the SIR and reverberation time. As shown in Fig. 9.13(a), in the absence of reverberation at 0-dB SIR, both the fixed ITD system and the automatic-ITD system provide comparable performance. If reverberation is present, however, the automatic-ITD system PDCW-AUTO provides substantially better performance than the PDCW-FIXED signal separation system.

In the second set of the experiments we changed the location of the interfering speaker while maintaining the SIR at 0 dB. As shown in Fig. 9.14, even if the SIR is the same as in the calibration environment, the performance of the fixed-ITD threshold system becomes significantly degraded if the actual interfering speaker location is different from the location used in the calibration environment. The PDCW-AUTO selection system provides recognition results that are much more robust with respect to the locations of the interfering sources. In this figure we observe that as the interfering speaker moves toward the target, the fixed-ITD threshold PD system provides increased word error rate. We repeated this experiment with different reverberation times. As shown in Fig. 9.14, the automatic-threshold-selection algorithm provides consistently better recognition accuracy than the fixed threshold system, as expected.

In the third set of the experiments we conducted experiments in which the target angle

θ_T was varied from -30° to 30°. In our previous work ([46, 78]), we assumed that the target is located along the bisector of the line between two microphones, but this is not always the case in a real environment, and θ_T may not be exactly zero. As shown in Fig. 9.15, if the target angle $|\theta_T|$ becomes larger than 20° the PDCW-FIXED and ZCAE algoroithms fail to separate the sound sources, resulting in poor performance. In contrast (and as expected), both the PDCW-AUTO and PD-AUTO provide substantial robustness against deviation in the target direction.

9.4.2 Experimental results using three randomly-positioned interfering speakers

In the second set of experiments we assumed the same room dimension (5 x 4 x 3 m) as the experiments in Sec. 9.4.1. We also still assume that the distance between two microphones is 4 cm, the target speaker is located along the perpendicular bisector to the line connecting two microphones, and the distance between the target and microphones is 1.5 m. In this experiment we assume that the target speech is masked by three interfering speakers, as shown in Fig. 9.16. The location of each interfering speaker is uniformly distributed on the plane at the same height as the microphones. Thus, in some cases, the interfering speaker might be in a similar direction as the target. The locations of the interfering speakers is changed for each utterance in the test set. Experimental results for this configuration are shown in Fig. 9.17. The general tendencies of the experimental results is similar to those in Fig. 9.13 where there is a single interfering speaker along the direction of $\theta_I = 30^\circ$. The greatest difference between the results in Figs. 9.17 and 9.13 is that the improvement in performance observed when the automatic threshold ITD selection of the PDCW-AUTO and PD-AUTO algorithms is invoked becomes much more profound with three randomly-placed interfering speakers than with only a single interfering speaker.

We believe that if there are multiple noise sources, the mask pattern becomes more varied. In this case, the use of a fixed narrow ITD threshold as in PD-FIXED introduces artifacts, which harm speech recognition accuracy. As will be seen in Sec. 9.4.3, the same tendency is observed in the presence of omnidirectional natural interfering sources as well.

9.4.3 Experimental results using natural omnidirectional noise

In the third set of experiments, we still assume that the distance between the two microphones is the same as before (4 cm), but we added noise recorded with two microphones in real environments such as a public market, a food court, a city street and a bus stop. These real noise sources are at all locations around the two microphones, and the signals from these recordings are digitally added to clean speech from the test set of the RM database. As before, all fixed-ITD-threshold algorithms use a threshold value of $\theta_{TH} = 20^\circ$. Fig. 9.18 shows speech recognition accuracy for this configuration. Again we observe that the PDCW-AUTO algorithm provides the best performance by a significant margin, while the PDCW-FIXED, PD-AUTO, and ZCAE show similar performance to each other. As previously seen in Fig. 9.8, in the case of omnidirectional natural noise, an ITD threshold θ_{TH} smaller than 20° results in better speech recognition accuracy. If we use the automatic ITD threshold algorithm, then it chooses a better ITD threshold than $\theta_{TH} = 20^\circ$ that is used in the PDCW-FIXED or PD-FIXED algorithms.

9.5 Computational Complexity

We profiled the run times of implementations in C of the PDCW-FIXED and ZCAE algorithms on two machines. The PDCW-FIXED algorithms ran in only 9.03% of the time required to run the ZCAE algorithm on an 8-CPU Xeon E5450 3-GHz system, and in only 9.68% of the time to run the ZCAE algorithm on an embedded system with an ARM11 667-Mhz processor using a vector floating point unit. The major reason for the speedup is that in ZCAE the signal must be passed through a bank of 40 filters while PDCW-FIXED requires only two FFTs and one IFFT for each feature frame. The PDCW-AUTO algorithm requires more computation than the PDCW-FIXED algorithm, but it still requires much less computation than ZCAE.

9.6 Summary

In this work, we present a speech separation algorithm, PDCW, based on inter-microphone time delay that is inferred from phase information. The algorithm uses gammatone channel

weighting and medium-duration analysis windows. While the use of channel weighing and longer analysis windows does not provide substantial improvement in recognition accuracy when there is only one interfering speaker in the absence of reverberation, this approach does provide significant improvement for more realistic environmental conditions where speech is degraded by reverberation or by the presence of multiple interfering speakers. This PDCW approach also provides significant improvements for noise sources recorded in natural environments as well.

We also developed an algorithm that blindly determines the ITD threshold that is used for sound source separation by minimizing the cross-correlation between spectral regions belong to the putative target and masker components after nonlinear compression. The combination of the PDCW algorithm and the automatic threshold selection is referred to as the PDCW-AUTO algorithm. We conducted experiments in various configurations, and we observed that PDCW-AUTO provides significant improvement in speech recognition accuracy for speech in various types of interfering noise sources and reverberation, compared to state-of-the-art algorithms that rely on a fixed ITD threshold. The use of the automatic ITD threshold selection is particularly helpful in the presence of multiple interfering sources or reverberation, or when the location of the target source is not estimated properly.

The PDCW and PDCW-AUTO algorithms are also more computationally efficient than the other algorithms to which they are compared, all of which obtain inferior recognition accuracy compared to PDCW.

9.7 Open Source Software

An open source implementation of the version of PDCW-AUTO used for the calculations in this paper is available at `http://www.cs.cmu.edu/~robust/archive/AUTO_PDCW`. While the PDCW algorithm itself is not patent protected, a US patent has been applied for the automatic ITD threshold selection algorithm [68]

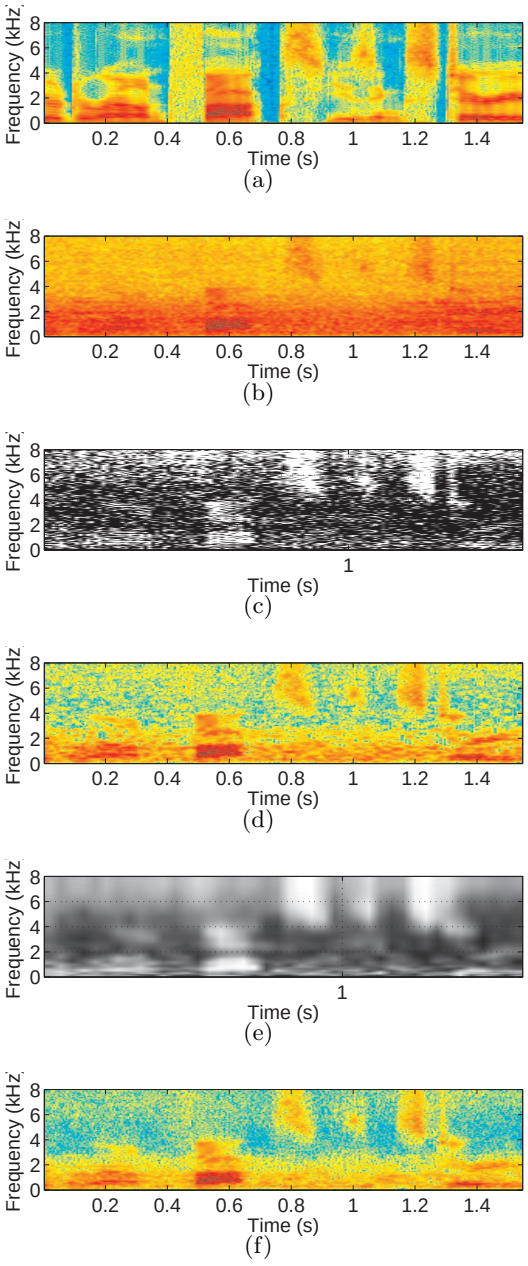

Fig. 9.5: Sample spectrograms illustrating the effects of PDCW processing. (a) original clean speech, (b) noise-corrupted speech (0-dB omnidirectional natural noise), (c) the time-frequency mask $\mu[m,k]$ in Eq. (9.9) with windows of 25-ms length, (d) enhanced speech using $\mu[m,k]$ (PD), (e) the time-frequency mask obtained with Eq. (9.9) using windows of 75-ms length, (f) enhanced speech using $\mu_s[m,k]$ (PDCW).

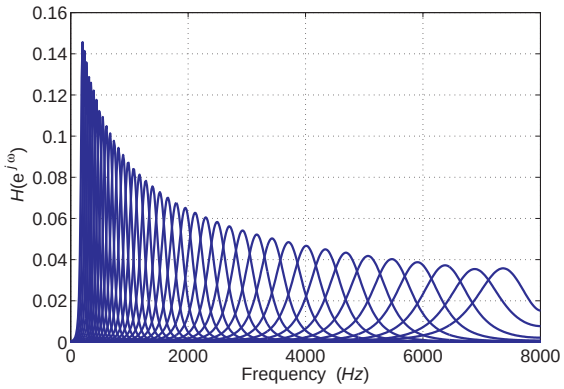

Fig. 9.6: The frequency response of a gammatone filterbank with each area of the squared frequency response normalized to be unity. Characteristic frequencies are uniformly spaced between 200 and 8000 Hz according to the Equivalent Rectangular Bandwidth (ERB) scale [4].

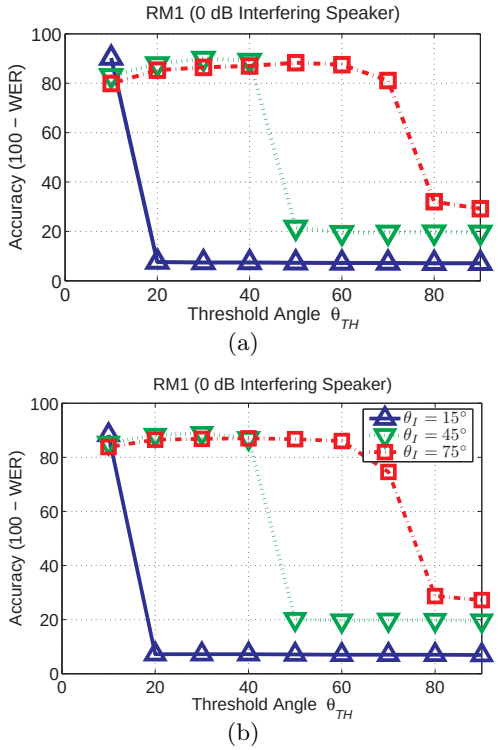

Fig. 9.7: The dependence of word recognition accuracy on the threshold angle θ_{TH} and the location of the interfering source θ_I using PD-FIXED, and (b) PDCW-FIXED. The target is assumed to be located along the perpendicular bisector of the line between two microphones ($\theta_T = 0°$).

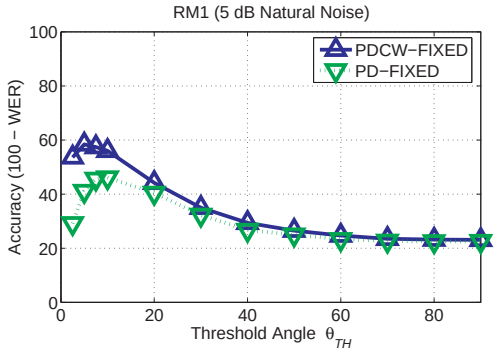

Fig. 9.8: The dependence of word recognition accuracy on the threshold angle θ_{TH} in the presence of natural omnidirectional noise. The target is assumed to be located along the perpendicular bisector of the line between the two microphones ($\theta_T = 0°$).

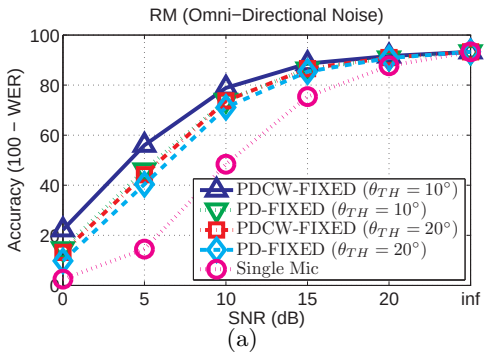

Fig. 9.9: The dependence of word recognition accuracy on SNR in the presence of natural omnidirectional real-world noise, using different values of the threshold angle θ_{TH}. Results were obtained using the PDCW-FIXED algorithm.

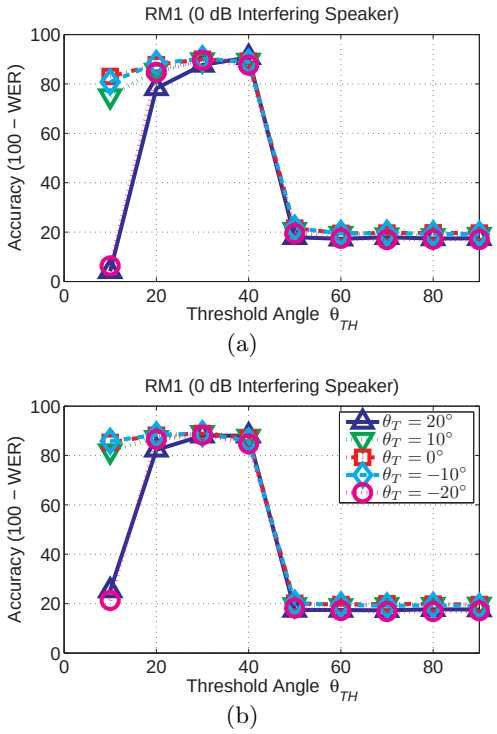

Fig. 9.10: The dependence of word recognition accuracy on the threshold angle θ_{TH} and the location of the target source θ_T using (a) the PD-FIXED, and (b) the PDCW-FIXED algorithms.

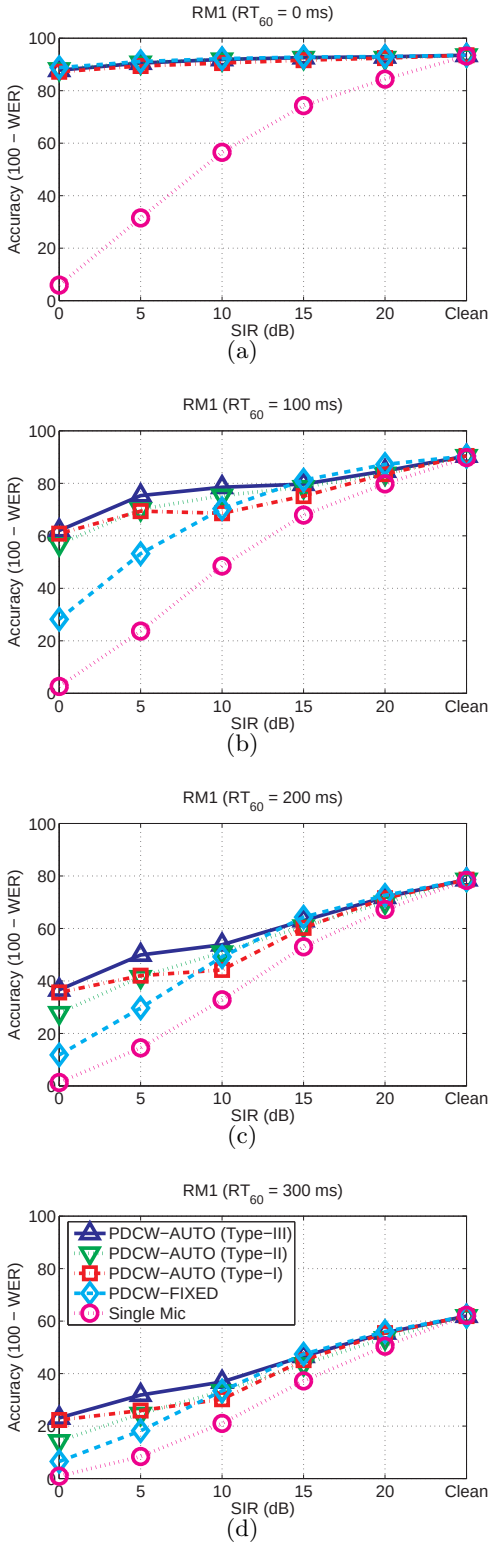

Fig. 9.11: Comparison of recognition accuracy using the DARPA RM database for speech corrupted by an interfering speaker located at 30 degrees at different reverberation times: (a) 0 ms, (b) 100 ms, (c) 200 ms, and (d) 300 ms.

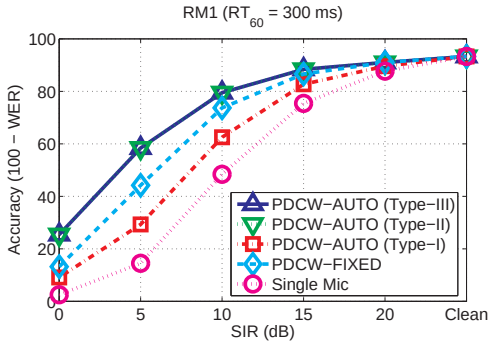

Fig. 9.12: Speech recognition accuracy obtained using different algorithms in the presence of natural real-world noise. Noise was recorded in real environments with real two-microphone hardware in locations such as a public market, a food court, a city street, and a bus stop with background babble. This noise was digitally added to the clean test set.

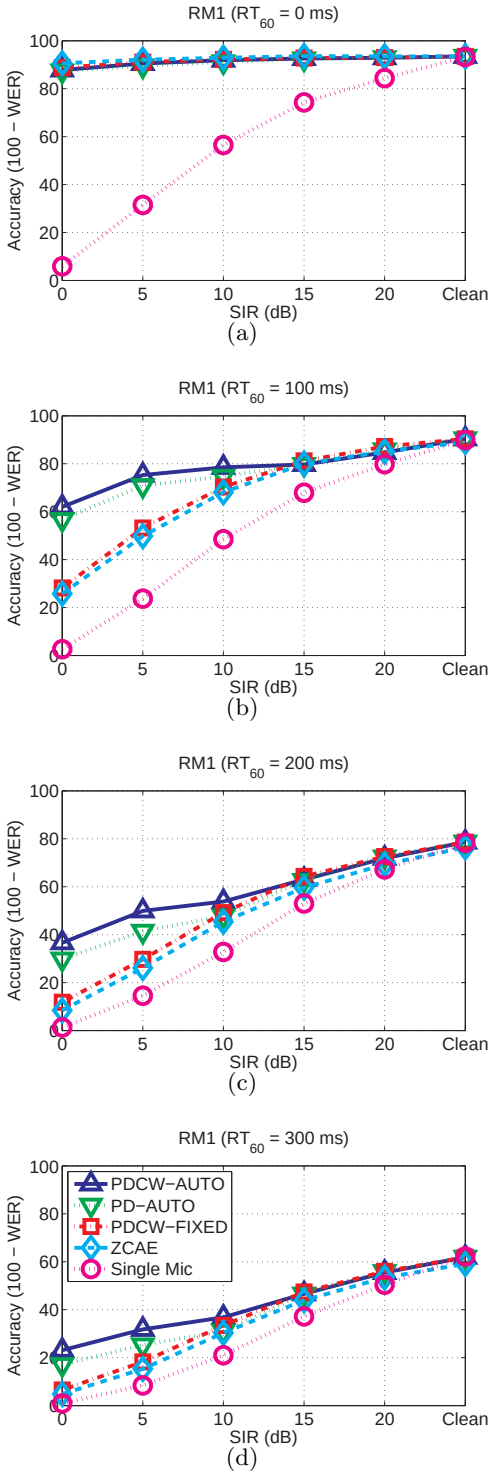

Fig. 9.13: Comparison of recognition accuracy for the DARPA RM database corrupted by an interfering speaker located at 30 degrees at different reverberation times: (a) 0 ms, (b) 100 ms, (c) 200 ms, and (d) 300 ms.

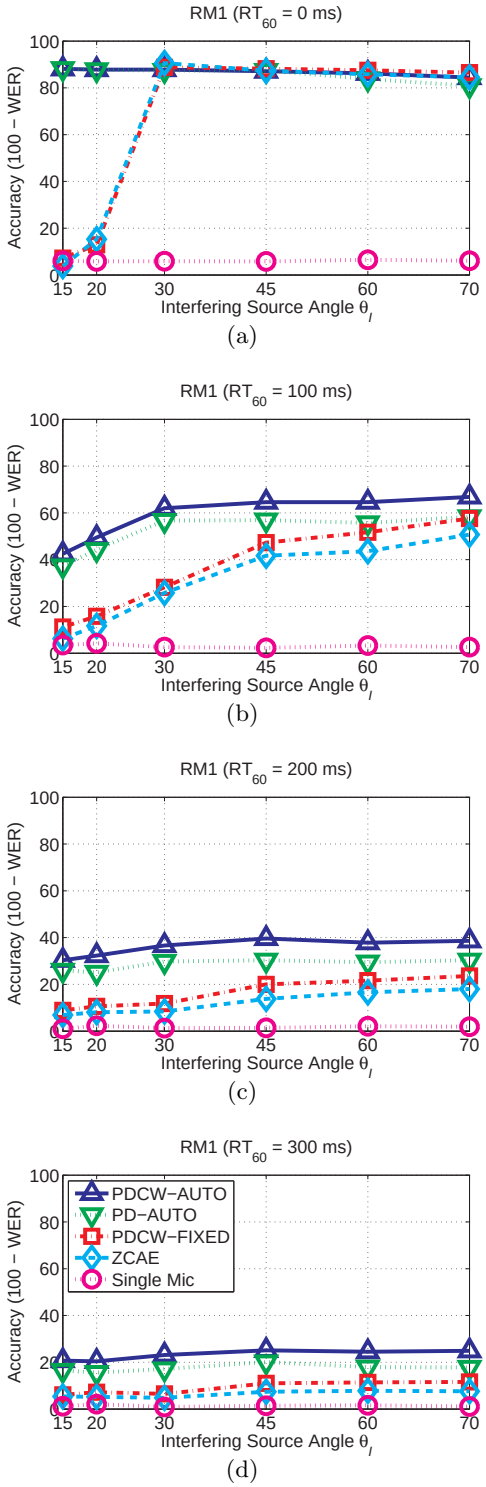

Fig. 9.14: Comparison of recognition accuracy for the DARPA RM database corrupted by an interfering speaker at different locations in a simulated room with different reverberation times: (a) 0 ms, (b) 100 ms, (c) 200 ms, and (d) 300 ms. The *signal-to-interference ratio* (SIR) is fixed at 0 dB.

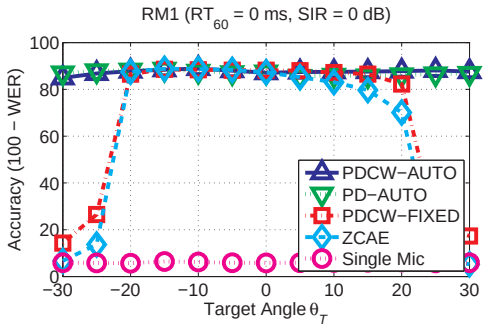

Fig. 9.15: Comparison of recognition accuracy for the DARPA RM database corrupted by an interfering speaker located at 45 degrees ($\theta_I = 45°$) in an anechoic room. The SIR is fixed at 0 dB. The target angle θ_T is varied from $-30°$ to $30°$

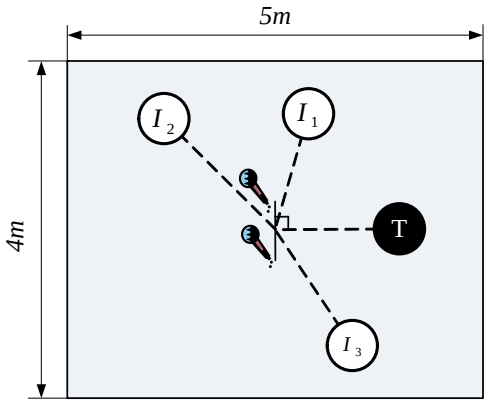

Fig. 9.16: The experimental configuration using three interfering speakers. The target speaker is represented by T, and the interfering speakers are represented by I_1, I_2, and I_3, respectively. The locations of the interfering speakers are random for each utterance.

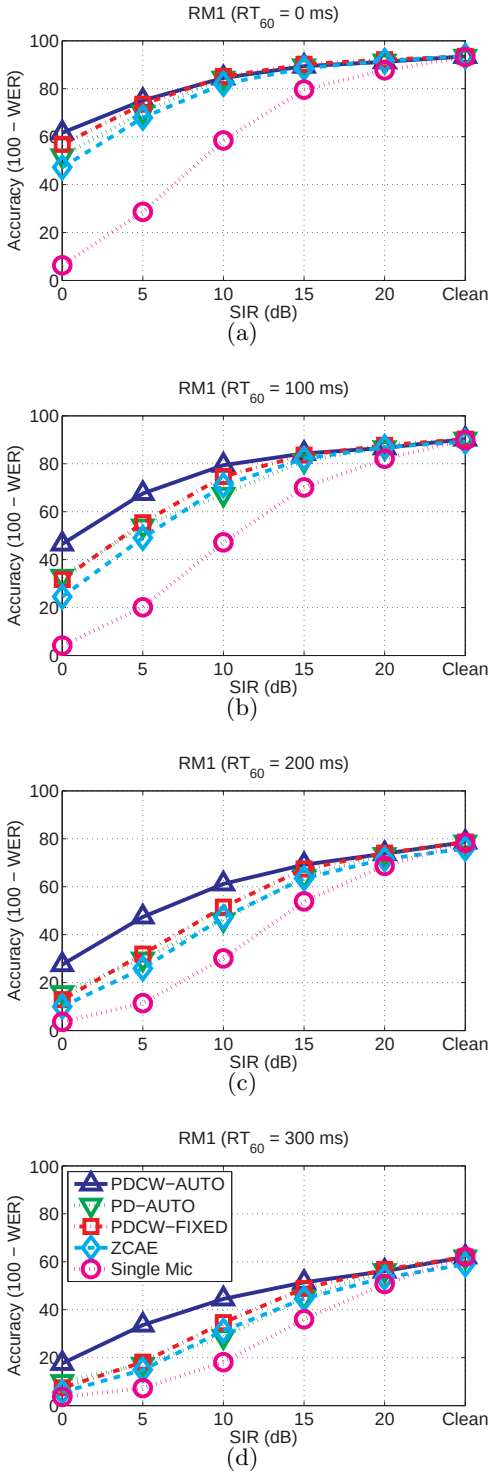

Fig. 9.17: Comparison of recognition accuracy for the DARPA RM database corrupted by three interfering speakers that are randomly placed in a simulated room with different reverberation times: (a) 0 ms, (b) 100 ms, (c) 200 ms, and (d) 300 ms.

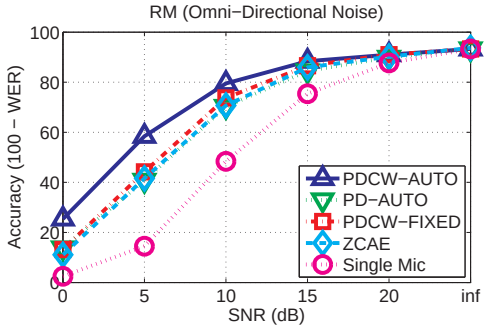

Fig. 9.18: Speech recognition accuracy using different algorithms in the presence of natural real-world noise. Noise was recorded in real environments with real two-microphone hardware in locations such as a public market, a food court, a city street, and a bus stop with background babble. This noise was digitally added to the clean test set.

10. COMBINATION OF SPATIAL AND TEMPORAL MASKS

In this study we combine the use of a newly-developed form of single-microphone temporal masking that has proved to be very effective in reverberant environments with a new type of spatial masking that is both simple to implement and effective in noise. We evaluate the effectiveness of this combination of spatial and temporal masking (STM) in a variety of degraded acoustical environments.

10.1 Signal separation using spatial and temporal masks

10.1.1 Structure of the STM system

The structure of our sound source separation system, which crudely models some of the processing in the peripheral auditory system and brainstem, is shown in Fig. 10.1. Signals from the two microphones are processed by a bank of 40 modified gammatone filters [57] with the center frequencies of the filters linearly spaced according to Equivalent Rectangular Bandwidth (ERB) [4] between 100 Hz and 8000 Hz, using the implementation in Slaney's

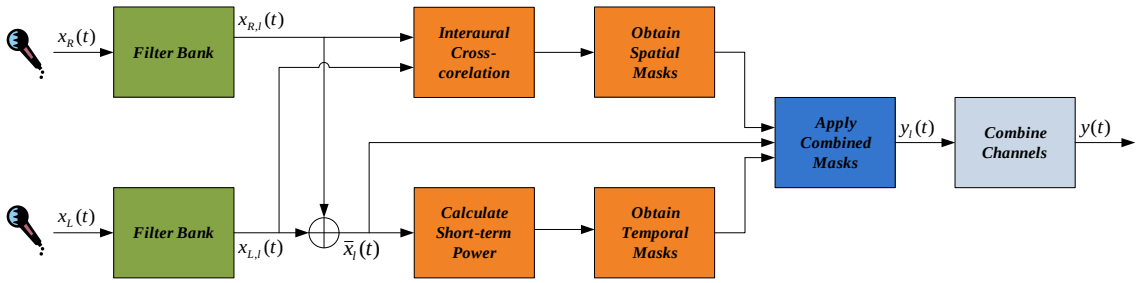

Fig. 10.1: The block diagram of the sound source separation system using spatial and temporal masks (STM).

Auditory Toolbox [47]. As we have done previously (*e.g.* [19]), we convert the gammatone filters to a zero-phase form in order to impose identical group delay on each channel. The impulse responses of these filters $h_l(t)$ are obtained by computing the autocorrelation function of the original filter response:

$$h_l(t) = h_{g,l}(t) * h_{g,l}(-t) \tag{10.1}$$

where l is the channel index and $h_{g,l}(t)$ is the original gammatone response. While this approach compensates for the difference in group delay from channel to channel, it also causes the magnitude response to become squared, which results in bandwidth reduction. To compensate for this, we intentionally double the bandwidths of the original gammatone filters at the outset. We obtain binary spatial masks by calculating the normalized cross-correlation coefficient and comparing its value to a pre-determined threshold value, as described in detail in Sec. 10.1.2. Along with the spatial masks, we also generate binary temporal masks. This is accomplished by calculating the short-time power for each time-frequency bin and comparing this value to a short-time average value that had been obtained by IIR lowpass filtering, as described in detail in Sec. 10.1.3. We obtain the final masks by combining these temporal masks and spatial masks as described in Sec. 10.1.4. To resynthesize speech, we combine the signals from each channel:

$$y(t) = \sum_{l=0}^{L-1} y_l(t) \tag{10.2}$$

where L is the number of channels (40 at present), and $y_l(t)$ is the signal from in each channel l after applying the masks. $y(t)$ is the final output of the system.

10.1.2 Spatial mask generation using normalized cross-correlation

In this section, we describe the construction of the binary masks using normalized cross-correlation. In our previous research (*e.g.* [46] [67]), which is also described in Chaps. 7 and 9 in this thesis, we have frequently observed that an analysis window that is longer than the conventional window of about 25 ms typically used for speech recognition, is more effective in noise-robustness algorithms. Hence, we use a window length of 50 ms with 10 ms between analysis frames as in [66] for the present study. We define the normalized correlation $\rho(t_0, l)$

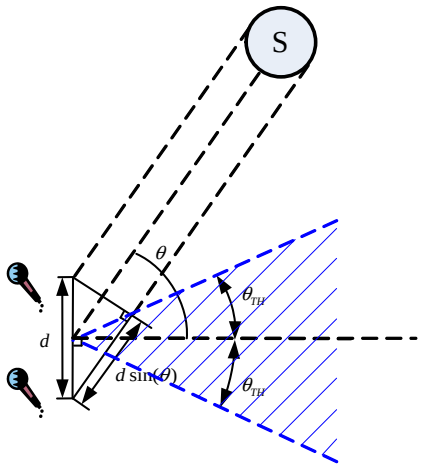

Fig. 10.2: Selection region for a binaural sound source separation system: if the location of the sound source is determined to be inside the shaded region, we assume that the signal is from the target.

for the time-frequency segment that begins at $t = t_0$ and belongs to frequency bin l to be

$$\rho(t_0, l) = \frac{\frac{1}{T_0}\int_{T_0} x_{R,l}(t;t_0)x_{L,l}(t;t_0)dt}{\sqrt{\frac{1}{T_0}\int_{T_0}(x_{R,l}(t;t_0))^2dt}\sqrt{\frac{1}{T_0}\int_{T_0}(x_{L,l}(t;t_0))^2dt}} \tag{10.3}$$

where l is the channel index, $x_{R,l}(t;t_0)$ and $x_{L,l}(t;t_0)$ are the short-time signals from the left and right microphones after Hamming windowing, and t_0 refers to the time when each frame begins. If $x_{R,l}(t;t_0) = x_{L,l}(t;t_0)$, then $\rho(t_0, l) = 1$ in Eq. (10.3). $|\rho(t_0, l)|$ is less than one otherwise. We note that this statistic is widely used in models of binaural processing (*e.g.* [87]), although typically for different reasons.

Let us consider the case where the sound source is located at an angle θ as shown in Fig. 10.2. We assume that the desired signal is along the perpendicular bisector of the line between the two mics. This leads to a decision criterion in which a component is accepted if the putative location of the sound source for a particular time-frequency segment is within the shaded region (*i.e.* $|\theta| < \theta_{TH}$), and rejected otherwise. If the bandwidth of a filter is sufficiently narrow, then the signal after filtering can be approximated by the sinusoidal function [18]:

$$x_{R,l}(t;t_0) = A\sin(\omega_0 t) \tag{10.4a}$$

$$x_{L,l}(t;t_0) = A\sin(\omega_0(t-\tau)) \tag{10.4b}$$

where ω_0 is the center frequency of channel l. By inserting (10.4) into (10.3), we obtain the following simple relation:

$$\rho(t_0, l) = \cos(\omega_0 \tau) = \cos\left(\omega_0 d \sin(\theta)\right) \tag{10.5}$$

As long as the microphone distance is small enough to avoid spatial aliasing, Eq. (10.5) implies that $\rho(t_0, l)$ decreases monotonically as $|\theta|$ increases. Thus, we can retain a given time-frequency bin if $\rho(t_0, l) \geq \rho_{TH}$ and reject it if $\rho(t_0, l) < \rho_{TH}$, where for each channel ρ_{TH} is given by $\rho_{TH} = \cos\left(\omega_0 d \sin(\theta_{TH})\right)$.

10.1.3 Temporal mask generation using modified SSF processing

Our temporal masking generation approach is based on a modification of the SSF approach introduced in [55] and elaborated in Chap. 7 of this thesis. First, we obtain the short-time power for each time-frequency bin:

$$P_l[m] = \int_{T_0}^{T_0+T_f} \left(\bar{x}_l(t; t_0)\right)^2 dt \tag{10.6}$$

where $\bar{x}(t; t_0)$ is the short-time average of $x_{L,l}(t; t_0)$ and $x_{R,l}(t; t_0)$, which are the Hamming-windowed signals at time t_0 in Channel l from the two microphones. The index of the frame that begins at $t = t_0$ is m, and T_f is the window length. As in [55], we obtain a first-order IIR lowpassed output:

$$Q_l[m] = \lambda Q_l[m-1] + (1-\lambda) P_l[m] \tag{10.7}$$

where λ is the forgetting factor which determines the bandwidth of the filter. Based on a pilot study in [55], we use the value $\lambda = 0.04$. If the power in a specific time-frequency bin is less than the lowpassed output developed in Eq. (10.7), we assume that it is masked by temporal masking, so we accept a time-frequency segment if $P_l[m] \geq Q_l[m]$ and reject it if $P_l[m] < Q_l[m]$.

10.1.4 Application of spatial and temporal masks

If a specific time-frequency bin is accepted by both the spatial and temporal masking processes described Secs. 10.1.2 and 10.1.3, then this time-frequency bin is selected; otherwise

it is rejected. Binary masking is applied according to the following equation:

$$\begin{cases} y_l(t,t_0) = \bar{x}_l(t,t_0) & \texttt{if selected} \\ y_l(t,t_0) = \mu \bar{x}_l(t,t_0) & \texttt{if rejected} \end{cases} \tag{10.8}$$

where μ is a scaling factor that suppresses (but does not annihilate) the signal in the rejected time-frequency bin. The signal $y_l(t,t_0)$ is the short-time signal in each time-freqeuency bin after applying the mask, and $\bar{x}_l(t,t_0)$ is the average of the left and right short-time signals starting at time t_0 in the l^{th} channel.

In previous work (*e.g.* [35]) and in Chaps. 4 and 5 of this thesis we have observed that power flooring (*i.e.* the imposition of a minimum power) is very important for robust speech recognition. In this study as in others the choice of the power flooring coefficient μ is important to prevent power from approaching zero too closely. In pilot work we have found the following scaling factor to be useful:

$$\mu = \sqrt{\frac{\delta\left(\frac{1}{T}\int_0^T \bar{x}_l^2(t)dt\right)}{\frac{1}{T_f}\int_0^{T_f} \bar{x}_l^2(t;t_0)dt}} \tag{10.9}$$

In the above equation, $\bar{x}_l(t)$ is the average of the left and right signals for this l^{th} channel for this utterance, T is the length of the entire utterance, and T_f is the frame length (which is 50 ms in our implementation). The above equation means that the input power of time-frequency bins that are rejected is reduced to δ times the average power $\left(\frac{1}{T}\int_0^T \bar{x}_l^2(t)dt\right)$ in this channel. We have found that $\delta = 0.01$ is a suitable coefficient.

10.2 Experimental results and Conclusions

In this section we present experimental results using the STM algorithm described in this paper. We assume a room of dimensions 5 x 4 x 3 m, with two microphones located at the center of the room. The distance between two microphones is 4 cm. The target is located 1.5 m away from the microphones along the perpendicular bisector of the line connecting two microphones, and an interfering speaker is located at 30 degrees to one side and 1.5 m away from the microphones. The target and interfering signals are digitally added after simulating reverberation effects using the *RIR* software package. We used `sphinx_fe`

included in `sphinxbase 0.4.1` for speech feature extraction, `SphinxTrain_1.0` for speech recognition training, and `Sphinx3.8` for decoding, all of which are readily available in Open Source form. We used a subset of 1600 utterances from the DARPA Resource Management (RM1) training data for acoustic modeling and a subset of 600 utterances from the RM test data for evaluation.

Figure 10.3 describes the contributions of spatial masking and temporal masking in the environments considered. We note that while temporal masking scheme must be applied both to training and test data to avoid increased WER due to environmental mismatch, the system performance is essential the same regardless of whether spatial masking is used in training or no. This is not surprising, as spatial masking should routinely accept all components of clean speech from the target location.

In the anechoic environment (Fig. 10.3(a)), we observe that improvement with the STM algorithm is mostly provided by spatial masking, with temporal masking providing only marginal improvement. If T_{60} is increased to 200 ms (Fig. 10.3(b)), or 500 ms (Fig. 10.3(c)), however, we observe that the contribution of temporal masking becomes quite substantial. When both noise and reverberation are present, the contributions of temporal and spatial maskings are complementary and synergistic.

Figure 10.4 compares speech recognition accuracy for several algorithms including the STM system described in this paper, PDCW [46], and ZCAE in [18], all using binary masking. To compare the performance of these different systems in the same condition, we used a threshold angle of 15 degrees with all algorithms to obtain binary masks. In the anechoic condition (Fig. 10.4(a)), the STM approach provided slightly worse performance than the PDCW and ZCAE algorithms. In reverberant environments , the STM system provides the best results by a very large margin, and the PDCW results were slightly better than the corresponding ZCAE results. In terms of computational cost, PDCW requires the least amount of computation due to its efficient frequency-domain implementation, while STM and ZCAE require much more computation because they involve time-domain filtering.

The MATLAB code for the STM algorithm can be found at `http://www.cs.cmu.edu/~robust/archive/algorithms/SMT_ICASSP2011/`.

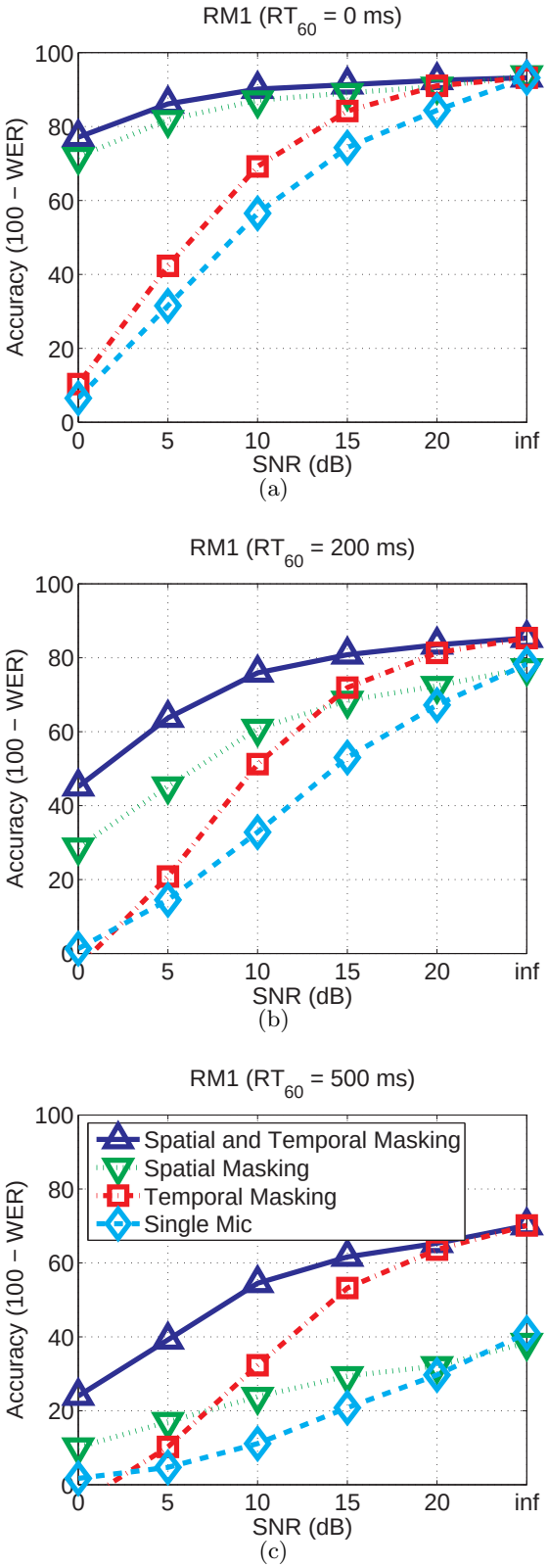

Fig. 10.3: Dependence of recognition accuracy on the type of mask used (spatial *vs* temporal) for speech from the DARPA RM corpus corrupted by an interfering speaker located at 30 degrees, using various simulated reverberation times: (a) 0 ms (b) 200 ms (c) 500 ms.

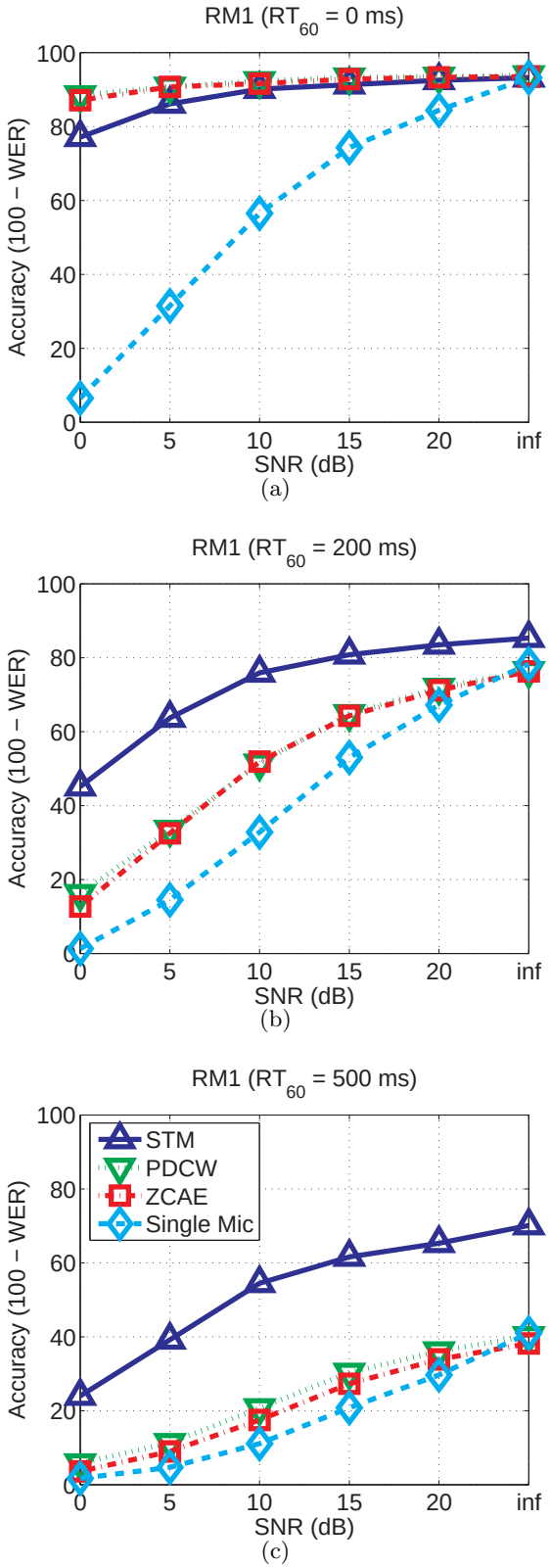

Fig. 10.4: Comparison of recognition accuracy using the STM, PDCW, and ZCAE algorithms for the DARPA RM database corrupted by an interfering speaker located at 30 degrees, using various simulated reverberation times: (a) 0 ms (b) 200 ms (c) 500 ms.

11. SUMMARY AND CONCLUSIONS

11.1 Introduction

In this thesis we have sought to improve speech recognition accuracy in noisy environment using techniques motivated by auditory processing. Our goal in this thesis has been to enhance robustness, especially in more difficult environments such as the presence of non-stationary noise, reverberation, or interfering speakers using techniques motivated by auditory processing.

After the introduction of Hidden Markov Models (HMMs), speech recognition accuracy has significantly improved. However, if the test environment is different from the training environment, then speech recognition accuracy is seriously degraded. Conventional approaches for enhancing robustness against environmental mismatch are usually based on statistical feature normalization. For example, it is usually assumed that the mean of each element of features is the same for all utterances. One can also make a similar assumption for variance as well as mean. Cepstral Mean Normalization (CMN) and Mean Variance Normalization (MVN) are based on these assumptions. Alternatively, one can assume that the histogram is the same for all utterances. As mentioned in Chapter 2, these techniques are somewhat sensitive to the lengths of silences that precede and follow each utterance, but if they are combined with a reliable Voice Activity Detector (VAD), they usually proivide significant performance improvement, especially for stationary noise. Another type of approaches is based on the development of a statistical model (usually represented by a Gaussian Mixture Model, GMM) of log spectra or features obtained from a clean training set. The effects of noise and/or reverberation can be represented analytically by a nonlinear environmental function. Using the statistical model obtained from training data, the environmental function is developed and then applied in inverse fashion to eliminate the effects of noise. These

kinds of approaches are typically successful for stationary noise, but they do not provide substantial improvements in non-stationary noise or reverberation.

In this thesis we first attempt to understand why the human auditory system demonstrates such a remarkable ability to understand speech, even in non-stationary noise or under reverberation. We then apply our insights toward the development of signal processing that improves speech recognition accuracy. We focus especially on the characteristics of nonlinearity, temporal masking, temporal resolution, and modulation filtering that are observed in peripheral auditory processing, as well as the sound separation based on timing differences to multiple sensors (or ears) and the precedence effect, both of which are essential components of binaural hearing.

11.2 Summary of Findings and Contributions of This Thesis

We found that there are a number of auditory phenomena which have not been exploited at all or which have been inefficiently exploited in conventional feature extraction and/or noise compensation algorithms. Some examples include the rate-intensity nonlinearity, onset enhancement, and temporal masking. Our conclusion is that if we make use of a more faithful model of human auditory processing, we can obtain improvements under unmatched conditions (when the system is trained on clean speech and deployed in a degraded environment). Unfortunately, detailed modeling of the human auditory system is prohibitive, since the models are too complicated and impractical for real-time applications. Thus, in our work, we have attempted to make develop simple mathematical models that are motivated by human auditory processing. Our objective is building simple models which can be useful for real applications, so we also put emphasis on online processing and computational cost as well. Our contributions are summarized in this Section.

First, we observe that the logarithmic nonlinearity employed in baseline MFCC processing is not very robust in the presence of additive noise. The reason is that the logarithmic nonlinearity does not include an auditory threshold as discussed in Chapter 4. If the short-time power in a particular time-frequency bin is below the auditory threshold level for human listeners, the signal effectively should be considered to represent a silence segment, regardless of the actual power level. In contrast with a logarithmic nonlinearity, small power differences

in the inaudible range (power below the threshold level) can greatly affect the feature values. This is especially true in situations in which the power in a certain time-frequency bin approaches zero, as the logarithmic output approaches negative infinity. For these small-power regions, even very small changes in the input power level will produce very large changes in the output of the nonlinearity, which results in vulnerability to additive noise.

While the human auditory nonlinearity does not have this problem because it includes a threshold, the rate-intensity function is highly nonlinear and not so suitable for automatic speech recognition applications. Because of this we adopted a simplified nonlinearity that is based on the power function. From an MMSE approximation to the human rate-intensity curve, we obtained a power-function exponent between 1/10 and 1/15. As shown in experimental results in Chapter 4, this range also shows good balance in terms of trade offs between performance in clean speech and robustness in noise. In our proposed feature extraction procedure known as Power Normalized Cepstral Coefficients (PNCC), we use an exponent of 1/15. As shown in Chapter 8, PNCC processing provides recognition accuracy that is as good as or better than that obtained with MFCC processing in clean speech, while obtaining much better speech recognition accuracy than MFCC processing in noisy environments.

Small Power Boosting (SPB), discussed in Chapter 5, is another approach based on this observation. As mentioned above, for these small power regions, even for a very small change in the input power level, there is a very big change in the output of the nonlinearity. Because this is the case, we can enhance robustness by systematically removing all small-power regions. The SPB approach results in a slight degradation of speech recognition accuracy for clean speech, but it provides superior performance especially in the case of background music.

We discuss in Chapter 6 the PPDN algorithm, which reconstructs degraded speech signals based on an equalization of the probability distribution that characterizes the power coefficients.

In addition, we also observe that in Chapter 7 onset enhancement plays an important role in enhancing robustness especially in reverberant environments. Neurophysiological measurements of the response of individual auditory-nerve fibers in mammals indicate that the onset rate is much greater than the sustained rate, and it does not exhibit saturation. In reverberant environments the effects of reverberation generally have more impact on the

trailing portion than the onset portion of the response to sound. Thus, we understand that emphasizing the onset and suppressing the trailing portion is helpful in reverberant environments, and this is the concept that is the basis for the SSF algorithm.

While temporal masking is in some sense similar to onset enhancement, they are not exactly the same. In case of onset enhancement we provide a relative emphasis to the onset portions (or a relative de-emphasis to the trailing portions). Temporal masking, in contrast, refers to the diminished perception of smaller peaks of short-time power after a sufficiently large peak in sound pressure. We also developed a simple mathematical model that captures this phenomenon. The application of temporal masking also provided improvements of speech recognition in reverberation and in the presence of interfering speakers.

We also observed that temporal resolution plays an important role in robust speech recognition. For human listeners it is well known that we largely ignore slowly-varying spectral components. If we try to remove such slowly-varying components, it is better to use a longer-duration analysis window than then the shorter-duration window that has been typically been used in speech analysis. This poses a challenge in that a longer-duration window is best for estimating the characteristics of the slowly-varying noise components, while a shorter window is best for analyzing the speech itself, which varies more rapidly. We solved this problem through the use of a novel two-stage window system, which was realized either using the Medium-duration Analysis Synthesis (MAS) approach or the Medium-duration-window Running Average (MRA) approach. This two-stage window length system has been incorporated into many algorithms such as Power Normalized Cepstral Coefficients (PNCC), Power-function-based Power Distribution Normalization (PPDN), Phase Difference Channel Weighting (PDCW), etc.

As noted in the paragraph above, the human auditory systems pays less attention to slowly-varying components. Motivated by this, researchers have developed various types of approaches referred to as modulation spectrum analysis, based on filtering of the envelopes of the signal that emerges from each of a bank of bandpass filters. We propose a new technique along these lines that is based on nonlinear asymmetric filtering. The asymmetric filter has the ability to track the lower-level envelope, which is especially useful in compensating for slowly-varying noise components. The algorithm also uses medium-duration windows for better temporal resolution, and applies the filtering before the nonlinearity to facilitate the

removal of additive noise.

All of the major fundamental insights that are developed in Chapters 3 to 6 are integrated into a practical integrated feature extraction scheme called power-normalized cepstral coefficients (PNCC) that are computationally efficient and that provide better recognition accuracy than MFCC and PLP features, as well as several popular noise compensation algorithms.

All of the approaches above are based on single-channel (or monaural) processing of sound. It is also well known that the human auditory system makes use of differences of timing information at low frequency to separate sound sources that arrive from different azimuths. Motivated by binaural hearing phenomena, we developed an efficient sound source separation algorithm called PDCW, which is described in Chapter 9. In this approach we calculate the inter-microphone time delay (ITD) from phase difference information in the frequency domain, and reconstruct an estimate of the target signal using only those time-frequency segments that are believed to have ITDs that are consistent with the direction of the target source. We make use of a smoothed frequency-weighting scheme based on the gammatone frequency response that provides better recognition accuracy than the direct use of binary masks for each frequency index.

An important parameter in the PDCW algorithm is the threshold ITD that is the basis for decisions about which time-frequency components are considered to belong to the target signal, and the optimal value of this threshold is a complex function of the locations of the target and interfering sources, the SNR, and amount of reverberation in the environment. We propose a novel and very successful algorithm to identify the optimal ITD threshold blindly, by exploiting the cross correlation between the power from the target segments and the other segments, passing both through a compressive nonlinearity. This approach, when combined with PDCW, is called PDCW-AUTO and is discussed in detail in Chapter 9.

Finally, in Chapter 10 we discuss the advantages that can be obtained by combining masks that are developed using temporal and spatial considerations.

11.3 Suggestions for Further Research

In this thesis we considered a number of aspects of human auditory processing, but still there are other attributes that remain to be considered. For example, the only type of masking considered was temporal masking. It is quite likely that appropriate consideration of other types of masking such as two-tone suppression could provide additional improvements in recognition accuracy.

In PDCW algorithm we calculated the ITD in the frequency domain for reasons motivated by computational efficiency. This approach should be compared with the estimation of ITDs using a correlation-based approach, which is closer to actual human binaural processing.

Finally, our work has all been based on the use of a fixed rate-level nonlinearity. It may well be the case that a time-varying nonlinearity could provide superior performance. In addition, it may be worthwhile to consider the incorporation of a time-varying filter bandwidth (such as the one used in the auditory-nerve model of Zhang and Carney).

BIBLIOGRAPHY

[1] M. G. Heinz, X. Zhang, I. C. Bruce, and L. H. Carney, "Auditory-nerve model for predicting performance limits of normal and impaired listeners," *Acoustics Research Letters Online*, vol. 2, no. 3, pp. 91–96, July 2001.

[2] H. G. Hirsch, P. Meyer , and H. W. Ruehl, "Improved speech recognition using high-pass filtering of subband envelopes," in *EUROSPEECH '91*, Sept. 1991, pp. 413–416.

[3] H. Hermansky and N. Morgan, "RASTA processing of speech," *IEEE. Trans. Speech Audio Process.*, vol. 2, no. 4, pp. 578–589, Oct. 1994.

[4] B. C. J. Moore and B. R. Glasberg, "A revision of Zwicker's loudness model," *Acustica - Acta Acustica*, vol. 82, pp. 335–345, 1996.

[5] B. Atal, "Effectiveness of linear prediction characteristics of the speech wave for automatic speaker identification and verification," *Journal of the Acoustical Society of America*, vol. 55, pp. 1304–1312, 1974.

[6] X. Huang, A. Acero, H-W Won, *Spoken Language Processing: A Guide to Theory, Algorithm, and System Development.* Upper Saddle River, NJ: Prentice Hall, 2001.

[7] P. Pujol, D. Macho, and C. Nadeu, "On real-time mean-and-variance normalization of speech recognition features," in *IEEE Int. Conf. Acoust., Speech and Signal Processing*, vol. 1, May 2006, pp. 773–776.

[8] Y. Obuchi,N. Hataoka, and R. M. Stern, "Normalization of time-derivative parameters for robust speech recognition in small devices," *IEICE Transactions on Information and Systems*, vol. 87-D, no. 4, pp. 1004–1011, Apr. 2004.

[9] A. Acero and R. M. Stern, "Environmental Robustness in Automatic Speech Recognition," in *Proc. IEEE Int. Conf. Acoust., Speech, Signal Processing (Albuquerque, NM)*, vol. 2, Apr. 1990, pp. 849–852.

[10] P. J. Moreno, B. Raj, and R. M. Stern, "A vector Taylor series approach for environment-independent speech recognition," in *IEEE Int. Conf. Acoust., Speech and Signal Processing*, May. 1996, pp. 733–736.

[11] S. F. Boll, "Suppression of acoustic noise in speech using spectral subtraction," *IEEE Trans. Acoust., Speech and Signal Processing*, vol. 27, no. 2, pp. 113–120, Apr. 1979.

[12] R. Singh, R. M. Stern, and B. Raj, "Signal and feature compensation methods for robust speech recognition," in *Noise Reduction in Speech Applications*, G. M. Davis, Ed. CRC Press, 2002, pp. 219–244.

[13] R. Singh, B. Raj, and R. M. Stern, "Model compensation and matched condition methods for robust speech recognition," in *Noise Reduction in Speech Applications*, G. M. Davis, Ed. CRC Press, 2002, pp. 245–275.

[14] B. Raj, V. N. Parikh, and R. M. Stern, "The effects of background music on speech recognition accuracy," in *IEEE Int. Conf. Acoust., Speech and Signal Processing*, vol. 2, Apr. 1997, pp. 851–854.

[15] C. Kim, Y.-H. Chiu, and R. M. Stern, "Physiologically-motivated synchrony-based processing for robust automatic speech recognition," in *INTERSPEECH-2006*, Sept. 2006, pp. 1975–1978.

[16] B. Raj and R. M. Stern, "Missing-Feature Methods for Robust Automatic Speech Recognition," *IEEE Signal Processing Magazine*, vol. 22, no. 5, pp. 101–116, Sept. 2005.

[17] S. Srinivasan, M. Roman, and D. Wang, "Binary and ratio time-frequency masks for robust speech recognition," *Speech Comm.*, vol. 48, pp. 1486–1501, 2006.

[18] H. Park, and R. M. Stern, "Spatial separation of speech signals using amplitude estimation based on interaural comparisons of zero crossings," *Speech Communication*, vol. 51, no. 1, pp. 15–25, Jan. 2009.

[19] R. M. Stern, E. Gouvea, C. Kim, K. Kumar, and H .Park, "Binaural and multiple-microphone signal processing motivated by auditory perception," in *Hands-Free Speech Communication and Microphone Arrys, 2008*, May. 2008, pp. 98–103.

[20] R. M. Stern and C. Trahiotis, "Models of binaural interaction," in *Hearing*, B. C. J. Moore, Ed. Academic Press, 2002, pp. 347–386.

[21] H. S. Colburn and A. Kulkarni, "Models of sound localization," in *Sound Source Localization*, A. N. Popper and R. R. Fay, Eds. Springer-Verlag, 2005, pp. 272–316.

[22] S. B. Davis and P. Mermelstein, "Comparison of parametric representations for monosyllabic word recognition in continuously spoken sentences," *IEEE Trans. Acoust., Speech, and Signal Processing*, vol. 28, no. 4, pp. 357–366, Aug. 1980.

[23] J. Volkmann, S. S. Stevens, and E. B. Newman, "A scale for the measurement of the psychological magnitude pitch (A)," *J. Acoust. Soc. Am.*, vol. 8, no. 3, pp. 208–208, Jan 1937.

[24] E. Zwicker, "Subdivision of the audible frequency range into critical bands," *J. Acoust. Soc. Am.*, vol. 33, no. 2, pp. 248–248, Feb 1961.

[25] H. Hermansky, "Perceptual linear prediction analysis of speech," *J. Acoust. Soc. Am.*, vol. 87, no. 4, pp. 1738–1752, Apr. 1990.

[26] A. V. Oppenheim and R. W.Scafer, with .J. R. Buck, *Discrete-time Signal Processing*. Englewood-Cliffs, NJ: Prentice-Hall, 1999.

[27] L. R. Rabiner and R. W. Schafer, *Digital Processing of Speech Signals*. Englewood-Cliffs, NJ: Prentice-Hall, 1978.

[28] S. S. Stevens, "On the psychophysical law," *Psychological Review*, vol. 64, no. 3, pp. 153–181, 1957.

[29] B. G. Gold and N. Morgan, *Speech and Audio Signal Processing:Processing and Perception of Speech and Music*. New York: John Wiley & Sons, Inc., 2000.

[30] D. Ellis. (2006) PLP and RASTA (and MFCC, and inversion) in MATLAB using melfcc.m and invmelfcc.m. [Online]. Available: http://labrosa.ee.columbia.edu/matlab/rastamat/

[31] H. G. Hirsch and C. Ehrlicher, "Noise estimation techniques or robust speech recognition," in *IEEE Int. Conf. on Acoustics, Speech, and Signal Processing*, May 1995, pp. 153–156.

[32] B. E. D. Kingsbury, N. Morgan, and, S. Greenberg, "Robust speech recognition using the modulation spectrogram," *Speech Communication*, vol. 25, no. 1–3, pp. 117–132, Aug. 1998.

[33] R. Drullman, J. M. Festen and R. Plomp, "Effect of temporal envelope smearing on speech recognition," *J. Acoust. Soc. Am.*, vol. 95, no. 2, pp. 1053–1064, Feb. 1994.

[34] ——, "Effect of reducing slow temporal modulations on speech recognition," *J. Acoust. Soc. Am.*, vol. 95, no. 5, pp. 2670–2680, May 1994.

[35] C. Kim and R. M. Stern, "Feature extraction for robust speech recognition based on maximizing the sharpness of the power distribution and on power flooring," in *IEEE Int. Conf. on Acoustics, Speech, and Signal Processing*, March 2010, pp. 4574–4577.

[36] ——, "Power function-based power distribution normalization algorithm for robust speech recognition," in *IEEE Automatic Speech Recognition and Understanding Workshop*, Dec. 2009, pp. 188–193.

[37] C. Kim, K. Kumar and R. M. Stern, "Robust speech recognition using small power boosting algorithm," in *IEEE Automatic Speech Recognition and Understanding Workshop*, Dec. 2009, pp. 243–248.

[38] X. Huang, A. Acero, H-W Won, *Spoken Language Processing: A Guide to Theory, Algorithm, and System Development*. Upper Saddle River, NJ: Prentice Hall, 2001.

[39] O. Vikki, and K. Laurila, "Cepstral domain segmental feature vector normalization for noise robust speech recognition," *Speech Communication*, vol. 25, pp. 133–147, Aug. 1998.

[40] M. C. Benitez, L. Burget, B. Chen, S. Dupont, H. Garudadri, H. Hermansky , P. Jain, S. Kajarekar, N. Morgan, S. Sivadas, "Robust asr front-end using spectral-based and discriminant features: experiments on the aurora tasks," in *EUROSPEECH-2001*, Sept. 2001, pp. 429–432.

[41] R. M. Stern, B. Raj, and P. J. Moreno, "Compensation for environmental degradation in automatic speech recognition," in *Proc. of the ESCA Tutorial and Research Workshop on Robust Speech Recognition for Unknown Communication Channels*, Apr. 1997, pp. 33–42.

[42] B. Raj, V. N. Parikh, and R. M. Stern, "The effects of background music on speech recognition accuracy," in *IEEE Int. Conf. Acoust., Speech and Signal Processing*, vol. 2, Apr. 1997, pp. 851–854.

[43] J. W. Strutt (Lord Rayleigh), "On our perception of sound direction," *Philosophical Magazine*, vol. 13, pp. 214–232, 1907.

[44] R. H. Gilkey and T. R. Anderson, Eds., *Binaural and Spatial Hearing in Real and Virtual Environments*. Psychology Press (reprint), 1997.

[45] R. M. Stern, D. Wang, and G. J. Brown, "Binaural sound localization," in *Computational Auditory Scene Analysis: Principles, Algorithms and Applications*, D. Wang and G. J. Brown, Eds. Wiley-IEEE Press, 2006.

[46] C. Kim, K. Kumar, B. Raj, and R. M. Stern, "Signal separation for robust speech recognition based on phase difference information obtained in the frequency domain," in *INTERSPEECH-2009*, Sept. 2009, pp. 2495–2498.

[47] M. Slaney, "Auditory toolbox version 2," *Interval Research Corporation Technical Report*, no. 10, 1998. [Online]. Available: http://cobweb.ecn.purdue.edu/~malcolm/interval/1998-010/

[48] D. M. Green, *An Introduction to Hearing, 6th edition*. Hillsdale, NJ: Lawrence Erlbaum Associates, Inc., Publishers, 1976.

[49] B. G. Gold and N. Morgan, *Speech and Audio Signal Processing:Processing and Perception of Speech and Music*. New York: John Wiley & Sons, Inc., 2000.

[50] X. Zhang and M. G. Heinz and I. C. Bruce and L. H. Carney, "A phenomenological model for the responses of auditory-nerve fibers: I. Nonlinear tuning with compression and suppression," *J. Acoust. Soc. Am.*, vol. 109, no. 2, pp. 648–670, Feb 2001.

[51] H. Hermansky, "Perceptual linear prediction analysis of speech," *J. Acoust. Soc. Am.*, vol. 87, no. 4, pp. 1738–1752, Apr. 1990.

[52] S. S. Stevens, "On the psychophysical law," *Psychological Review*, vol. 64, no. 3, pp. 153–181, 1957.

[53] S. G. McGovern, "A model for room acoustics," http://2pi.us/rir.html.

[54] B. Raj, M. L. Seltzer, and R. M. Stern, "Reconstruction of Missing Features for Robust Speech Recognition," *Speech Communication*, vol. 43, no. 4, pp. 275–296, Sept. 2004.

[55] C. Kim and R. M. Stern, "Feature extraction for robust speech recognition using a power-law nonlinearity and power-bias subtraction," in *INTERSPEECH-2009*, Sept. 2009, pp. 28–31.

[56] D. Kim, "Auditory processing of speech signals for robust speech recognition in real-world noisy environments," *IEEE Trans. Speech and Audio Processing*, vol. 7, no. 1, pp. 55–69, Jan. 1999.

[57] P. D. Patterson, K. Robinson, J. Holdsworth, D. McKeown, C. Zhang, and M. H. Allerhand, "Complex sounds and auditory images," in *Auditory and Perception*. Oxford, UK: Y. Cazals, L. Demany, and K. Horner, (Eds), Pergamon Press, 1992, pp. 429–446.

[58] P. Jain and H. Hermansky, "Improved mean and variance normalization for robust speech recognition," in *IEEE Int. Conf. Acoust., Speech and Signal Processing*, May. 2001.

[59] Y. Obuchi,N. Hataoka, and R. M. Stern, "Normalization of time-derivative parameters for robust speech recognition in small devices," *IEICE Transactions on Information and Systems*, vol. 87-D, no. 4, pp. 1004–1011, Apr. 2004.

[60] R. Balchandran and R. Mammone, "Non-parametric estimation and correction of non-linear distortion in speech system," in *IEEE Int. Conf. Acoust., Speech and Signal Processing*, May. 1998, pp. 749–752.

[61] S. Molau, M. Pitz, and H. Ney, "Histogram based normalization in the acoustic feature space," in *Proc. of Automatic Speech Recognition*, Nov. 2001, pp. 21–24.

[62] S. Dharanipragada and M. Padmanabhan, "A nonlinear unsupervised adaptation technique for speech recognition," in *Proc. Int Conf. Spoken Language Processing*, Oct. 2001, pp. 556–559.

[63] C. Kim and R. M. Stern, "Robust signal-to-noise ratio estimation based on waveform amplitude distribution analysis," in *INTERSPEECH-2008*, Sept. 2008, pp. 2598–2601.

[64] C. Kim and R. M. Stern, "Power-normalized cepstral coefficients (pncc) for robust speech recognition," *IEEE Trans. Audio, Speech, Lang. Process.*, (in submission).

[65] ——, "Sound source separation algorithm using phase difference information and automatic selection of itd threshold (name needs to be revised)," *IEEE Trans. Audio, Speech, Lang. Process.*, (in submission).

[66] C. Kim and R. M. Stern, "Nonlinear enhancement of onset for robust speech recognition," in *INTERSPEECH-2010*, Sept. 2010, pp. 2058–2061.

[67] J. L. C. Kim, K. Eom and R. M. Stern, "Automatic selection of thresholds for signal separation algorithms based on interaural delay," in *INTERSPEECH-2010*, Sept. 2010, pp. 729–732.

[68] C. Kim, R. M. Stern, K. Eom, and J. Lee, "Automatic Interaural Time Delay Threshold Selection Method for Sound Source Separation," *United States Patent (Filed)*, 2010.

[69] P. M. Zurek, *The precedence effect*. New York, NY: Springer-Verlag, 1987, ch. 4, pp. 85–105.

[70] K. D. Martin, "Echo suppression in a computational model of the precedence effect," in *IEEE ASSP Workshop on Applications of Signal Processing to Audio and Acoustics*, Oct. 1997.

[71] Y. Park and H. Park, "Non-stationary sound source localization based on zero crossings with the detection of onset intervals," *IEICE Electronics Express*, vol. 5, no. 24, pp. 1054–1060, 2008.

[72] L. R. Rabiner and B.-H. Juang, *Fundamentals of Speech Recognition*. Englewood Cliffs, New Jersey: PTR Prentice Hall, 1993.

[73] F. Jelinek, *Statistical Methods for Speech Recognition (Language, Speech, and Communication)*. MIT Press, 1998.

[74] *Speech Processing, Transmission and Quality Aspects (STQ); Distributed Speech Recognition; Advanced Front-end Feature Extraction Algorithm; Compression Algorithms*, European Telecommunications Standards Institute ES 202 050, Rev. 1.1.5, Jan. 2007.

[75] C. Kim, "Signal processing for robust speech recognition motivated by auditory processing," Ph.D. dissertation, Carnegie Mellon University, Pittsburgh, PA USA, October 2010.

[76] C. Lemyre, M. Jelinek, and R. Lefebvre, "New approach to voiced onset detection in speech signal and its application for frame error concealment," in *IEEE Int. Conf. on Acoustics, Speech, and Signal Processing*, May 2008, pp. 4757–4760.

[77] S. R. M. Prasanna and P. Krishnamoorthy, "Vowel onset point detection using source, spectral peaks, and modulation spectrum energies," *IEEE Trans. Audio, Speech, and Lang. Process.*, vol. 17, no. 4, pp. 556–565, May 2009.

[78] C. Kim, K. Kumar, and R. M. Stern, "Binaural sound source separation motivated by auditory processing," in *IEEE Int. Conf. on Acoustics, Speech, and Signal Processing*, 2011,(submitted).

[79] S. Seneff, "A joint synchrony/mean-rate model of auditory speech processing," *J. Phonetics*, vol. 16, no. 1, pp. 55–76, Jan. 1988.

[80] J. Tchorz and B. Kolllmeier, "A model of auditory perception as front end for automatic speech recognition," *J. Acoust. Soc. Am.*, vol. 106, no. 4, pp. 2040–2050, 1999.

[81] X. Zhang and M. G. Heinz and I. C. Bruce and L. H. Carney, "A phenomenological model for the responses of auditory-nerve fibers: I. Nonlinear tuning with compression and suppression," *J. Acoust. Soc. Am.*, vol. 109, no. 2, pp. 648–670, Feb 2001.

[82] J. Allen and D. Berkley, "Image method for efficiently simulating small-room acoustics," *J. Acoust. Soc. Am.*, vol. 65, no. 4, pp. 943–950, April 1979.

[83] C. S. C. S. Consortium. CMU sphinx open source toolkit for speech recognition: Downloads. [Online]. Available: http://cmusphinx.sourceforge.net/wiki/download/

[84] W. Grantham, "Spatial hearing and related phenomena," in *Hearing*, B. C. J. Moore, Ed. Academic, 1995, pp. 297–345.

[85] P. Arabi and G. Shi, "Phase-based dual-microphone robust speech enhancement," *IEEE Tran. Systems, Man, and Cybernetics-Part B:*, vol. 34, no. 4, pp. 1763–1773, Aug. 2004.

[86] D. Halupka, S. A. Rabi, P. Aarabi, and A. Sheikholeslami, "Real-time dual-microphone speech enhancement using field programmable gate arrays," in *IEEE Int. Conf. on Acoustics, Speech, and Signal Processing*, March 2005, pp. v/149 – v/152.

[87] C. Trahiotis, L. Bernstein, R. M. Stern, and T. N. Buell, "Interaural correlation as the basis of a working model of binaural processing," in *Sound Source Localization*, ser. Springer Handbook of Auditory Research, R. Fay and T. Popper, Eds. Springer-Verlag, 2005, vol. 25, pp. 238–271.

[88] D. M. Green, *An Introduction to Hearing, 6th edition*. Hillsdale, NJ: Lawrence Erlbaum Associates, Inc., Publishers, 1976.

[89] C. Kim, Y-H. Chiu, and R. M. Stern, "A robust voice adtivity detection algorithm based on power normalization and statistical hypothesis testing," in *IEEE Int. Conf. on Acoustics, Speech, and Signal Processing*, 2011, (submitted).